Molecular Mechanisms Regulating the Epithelial Barrier: Key Roles for Cx26 and ADAM17 during Bacterial Infection

Charlotte Louise Simpson

Supervisors: **Dr Olivier Marchès**

Prof David Kelsell

Submitted for the Degree of

Doctor of Philosophy

Abstract

This study investigated how gastrointestinal and skin bacterial infections were affected by differential expression of connexin (Cx) 26 and a disintegrin and metalloprotease (ADAM) 17 *in vitro*.

Cx26 is a component of gap junctions, which facilitate the transfer of small molecules between two cells. Recessive mutations in Cx26 cause non syndromic hearing loss (NSHL), and in certain populations, specific mutations account for the majority of Cx26 related NSHL. Their common occurrence suggests that they may provide a heterozygous, protective advantage to carriers. In this study adherence by the attaching and effacing pathogen Enteropathogenic *Escherichia coli* (EPEC) was significantly reduced in cells expressing mutant Cx26 compared to wild type Cx26. Furthermore, EPEC adherence and invasion of an alternative enteric pathogen, *Shigella flexneri* were reduced following treatment with Cx26 short-interfering-RNA in intestinal cells. These findings suggest that the loss of functional Cx26 expression improves protection against enteric bacteria.

ADAM17 releases substrates including tumour necrosis factor alpha and ligands of the epidermal growth factor receptor and therefore is involved in the induction of immune responses and maintenance of the epidermal barrier. This study demonstrated that ADAM17 provides protection during *Staphylococcus aureus* infection of keratinocytes. Subsequently the protective effects of ADAM17 mediated protection were explored. Secretion of the proinflammatory cytokines Interleukins 6 and 8 correlated with ADAM17 activity. Additionally gene expression profiling was performed which identified the IL-17 signalling pathway, which is known to be important during *S. aureus* infection, as a potential downstream target of ADAM17.

In summary, based on these findings, Cx26 and ADAM17 may represent potential therapeutic targets for gastrointestinal and skin bacterial pathogens.

Table of Contents

List of Figures and Tables

List of Figures

List of Tables

Publications and abstracts

Peer reviewed publications:

C Simpson, D Kelsell & O Marchès (2013). Connexin 26 facilitates gastrointestinal bacterial infection *in vitro*. Cell and Tissue Research, 351: 107-116. (2013)

M Brooke, S Etheridge, N Kaplan, **C Simpson**, E O'Toole, A Ishida-Yamamoto, O Marchès, S Getsios, D Kelsell. iRHOM2-dependent regulation of ADAM17 in cutaneous disease and epidermal barrier function (in preparation for publication).

Abstracts

C. Simpson, M. Brooke, O. Marchès & D. Kelsell (May 2013). A specific requirement for a disintegrin and metalloprotease (ADAM) 17 in protection against cutaneous *Staphylococcus aureus* infection. (Abstract #1132). Poster presented at the International Investigative Dermatology Meeting, Edinburgh. Available at [1].

C. Simpson, O. Marchès & D. Kelsell (March 2013). Investigating a link between connexion 26 (Cx26) and the intestinal barrier. Oral presentation, Society for General Microbiology, Dublin. Available at http://www-07.all-portland.net/meetings/SGM%20Dublin%202012_Abstracts.pdf

Acknowledgements

I would like to thank my supervisors Olivier Marchès and David Kelsell for their expert knowledge, guidance and support throughout my PhD. I also thank Dr Patricia Martin (Glasgow Caledonian University) for the (WT)Cx26-mCherry plasmid, Dr Sahira Khalaf for the Caco-2 and HT-29 cell lines, Dr Ann Wheeler for help with imaging and developing the assay for quantifying EPEC infection and Mimoza Hoti for carrying out the gene expression array.

I would also like to thank everybody in the laboratory group including Dr Claire Scott, Dr Diana Blaydon, Dr Daniel Tattersall, Matthew Brooke, Sarah Etheridge, Daniela Nitiou, Benjamin Fell and Phil Bland. Special thanks in particular to Dr Claire Scott, Dr Daniel Tattersall and Dr Joseph Aduse-Opoku for technical training and Matthew Brooke for primer design.

Thanks to my family and friends for their support.

Finally I acknowledge the financial assistance of Barts and the London School of Medicine and Dentistry and the Medical Research Council, UK.

List of Abbreviations

-/-	Homozygous mutant
+/-	Heterozygous
+/+	Wild type
+ve	Positive
<	Less than
>	Greater than, or substitution (mutation)
℃	Degrees celcius
A	Amp
A	Adenine (nucleic acid)
Ab	Antibody
ADAM	A disintegrin and metalloprotease
ADF	Actin depolymerising factor
ADP	Adenosine diphopshate
agr	Accessory gene regulator
AJ	Adherens junction
APC	Antigen presenting cell
AQP	Aquaporin
Arp	Actin-related-protein
AS	Individuals heterozygous for the sickle gene
ATG	Methionine start codon
ATP	Adenosine triphosphate
ATPase	Adenosine triphosphatase
BFP	Bundle forming pili
BPS	Bart-Pumphrey syndome
BSA	Bovine serum albumin
c	Coding DNA reference sequence
C	Cytosine (nucleic acid)
C (Cys)	Cysteine (amino acid)
C. albicans	*Candida albicans*
C. rodentium	*Citrobacter rodentium*
Ca	Calcium
cAMP	Cyclic adenosine monophosphate
CD	Cluster of differentiation
cDNA	Complementary deoxyribonucleic acid
CE	Cornified envelope
Ces	Chaperone of *E. coli* secretion
CFTR	Cystic fibrosis transmembrane conductance regulator
CHIPs	Chemotaxis inhibitory protein of S. aureus
CL	Cytoplasmic loop
Cl^-	Chloride
CNS	Central nervous system
CO_2	Carbon dioxide
CSF	Colony stimulating factor
Ct	Cycle threshold
Cx	Connexin
CXCL	Chemokine (C-X-C motif) ligand
D (Asp)	Aspartic acid (amino acid)
DAPI	Diamidino-2-phenylindole
DEFB103A	Defensin, beta 103A (encoding hBD-3)
DEFB4A	Defensin, beta 4A (encoding hBD-2)

Del	Deletion
DFNA	Deafness, autosomal dominant
DFNB	Deafness, neurosensory autosomal recessive
DFNX	Deafness, X linked
dH_20	Distilled water
dIL	Decilitre
DMSO	Dimethyl sulphoxide
DNA	Deoxyribonucleic acid
DNase	Deoxyribonuclease
dNTP	Deoxyribonucleotide triphosphate
DRA	Downregulated in adenoma
DSS	Dextran sodium sulphate
E (Glu)	Glutamic acid (amino acid)
E. coli	*Escherichia coli*
Eae	*E. coli attaching and effacing* (encoding Intimin)
EAF	EPEC adherence factor
ECM	Extracellular matrix
EDTA	Ethylenediaminotetraacetic acid
EGF	Epidermal growth factor
EGFR	Epidermal growth factor receptor
EHEC	Enterohemorrhagic *Escherichia coli*
EL	Extracellular loop
EPEC	*Enteropathogenic Escherichia coli*
ER	Endoplasmic reticulum
ERAD	Endoplasmic reticulum associated degradation
ErbB	Erythroblastic leukaemia viral oncogene homolog
ERK	Extracellular-signal-regulated kinase
Esc	*E. coli* secretion
Esp	*E. coli* secreted protein
F (Phe)	Phenylalanine (amino acid)
F-actin	Filament actin
FBS	Foetal bovine serum
Fnbp	Fibronectin binding protein
FSC-A	Forward scatter
Fx	Frameshift
G	Guanine (nucleic acid)
G (Gly)	Glycine (amino acid)
G-actin	Globular actin
GAP	Guanosine triphosphate phosphohydrolase activating protein
GAPDH	Glyceraldehyde-3-phosphate dehydrogenase
GDI	Guanine nucelotide dissociation inhibitor
GDP	Guanosine diphosphate
GEF	Guanine nucleotide exchange factor
GFP	Green fluorescent protein
GJ	Gap junction
GJB	*Gap junction protein beta*
GJB2	Gap junction protein beta 2 (encoding Cx26)
GJIC	Gap junction intracellular communication
gp130	Glycoprotein 130
GPCR	G Protein coupled receptor
GrlA	Global regulator of locus of enterocyte effacement activator
GrlR	Global repressor of locus of enterocyte effacement repressor
GTP	Guanosine triphosphate
GTPase	Guanosine triphosphate phosphohydrolase

H (his)	Histidine (amino acid)
H_2O	Water
H_2O_2	Hydrogen peroxide
H_2SO_4	Sulphuric acid
hBD	Human beta defensin
HB-EGF	Heparin-binding EGF-like growth factor
HID	Hystrix-like icthyosis deafness
HLY	Human lysozyme promoter
HPV	Human papiloma virus
HRP	Horseradish peroxidase
I	Ionomycin
ICAM1	Intracellular adhesion molecule 1
IDP	Inner denser plaque
IEC	Intestinal epithelial cell
IFN	Interferon
Ig	Immunoglobulin
IL	Interleukin
IL6-R	Interleukin 6 receptor
ins	Insertion
IP_3	Inositol trisphosphate
Ipa	Invasion plasmid antigen
Ipg	Invasion plasmid gene
iRhom	Inactive rhomboid protein
ITGB1	Integrin, beta 1
Ix	Innexin
IκBα	Inhibitor of nuclear factor kappa B alpha
JNK	Jun N-terminal protein kinase
K	Potassium
K (Lys)	Lysine (amino acid)
kB	Kilobase
kDa	Kilodalton
KID	Keratitis-icthyosis deafness
L (Leu)	Leucine
L. monocytogenes	*Listeria monocytogenes*
LB	Luria Bertani
LEE	Locus of enterocyte effacement
ler	Locus of enterocyte effacement encoded regulator
LFA1	Lymphocyte function-associated antigen 1
LOF	Loss of function
LPS	Lipopolysaccharide
M	Molar
M (Met)	Methionine (amino acid)
M cell	Microfold cell
MA	Milliamp
MAPK	Mitogen activated protein kinase
MFI	Mean fluorescent intensity
Mg	Miligram
$MgCl_2$	Magnesium chloride
MLC	Myosin light chain
mg	Miligram
ml	Millilitre
mM	Millimolar or milimetre
MMP	Matrix metalloprotease

MOI	Multiplicity of infection
mRNA	Messenger ribonucleic acid
MS	Multiple sclerosis
MSCRAMM	Microbial surface components recognising adhesive matrix molecules
MV	Millivolt
Mxi	Membrane excretion protein
N (Asn)	Asparginine (amino acid)
Na	Sodium
NaN_3	Sodium azide
NF-κB	Nuclear factor kappa B
Ng	Nanogram
NHE	Sodium hydrogen exchanger
NK	Natural killer
nM	Nanomolar or nanometre
NOD	Nucleotide-binding oligomerisation-domain-containing
NSHL	Non syndromic hearing loss
NT	N terminal
NTP	Non-targeting pool
O_2	Oxygen
ODP	Outer denser plaque
P	Protein reference sequence
P (Pro)	Proline
P. falciparum	*Plamsodium falciparium*
PAMP	Pathogen associated molecular pattern
Panx	Pannexin
PAT	Putative anion transporter
PBMC	Peripheral blood mononuclear cell
PBS	Phosphate buffered saline
PCR	Polymerase chain reaction
PFA	Paraformaldehyde
pg	Picogram
PGN	Peptidoglycan
Pixel	Picture element
PKC	Protein Kinase C
PMA	Phorbol-12-myristate-13-acetate
PPK	Palmoplantar keratoderma
PPR	Pattern recognition receptor
PVL	Panton-Valentine leukocidin
Q (Gln)	Glutamine (amino acid)
qRT-PCR	Quantitative reverse transcriptase polymerase chain reaction
R (Arg)	Arginine (amino acid)
RE	Relative expression
RGB	Red green blue
RHBDF2	Rhomboid 5 homolog 2 (*Drosophila) (*encoding iRhom2*)*
RNA	Ribonucleic acid
RNase	Ribonuclease
RPM	Revolutions per minute
RT-PCR	Reverse transcriptase polymerase chain reaction
S (Ser)	Serine (amino acid)
S. aureus	*Staphylococcal aureus*
S. boydii	*Shigella boydii*
S. dysenteriae	*Shigella dysenteriae*
S. flexneri	*Shigella flexneri*
S. sonnei	*Shigella sonnei*

S. typhi	*Salmonella typhi*
sarA	*Staphylococcal* accessory regulator
SCIN	*Staphylococcal* complement inhibitor
SDS	Sodium-dodecyl-sulphate
SEM	Standard error of the mean
SGLT	Sodium dependent glucose transporter
SH	Src Homology
sIL-6R	Soluble interleukin 6 receptor
siRNA	Small interfering RNA
SNP	Single nucleotide polymorphism
Spa	Surface presentation antigen (*Shigella*) or *Staphylococcal* Protein A (*S. aureus*)
SSC-A	Side scatter
SVMP	Snake venom metalloprotease
T	Thymine (nucleic acid)
T (Thr)	Threonine (amino acid)
TACE	Tumour necrosis factor alpha converting enzyme
TBE	Tris borate EDTA
TBS	Tris buffered saline
TCR	T cell receptor
TE	Tris-EDTA buffer
TER	Transepithelial resistance
TGF	Transforming growth factor
TGM	Transglutaminase
Th	T helper
TIMP	Tissue inhibitor of matrix metalloprotease
Tir	Translocated intimin receptor
TJ	Tight junction
TLR	Toll like receptor
TM	Transmembrane
TNFR	Tumour necrosis factor alpha receptor
TNFα	Tumour necrosis factor alpha
TOC	Tylosis with oesophageal cancer
TRAPS	Tumour necrosis factor receptor associated periodic syndrome
TWL	Transepithelial water loss
U/ml	Units/millilitre
UV	Ultraviolet
V	Volts
V/v	Volume/volume
V (Val)	Valine (amino acid)
-ve	Negative
Vir	Virulence protein
VS	Vohwinkel syndrome
W (Trp)	Tryptophan (amino acid)
W/v	Weight/volume
WASP	Wiskott-Aldrich-syndrome protein
WAVE	Wiskott-Aldrich-veprolin-homologous
WT	Wild type
X	Any amino acid residue
Y (Tyr)	Tyrosine (amino acid)
Y. enterocolitica	*Yersinia enterocolitica*
Zn	Zinc
ZO	Zona occludens
µg	Microgram

µl	Microlitre
µM	Micromolar or micrometre

~ Chapter 1 ~

Introduction

1.1 Effect of Connexin (Cx) 26 expression on gastrointestinal bacterial infection

1.1.1 Gap junction intercellular communication (GJIC)

In multicellular organisms, intercellular communication is mediated by gap junctions (GJ) and is required to maintain cellular homeostasis and to orchestrate responses to extracellular stimuli[2]. Before GJ proteins were identified, the structure of GJs was discovered using electron microscopy and X-ray diffraction. A GJ plaque consists of hundreds of tightly clustered individual channels which connect two cells by spanning the cell membranes and the space between the cells[3,4] (figure 1.1.1). GJs permit the sharing of small molecules including ions (e.g. Ca^{2+}), metabolites (e.g. adenosine triphosphate (ATP)), nutrients (e.g. glucose) and second messengers (e.g. inositol trisphosphate (IP_3))[5], whilst restricting the passage of molecules exceeding 1kDa in size, for example nucleic acids and proteins[6]. By facilitating electrical and metabolic coupling between cells[7], gap junction intercellular communication (GJIC) is important for processes including cell growth and development[8]. For example, GJs expressed in periventricular precursor cells in the developing brain play a role in Ca^{2+} signalling, which regulates the proliferation of neural cells[9].

Figure 1.1.1: Structure of a gap junction. Six Cx subunits oligomerise and form a Cx hemichannel. At the cell surface hemichannels from adjacent cells dock end to end. This forms a GJ channel, which spans the cell membranes and intracellular space thereby connecting two cells. Small molecules are shared between cells via GJs facilitating intercellular communication.

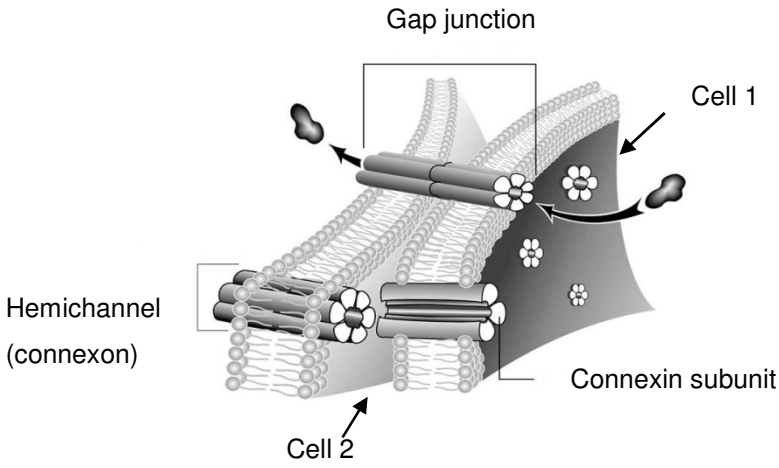

(Image modified from http://www.landesbioscience.com/curie/chapter/852/)

1.1.2 GJ proteins

Three families of GJ proteins have been described which are connexins (Cxs), innexins (Ixs) and pannexins (Panxs). In vertebrates most GJs are formed from Cxs, and the first Cx was cloned in 1986[10]. To date 21 Cx genes have been described in humans and 20 in mice[11]. Cx genes have been allocated to α, β, γ, δ and ε subgroups based on their structure and sequence homology[12]. The genomic structure of the majority of Cx genes consists of two exons, the first of which is non-coding and the second which contains the entire coding region of the gene[13]. Cx proteins are named according to their molecular mass, for example Cx26 is approximately 26kDa[7]. In invertebrates GJ form from Ixs, which are proteins specific to invertebrates, and which are unrelated to Cxs[8,14]. Although both groups of proteins share a similar topological structure, their primary amino acid sequences are only 16% homologous to each other[15]. Invertebrate GJ proteins were termed Ixs, which was a name given to describe a group of proteins that were invertebrate analogs of Cx proteins[16]. More recently three *PANX* genes were cloned in humans, and as they were homologs of Ixs, Ixs were subsequently reclassified with their vertebrate homologs in the Panxs family[14].

1.1.3 Cx expression in human tissue

With the exception of erythrocytes, mature sperm cells and skeletal muscle, Cxs are expressed by all tissue types[7]. Cx43 is the most widely expressed Cx and localises to at least 35 different cell types including astrocytes, keratinocytes and cardiomyocytes[17]. Commonly two or more Cx proteins are coexpressed by cells and tissues. For example keratinocytes express Cx26, Cx30, Cx30.3, Cx31.1 and Cx43, and Cx26 is coexpressed with Cx32 in hepatocytes[17].

1.1.4 Cx protein structure

Cx proteins consist of four transmembrane (TM) alpha helices, two extracellular loops, a cytoplasmic loop, a cytoplasmic amino (N) terminus and a cytoplasmic carboxyl (C) terminus[9] (figure 1.1.2). The extracellular loops harbour three

conserved cysteine residues, which form disulphide bonds connecting the two extracellular loops. The cysteine residues are required for the formation of functional GJ channels and if they are mutated, the ability of Cxs to form functional GJs is compromised[9].

Figure 1.1.2: Cx protein structure. Cx proteins consist of 4 transmembrane domains (m1-m4), 2 extracellular loos (el1 and 2), one cytoplasmic loop (cl), a cytoplasmic amino terminus (NH_2) and a cytoplasmic carboxyl terminus (HOOC).

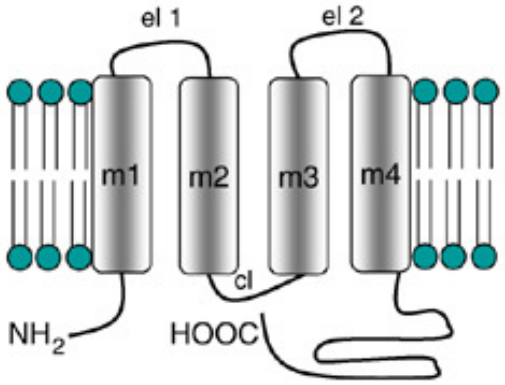

(Image modified from[18])

While the transmembrane domains and extracellular loops are conserved among different Cx proteins, the length and sequence of the cytoplasmic terminus and cytoplasmic loop of different Cx proteins varies. Cx50 has a long cytoplasmic terminus whereas Cx26 has a short cytoplasmic terminus[19]. The variation in the sequence of the cytoplasmic terminus and the cytoplasmic loop of different Cx proteins confers specific properties to GJ channels formed by different Cx proteins, including voltage and pH dependency[7,19]. For example, Cx26 and Cx43 channels are closed at positive and negative voltages respectively on the cytoplasmic side of the GJ[7]. Decreasing the intracellular pH also tends to reduce junctional conductance, and Cxs exhibit different sensitivities to pH, for instance Cx50 is more sensitive than Cx32 to a fall in pH[20]. Sensitivity to voltage and pH changes thus likely affects GJ permeability to small molecules.

1.1.5 GJ assembly

1.1.5.1 Cx protein synthesis

Cx proteins have a short half-life of a few hours meaning that they are continuously biosynthesised and degraded[17]. Consequently the level of Cx protein expression and GJIC can rapidly be upregulated or downregulated to accommodate changes in physiological conditions[17]. After gene transcription, with the exception of Cx26 which may be inserted into the endoplasmic reticulum (ER) membrane both post- and co-translationally[21], Cx proteins are co-translationally incorporated into the ER membrane[17].

1.1.5.2 Cx hemichannel formation

Six individual Cx subunits oligomerise to form a hemichannel (connexon)[2,17]. While this occurs predominantly in the ER[2,17] some Cxs including Cx43 and Cx46 oligomerise in the *trans*-Golgi network[22,23]. The hemichannel formed can be either homomeric, when the Cxs in the hemichannel are the same, or heteromeric, when the Cxs in the channel are different[9,17].

1.1.5.3 Cx hemichannel trafficking to the cell surface, GJ assembly and degradation

After exiting the ER, most Cxs pass through the Golgi apparatus and then traffic to the cell surface[2,17]. However, the incorporation of Cx26 into functional GJs is relatively unaffected by disruption of the Golgi apparatus, demonstrating that Cx26 can traffic to the cell surface via a Golgi independent pathway[24]. Upon exiting the Golgi apparatus, hemichannels are packaged into transport vesicles. These are loaded onto microtubules and undergo anterograde transport to the cell surface via plus ended motor proteins, for example kinesins [17,25,26]. After insertion into the plasma membrane, Cx hemichannels from adjacent cells dock end to end, which is guided by the adherens junction components N- and E-cadherin. This forms a GJ channel which connects the cytoplasms of the two

cells. GJ channels can be either homotypic, composed of two identical hemichannels, or heterotypic, composed of two different hemichannels (figure 1.1.3). Homotypic and heterotypic GJ channels are composed of either homomeric or heteromeric hemichannels. Tens to thousands of these individual GJ channels subsequently cluster together and form a GJ plaque[9]. The combination of Cx proteins which interact with each other is different in different tissue types and this affects the permeability of GJs to specific molecules[9,17]. For example, although the transfer of cAMP and cGMP is equally efficient through homomeric channels formed by Cx32, cGMP passes more efficiently through heteromeric hemichannels composed of Cx32 and Cx26[27].

Figure 1.1.3: GJ channels. GJ channels form from the end to end docking of two Cx hemichannels from adjacent cells. Homotypic GJ channels are composed of two identical hemichannels. Each hemichannel may be homomeric (composed of the same Cx) or heteromeric (composed of different Cxs). Heterotypic GJ channels are composed of two different hemichannels. Each hemichannel of a heterotypic GJ channel may be homomeric or heteromeric. GJ are composed of clusters of tens to thousands of GJ channels.

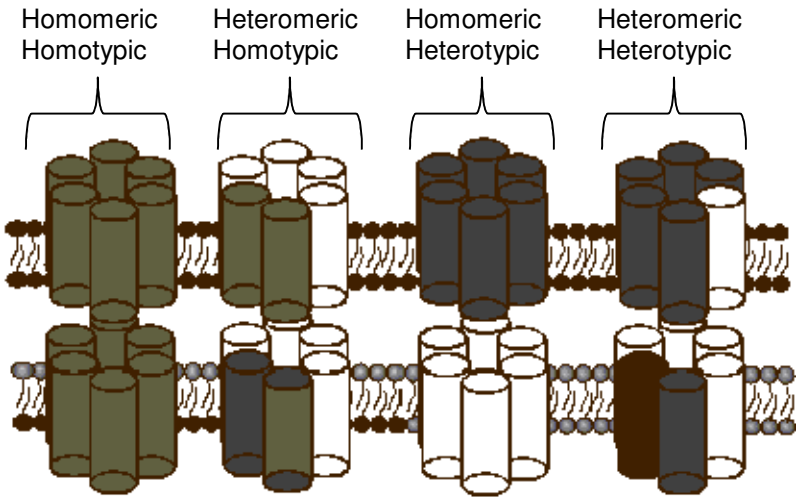

(Image modified from http://herkules.oulu.fi/isbn9514259351/html/i245454.html)

Hemichannel clustering at the cell surface is a continually active, dynamic process[7,17]. Pulse chased experiments using tetracysteine-tagged Cx43 revealed that hemichannels continually traffic to the cell surface[28]. Newly formed GJ channels localise to the outer margin of the GJ, and as they mature they migrate into the centre of the GJ plaque[28]. Older GJ channels are removed from the plaque by endocytosis, and certainly for Cx43, this step is initiated by ubiquitination. Cx43 endocytosis may then result from the internalisation of uncoupled hemichannels, or the internalisation of whole GJs into double-

membrane vesicles termed ‘annular junctions’. Following internalisation, degradation has subsequently been shown to occur in the lysosome or proteasome, or by the process of autophagy[7,17,19]. The life cycle of Cx proteins is shown in figure 1.1.4.

Figure 1.1.4: Life cycle of Cx proteins. Upon exiting the Golgi apparatus Cx hemichannels are packaged into transport vesicles. These are loaded onto microtubules for their transport to the cell surface via plus-ended motor proteins, e.g. kinesins. After insertion into the plasma membrane at the intercalated disc, Cx hemichannels from adjacent cells dock end to end forming a GJ channel, which is guided by adherens junction components. Unpaired Cx hemichannels are endocytosed and whole GJs can be internalised into double membrane ‘annular junction’ vesicles. Cx hemichannels and GJs may then be degraded in the lysosome or proteasome, or by the autophagy process.

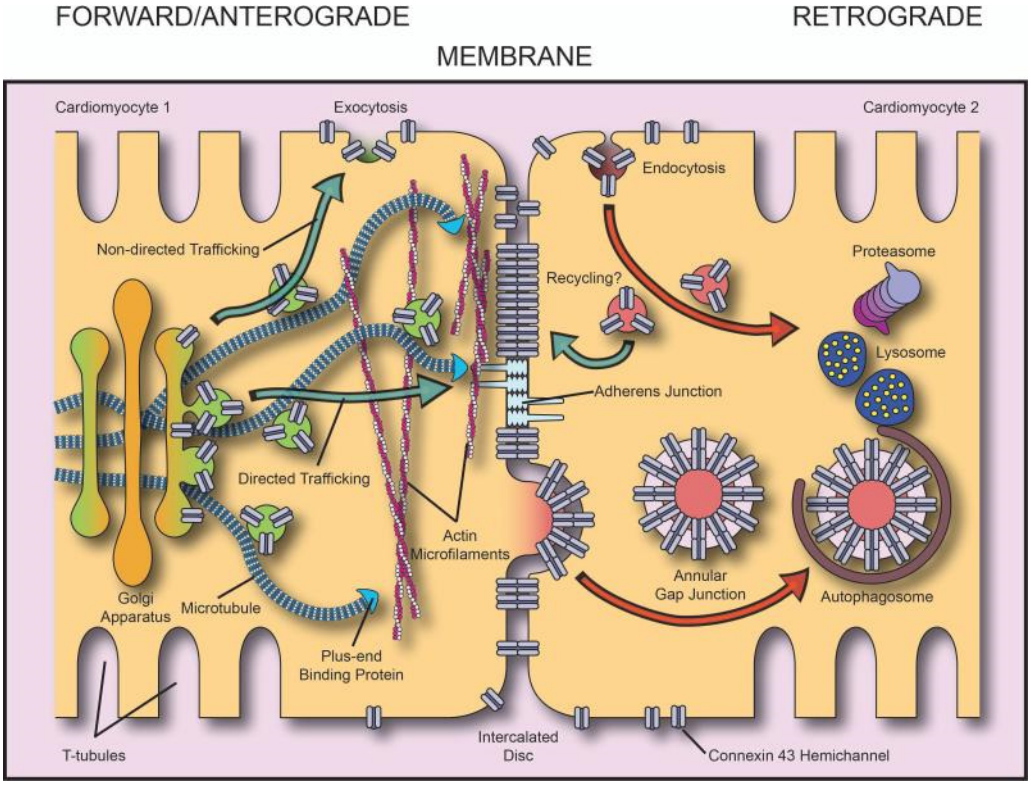

(Image from Smyth, J. W. and Shaw R. M. The Gap Junction Life Cycle. *Heart Rhythm*. **9**, 151-153 (2012).)

1.1.6 GJ regulation

The cytoplasmic loop and cytoplasmic terminus of Cx proteins are sites subject to post-translational modifications which serve to regulate GJs. GJ opening and permeability are regulated by various factors including the intracellular concentration of Ca^{2+}, voltage, pH and phosphorylation[7]. Phosphorylation of serine, threonine and tyrosine residues located in the cytoplasmic terminus can

alter the unitary conductance, mean open time, or voltage and pH sensitivity of GJ channels, thereby modifying the sharing of ions and small molecules between cells[7]. With the exception of Cx26[29], all other known Cxs can be phosphorylated[30].

1.1.7 Cx phosphorylation

Cx phosphorylation is thought to be important at various stages during the lifecycle of Cx proteins. For example, phosphorylation of the C-terminus of Cx43 by Protein Kinase A increases its incorporation into the plasma membrane[31], while phosphorylation by casein kinase regulates the assembly of Cx43 hemichannels into GJ plaques[32]. Conversely epidermal growth factor (EGF) signalling induces Cx43 phosphorylation via the mitogen activated protein kinase (MAPK) pathway, which accelerates the internalisation and subsequent degradation of Cx43[33]. In many tumours, EGF signalling is enhanced, and the authors suggested that it could lead to enhanced Cx degradation, which in turn could account for the reduction in GJIC which occurs in some tumour types[33].

1.1.8 Unpaired Cx hemichannels

In addition to forming GJs, Cx hemichannels also exist as isolated channels at the cell surface. This was first observed when individual *Xenopus* oocytes injected with Cx46 mRNA displayed conductance at low concentrations of extracellular Ca^{2+} and incorporated fluorescent dyes from the extracellular medium[34]. Treating cells with GJ blockers including heptanol and octanol reduced dye uptake by 50%[35]. Unpaired Cx hemichannels were subsequently discovered in astrocytes[36] and ventricular myocytes[37]. Subsequently other Cx proteins including Cx26, Cx45[38] and Cx50[39] were shown to form functional unpaired Cx hemichannels[40].

1.1.8.1 Unpaired Cx hemichannel function

In a resting cell Cx hemichannels are closed, but certain stimuli trigger their opening[41]. These include a decrease in the concentration of extracellular Ca^{2+} to below the physiological concentration, mechanical membrane stress, membrane depolarisation, ischemia, metabolic inhibition, changes in pH and phosphorylation[41]. Open hemichannels permit the exchange of molecules between the intracellular and extracellular environment, thereby facilitating paracrine signalling[2]. ATP was the first molecule shown to be released by Cx hemichannels[41]. More recently Cx hemichannels have been shown to release other molecules including glutamate by astrocytes[42] and prostaglandins by osteoclasts[43].

In humans Ca^{2+} plays important roles in numerous physiological processes including fertilisation, programmed cell death, neurotransmitter release and muscle contraction[44]. Ca^{2+} signalling is facilitated by Cx hemichannels which propagate Ca^{2+} waves to neighbouring cells[2]. In response to changes in the cytoplasmic concentration of Ca^{2+}, Cx hemichannels open leading to the release of ATP from the cell[2]. ATP binds to purinergic receptor 2Y, which is a G-protein-coupled-receptor (GPCR) on neighbouring cells, activating phospholipase C[2]. This leads to the formation of inositiol trisphosphate, triggering the release of Ca^{2+} from ER stores, and the opening of new Cx hemichannels, which in turn transmits the Ca^{2+} wave to surrounding cells[2].

1.1.9 Experimental approaches used to study GJs and unpaired hemichannels

Many functional assays performed *in vitro* have been used to study the activity of GJs[14].

1.1.9.1 Cx protein labelling with fluorescent tags

Over-expression of proteins labelled with fluorescent tags, for example green fluorescent protein (GFP) or mCherry fluorescent protein, enables their

behaviour and function to be visualised in transfected cells. This technique has been used to investigate differences between the localisation of wild type and mutant Cx proteins[2].

1.1.9.2. Dye transfer assays

Dye transfer assays (figure 1.1.5) have been used to measure whether a dye can pass between cells via GJs, or between the intracellular and extracellular environment via unpaired Cx hemichannels. Using dyes with different molecular sizes provides an indication of the size of molecules which can pass through specific hemichannels. This technique has been used to study the permeabilities of specific GJs and unpaired hemichannels formed from different Cx proteins, and to assess how the passage of small molecules is affected by specific Cx mutations[45].

Figure 1.1.5: Dye transfer assay. Lucifer yellow dye is injected into the cells marked with an asterisk. Lucifer yellow binds to DNA labelling the nuclei of cells. If the injected cell forms GJs with neighbouring cells, dye will be transferred from the injected cell. **a** is an example of a cell which is not coupled to many other cells, whilst **b** shows a cell which has formed GJs with multiple adjacent cells.

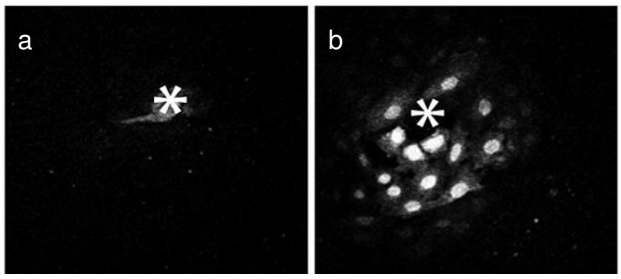

(Image modified from[46])

1.1.9.3 Dual clamp voltage technique

The dual clamp voltage technique (figure 1.1.6) is used to measure electrophysical coupling between cells. *Xenopus* oocytes which have been injected with Cx DNA or RNA are commonly used in this assay. The dual voltage clamp technique measures the flow of ions between cells/oocytes which is termed the transjunctional voltage[47]. Each cell/oocyte is clamped individually

and has a recording electrode and a current injecting electrode inserted into it[48]. The voltage within the second cell/oocyte is measured, while the current is varied in the first cell/oocyte but kept constant in the second cell/oocyte[48]. As the current is kept constant in the second cell/oocyte, any variation in the voltage in the second cell/oocyte results from current passing from the first cell/oocyte into the second cell/oocyte via GJs[48]. This technique can be used to compare the transjunctional voltage between WT and Cx mutants thereby determining any effect which the mutant may have on the GJ channel function.

Figure 1.1.6: Dual clamp voltage technique

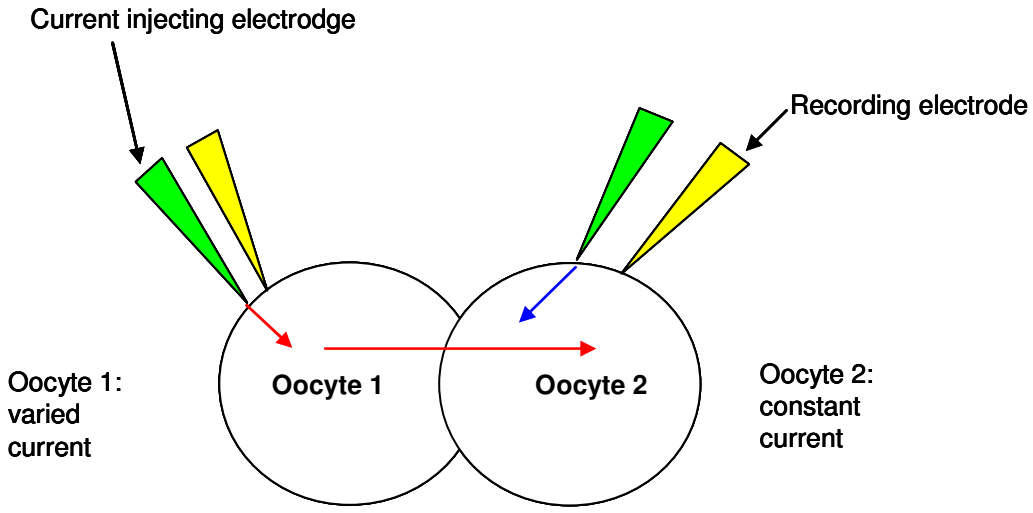

Any change in voltage in oocyte 2 results from current passing from oocyte 1 (red arrows) to oocyte 2.

1.1.9.4 Cx hemichannel blockers

Using chemicals to block hemichannel activity permits the study of GJs and unpaired hemichannels. However many of the chemicals available are not specific to Cx channels and also target other membrane channels[41]. For example, whilst aliphatic alcohols such as heptanol and octanol disrupt the plasma membrane compressing Cx channels, they also compress other membrane channels[41]. Other chemicals, for example 18α-glycyrrhetinic acid may be more specific to Cx hemichannels[49]. It has been suggested that 18α-glycyrrhetinic acid can bind directly to Cx proteins and induce hemichannel

closure. Additionally it has also been shown to interfere with the incorporation of Cx hemichannels into GJ plaques[49].

1.1.9.5 Cx mimetic peptides

Cx mimetic peptides are short amino acid sequences corresponding to part of the sequence contained by the Cx protein. For example, the mimetic peptide Gap 26 is identical to a sequence on extracellular loop 1, while Gap 27 is identical to a sequence on extracellular loop 2 of Cx43[41]. They have been designed to specifically inhibit Cx channels and have facilitated the study of GJs and unpaired hemichannels[41]. Incubating cells with Cx mimetic peptides for 10-30 minutes inhibits unpaired hemichannels, whereas GJ inhibition requires an incubation of one hour minimum[41]. The hypotheses are that Cx mimetic peptides might inhibit Cx function by preventing the incorporation of Cx hemichannels into GJ channels, by damaging the structure of existing GJ channels or by becoming incorporated inside GJ channels [41].

1.1.9.6 Mouse models

Mouse models in which specific Cx genes are knocked out, or in which specific Cx mutations are expressed have been used to study the functions of WT Cx proteins and the mechanisms of disease associated with specific Cx mutations. However it is important to remember that differences exist between humans and mice. For example, creating a mouse with a double knockout out of WT Cx26 led to embryonic lethality approximately 11 days post coitum, which the authors suggested was due to an inability to grow properly resulting from the defective uptake of glucose[50]. However in humans the loss of both Cx26 alleles only causes deafness, thus suggesting that Cx proteins may have different functions between the two species[2].

1.1.10 Mutations in Cx26

Cx26 mutations cause disease in a tissue specific fashion[2]. Recessive mutations in Cx26 cause non syndromic hearing loss (NSHL) in which only hearing is affected. Some dominant mutations in Cx26 solely cause NSHL, whereas others are linked to syndromic diseases. In addition to deafness, patients also present with cutaneous involvement. Mutations causing NSHL span the entire Cx26 coding region, but those that cause syndromic disease tend to be concentrated within the N-terminus and extracellular loop 1[51]. Many Cx26 NSHL mutations are small insertions or deletions, or nonsense mutations where an amino acid is substituted with a stop codon. Cx26 syndromic mutations result from a single missense mutation, which results in the substitution of a different amino acid, and production of full length, mutated Cx26[51].

1.1.11 Structure of the ear and deafness

The mammalian ear is composed of the outer, middle and inner ear (figure 1.1.7). Sound waves are collected by the pinna and then channelled down the auditory canal of the outer ear onto the tympanic membrane (ear drum). The middle ear contains three ossicles (bones) which conduct vibrations of the tympanic membrane to the cochlear located within the inner ear[52]. The cochlear comprises three fluid filled tubular compartments: the scala media which contains endolymph and the scala tympani and scala vestibule which contain perilymph[52-54]. Endolymph is highly concentrated with K^+ and has an electrical potential of +80 mV[53,54]. Vibrations of the ossicles causes endolymphatic K^+ to enter the hair cells of the organ of Corti and leads to their depolarisation[53,54]. K^+ then circulates to the perilymph before returning to the endolymph[53,54]. Nerve impulses are subsequently transmitted to the brain via the cochlear nerve for interpretation.

Two types of hearing impairment exist. Conductive hearing loss occurs when abnormalities of the outer ear, tympanic membrane or ossicles prevent sound travelling to the inner ear. Sensorineural hearing loss manifests itself when the

inner ear or components of the brain involved in sound interpretation are dysfunctional.

Figure 1.1.7: Structure of the ear and movement of K^+ in response to sound

a

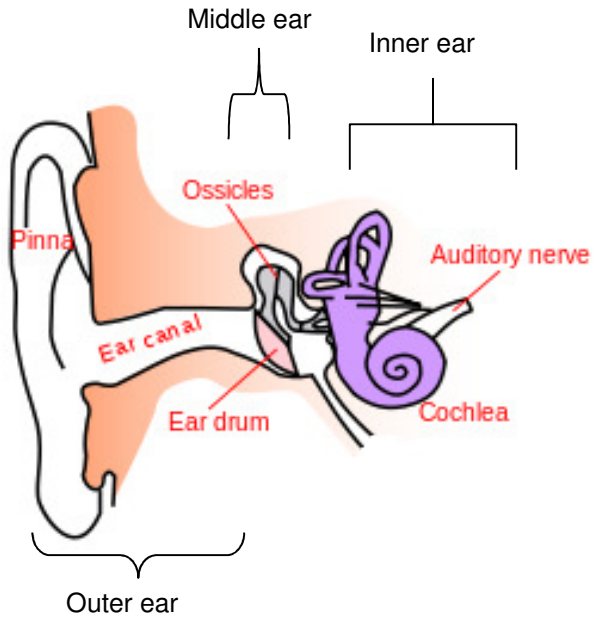

Sound vibrations captured by pinna are channelled down the ear canal onto the ear drum. Vibrations of the ear drum are conducted by the three ossicles to the cochlear.

b

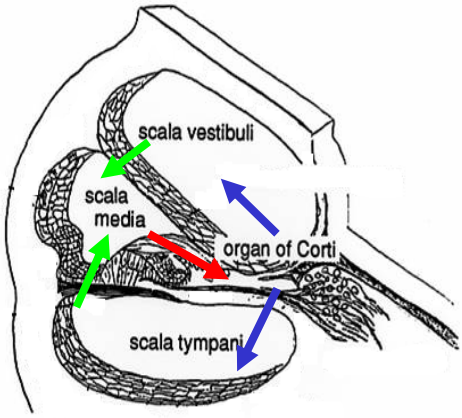

In response to sound endolymphatic K^+ in the scala media enters the hair cells of the Organ of Corti (red arrow), circulates to the perilymph in the scala vestibuli and scala tympani (blue arrows) and then returns to the endolymph in the scala media (green arrows).

(Image modified from http://www.d.umn.edu/~jfitzake/Lectures/UndergradPharmacy/SensoryPhysiology/Audition/CochleaStructure.html)

1.1.11.1 Cx expression in the ear

Several Cx proteins, including Cx26, Cx30, Cx31 and Cx32 have been detected within the epithelia and connective tissue of the rodent cochlea demonstrating a requirement for Cx mediated GJIC in hearing[53]. Mutations in various Cxs including Cx26, Cx30 and Cx31 cause deafness[53]. The expression of other

functional Cx proteins is not sufficient to prevent the development of deafness resulting from mutations. This suggests that all the Cx proteins expressed in the ear are required for hearing, with each having specific, slightly different functions within the ear.

It has been proposed that GJs present in the cochlear mediate K^+ recycling to ensure that the high concentration of K^+ required for transmitting the auditory signal is maintained in the endolymph[2]. GJs may also be important for the maintenance of cells within the organ of Corti. Conditionally knocking out Cx26 in cochlear epithelial tissue of mice results in the death of epithelial support cells at postnatal day 14, which subsequently extends to hair cells[55], thus demonstrating that Cx26 mediated GJIC is required for the survival of cells within the cochlear.

1.1.12 Structure of the skin

The skin forms a protective barrier between the body and the external environment, which provides protection against invading pathogens and prevents excessive water and solute loss[56]. The skin also functions to regulate body temperature, acts as a sensory organ and as a storage organ for lipids and water.

The skin is composed of three main layers, the epidermis, dermis and hypodermis (figure 1.1.8). The epidermis is the outermost layer of the skin and will be discussed in detail in section 1.1.12.1. The dermis lies below the epidermis. The epidermis and dermis are separated by the basement membrane, which primarily functions to connect the two layers. The hypodermis is the deepest layer of the skin and is found beneath the dermis.

The dermis consists of connective tissue[57]. It has an extracellular matrix (ECM) composed of collagen and elastin fibres which are synthesised by fibroblasts[57]. The structure of the ECM provides the skin with structural support, extensibility (ability to be stretched) and elasticity (ability to return to its original form). The dermis contains mechanoreceptors which are sensitive to touch and heat, hair follicles, sebaceous (sweat) glands, lymphatic vessels and blood vessels. The blood vessels function to transport nutrients to and remove waste products from

cells within the epidermis and the dermis. The dermis can be divided into two layers, with the papillary layer being more superficial to the reticular layer[57]. It contains dermal papillae which are finger-like projections which extend into the epidermis to provide improved strength to the connection between the epidermis and the dermis[57]. The deeper reticular layer is usually much thicker than the papillary layer and contains the majority of the elastin and collagen fibres [57].

The hypodermis contains nerves, blood vessels and adipocytes which store fat[58], thus meaning that the hypodermis acts as an energy reserve and an insulating layer. The hypodermis also functions to connect the skin to the underlying bone and muscle[58].

Figure 1.1.8: Structure of the skin and localisation of Cx proteins in the epidermis.

a

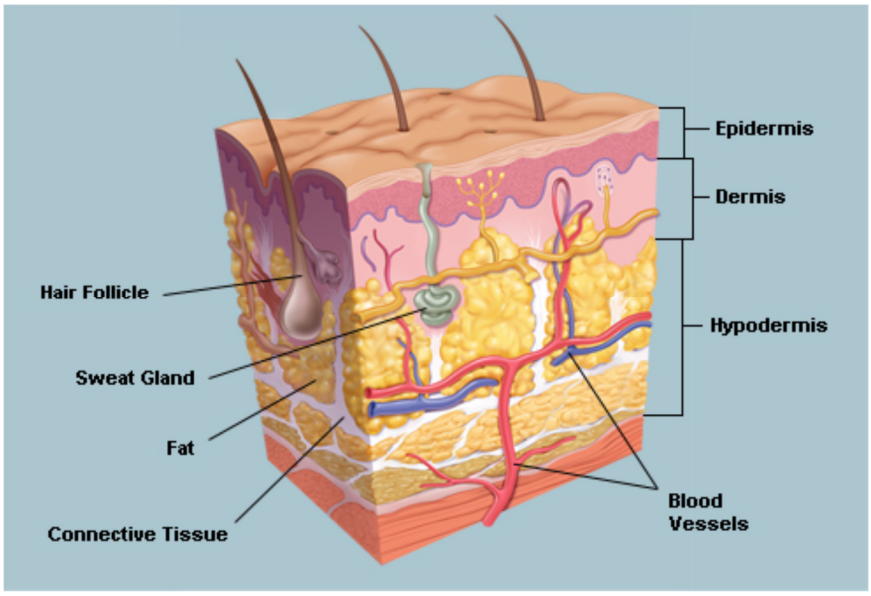

b

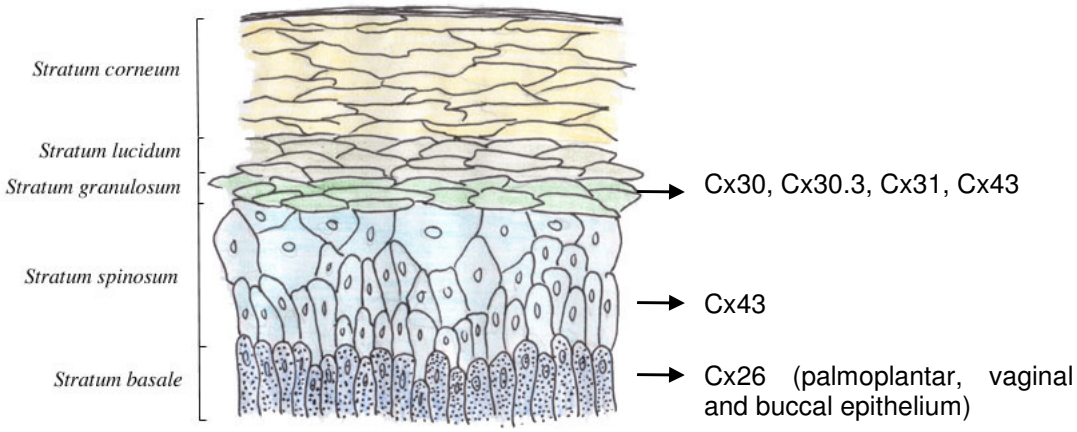

(Images taken from http://www.webmd.com/skin-problems-and-treatments/picture-of-the-skin (a) and http://www.standardofcare.com/mwiki/index.php?title=Epidermis&redirect=no&printable=yes (b))

1.1.12.1 Epidermis

The epidermis is a stratified epithelium, which means that it is two or more cells thick[59]. This is in contrast to simple epithelia, such as intestinal epithelium, which is only one cell thick[59]. 95% of the cells in the epidermis are keratinocytes. In addition to acting as first line defence and forming a barrier

preventing pathogens from entering the body, keratinocytes also play an important role in the stimulation of immune responses. They express pattern recognition receptors including toll-like receptors (TLRs) and nucleotide-binding oligomerisation domain (NOD) receptors which recognise conserved sequences expressed by pathogens, leading to the production of proinflammatory and chemotactic signals. Keratinocytes also secrete peptides including cathelicidins and defensins which display antimicrobial activity towards invading pathogens, in turn contributing towards their elimination.

The epidermis is formed and continuously regenerated by terminally differentiating keratinocytes by the process of cornification (also termed terminal differentiation or keratinisation)[60]. It is composed of five layers which will be discussed below.

The basal layer *(Stratum basale)* is the deepest layer of the epidermis (figure 1.1.8) and the only layer to contain proliferating cells, which give rise to keratinocytes[60]. Keratinocytes are anchored to the basement membrane by hemidesmosomes. Basal keratinocytes express the structural components keratin 5 and keratin 14, which assemble into keratin intermediate filaments[60]. Intermediate filaments, along with microtubules composed of tubulin, and microfilaments composed of actin form the cytoskeleton of epithelial cells[60]. The basal layer of the epidermis also contains melanocytes which produce melanin pigment which confers resistance to UV light, and Merkel cells which are involved in light touch sensation[60].

The spinous layer *(Stratum spinosum)* of the epidermis is above the basal layer (figure 1.1.8). Keratinocytes which have lost their mitotic potential migrate from the basal layer into the spinous layer and are connected to each other by desmosomes[60]. Desmosomes are intracellular junctions which link cell surface adhesion proteins to the actin cytoskeleton, and which connect neighbouring cells to each other. The structure of a desmosome is shown in figure 1.1.9. Desmosomes contain desmoglein and desmocollin, which are transmembrane proteins belonging to the cadherin family of proteins[61]. In humans three desmocollins and four desmogleins have been described[61]. The interactions between the extracellular domains of desmoglein and desmocollin connect two keratinocytes[61]. The cytoplasmic side of the desmosome consists of an outer

denser plaque (ODP) and an inner denser plaque (IDP) spanned by the desmoplakin protein[61]. At the ODP the cytoplasmic domains of desmocollin and desmoglein attach to desmoplakin via plakoglobin and plakophillin, while at the IDP desmoplakin attaches to the keratin intermediate filaments of the keratinocyte[61].

Figure 1.1.9: Structure of a desmosome. Keratinocytes are connected by interactions between desmoglein (Dsg) and desmocollin (Dsc). At the cytoplasmic face the outer denser plaque (ODP) and the inner denser plaque (IDP) are spanned by desmoplakin (DP). At the ODP DP attaches to Dsg and Dsc via plakoglobin (PG) and plakophillin (PP). At the IDP DP attaches to keratin intermediate filaments (IF) of the cell cytoskeleton.

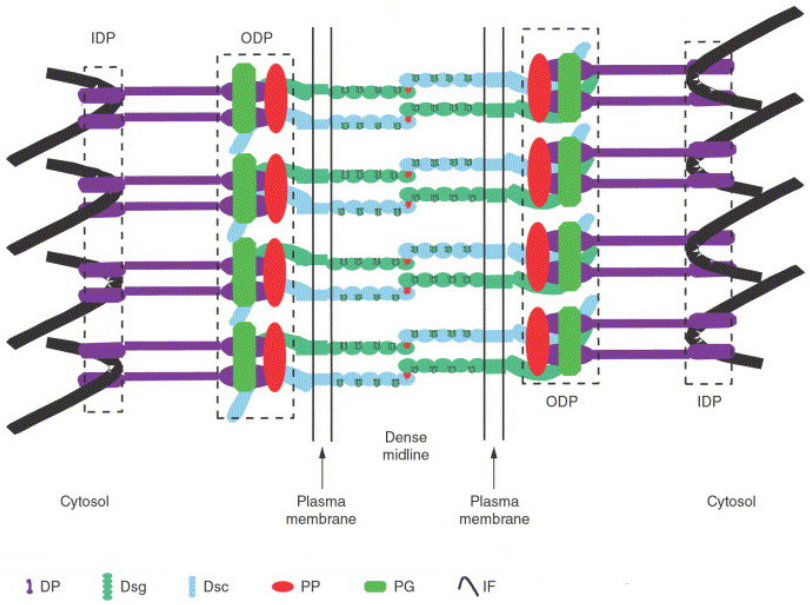

(Image modified from[62])

In the spinous layer of the epidermis keratinocytes begin to differentiate and express keratin 1 and keratin 10 which replace the expression of keratin 5 and keratin 14[60]. The spinous layer also contains Langerhan cells, which are a component of the immune system that function as antigen presenting cells[60]. They continuously monitor the environment for danger signals, and when activated they migrate to the regional lymph nodes and present antigen to T cells, which in turn stimulates the adaptive immune response[63].

The granular layer *(Stratum granulosum)* of the epidermis is above the spinous layer (figure 1.1.8). Keratinocytes migrate from the spinous layer upwards to the granular layer[60]. Within the granular layer the cornified envelope (CE) protein fillagrin is produced following cleavage of its precursor pro-fillagrin[60]. Fillagrin

forms aggregates with tightly packed keratin filaments and leads to their flattening[60].

The transitional layer *(Stratum lucidium)* is located above the granular layer (figure 1.1.8). This layer is normally absent from thin epithelium, and is usually only present in thick epithelium, including the palms and soles.

The CE (*Stratum corneum*) is the outer layer of the epidermis (figure 1.1.8) and is the product of the cornification process which produces dead corneocytes from terminally differentiated keratinocytes[60]. When keratinocytes are permeabilised by Ca^{2+}, trans-glutaminases are activated which mediate the cross linking of CE proteins including loricrin, involucrin and small proline-rich proteins. CE proteins are synthesised and deposited under the plasma membrane in the granular layer[60]. As keratinocytes migrate upwards from the granular layer, lipids are released from their lamellar bodies, which are cross linked onto the preassembled CE proteins by transglutaminases[60]. Also during the cornification process, organelles within the keratinocytes including the nucleus are destroyed[60]. The cornified layer is continuously renewed by cells migrating up through the inner layers and subsequently being sloughed off the top of the epidermis by desquamation[60].

1.1.12.2 Cx expression in the skin

In human and rodent epithelia, GJs exist in the basal, spinous and granular layers, but not the cornified layers[2] (figure 1.1.8). Cx expression within the epidermis undergoes spatial and temporal regulation[19] which leads to a distinct expression pattern of specific Cx proteins at different layers within the epidermis[2]. For example, whereas Cx43 expression is present throughout the suprabasal epidermal layers of interfollicular skin[19], albeit with highest expression being detected in the granular layer[64,65]; Cx30.3 and Cx31 expression appears to be restricted specifically to the granular layer[66]. It has thus been suggested that Cx proteins are differentially expressed because they might be required for specific stages of keratinocyte differentiation[2]. Cx26 is only detected in the sweat glands and hair follicles of the normal interfollicular epidermis[66], but is expressed by normal vaginal and buccal epithelium[67]. Cx26

expression has also been found in the basal and granular layers of palmoplantar epithelium[67], and within damaged and diseased epithelium[66]. Thus Cx26 may have a role during keratinocyte differentiation in normal vaginal and buccal epithelium, within hyperproliferative epithelium and during wound healing.

1.1.12.3 Cx26 expression and wound healing

Various studies have suggested a requirement for Cx26 expression during wound healing. A hypothesis is that Cx26 may facilitate keratinocyte proliferation, differentiation and migration into the wound site[2,68]. The exact localisation of Cx26 expression within the epidermis has shown some variation depending on the species used in the wound healing studies[68]. For example, Cx26 is upregulated behind the leading edge of the wound in both rats[69] and mice[70], but increased Cx26 expression in the leading edge of the wound only occurs in mice[70,69]. Moreover tape stripping of human skin also results in the upregulation of Cx26 expression throughout the epidermis[67]. Interestingly deregulated Cx26 expression has been shown to be detrimental for wound healing resolution[68]. For example, in mice persistent expression of Cx26 in the epidermis results in hyperproliferation of keratinocytes and prevents wound remodelling[71]. Furthermore in humans, psoriasis is associated with keratinocyte hyperproliferation, and upregulated Cx26 expression has been observed in psoriatic lesions compared to normal skin[72]. Taken together these findings suggest that the early stages of wound healing require Cx26, but the process may be compromised by abnormal expression of Cx26 during the later stages[68].

1.1.13 Mechanism of Cx26 mutations in human disease

Although the mechanisms by which Cx26 mutations cause disease are poorly understood, analysis of different Cx26 mutants *in vitro* has identified four possible ways Cx26 mutations might affect the function of GJs.

Some Cx26 mutations, particularly many of those associated with NSHL are loss of function (LOF) mutations which prevent the formation of functional GJs

at the cell surface. Consequently these mutations may lead to a disruption in K^+ recycling[2], and the death of cells within the cochlear which could lead to deafness. Mutants may not traffic correctly to the cell surface, or if they successfully reach the cell surface, may not be incorporated into the appropriate homotypic/heterotypic GJ required for normal function in healthy tissue[2]. Many Cx26 NSHL mutations including the most frequent recessive c.35delG mutation, lead to a premature termination of protein translation[73]. The c.35delG mutation leads to the deletion of a guanine at position 35, resulting in the introduction of a stop codon after residue 13[74]. The early termination of protein translation truncates the Cx26 protein, and when HeLa cells are transfected with the c.35delG mutant *in vitro,* GJ do not form[75].

Some mutations mistraffic and may accumulate in the cytoplasm or organelles[2]. For example, immunofluorescence revealed that the p.R143W NSHL mutation accumulates in the cytoplasm of transfected HeLa cells rather than trafficking to the GJ[45]. Accumulation of Cx26 mutations has also been observed in the Golgi apparatus, for example in the trans-*Golgi* network by the p.D66H mutant[76].

Other mutations may act in a dominant negative fashion affecting the function of WT Cx26[2]. For example, coexpression of the p.R75W mutation with WT Cx26 in *Xenopus* oocytes, suppresses the electrical activity of WT Cx26[77]. Furthermore such mutations may affect the function of a different Cx protein expressed within the cell. For example, expression of certain Cx26 mutations which cause skin disease in *Xenopus* oocytes, suppresses the activity of coexpressed WT Cx43[78]. Moreover, the Cx26-D66H mouse which mimics Vohwinkel syndrome (VS), in which p.D66H is expressed in the suprabasal epidermal layers, exhibits defective transport of WT Cx26 and Cx30 to the cell surface[79]. When mutant Cx proteins act in a dominant negative fashion, the type of hemichannel which can form GJs may be altered. This potentially alters the specific properties of the GJ including its permeability, which could influence GJIC between cells and possibly contribute to the development of disease[19]. Many of the dominant Cx26 mutations associated with palmoplantar keratoderma (PPK) with deafness, Bart-Pumphrey syndrome (BPS) and VS are thought to act in a dominant negative fashion[51].

Other mutations, particularly those associated with Keratitis–ichthyosis deafness (KID) syndrome and Hystrix-like ichthyosis deafness (HID) syndrome may traffic to the cell surface but induce aberrant hemichannel activity[51,19]. For example, expression of the p.A40V mutation in *Xenopus oocytes* results in the production of membrane currents which are absent in oocytes expressing WT Cx26[80]. Such activity of unpaired hemichannels could result in the deregulated release of molecules into the extracellular environment, which could induce cell death and alter the behaviour of neighbouring cells[2,19].

1.1.14 Mutations in Cx26 linked to NSHL

Approximately one in one thousand individuals is affected with deafness at birth or in early childhood[81]. Hereditary NSHL is classified as autosomal dominant, (DFNA – Deafness, Autosomal Dominant), autosomal recessive (DFNB – Deafness, Neurosensory Autosomal Recessive) or X-linked (DFNX – Deafness, X Linked) and more than 100 genetic loci have been linked to deafness[81]. 80% of hereditary NSHL cases arise from recessive mutations[82] and between 30-60% of these cases are attributed to mutations in Cx26[83]. Dominant mutations in Cx26 have also been linked to NSHL[73].

1.1.14.1 Recessive mutations in Cx26 linked to NSHL

DFNB NSHL was first linked to a locus on chromosome 13q11, which was termed DFNB1 by homozygosity mapping in two consanguineous Tunisian families[84]. Subsequently a locus identified in a French family affected by dominant deafness, which was termed DFNA3, was linked to the same region of the chromosome, 13q12[85]. The *GJB2* gene localises to this area of the chromosome, which led to the hypothesis that mutations in Cx26 were responsible for both deafness forms[81]. Screening the *GJB2* gene in three consanguineous Pakistani families affected by recessive deafness identified the two nonsense mutations p.W24X and p.W77X[86]. In a separate study the size of the DNB1 locus was reduced and found to include the *GJB2* gene, and subsequently, screening *GJB2* identified the most frequent recessive c.35delG mutation[74]. This mutation leads to the deletion of a guanine at position 35,

which results in the introduction of a stop codon after residue 13[74]. The early termination of protein translation truncates the Cx26 protein, and not surprisingly, when HeLa cells are transfected with the c.35delG mutant *in vitro,* GJs do not form[75]. The p.W24X, p.W77X and c.35delG mutations were some of the first recessive Cx26 mutations linked to NSHL.

GJB2 was also screened in a family with palmoplantar keratoderma (PPK) and deafness[86]. Although none of the mutations showed linkage to PPK, the p.M34T mutation was identified in individuals with deafness and originally reported as a dominant mutation[86]. However, further analysis of the family showed that deafness only manifest in individuals when a dominant Cx26 mutant, p.D66H was also present[87]. Other studies reported that the p.M34T mutation was present in individuals with normal hearing, and consequently p.M34T was reclassified as a recessive Cx26 NSHL mutation[88].

To date, more than ninety recessive Cx26 NSHL mutations have been identified and the full list can be found on the Connexin-deafness homepage (http://davinci.crg.es/deafness). The Cx26 NSHL mutations most relevant to the background and experiments for this work are detailed in table 1.1.1 and their location within the Cx26 protein in shown in figure 1.1.9 a.

Table 1.1.1: Recessive mutations in Cx26 associated with NSHL

TM= transmembrane domain, EL=extracellular loop, NT=N terminal, fx=framshift

Nucleotide change	Amino acid	Protein domain	Ref
c.71G>A	p.W24X	TM1	86
c.231G>A	p.W77X	TM2	86
c.101T>C	p.M34T	TM1	88
c.35delG	p.G12fx	NT	74
c.427C>T	p.R143W	TM3	89
c.235delC	p.L78fx	TM2	90
c.167delT	p.L81fx	EL2	74

1.1.14.2 Dominant mutations in Cx26 linked to NSHL

The first mutation in Cx26 linked to the DFNA3 locus (dominant NSHL) was p.W44C[91]. Although the p.R75W mutation was linked to PPK and deafness in an Egyptian family, it was also identified in a control subject with no skin

disease[77]. This suggested that the p.R75W mutation could solely cause dominant NSHL hearing loss, without necessarily causing syndromic disease. The dominant mutations in Cx26 associated with NSHL discovered to date[82] are listed in table 1.1.2 and their location within the Cx26 protein in shown in figure 1.1.9 b.

Table 1.1.2: Dominant mutations in Cx26 associated with NSHL

EL=extracellular loop, TM= transmembrane domain

Nucleotide change	Amino acid	Protein domain	Ref
c.131G>C	p.W44S	EL1	82
c.132G>C	p.W44C	EL1	91
c.223C>T	p.R75W	EL1	77
c.428G>A	p.R143Q	TM3	92
c.487A>C	p.M163L	EL2	93
c.534G>A	p.D179W	EL2	94
c.551G>A	p.R184Q	EL2	95
c.605G>T	p.C202F	TM4	96
c.125delAGG	p.del42E	EL1	78

1.1.15 Syndromic diseases associated with Cx26 mutations

Syndromic diseases are caused by dominant Cx26 mutations. In addition to deafness such mutations also cause ectodermal dysfunction and skin disorders[51]. Diseases include Vohwinkel syndrome (VS), Bart-Pumphrey syndrome (BPS), Palmoplantar keratoderma (PPK) with deafness, Keratitis–ichthyosis deafness (KID) syndrome and Hystrix-like ichthyosis deafness (HID) syndrome. The symptoms of these diseases are described in table 1.1.3, the Cx26 mutations listed in table 1.1.4 and the location of the mutations within the Cx26 protein are shown in figure 1.1.9 c.

Table 1.1.3: Symptoms of syndromic diseases caused by dominant mutations in Cx26

Disease	Symptoms
VS [51]	• Sensorineural deafness • Palmoplantar hyperkeratosis (thickening of the *stratum corneum* of the palms and soles) • Pseudoainhum (constrictions of the circumference of the fingers and toes) • Pseudoainhum can lead to autoamputation (spontaneous detachment) of the fingers and toes
BPS [51]	• Palmoplantar hyperkeratosis • Sensorineural deafness • Hyperkeratosis of the metacarpophalangeal and interphalangeal joints of the hand, termed as knuckle pads • Leukonychia (whitening, thickening and crumbling of the nails)
PPK with deafness [51]	• Palmoplantar hyperkeratosis • Sensorineural hearing loss, a form less severe than results from other syndromic Cx26 mutations
KID syndrome [51]	• Mild to severe sensorineural hearing loss • Loss of eyebrows and eyelashes • Mild to severe keratitis (inflammation of the cornea) • Keratitis may eventually lead to blindness • Skin lesions may be present all over the body of patients and are usually accompanied by ichthyosis (scaling of the skin) • Skin lesions and ichthyosis lead to an increased susceptibility to bacterial, viral and fungal infections. • Increased probability of developing carcinomas
HID like syndrome [51]	• Excluding keratosis, HID syndrome presents with similar symptoms to KID syndrome • Skin of HID syndrome patients is characterised by the presence of spiky hyperkeratotic masses with a cobblestone-like appearance all over the body

Table 1.1.4: Dominant mutations in Cx26 associated with syndromic diseases

VS=Vohwinkel syndrome, BPS=Bart Pumphrey syndrome, PPK=palmoplantar keratoderma, KID=keratitis-ichthyosis-deafness syndrome, HID=hystrix-like-ichthyosis-deafness syndrome EL=extracellular loop, CL=cytoplasmic loop, CT=C terminus, NT= N terminus

Disease	Nucleotide change	Amino acid	Protein domain	Ref
VS	c.175G>A	p.G59S	EL1	97
	c.196G>C	p. D66H C	EL1	98
	c.389G>T	p.G130V	CL	99
BPS	c.162C>A	p.N54K	EL1	100
	c.175G>A	p.G59S	EL1	101
PPK with deafness	c.160A>C	p.N54H	EL1	102
	c.176C>G	p.G59A	EL1	103
	c.175G>C	p.G59R	EL1	104
	c.219A>G	p.H73R	EL1	105
	c.224G>A	p.R75Q	EL1	106
	c.389G>T	p.G130V	CL	107
	c.458C>T	p.S183F	EL2	108
	c.223C>T	p.R75W	EL1	77
	c.125delAGG	p.del42E	EL1	78
KID syndrome	c.34G>C	p.G12R	CT	109
	c.40A>C	p.N14Y	NT	110
	c.50C>T	p.S17F	CT	109
	c.119C>T	p.A40V	EL1	80
	c.134G>A	p.G45E	EL1	111
	c.148G>A	p.D50N	EL1	109
	c.148G>T	p.D50Y	EL1	112
HID like syndrome	c.148G>T	p.D50Y	EL1	113

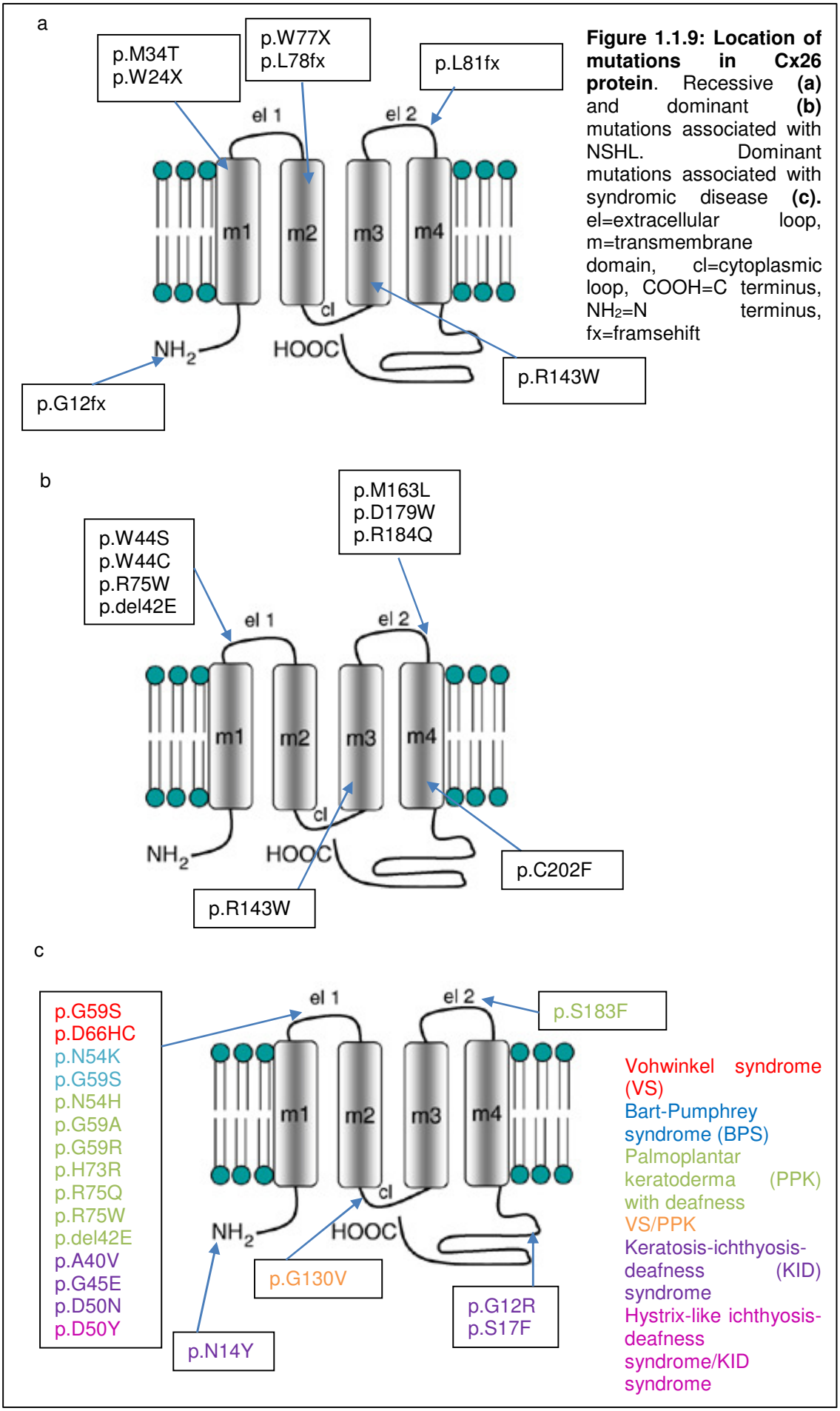

Figure 1.1.9: Location of mutations in Cx26 protein. Recessive **(a)** and dominant **(b)** mutations associated with NSHL. Dominant mutations associated with syndromic disease **(c).** el=extracellular loop, m=transmembrane domain, cl=cytoplasmic loop, COOH=C terminus, NH_2=N terminus, fx=framsehift

The same mutation within Cx26 can give rise to different diseases. For example the p.G59S mutation is associated with VS[97] and BPS[101], while the p.D50Y mutation is linked to KID[112] and HID-like[113] syndromes. This demonstrates that some of the symptoms associated with specific disease differ, but there is also overlap in the clinical presentation of the diseases[51]. The emerging view is that there are two broad groups of diseases associated with syndromic Cx26 mutations, the VS-BPS-PPK group and the KID-HID group[51].

1.1.16 Potential heterozygote advantage linked to recessive NSHL Cx26 mutations

With a few exceptions most of the recessive Cx26 NSHL mutations described are only found in a few individuals[82]. However specific Cx26 NSHL mutations are more prevalent in certain geographic locations or ethnic groups. For example, the c.35delG mutation is responsible for 20% of childhood hereditary hearing loss in European descendants[114] with carrier frequencies ranging from 1/35 in southern Europe to 1/79 in central and northern Europe[115]. The c.235delC mutation has a carrier frequency of 2% in Japanese populations, and of 70 mutant *GJB2* alleles screened in deaf Japanese individuals, 10 were c.235delC[116]. In Ghana the p.R143W mutation is the most prevalent recessive Cx26 NSHL mutation, and of 121 mutant *GJB2* alleles screened in unrelated deaf individuals, 110 were p.R143W[95]. Additionally the p.167delT mutation has been reported to have a carrier frequency of 4% in Ashkenazi Jews[117].

It has been hypothesised that high carrier frequencies of specific Cx26 NSHL mutations exist because they confer a heterozygote advantage to carriers[45,118-120]. Heterozygous advantage exists when a heterozygous individual who carries one wild type copy and one mutated copy of a gene, has an advantage over a homozygous individual who carries two wild type copies of a gene. For example, sickle cell anaemia is a recessively inherited condition where red blood cells develop abnormally. In Africa the occurrence of individuals who are heterozygous for the sickle gene (AS) is relatively common, and it has been shown that these individuals are better protected from death with *Plasmodium falciparum* malaria[121]. The red bloods cells of healthy individuals are disc-shaped and flow easily in the bloodstream, whereas those of sickle cell patients

are crescent shaped and block the flow of blood. When sickle cell anaemia patients are exposed to low O_2 conditions, their red blood cells undergo sickling and removal by phagocytosis. AS heterozygotes produce normal and abnormal haemoglobin which means that some of their red blood cells will also undergo sickling. Invasion of red blood cells by *P. falciparum* causes decreases in the intracellular pH and O_2 concentration[121]. This causes the red blood cells to sickle, which in turn leads to their phagocytosis and removal from the blood stream[121]. This occurs preferentially in AS heterozygotes compared to healthy individuals, meaning they have a reduced number of parasites circulating within the bloodstream[121].

Another example of heterozygous advantage is where cystic fibrosis patients who carry a mutated copy of the cystic fibrosis transmembrane conductance regulator gene (CFTR) have improved protection against infection with *Vibrio cholerae*, the causative agent of cholera[122]. The cholera toxin induces cAMP mediated Cl^- secretion via CFTR channels from enterocytes into the intestinal lumen, which in turn acts to drive Na^+ and water movement out of the cell[122]. Individuals heterozygous for the CFTR gene have reduced diarrhoea production compared to healthy individuals. CFTR heterozygotes also have improved protection against *Salmonella typhi*, the causative agent of typhoid[123]. *S. typhi* utilises the CFTR protein to translocate into intestinal epithelial cells, meaning that bacterial uptake is significantly reduced into cells expressing CFTR mutants compared to WT CFTR[123].

The examples described above represent instances of when having one wild type and one mutated copy of a gene may be more beneficial than two wild type copies. Carrying the mutation confers a protective advantage by reducing susceptibility to infection. If carrying a Cx26 NSHL mutation conferred a heterozygote advantage, it could account for the high carrier frequencies of specific Cx26 NSHL mutations within certain geographic locations or ethnic groups[45,118-120].

1.1.16.1 Recessive NSHL Cx26 mutations linked to epidermal thickness

Interestingly, although Cx26 NSHL mutations do not cause skin disease, expression of the p.143W and c.35delG mutations is linked to a thicker epidermis (figure 1.1.10). Measurements of the epidermal thickness of skin sections taken from biopsies of heterozygote carriers of the p.R143W allele and p.R143W Cx26 homozygotes, revealed that the epidermis was significantly thicker compared to WT Cx26 homozygotes[120]. When the epidermal thickness of carriers of the c.35delG allele was measured by sonography and compared to WT Cx26 homozygotes it was found to be twice as thick[118]. The epidermis of organotypic cultures grown with keratinocytes was also significantly thicker when the pR143W mutation was expressed[4]. Organotypic models of the skin provide a three-dimensional model in which the skin can be studied *in vitro.* They mimic more accurately what happens during keratinocyte growth and differentiation *in vivo* than cell monolayers. The technique involves growing keratinocytes on de-epidermalised dermis (DED) until they form an epidermis. The thicker epidermis associated with p.143W expression did not result from increased cell proliferation, since there was no difference in expression of the proliferation marker Ki67 in organotypic cultures expressing p.R143W or WT Cx26[45]. Staining for the epidermal differentiation marker Keratin 14 was restricted to the basal layer of organotypic cultures expressing WT Cx26, but was detected in both the basal and suprabasal epidermal layers in organotypic cultures expressing p.R143W[45]. The authors suggested this was indicative of keratinocytes undergoing an extended terminal differentiation program which in turn may produce a thicker epidermis[45]. The thicker epidermis that is associated with heterozygote carriers of the p.R143W allele could also result from increased cell viability as keratinocytes transfected with p.R143W exhibited significantly reduced cell death compared to keratinocytes expressing WT Cx26[119]. It has been suggested that a thicker epidermis could be beneficial to carriers, if it acts as a more robust barrier, which in turn provides improved barrier against infection and trauma[118,120].

Figure 1.1.10: Epidermal thickness of p.R143W and c.35delG heterozygotes. Measurements of biopsies taken from WT Cx26 homozygotes, heterozygous carriers of the p.R143W allele and p.R143W Cx26 homozygotes **(a)** and epidermal thickness of WT Cx26 homozygotes and heterozygous carriers of the c.35delG allele **(b).** Heterozygous carriers of p.R143W and c.35delG have a si\gnificantly thicker epidermis than WT Cx26 homozygotes.

a

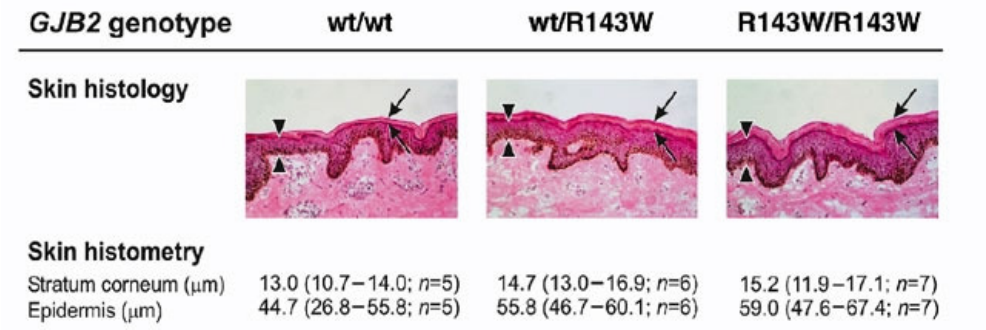

b Epidermal thickness (mm)

	wt/wt	wt/c.35delG
Females	0.38	0.81
Males	0.42	0.93

(Images obtained from[118,120])

1.1.17 Cx protein expression linked to gastrointestinal bacterial infection

Recent evidence has indicated a role for intercellular communication mediated by Cx26 during *Shigella flexneri* infection, the causative agent of bacillary dysentery. Cx43 has also been implicated in mice during infection with the attaching and effacing pathogen *Citrobacter rodentium. C. rodentium* is the *in vivo* model used to study human Enteropathogenic *Escherichia coli* (EPEC) and Enterohemorrhagic *Escherichia coli* (EHEC) infection. *Shigella* and EPEC will be discussed in detail in sections 1.1.18-22.

1.1.18 *Shigella*

The gastrointestinal pathogens *Shigella* and EPEC are gram negative bacteria belonging to the family *Enterobacteriaceae. Shigella* is the causative agent of bacillary dysentery or shigellosis. Shigellosis presents with symptoms ranging from watery diarrhoea to dysentery. Dysentery is diarrhoea which contains

blood and mucus within the faeces, and is accompanied by fever and abdominal cramps[124]. Complications may arise from shigellosis which can lead to death, particularly in toddlers and young children[124]. These include hypoglycaemia (when the concentration of blood glucose has fallen below 70 mg/dlL[125]), bacteraemia (viable bacteria are present within the circulating blood) and septicaemia (an infection caused by bacteraemia). Severe dehydration results from fever and diarrhoea and can lead to problems[124] including hypovolemia (a decreased volume of circulating blood), haemolytic uraemic syndrome (haemolytic anaemia (anaemia resulting from the destruction of red blood cells) and uraemia (accumulation of urea in the blood)) and toxic megacolon (dilation of the colon leading to its obstruction[126]).

Four species of *Shigella* have been identified which are *S. flexneri, S. sonnei, S. dysenteriae* and *S. boydii*. With the exception of *S. sonnei,* the other three serogroups are further subcategorised into specific serotypes. This classification is based on the carbohydrate composition of the O-antigenic polysaccharide chain of the Lipopolysaccharide (LPS) surface antigen[124]. *Shigella* is a highly invasive bacterium, and as few as ten to one hundred bacteria are sufficient to establish disease in humans[127]. Shigellosis therefore represents an important issue for public health. Although Shigellosis occurs worldwide, it is significantly more prevalent in developing countries. Of an estimated 164.7 million annual cases of Shigellosis, only 1.5 million cases were observed in developed countries, while 163.2 million cases, with 1.1 million deaths, were identified in developing countries[128]. Shigellosis in developing countries tends to be associated with infection with *S. flexneri* and *S. dysenteriae*, while *S. sonnei* is responsible for many cases in developed countries. Whereas shigellosis endemics tend to be caused by *S. flexneri* and *S. sonnei,* shigellosis epidemics and pandemics are usually associated with *S. dysenteriae* type I[124]. Shigellosis is associated with poor hygiene and can be transmitted directly by the faecal-oral route, where bacteria in the faeces of an infected individual are ingested by a non-infected individual, or indirectly through the ingestion of contaminated food or water[124]. Shigellosis thus affects individuals who exhibit poor levels of hygiene, and therefore is most predominant in young children. 69% of shigellosis cases and 61% of deaths associated with shigellosis occur in children under the age of five years old[128].

1.1.19 Enteropathogenic *Escherichia coli* (EPEC)

Escherichica coli (E. coli) is the most abundant non-pathogenic organism of the mammalian colon microflora[129] and represents the most common cause of diarrhoea worldwide[130]. Certain strains of *E. coli* have acquired virulence factors making them pathogenic[129,131] such as Enteropathogenic *E .coli* (EPEC) and Enterohemorrhagic *E. coli* (EHEC), which are human pathogens belonging to the attaching and effacing lesion forming family of bacteria. EHEC produces Shiga toxins which enable the bacteria to cause haemorrhagic colitis which can progress to haemolytic uraemic syndrome[132]. EPEC induces watery diarrhoea, which may be accompanied by low grade fever, nausea and vomiting, and is also a major cause of acute gastroenteritis (inflammation of the gastrointestinal tract). EPEC can be divided into typical and atypical strains, which will be discussed in section 1.1.22.1. Typical EPEC is a leading cause of diarrheal disease and dehydration associated deaths in infants aged between six months and two years of ages in developing countries, where it is associated with a mortality rate of 10-40%[131,133]. Atypical EPEC is more common than typical EPEC in developed countries, and causes disease in a broader age group[134]. EPEC can be transmitted by the faecal-oral route or through contact with an infected individual.

Shigella and EPEC infections are treated with oral rehydration in combination with antibiotics. Although antibiotic courses have proved useful for the treatment of many cases of diarrhoea, one of the major problems is the emergence of multiple antibiotic resistance[124,130]. Current therapies are not sufficient to eradicate the problems associated with gastrointestinal pathogens, and as diarrhoea represents a leading cause of death in developing countries, there is an urgent need to find new treatments for gastrointestinal bacterial infection.

1.1.20 Type III secretion system

The ability of *Shigella* and EPEC to establish an infection is mediated by a type III secretion system, which is inserted into the host cell plasma membrane[135]. It is used to deliver bacterial proteins, which are termed effectors, from the

cytoplasm of the bacteria into the host cell cytoplasm, where they can manipulate host cell functions and contribute to the establishment of disease[135].

1.1.20.1 Shigella secretion apparatus

The genes encoding components of the *Shigella* secretion apparatus localise to a 31 kb region, termed the entry region, of a 213 kb virulence plasmid[124,136]. The entry plasmid contains the genes which encode the structural components of the secretion apparatus, *mxi (*membrane excretion proteins) and *spa* (surface presentation antigens) genes; genes which encode proteins secreted by the apparatus including i*pa* (invasion plasmid antigens) *A*, *B*, *C* and *D*, *ipg* (invasion plasmid gene) *B1* and *IcsB*; chaperones including *ipgA, IpgC, IpgE* and *Spa 15*; and transcriptional activators *Vir (*virulence protein) *B* and *MxiE*[124,136]. Chaperone proteins bind to specific effectors in the bacterial cytoplasm before they are secreted[124]. For example, the chaperone protein encoded by *IpgE* binds to IpgD[136]. When *IpgE* is mutated, the amount of IpgD protein found in whole *IpgE* mutant cell extracts is significantly decreased, demonstrating that IpgE is required for the production and stability of IpgD[137]. Additional virulence factors are also encoded by genes outside the entry region of the virulence plasmid[124].

In order for secreted proteins to pass from the cytoplasm of the bacteria into the host cell cytoplasm, they must pass through three membranes, the outer and inner membranes of the bacteria and the host cell membrane (figure 1.1.11). The base of the secretion apparatus is anchored in the cytoplasm of the bacteria[135]. It consists of protein ring structures spanning the inner (MxiG) and outer (MxiD) bacterial membranes, which are connected to each other by MxiJ[138]. A 60 nm needle formed from MxiH[138] is attached to the base of the secretion apparatus, and projects from the surface of the bacterial cell into the extracellular milieu[139]. Prior to contact with the host cell, IpaB and IpaD are assembled in a complex at the tip of the needle, where they have been proposed to have roles in recognising host cell components[140]. Upon contact of IpaB with the host cell membrane, IpaB is inserted into the membrane and undergoes a conformational change[140]. This signal is transduced through IpaD, which results in the activation of the secretion apparatus[140]. This leads to the

secretion of IpaC, which now localises to the tip of the needle complex, and also inserts into the host cell membrane[140]. The complex formed by IpaB and IpaC is a translocation pore, through which secreted proteins which have been transported down the needle complex can be delivered into the host cell membrane[141]. In order for effectors to be secreted, the secretion apparatus must be energised, which is achieved through the hydrolysis of ATP molecules into ADP molecules by the cytoplasmic ATPase Spa47[135].

Figure 1.1.11: Structure of type III secretion system of *Shigella*. The base of the secretion system apparatus consists of MxiM and MxiG protein rings spanning the outer and inner membranes connected to each other by MxiJ. A needle composed of MxiH is connected to the base of the secretion apparatus and projects into the extracellular milieu. Effector proteins are delivered into the host cell through the translocator, which is composed of IpaB and IpaC. The cytoplasmic ATPase Spa47 energises the secretion apparatus.

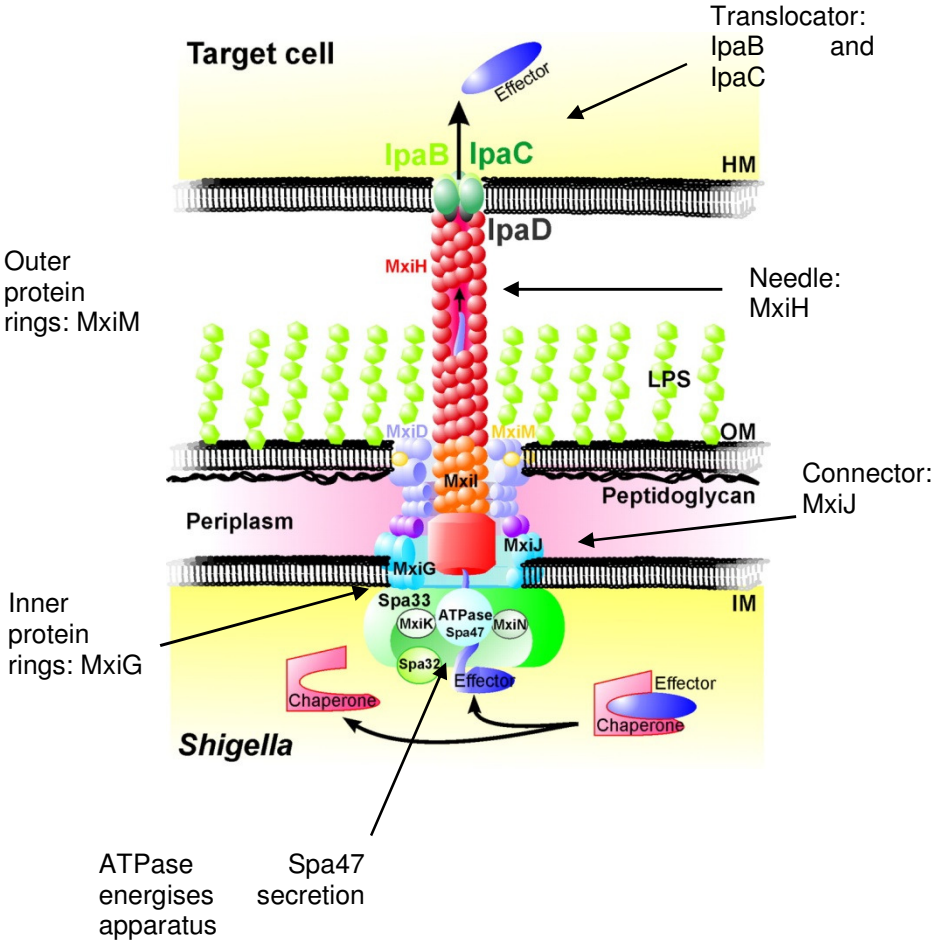

(Image modified from[142])

1.1.20.2 EPEC secretion apparatus

The genes encoding the EPEC secretion apparatus localise to the chromosomal locus of enterocyte effacement (LEE)[143,144]. The base of the secretion apparatus consists of *E. coli* secretion (Esc) C rings spanning the outer bacterial membrane, connected to rings composed of EscR, EscS EscT, EscU and EscV spanning the inner bacterial membrane, by means of EscJ (figure 1.1.12). The needle complex, which is composed of EscF, forms a projection channel, and is directly connected to the *E. coli* secreted protein (Esp) A filamentous extension. The filamentous extension is unique to the secretion apparatus found in EPEC[138]. EspA is also connected to the EspB/D translocator complex[138]. The LEE also contains the *E. coli* attaching and effacing (*eae)* gene, which encodes the bacterial outer membrane protein Intimin; and secreted effector proteins including the translocated intimin receptor (Tir), Map, EspB, EspF, EspG, EspH and EspZ [138,145]. Similarly to *Shigella*, EPEC encodes chaperone proteins which ensure efficient secretion of secreted proteins[138]. For example, Chaperone of *E. coli* secretion (Ces) F chaperones EspF[146] and CesAB chaperones EspA and EspB[147]. Up to 20 or 30 other effectors also exist which are encoded by genes outside of the LEE.

1.1.20.3 Secretion system gene expression regulation

The expression of secretion system genes is tightly regulated to ensure that proteins are expressed in sufficient quantities at the appropriate time point during infection. It also means that gene expression can be adjusted by the bacteria to accommodate changes within their environment. Gene expression is regulated by temperature in *Shigella* where the *mxi*, spa and *ipa* genes are transcribed at 37°C, but not at 30°C[148]. Their transcription is also regulated by the transcriptional activators *VirB* and *VirF*[148]. So if *Shigella* is growing in culture at 37°C, transcription of genes which are under the control of *VirB* and *VirF* occurs. Contact with epithelial cells leads to increased activation of the secretion apparatus[148]. This leads to increased transcription of genes encoding effector proteins. The transcription of these genes is regulated by the transcriptional activator *MxiE*[148]. Gene expression in EPEC is also regulated by

temperature, and is activate and inactive at 37ºC and 28ºC respectively[149]. Gene expression is influenced by nutrient availability, with EPEC undergoing localised adherence to intestinal epithelial cells (IEC) more efficiently in the presence of extracellular glucose than galactose[150]. The LEE-encoded regulator (*ler*) is a key regulator of EPEC virulence factors including the Esp proteins, Intimin and Tir[151]. *Ler* transcription is activated by the global regulator of LEE activator (GrlA) and repressed by the global regulator of LEE repressor (GrlR)[129,138]. *Ler* expression is also activated by quorum sensing[152]. Bacteria constitutively secrete signalling molecules termed autoinducers[152]. They have receptors for these signalling molecules, so they can detect other bacteria within the local environment, and respond by inducing the transcription of specific genes[152]. Thus tight regulation of gene expression in *Shigella* and EPEC helps to establish a successful infection.

Figure 1.1.12: Structure of type III secretion system of EPEC. Protein rings composed of EscC span the outer bacterial membrane and EscR, S, T, U and V span the inner bacterial membrane. The rings are connected to each other by EscJ. The needle complex is composed of EscF and is connected to the EspA filamentous extension, which is unique to the EPEC secretion system. The translocator is composed of EspD/B. The cytoplasmic ATPase EscN energises the secretion apparatus.

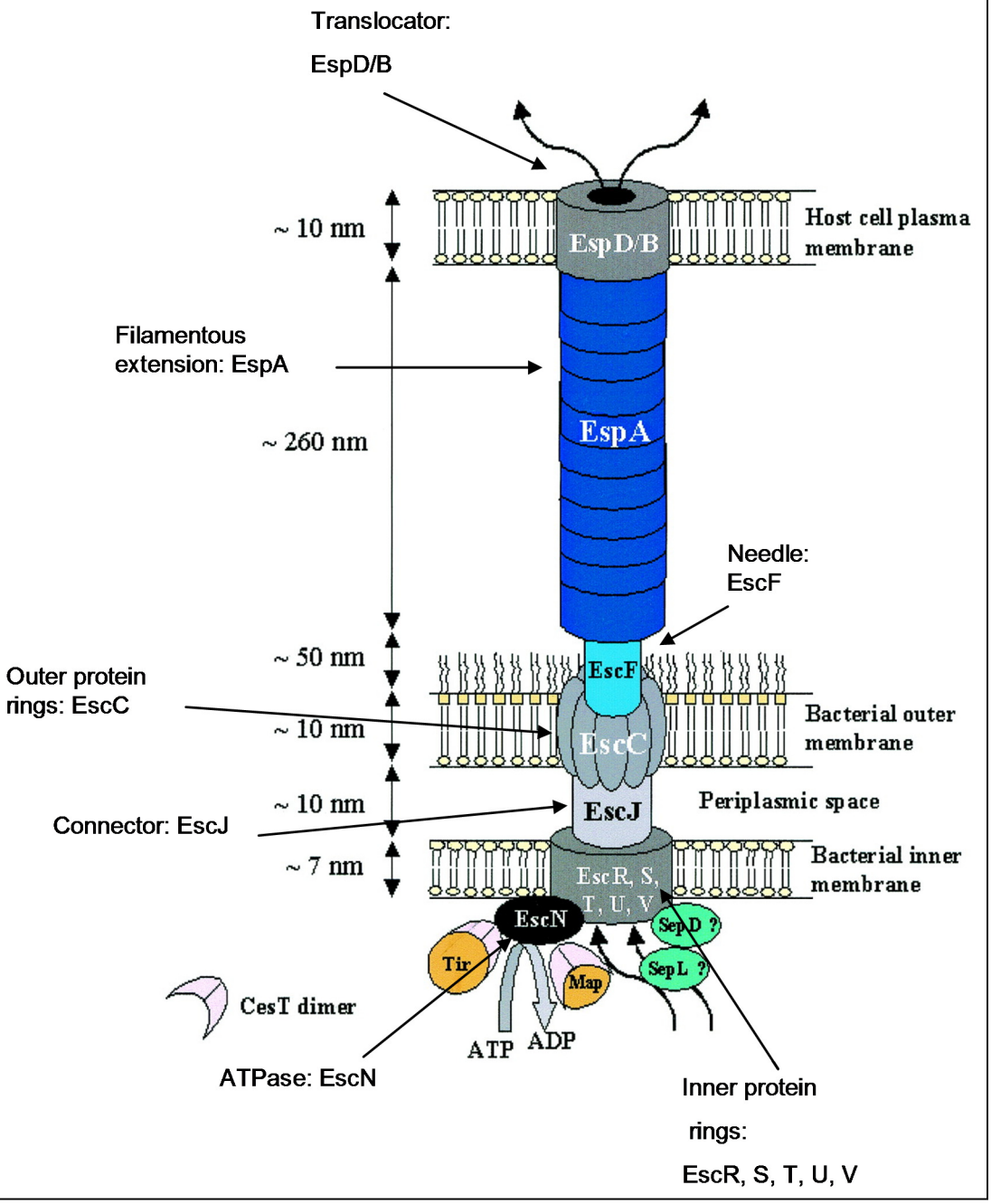

(Image modified from[138])

A major difference between *Shigella* and EPEC is how they cause disease. *Shigella* is an intracellular pathogen which invades colonic epithelial cells. EPEC is an extracellular pathogen which colonises the surface of the intestinal epithelium. EPEC forms attaching and effacing lesions which allow it to adhere

intimately to IECs. *Shigella* and EPEC infections will be discussed in detail in sections 1.1.21 and 1.1.22.

1.1.21 *Shigella* infection

1.1.21.1 Macrophage apoptosis and the inflammatory response during Shigella infection

1.1.21.1.1 Mucosal immune response

To understand how *Shigella* invades the colonic epithelium, a description of the mucosal immune system is required. Immune responses are induced in the Peyer's Patches (figure 1.1.13)[153]. Peyer's Patches contain central B cell follicles, which are surrounded by areas of T cells[153]. The subepithelial dome contains antigen presenting cells (APCs) including macrophages and dendritic cells[153]. It is superficial to the lymphoid follicles of Peyer's patches and lies below the follicular associated epithelium, which contains specialised epithelial microfold (M) cells[153]. M cells transfer antigen from the intestinal lumen by transcytosis to APCs within the subepithelium dome[153]. In turn APCs migrate to the lymphoid follicles and interact with naïve lymphocytes[153]. Once lymphocytes have been primed, they leave the Peyer's patches via draining nodes and migrate into the mesenteric lymph node[153]. From here they travel through the thoratic duct into the bloodstream before migrating to the lamina propria[153]. The lamina propria is the site of effector immune responses in the mucosal immune system and comprises immune cells including T and B lymphocytes, macrophages, dendritic cells, neutrophils and mast cells[153].

Figure 1.1.13: Mucosal immune system. Immune responses are induced in the Peyer's patches (PP). M cells transfer luminal antigen to antigen presenting cells (APCs) such as macrophages and dendritic cells in the subepithelial dome. APCs migrate into the lymphoid follicle which consists of a central B cell area surrounded by T cell areas, where they interact with naïve lymphocytes. Once primed, lymphocytes exit the PP and migrate into the mesenteric lymph node before entering the bloodstream via the thoratic duct. They then migrate to the lamina propria (LP) which is the site of effector immune responses. The LP contains immune cells including T and B cells, macrophages, dendritic cells, neutrophils and mast cells.

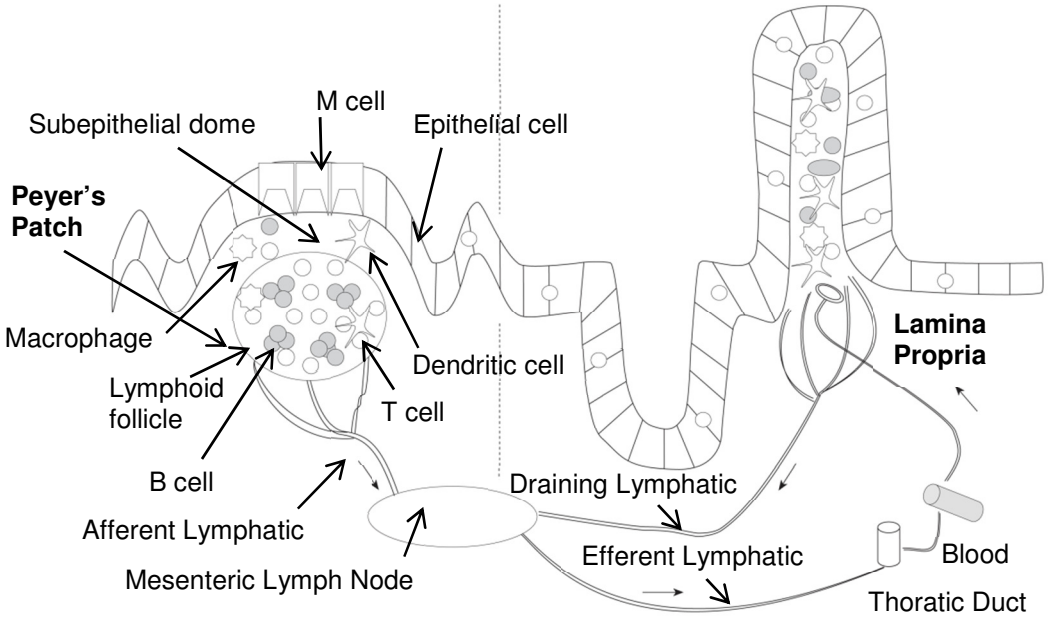

(Image modified from[153])

1.1.21.1.2 Macrophage apoptosis and inflammatory response

Shigella uses M cells to cross the epithelial barrier by transcytosis into the subepithethial dome[124], where the bacteria invade resident macrophages (figure 1.1.14)[154]. *Shigella* lyses the phagocytic vacuole in which they were internalised in, enabling them to escape into the macrophage cytoplasm, where they replicate before triggering macrophage apoptosis[154]. Macrophage cell death results from inflammasome mediated activation of Caspase 1. Inflammasome activity can be stimulated by lipopolysaccharide (LPS), which is released as the bacteria escape from the phagocytic vacuole[154], and by the effector IpaB[71]. The production of interleukin (IL) 1β contributes to inflammation within the intestine, and leads to immune cell recruitment into the tissue. This is important because it damages the epithelial surface, which allows more bacteria to cross the

intestinal barrier and gain access to the basolateral pole of epithelial cells, to disseminate to neighbouring cells and in turn spread throughout the tissue. *Shigella* invasion into enterocytes will be discussed in section 1.1.21. Epithelial cells infected with *Shigella* are an importance source of IL-8, and because of its role in neutrophil recruitment into the intestine, IL-8 also has a pivotal role during *Shigella* infection. The persistence of *Shigella* within the intestine activates the innate immune system through the release of bacterial products including LPS and peptidoglycan (PGN), which are pathogen-associated molecular patterns (PAMPs). PAMPs are patterns conserved among a specific group of pathogens, which are recognised by pattern recognition receptors (PRRs). PPRs may be expressed at the cell surface, for example toll-like-receptor (TLR) 4, which is activated by LPS[155], or they may be found intracellularly, such as nucleotide-binding oligomerisation-domain-containing protein 1 (NOD1), which recognises PGN[156]. This triggers signalling cascades involving nuclear factor (NF)-κB, and MAPKs including extracellular-signal-regulated kinase (ERK) and p38, which serve to induce transcription of genes including cytokines, chemokines and adhesion molecules, which are involved in the immune response[157]. NF-κB is a transcription factor which directly induces inflammatory gene transcription. Its activity relies on its translocation to the nucleus, which occurs when its inhibitor, inhibitor of NF-κB alpha (IκBα) undergoes phosphorylation, and subsequent polyubiquitination and proteosomal degradation[157]. ERK and p38 MAP kinase signalling induces gene transcription by histone H3 phosphorylation, which permits transcription factors to gain access to chromatin[157]. Bacterial and inflammatory response dissemination throughout the intestine results in oedema (abnormal fluid volume between cells, and the production of a mucopurulent discharge (fluid containing mucus and pus), followed by the formation of abscesses and mucosal haemorrhaging, and thus accounts for the symptoms associated with *Shigella*[124].

Figure 1.1.14: Inflammatory responses during *Shigella* infection.

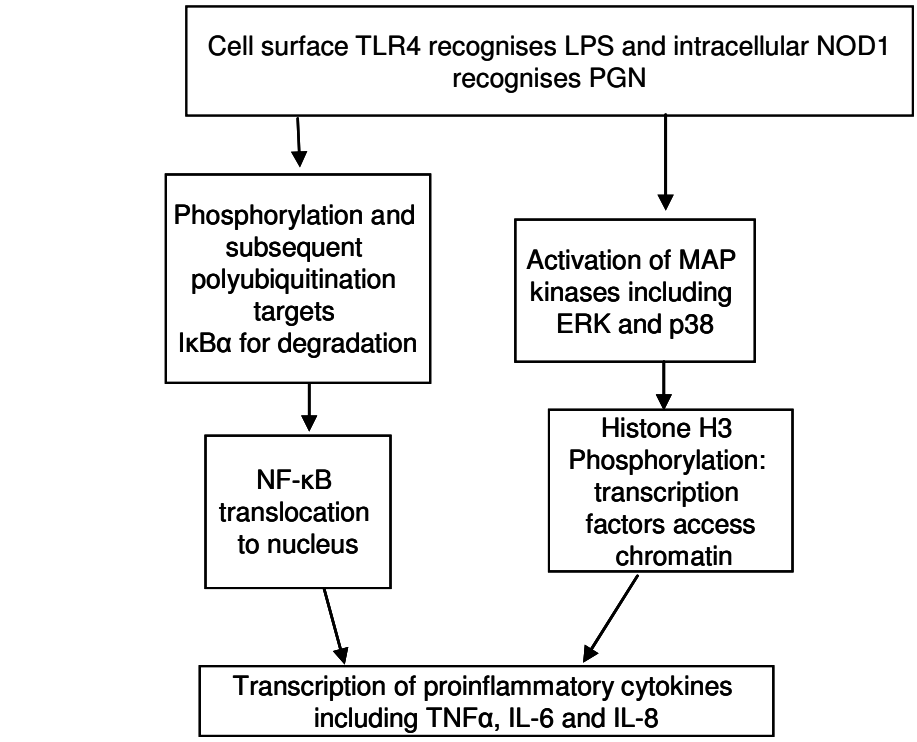

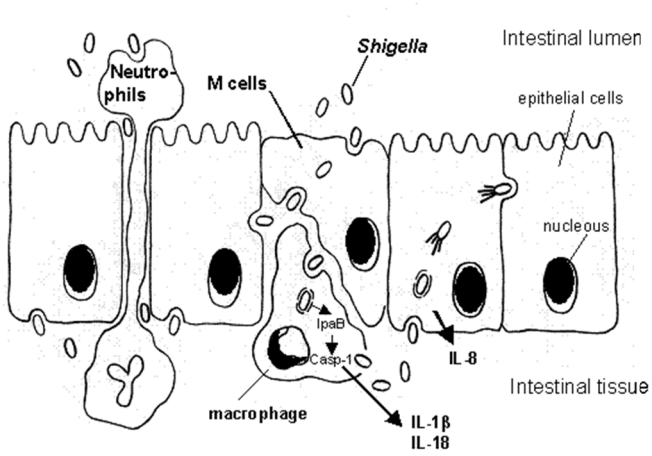

Shigella crosses the intestinal barrier by transcytosis via M cells. *Shigella* invades macrophages and triggers apoptosis by activation of caspase 1. Bacteria are released from macrophages which then invade epithelial cells. IL-1β and IL-18 released from dying macrophages act in combination with IL-8 released from infected epithelial cells to recruit neutrophils to the site of infection. This damages the epithelial surface, which allows more bacteria to cross the intestinal barrier, which subsequently invade epithelial cells.

(Image from http://edoc.hu-berlin.de/dissertationen/averhoff-petra-2006-05-24/HTML/chapter1.html.)

1.1.21.2 Shigella invasion into enterocytes

Following release from dying macrophages *Shigella* invades IECs. This relies on the production of effectors which target the host cell actin machinery. The

regulation of actin by the host cell (section 1.1.22.2.1) and its modification by *Shigella* effectors (section 1.1.22.2.2) will be discussed.

1.1.21.2.1 Actin dynamics within the host cell

The regulated assembly, turnover and spatial organisation of actin filaments is responsible for many processes which enable cells to change shape, to migrate and to extend membrane protrusions (e.g. filopodia)[158]. In cells actin exists in two forms, globular actin (G-actin) which can undergo polymerisation into actin filaments (F actin). F actin is polarised and comprises a fast growing, barbed, plus end and a slow growing, pointed, minus end[158,159]. Actin filaments are orientated such that the barbed end faces the plasma membrane of the cell, whilst the pointed end is at the rear of the cell[158]. Actin turnover is coupled with ATP hydrolysis[158,159]. Actin filaments undergo treadmilling in which the filament remains roughly the same length[158,159]. Whilst actin monomer subunits are added to the barbed end, they are also lost from the pointed end. Actin assembly and turnover is regulated by many actin binding proteins. For example, actin-depolymerising-factor ADF/cofilin family members promote actin depolymerisation[160] and also sever pre-existing actin filaments[161]. This results in an increase in the concentration of G-actin within the cell, which can be incorporated into the actin filament at the barbed end. Capping proteins bind to the end of actin filaments. This regulates the length of the actin filament by preventing the association and dissociation of actin monomer subunits[162,163]. Capping barbed ends also regulates filament growth direction, since G-actin subunits are guided to the small number of uncapped barbed ends that are available for subsequent actin polymerisation[158]. Multiple proteins including CapZ capping protein bind to barbed end filaments, whilst members of the tropomodulin protein family cap pointed end filaments[162,163]. The effect of capping actin filaments is balanced by the generation of new filaments [158]. The actin-related-protein (Arp) 2/3 complex is activated by members of the Wiskott-Aldrich-syndrome protein (WASP) and WASP family verprolin-homologous (WAVE) families of proteins, and plays an important role in the branching and nucleation of actin filaments[164,165]. WASP and WAVE proteins initiate new actin

filament polymerisation by bringing together actin monomers within the Arp2/3 complex. They also bind to existing actin filaments and stimulate the formation of additional new filaments. Two models have been proposed to explain how the Arp2/3 complex promotes branching: one which proposes that branching occurs at the barbed end of growing filaments; and the other which proposes that branching may occur at the side of existing filaments[166].

The RhoA GTPases RhoA, Rac and Cdc42 are master regulators of actin dynamics, whose downstream targets include the actin regulatory proteins discussed in the previous paragraph[158]. They are a subfamily within the Ras superfamily of small guanosine triphosphate phosphohydrolases (GTPases)[167], and are active and inactive when they are bound by GTP and GDP respectively[168]. They are regulated by three classes of proteins[168]. Guanine nucleotide exchange factors (GEFs) stimulate guanosine triphosphate (GTP) binding, and GTPase activating proteins (GAPs) trigger GTP hydrolysis to guanosine diphosphate (GDP)[168]. Additionally, the RhoA GTPases are inhibited by guanine nucleotide dissociation inhibitors (GDIs), which sequester them in a GDP bound state[168]. Once RhoA GTPases are activated in their GTP bound state, they can activate actin regulatory protein downstream targets, whose activities have been discussed above. Thus activated Rho GTPases regulate the assembly, spatial arrangement and turnover of actin filaments. They also represent the main target of *Shigella* effectors for invasion into cells.

1.1.21.2.2 Invasion of Shigella into IECs and spread from cell to cell

Shigella invasion into IECs requires the formation of filopodia and membrane ruffles, which are actin rich membrane protrusions that form phagocytic cups enclosing the bacteria[169]. A role for a number of effectors has been demonstrated in invasion through their activation of Rho GTPases. For example, IpaC activates Rac and Cdc42, which stimulates the activity of the Arp2/3 complex, and leads to the branching of new actin filaments[170,192]. IpgB1 also activates Rac, which may occur directly if IpgB1 has intrinsic GEF activity for Rac[170], or indirectly if it recruits the Rac GEF DOCK 180[171]. IpgD also acts to enhance actin polymerisation. IpgD possesses phosphatidylinositol

phosphatase activity, converting phosphatidylinositol 4,5-bisphosphate into phosphatidylinositol 5-monophosphate, and has been proposed to promote detachment of the actin cytoskeleton from the plasma membrane, which may favour actin polymerisation at the site of invasion[172]. In order for bacterial invasion into the enterocyte to take place, the phagocytic cup must close[173]. This has been proposed to occur by an inhibition of actin polymerisation, resulting from an interaction between IpaA, and vinculin[169,174]. IpaA binds to the cytoskeletal protein vinculin, and this interaction has been suggested to cause vinculin to act as a capping protein, binding to barbed end filaments and attenuating their growth[175,176].

Following uptake into IECs, *Shigella* lyse the vacuole they were internalised in, and escape into the cytoplasm where they become covered with F-actin. The outer surface membrane protein VirG, is asymmetrically distributed over the surface of the bacterium, and accumulates at one pole[154]. VirG recruits host cell components including N-WASP and the Arp2/3 complex[142]. Activation of the Arp2/3 complex by N-WASP, causes actin nucleation at one pole of the bacterium. This leads to the formation of an actin tail which propels the bacterium through the cytoplasm[142]. When the bacteria reach the plasma membrane, they trigger actin protrusions into neighbouring cells, which subsequently endocytose the bacteria. As this enables *Shigella* to disseminate through the tissue without being exposed to the extracellular environment, the bacteria evade the host immune response[142]. VirA also facilitates bacterial movement within the cytoplasm. *Shigella* movement is perturbed by microtubules, which are composed of α- and β- tubulin[154]. As VirA degrades α-tubulin, this creates a tunnel in the microtubule network through which the bacteria can move smoothly[177]. In summary, the bacteria hijack the host cell machinery which regulates the assembly and turnover of actin. As this is pivotal for their invasion into epithelial cells and spread throughout the intestine, it is an absolute requirement for setting up a successful infection.

1.1.22 EPEC infection

During EPEC infection a variety of mechanisms act in combination to induce diarrhoea development. These mechanisms include the formation of attaching

and effacing lesions, the disruption of the epithelial barrier and the modification of ion and water transport and will be discussed in the following sections.

1.1.22.1 Attaching and effacing lesion formation: intimate adherence to IECs

As previously mentioned, EPEC is a non-invasive extracellular bacterium, which colonises the surface of the intestinal mucosa by forming attaching and effacing lesions on the surface of IECs[131]. EPEC can be divided into typical and atypical strains. Both strains produce the chromosomal locus of enterocyte effacement (LEE), which encodes the type III secretion apparatus and has been described in section 1.1.20.2. A key difference between typical EPEC and atypical EPEC is the production of a ~95 kb plasmid termed EPEC adherence factor (EAF) plasmid. Typical EPEC express the EAF plasmid and undergo localised adherence to IECs[143,178], and this will be discussed in the next paragraph. Atypical EPEC do not produce the EAF plasmid and therefore do not undergo localised adherence to IECs.

For typical EPEC, the initial step in attaching and effacing lesion formation occurs when the bacteria undergo localised adherence to IECs, where tight clusters of bacteria bind and form micro-colonies on the cell surface[143]. This requires the production of type IV fimbriae produced by EPEC, which are known as bundle forming pili (BFP), and which are encoded by the EAF plasmid[143,178]. BFP are proteinaceous fibrillar organelles, which extend out of the surface of the bacterium, facilitating the adhesion of the bacterium to the host cell and the recruitment of additional bacteria into micro-colonies on the cell[143,178].

Following localised adherence, the bacteria induce actin pedestal formation beneath them, allowing them to adhere intimately to the enterocyte. They inject their own receptor, Translocated Intimin Receptor (Tir) into the host cell membrane via the type III secretion system[138,179]. Binding of Tir to the bacterial outer membrane protein Intimin, mediates intimate adherence to IECs[131]. Actin pedestal formation requires the activation of the Arp2/3 complex by N-WASP, which leads to actin polymerisation and cytoskeleton rearrangements. EPEC and the closely related bacteria, EHEC activate N-WASP in different ways.

EPEC Tir is phosphorylated on the Y474 tyrosine residue and recruits the host cell adaptor protein Nck, which in turn recruits and activates N-WASP[138]. On the other hand, instead of Nck, EHEC utilises its effector EspFu, which binds directly to and activates N-WASP[138]. EPEC Tir also recruits cytoskeletal proteins including α-actinin, ezrin and myosin light chain to the site of pedestal formation[131]. Such proteins may provide a direct link between the bacterium and the host cell cytoskeleton[180,181]. Thus EPEC and EHEC induce cytoskeleton rearrangements and actin pedestal formation so that they can adhere tightly to the IEC (illustrated in figure 1.1.15). This leads to the formation of the attaching and effacing lesions on the intestinal surface, which is the hallmark of EPEC and EHEC infections.

Figure 1.1.15: Attaching and effacing lesion formation. Transmission Electron Microscopy of the ileal loop of rabbits infected with WT EPEC **(a)** and mutant EPEC, Δ*escN* **(b)**. WT EPEC adheres intimately to the microvilli brush border, which leads to the formation of attaching and effacing lesions (red arrows) and causes the destruction of the microvilli. EPEC Δ*escN* is unable to form attaching and effacing lesions on cells because it is deficient in type III secretion and unable to deliver effectors into the host cell.

a

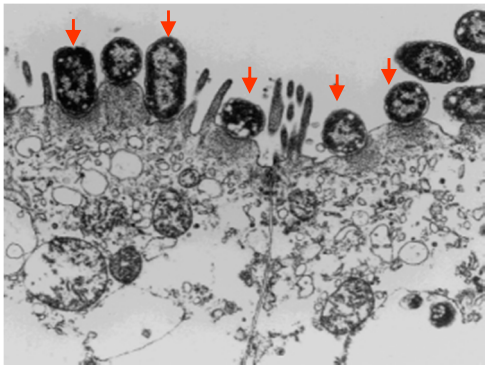

b

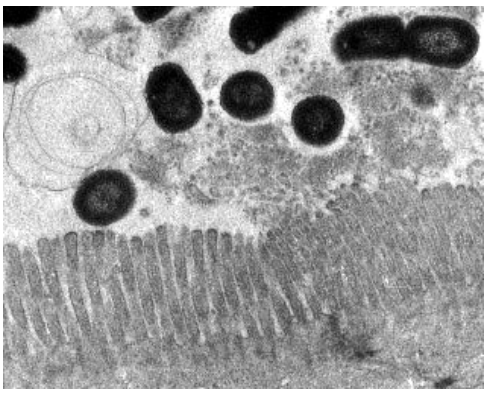

(Image obtained from Dr. Olivier Marchès)

1.1.22.2 Disruption of the epithelial barrier

1.1.22.2.1 Epithelial barrier structure

The intestinal epithelium separates the intestinal lumen and subepithelial tissue[131]. By acting as a physical, ion and size selective barrier, the passage of molecules between the two environments is tightly regulated[182]. Apical junctional complexes, which include tight junctions (TJ) and adherens junctions (AJ) (figure 1.1.16), provide adhesive contacts between neighbouring cells, and therefore function to maintain the intestinal barrier[131,182]. TJs maintain IEC polarity by preventing the lateral diffusion of membrane proteins between apical and basal surfaces[183]. TJs also prevent ions and solutes from passing between adjacent cells, meaning that they must enter cells by diffusion or active transport[183]. AJs are thought to initiate and stabilise cell: cell adhesion by connecting the actin cytoskeletons of neighbouring cells[183].

Localised clustering of transmembrane proteins including occludin, claudins and junctional adhesion molecules is necessary for their incorporation into TJs and is mediated through binding to the C-terminus of cytoplasmic zona occludens (ZO) proteins. The N-terminus of ZO proteins is anchored to the actin filaments and the myosin light chain (MLC) of the perijunctional actomyosin ring, which regulates TJ permeability[131,182,184]. AJs lie directly below TJs, and form from interactions of nectins and cadherins (transmembrane proteins) with afadins and catenins (cytoplasmic proteins). With regard to cadherin and catenin interactions, while β-catenin and p120 catenin bind directly to the cadherin, α-catenin binds via β-catenin[182]. AJs are closely connected to the actin cytoskeleton, through the direct binding of afadin and catenin protein family members to actin[182].

Figure 1.1.16: Apical junctional complex structure. Tight junctions (TJ) form from interactions of claudins, occludin and junctional adhesion molecules (transmembrane proteins) with zona occludens (cytoplasmic proteins). Adherens junctions (AJ) form from interactions of nectins and cadherins (transmembrane proteins) with afadins and catenins (cytoplasmic proteins). TJs and AJs are connected to the actomysoin ring via their cytoplasmic proteins.

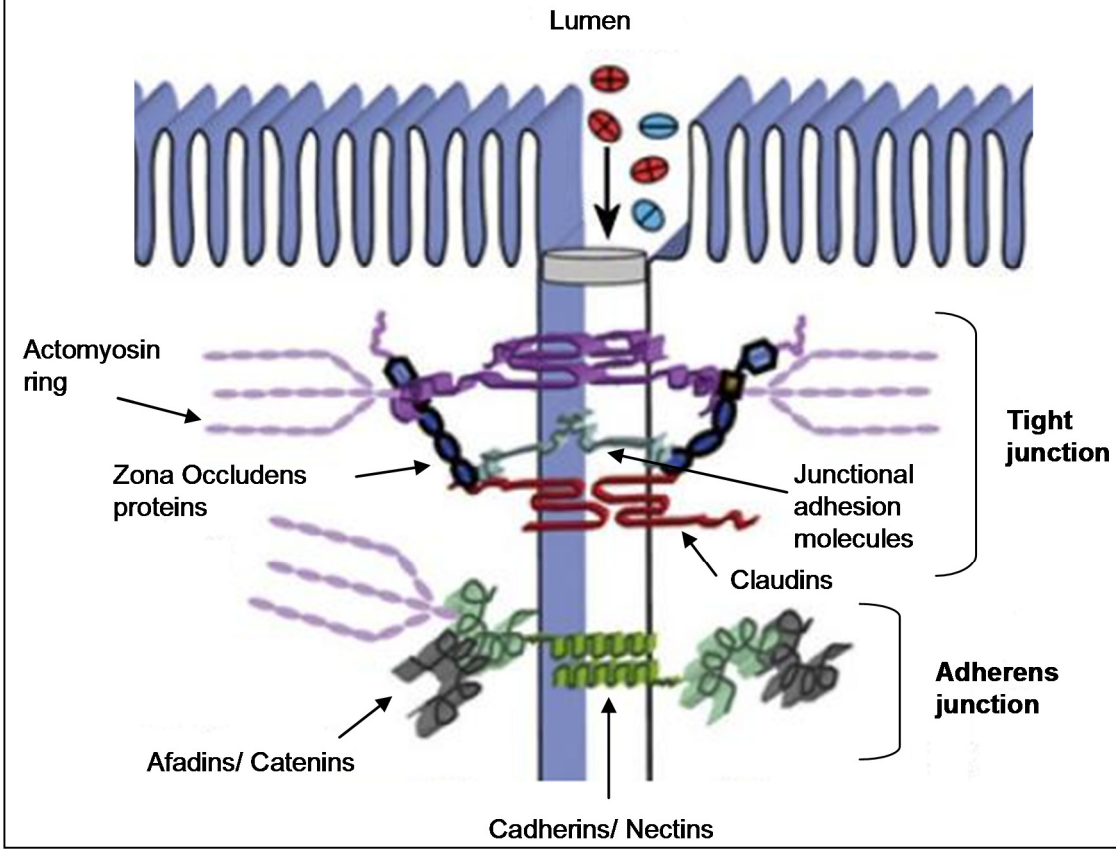

(Image modified from[185])

1.1.22.2.2 Epithelial barrier modification by EPEC

During EPEC infection both the structure and function of TJs are manipulated. One mechanism which regulates the permeability of TJs is phosphorylation of the myosin light chain (MLC) of the actomyosin ring by myosin light chain kinase. EPEC has been shown to induce MLC phosphorylation in IECs[186]. This stimulates the contraction of the actomyosin ring, which causes an increase in paracellular permeability and a decrease in transepithelial resistance (TER), indicating that the integrity of the barrier is compromised[131,187]. EPEC can directly modify the localisation of TJ proteins. For example, claudin-1 has been redistributed from TJs in EPEC infected IECs[188] and in *C. rodentium* infected mice[189]. Both EspF and Map have been shown to induce occludin redistribution during EPEC infection of IECs[190]. Phosphorylation is required for occludin

localisation to the TJ, and during EPEC infection, occludin is translocated from the TJ to the cytosol, which coincides with its dephosphorylation[187]. Mice with an EspF mutation infected with *C. rodentium,* highlight the importance of barrier modification during attaching and effacing bacterial infection *in vivo*[191]. Although the bacteria are able to adhere intimately to the epithelium, they do not disrupt TJs, and this leads to reduced water movement into the intestinal lumen compared to wild type mice[191]. In addition, EPEC has been shown to target AJs in an EspB dependent manner[192]. When EspB bound to α-catenin within a complex of E-cadherin/β-catenin/α-catenin, it induced a conformational change in the structure of α-catenin, leading its dissociation from the AJ[192]. Thus by targeting TJ and AJ proteins, EPEC manipulates the structure of the junction. This compromises the integrity of the intestinal epithelial barrier, which is confirmed by a decrease in TER and an increase in paracellular permeability. Compromising the intestinal barrier may facilitate bacterial penetration through the intestinal epithelium[192].

1.1.22.3 Modification of water and ion transport

1.1.22.3.1 Water and ion transport

The transport of water, electrolytes and solutes in the intestine is tightly regulated to maximise their absorption. Various transporter proteins including Na^+ dependent glucose transporter (SGLT) 1, Na^+/H^+ exchanger isoforms 2 and 3 (NHE_2/NHE_3), and Cl^-/HCO_3^- exchangers, down regulated in adenoma (DRA) and putative anion transporter (PAT) 1 mediate the absorption of water and solutes across the intestinal epithelium[131]. For example, amino acids and sugar absorption is coupled to Na^+ transport by SGLT-1[193]. As nutrients are absorbed by IECs, the osmolarity of the intestinal lumen decreases[194]. Osmosis is defined as the movement of water from a region of low solute concentration to a region of high solute concentration. Thus the reabsorption of nutrients also drives the reabsorption of water across the intestinal epithelium[194]. On the other hand, water is also secreted from IECs into the intestinal lumen[193]. Cl^- secretion from IECs is mediated by the opening of the cystic fibrosis transmembrane conductor regulator channel[193]. The exit of Cl^- from the cell drives the movement of Na^+

into the intestinal lumen[193], thereby increasing the luminal electrolyte concentration, and creating an osmotic gradient which causes water to move into the lumen. Water absorption through cellular membranes is also mediated by aquaporin channels expressed in colonic epithelial cells[131]. Thus various transporter proteins and channels act in combination to ensure maximum reabsorption of water and nutrients across the intestinal epithelium.

1.1.22.3.2 Modification of water and ion transport by EPEC

EPEC modifies host cell electrolyte reabsorption. For example, EspF targets NHE_3 to reduce Na^+ uptake[195]. EspG and EspG2 destroy the microtubule network to prevent DRA trafficking from intracellular compartments to the apical membrane of IECs, leading to reduce Cl^- uptake[196]. Moreover, the cooperative action of EspF, Map, Tir, and Intimin reduced the activity of the SGLT-1 co-transporter[197]. By reducing nutrient and electrolyte reabsorption across the intestinal epithelium, EPEC also reduces water reabsorption across the epithelial barrier. Additionally, EPEC directly reduces water reabsorption by manipulating aquaporin expression. For example, in *C. rodentium* infected mice, EspF and EspG mediated AQP2 and AQP3 redistribution from the apical and lateral membranes to the cytosol in colonocytes[198]. The authors suggested that this may contribute to diarrhoea production, and consistently, AQP2 and AQP3 returned to their normal localisation when the mice recovered from infection[198]. Thus by targeting transporter proteins and aquaporin channels, EPEC reduces solute and water reabsorption across the epithelial barrier. The resulting increase in luminal water contributes to the development of diarrhoea[131].

1.1.22.4 Diarrhoea development in EPEC

In summary, the formation of attaching and effacing lesions, epithelial barrier disruption and modification of water and ion transport act in combination to mediate diarrhoea development. The formation of attaching and effacing lesions on the epithelial surface leads to the shortening and destruction of intestinal microvilli[131,180]. Microvilli increase the absorptive area of the intestine so by

destroying them, EPEC reduces the area over which nutrient and water reabsorption across the epithelial barrier can occur[131,180]. The disruption of the epithelial barrier causes water to move between epithelial cells into the lumen, and concurrently, water reabsorption is also reduced because EPEC targets various transporter proteins and channels. The net effect is to increase the volume of water in the intestinal lumen. As diarrhoea production occurs before attaching and effacing lesion formation is complete, this suggests that the other mechanisms probably contribute to the initial onset of diarrhoea[204,221].

1.1.23 Cx hemichannels and gastrointestinal bacterial infection

Cx26 is expressed within the human colon[199]. Unpaired Cx26 hemichannels have been linked to infection with *S. flexneri. S. flexneri* induces transient peaks in the intercellular concentration of Ca^{2+}, which opens Cx26 hemichannels and in turn releases ATP into the extracellular medium[200]. Prior to invasion into cells, *Shigella* are captured by filopodial extensions[200]. ATP signalling stimulates the retrograde flow of filopodial actin, in a process dependent on ERK1/2 activation[200]. This in turn causes the filopodia to retract bringing the bacteria into contact with the cell body where invasion takes place[200]. Thus by opening Cx26 hemichannels, *S. flexneri* induces signalling cascades which result in their internalisation into IECs. Subsequently HeLa cells transfected with p.R143W were shown to be significantly less susceptible to invasion with *S. flexneri* than HeLa cells expressing WT Cx26[45]. This *in vitro* data suggests that WT Cx26 expression facilitates cellular invasion, whereas carrying the p.R143W mutation may provide improved protection against infection with *S. flexneri*. These results support the heterozygous advantage hypothesis. *In vivo* data demonstrate that heterozygote carriers of the c.35delG and p.R143W mutations have a thicker epidermis. One of the principal functions of the skin is to form a defensive barrier against invading pathogens. Similar protective properties of the skin also exist in the gut epithelium, so plausibly, the epidermis of the gut epithelium of Cx26 heterozygotes may also be thicker than normal individuals. This in turn could provide carriers of Cx26 NSHL mutations with improved protection against infection with enteric bacteria. This may be most beneficial in

developing countries where infection with gastrointestinal pathogens including *S. flexneri* is greatest.

Unpaired Cx43 hemichannels have been linked to *Citrobacter rodentium*[201] and *Yersinia enterocolitica*[202] infections. During *C. rodentium* infection, unpaired Cx43 hemichannels are detected at the apical plasma membrane of mouse colonocytes, which have been suggested to facilitate water secretion into the intestinal lumen, and in turn contribute to diarrhoea development[201]. Furthermore, diarrhoea production was significantly reduced in mice carrying a heterozygous mutation in Cx43[201]. *Y. enterocolitica* can be ingested by both phagocytic and non-phagocytic cells, including IECs and endothelial cells[202]. Following internalisation, *Y. enterocolitica* invades the intestinal epithelium and proliferates in underlying lymphoid tissue[202]. *Y. enterocolitica* invasion into Cx43 transfected HeLa cells was significantly reduced by treatment with a hemichannel blocker, thus indicating a role for Cx43 hemichannels during *Y. enterocolitica* infection[202]. *Y. enterocolitica* induced tyrosine phosphorylation of Cx43[202]. Cx phosphorylation regulates GJ function, for example by modifying GJ opening, which could favour bacterial uptake[202]. These results further support a hypothesis that a loss of functional Cx expression reduces infection with gastrointestinal bacteria

1.1.24 Aims and hypotheses (Results chapters 3 and 4)

As described in sections 1.1.16 and 1.1.22, high carrier frequencies of specific Cx26 NSHL mutations exist in certain geographic locations, and these have been suggested to confer a heterozygous advantage, namely that carriers have a thicker epidermis and may be better protected from infection with gastrointestinal bacteria. The aim of this project was to investigate how infection with gastrointestinal bacteria was affected by Cx26 expression *in vitro* using *S. flexneri* and EPEC as models of infection. EPEC adhesion and *S. flexneri* invasion were quantified in cells expressing a Cx26 NSHL mutation, and in intestinal cells that had been treated with siRNA to Cx26 (chapter 4). It was hypothesised that a loss of functional Cx26 expression would reduce infection by both pathogens. Methods were developed to quantify EPEC infection using an automated system (chapter 3). This aimed to quantify infection within a large

population of cells without any bias. An automated system would be more accurate than quantifying infection by manual counting, because humans may make mistakes over the number of cells which have been counted, or may be biased with regards to which cells to include in the analysis.

1.2 Effect of a disintegrin and metalloprotease (ADAM) 17 expression on cutaneous bacterial skin infection

1.2.1 Ectodomain shedding

Various membrane bound precursor proteins including cytokines, growth factors and receptors undergo regulated cleavage by specific enzymes from the surface of cells in a process termed ectodomain shedding[203], which is illustrated in figure 1.2.1. This results in the release of the soluble extracellular domains from the membrane bound portions of the proteins, which can participate in autocrine, juxtacrine or paracrine signalling, and which are important in a wide range of biological processes. Specific proteins can be activated, inhibited and functionally altered by proteolytic cleavage, meaning that ectodomain shedding provides a mechanism to regulate specific proteins. The majority of ectodomain shedding is mediated by proteins which belong to the membrane bound 'a disintegrin and metalloprotease' (ADAM) family of proteins[204]. ADAM17 was the first ADAM protein to be implicated in ectodomain shedding, because it was identified as the tumour necrosis factor alpha (TNFα) converting enzyme (TACE) [203,205,206]. TNFα is synthesised as a 26 kDa membrane bound precursor protein, and this undergoes proteolysis by ADAM17/TACE releasing a soluble, secreted 17 kDa biologically active protein into the bloodstream.

Figure 1.2.1: Principle of ectodomain shedding. Membrane bound precursor proteins undergo cleavage from the cell surface by proteases, e.g. ADAM17, to release a soluble, mature extracellular portion of the protein.

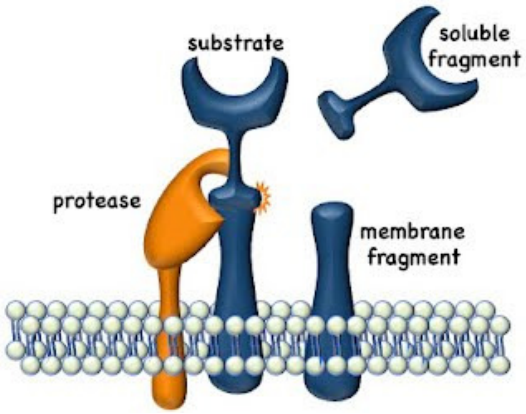

(Image taken from http://walchecklab.umn.edu/research-interests/ectodomain-shedding)

1.2.2 Structure of ADAM proteins

ADAM proteins are members of the metzincin super-family of metalloproteases. They are characterised by the possession of a catalytic Zn^{2+} in their active site, and their members also include the serralysin, the astacin and the adamalysin families of proteins[207]. ADAM proteins are multi-domain proteins, composed of a prodomain, a metalloprotease domain, a disintegrin domain, a cysteine-rich domain, a single transmembrane domain and a cytoplasmic tail. The cysteine-rich domain of many ADAMs also contain an epidermal growth factor (EGF)-like repeat[208]. The structure of ADAM proteins is shown in figure 1.2.2.

Figure 1.2.2: ADAM protein structure. ADAM proteins are multi-domain proteins consisting of a prodomain, metalloprotease domain, disintegrin domain, cysteine-rich domain, transmembrane domain and a cytoplasmic tail. The cysteine rich domain of many ADAM proteins also contains an epidermal growth factor (EGF)-like repeat. ADAM proteins are synthesised as precursor proteins, which undergo maturation following prodomain removal.

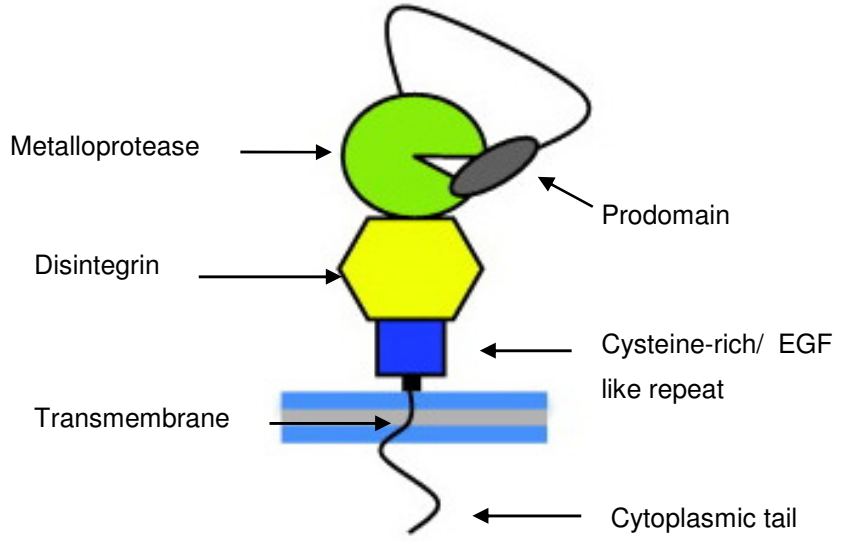

(Image adapted from [209])

1.2.2.1 Metalloprotease domain

X-ray crystallographic studies have revealed that the catalytic part of the metalloprotease domain of ADAM proteins consists of a globular structure with an active cleft located between two subdomains[210,211]. The active cleft contains a highly conserved Zn^{2+} binding motif, HEXXHXXGXXH, in which a catalytically active Zn^{2+} is bound by three histidines, a catalytic glutamate residue, and a

downstream methionine turn which loops around to face the HEXXHXXGXXH motif[212]. The specificity of substrates cleaved by the ADAM protein is determined by the structure of the active site.

1.2.2.2 N terminal signal sequence and prodomain

ADAMs are synthesised as proproteins in the rough ER. The N terminus of ADAMs contains a signal sequence, which directs the protein from the ER to its site of maturation in the Golgi apparatus[210,211]. The prodomain of ADAMs also localises to the N terminus of the protein, and functions to maintain the catalytic part of the metalloprotease domain in an inactive state. This is achieved by a cysteine switch mechanism, in which a conserved cysteine residue within the prodomain binds to the catalytic Zn^{2+} in the metalloprotease domain, blocking the active site[213]. Removal of the prodomain from ADAMs occurs by proprotein convertase mediated cleavage, e.g. by furin at a conserved Rx(R/K)R motif[214]. This results in the removal of the cysteine from the catalytic Zn^{2+}, which makes the active site accessible, and leads to the activation of the ADAM protein.

1.2.2.3 Disintegrin domain

The disintegrin domain of ADAMs was named because of its similarity to the disintegrin domain of metalloprotease proteins found in snake venom (SVMPs), which function to inhibit blood clotting[215]. SVMPs target integrins, which are cell surface receptors composed of an α and β chain, that mediate the attachment of cells to other surrounding cells, or to the extracellular matrix (ECM). Integrins expressed on the surface of activated platelets bind to ligands including fibrinogen, by means of an arginine-glycine-aspartic acid (RGD) motif. The disintegrin domain of SVMPs also contains an RGD motif, which enables SVMPs to bind to integrins expressed on the platelet surface, blocking the interaction between fibrinogen and integrins. This leads to an inhibition of platelet aggregation and blood clotting at the wound site[210]. The disintegrin domain of human ADAM15 contains an RGD motif, which is recognised by the α5β3 and α5β1 integrins, and which facilitates ADAM15 binding[216]. The disintegrin domain of most ADAM proteins does not contain an RGD motif.

However, all ADAMs excluding ADAM10 and ADAM17, can interact with members of the α4/α9 integrin subfamily through an aspartic acid located in their disintegrin domains[210],[217].

ADAM17 has recently been shown to interact with α5β1 integrin[218]. Although the precise amino acid sequence which mediates this interaction is unknown, binding was localised to the disintegrin and cysteine-rich domains of ADAM17. Whereas cells expressing either full length WT ADAM17, or a construct containing the disintegrin and cysteine-rich domains of ADAM17, adhered to α5β1 integrin coated beads, cells expressing a construct missing the disintegrin and cysteine-rich domains did not. This is an example of how the interaction of proteins with the disintegrin domain of an ADAM is supported by its cysteine rich-domain[210]. It has been suggested that the interaction of ADAM proteins with integrins may influence events including cell adhesion and migration, and consistently, colocalisation of ADAM17 and α5β1 integrin has been observed at membrane ruffles and focal adhesions[218].

1.2.2.4 Cytoplasmic tail

The length and sequence of the cytoplasmic tail varies between ADAM proteins[210]. ADAMs can interact with specific intracellular proteins by means of conserved sequences expressed within the cytoplasmic tail. The most common sequences are proline-rich PXXP motifs, which facilitate interactions with Src Homology (SH) 3 domain containing-proteins. Such interactions function to regulate the trafficking, maturation and metalloprotease activity of the ADAM protein. Phosphorylation of specific serine, threonine and tyrosine residues within the cytoplasmic tail also serves to regulate the ADAM protein. For example, ERK-mediated phosphorylation of residue Thr735 of pro-ADAM17, results in its trafficking from the ER to the cell surface[219] .

1.2.3 ADAM protein discovery

In mammals the first ADAM proteins identified were the human sperm protein fertilin components ADAM1 (fertilin-α) and ADAM2 (fertilin-β)[220]. The disintegrin

domains of ADAM1 and ADAM2 are left exposed because the ADAMs are cleaved after their metalloprotease domains[221]. Consequently they facilitate the binding of the sperm to the egg through their interaction with integrins expressed by the zona pelluicida, a specialised ECM which surrounds the developing oocyte. Subsequently, 25 *ADAM* genes have been identified in humans, of which 4 are pseudogenes[220]. Pseudogenes are genomic DNA sequences similar to normal genes, but which are non-functional, for example they are non-protein coding sequences. Of the 21 ADAM proteins encoded in humans, 13 are catalytically active, while the remaining 8 lack critical feature(s) in the active site of the metalloprotease domain[220]. ADAM1 is catalytically active, and ADAM2 is catalytically inactive, but knocking out either gene in mice results in male infertility, arising from defects in sperm migration and adhesion[222,223]. Thus both catalytically active and inactive ADAM proteins are required during development[220]. In humans a significant number of ADAM proteins are expressed in the testis, of which ADAM20, 21 and 30 are catalytically active, whilst ADAM2, 7, 18 and 29 are catalytically inactive[220]. The expression of specific ADAM proteins in the testis thus establishes a role for them in sperm function and spermatogenesis. However, it is not often possible to directly translate how ADAM proteins participate in fertility in rodents, into what occurs in humans, because some of the rodent testis-specific *ADAM* genes are only expressed as pseudogenes in humans. Of the remaining human *ADAM* genes which are catalytically active, *ADAM8* and *28* are restricted to haematopoietic cells, whilst *ADAM9, 10, 12, 15, 17, 19* and *33* exhibit expression throughout somatic tissue[220]. The widespread expression of both catalytically active and inactive ADAMs thus means they play a role in a large number of cellular and biological events in humans and other species.

1.2.4 ADAM protein regulation

As ADAM proteins are involved in a wide range of cellular processes including ectodomain shedding, cell migration, cell adhesion and cell signalling, they play important roles in development and cellular homeostasis. ADAM protein activity is dysregulated in many diseases including cancers, inflammatory diseases (e.g. rheumatoid arthritis and multiple sclerosis) cardiovascular diseases (e.g.

atherosclerosis), asthma and Alzheimer's[220], so it is important to understand how ADAM proteins are regulated. ADAM protein activity is both constitutive, and can be induced through natural and experimental stimuli. ADAM17 mediated substrate shedding can be stimulated by treatment of cells with phorbol esters including phorbol-12-myristate-13-acetate (PMA), in a process dependent on Protein kinase C (PKC) signalling[209]. ADAM17 activity can also be affected by intracellular signalling pathways, for example the ERK/MAPK pathway[203]. Tissue inhibitors of matrix metalloproteases (TIMPs) are expressed within cells which bind to active matrix metalloproteases (MMPs) and inhibit their proteolytic activity[220]. Although the specificity of TIMPs for MMPs is broad, it is a lot more restricted for ADAMs. For example, while ADAM10 can be inhibited by TIMP-1 and TIMP-3, TIMPs have no effect on ADAM8 and 9[220]. In addition as already mentioned, the cytoplasmic tail of ADAM proteins contains specific phosphorylation and proline rich motifs, which can also regulate the activity of the ADAM protein.

1.2.5 ADAM17 and inflammation

The immune response is associated with elevated levels of proinflammatory cytokines including TNFα, interleukin (IL) 1β and IL-6, which induce the transcription of proinflammatory effector molecules including cell adhesion molecules and chemokines involved in leukocyte recruitment[209,224]. ADAM17 mediated cleavage of TNFα thus makes it an important stimulator of immune responses. ADAM17 expression is elevated in inflammatory conditions including rheumatoid arthritis, Crohn's disease, pulmonary inflammation and multiple sclerosis[225]. ADAM17 activity also enhances IL-6 signalling, which contributes to inflammation. IL-6 signalling is transduced via the glycoprotein (gp) 130 signalling molecule. gp130 may be expressed on the surface of some cells from which the IL-6 receptor (IL-6R) is absent. When ADAM17 cleaves the IL-6R, a soluble form (sIL-6R) is released into the circulation, which binds to IL-6, and in turn this complex interacts with gp130[226]. IL-6 signalling can therefore occur in cells where the membrane bound IL-6R is absent[227]. Interestingly, ADAM17 also displays anti-inflammatory activity in the immune system. ADAM17 cleaves the membrane bound TNFα receptors, TNFR1 and TNFR2,

releasing soluble forms into the circulation. This acts to downregulate TNFα signalling by reducing the amount of TNFα which can bind to membrane associated TNFRs in two ways[224]. It leads to a decrease in the number of cell surface TNFRs, and the soluble receptors released by ADAM17 bind antagonistically to soluble TNFα. The importance of regulating TNFα signalling is demonstrated in patients with TNF receptor associated periodic syndrome (TRAPS)[228]. A mutation within the cleavage site of TNFR1 prevents ADAM17 mediated cleavage of the receptor, and consequently, the control of inflammation in patients is perturbed leading to inflammatory skin lesions and recurrent periods of high fevers[228]. In summary, the activities of ADAM17 are both pro- and anti-inflammatory within the immune system. ADAM17 plays a key role in the induction of immune responses, but also acts to control inflammation and prevent excessive inflammatory responses.

1.2.6 ADAM17 mediated regulation of epidermal growth factor receptor (EGFR) signalling

1.2.6.1 EGFR signalling

Signalling by ligands of the epidermal growth factor (EGF) family is involved in numerous cellular processes including proliferation, differentiation, motility, adhesion and death. The EGFR is a member of a family of receptor tyrosine kinases, whose other members compromise erythroblastic leukaemia viral oncogene homologs (ErbB) 2, 3 and 4[229]. Ligand binding to its receptor promotes homo- and hetro- dimerisation. This stimulates the cytoplasmic kinase activity, which triggers autophosphorylation on specific tyrosine residues within the cytoplasmic tail. Various intracellular signalling proteins are recruited to phosphorylated tyrosine residues, which subsequently activate downstream signalling cascades including the MAPK and phosphatidylinositol 3-kinase-activated Protein kinase B pathways. Ectodomain shedding of the EGF family of ligands is required for paracrine signalling. ADAM10 and ADAM17 are key upstream regulators of EGFR signalling. ADAM10 sheds EGF and betacellulin, whereas transforming growth factor alpha (TGFα), epiregulin, amphiregulin and heparin-binding EGF-like growth factor (HB-EGF) are released by ADAM17[230].

Different members of the EGF family bind to different receptors of the ErbB family. EGF, amphiregulin and TGF-α bind solely to the EGFR, while betacellulin, HB-EGF and epiregulin bind to the EGFR and ErbB4. Finally, some neuregulins bind solely to ErbB4, while other neuregulins bind to both ErbB3 and ErbB4[231].

Since ErbB signalling is involved in many biological processes, it follows that dysregulated signalling may be linked to disease. Insufficient ErbB signalling has been associated with neurodegenerative conditions including multiple sclerosis (MS)[232]. MS results from damage to glial and Schwann cell derived myelin sheaths that enclose neurons, which compromises the transmission of electrical impulses within the central nervous system (CNS). Mice with glial cells expressing a dominant negative ErbB receptor exhibit delayed myelination onset, which leads to thinner myelin fibre production[233]. This demonstrates that an appropriate level of ErbB signalling is required for the correct functioning of the CNS, and to prevent the development of neurodegenerative conditions. On the other hand, excessive ErbB signalling has been associated with many cancer types including lung, breast and colon carcinomas[232,234]. Excessive signalling leads to the uncontrolled proliferation of tumour cells, and can result from gene amplifications, which usually enhance subsequent ErbB protein translation, or mutations which permit ErbB receptor activation independently of ligand binding[234]. In summary, the ErbB signalling network has key roles in many different cellular processes, but must be tightly regulated to prevent the development of disease.

1.2.6.2 ADAM17$^{-/-}$ mice

As ADAM17 is an upstream regulator of EGFR signalling, *ADAM17*$^{-/-}$ mice are nearly phenotypically identical to mice lacking certain EGFR ligands. Both types of mice exhibit perinatal lethality and display developmental defects[203]. For example, similarly to *TGFα*$^{-/-}$ mice, *ADAM17*$^{-/-}$ mice have defects in epithelial structure, maturation and morphogenesis, including the inability to undergo eyelid fusion[235]. Both *amphiregulin*$^{-/-}$ mice and *ADAM17*$^{-/-}$ mice exhibit defective branching of the mammary glands[236] . Moreover, heart development is defective in *HB-EGF*$^{-/-}$ mice and *ADAM17*$^{-/-}$ mice, and is characterised by enlarged and

misshapen heart valves[237]. These observations demonstrate the absolute requirement for ADAM17 mediated shedding of EGFR ligands during developmental processes.

1.2.6.3 ADAM17 mediated regulation of EGFR signalling in epidermal barrier function

ADAM17 mediated regulation of EGFR signalling is required for epidermal barrier maintenance[238]. As discussed previously in section 1.1.16, the epidermal barrier is generated and maintained by the cornification process[60]. Keratinocytes which detach from the basal layer of the epidermis are committed to terminal differentiation, and migrate through the suprabasal layers to the surface of the epidermis where they form the cornified layer. The cornification process is initiated by the formation of the cornified envelope, in which its structural components are crosslinked by transglutaminases to form an insoluble protein network. Mice harbouring a conditional knock out of ADAM17 in keratinocytes (*ADAM17*$^{-/-}$) have dysregulated expression of keratinocyte differentiation markers[238]. For example, the expression of involucrin and transglutaminase 3, which are required to initiate cornification, was decreased[238]. The defect in terminal differentiation and cornified layer formation in *ADAM17*$^{-/-}$ mice resulted in a defective epidermal barrier, which led to increased transepidermal water loss and inflammatory cell infiltrates[238]. ADAM17 mediated shedding of EGFR ligands promotes keratinocyte terminal differentiation and stimulates transglutaminase activity, thereby facilitating the cornification process, which is required to maintain the epidermal barrier[238]. ADAM17 expression also prevents the development of chronic dermatitis in WT mice, which occurs in *ADAM17*$^{-/-}$ mice because of its role in barrier maintenance[238]. Therefore, targeting ADAM17 mediated regulation of the EGFR signalling pathway could represent a potential target for treatment of epidermal barrier defects.

The use of therapeutics targeting the ADAM17-EGFR signalling pathway for epidermal barrier defects however, must be considered carefully. Loss of functional ADAM17 expression results in the development of chronic dermatitis in mice[238], and led to the formation of pustular skin lesions in a patient suffering

from a neonatal onset inflammatory skin and bowel syndrome[239]. However, elevated ADAM17 mRNA expression has been associated with psoriatic skin lesions[225]. The skin barrier is also compromised in psoriasis, a condition which is associated with dysregulated inflammation, keratinocyte hyperproliferation and abnormal keratinocyte terminal differentiation[225]. Stimulating ADAM17 activity could improve the epidermal barrier function resulting from reduced ADAM17 expression, by promoting keratinocyte terminal differentiation and cornification. However, inhibiting ADAM17 activity was also beneficial in a murine model of psoriasis[240]. Inhibiting metalloprotease activity led to reduced inflammation and decreased abnormal keratinocyte proliferation and differentiation, presumably as a result of impaired proinflammatory cytokine and EGFR ligand shedding[240]. ADAM10 represents a second ADAM protein, which could also be carefully targeted for epidermal barrier defects. Adherens junctions (AJ) participate in the maintenance of the epidermal barrier. The AJ component E-cadherin is shed by ADAM10, which influences cell adhesion and migration *in vitro*[241]. Keratinocytes exhibit impaired cell adhesion in eczematous dermatitis, which may result from increased ADAM10 mediated shedding of E-cadherin[242]. Thus, depending on the requirements for specific conditions, ADAM proteins could be targeted to either increase or decrease their activity as a means to improve epidermal barrier function.

1.2.6.4 ADAM17 mediated regulation of EGFR signalling in intestinal barrier function

A study by Chalaris *et al*[243] highlights the importance of EGFR signalling to maintain the intestinal barrier. The authors created mice in which ADAM17 was conditionally knocked out in all tissues. In mice, colitis can be induced by treating them with dextran sodium sulphate (DSS). When *ADAM17*$^{-/-}$ mice were treated with DSS, they exhibited significantly worsened intestinal inflammation and ulceration compared to WT mice[243]. The impaired shedding of EGFR ligands in *ADAM17*$^{-/-}$ mice led to an inhibition of intestinal epithelial cell (IEC) proliferation following DSS treatment. However, under normal conditions, the proliferation of colonic tissue in *ADAM17*$^{-/-}$ mice was not significantly different to WT mice[243]. Thus ADAM17 mediated regulation of EGFR signalling would

appear to be required, not for the basal level of IEC proliferation, but rather for the regeneration of IECs in response to injury or inflammation. IEC regeneration is essential for maintenance of the intestinal barrier[243].

1.2.7 ADAM17 loss of function mutation in humans

Using high through-put sequencing technology, our group identified the first loss of function (LOF) mutation in ADAM17 as the cause of a recessively inherited neonatal onset inflammatory skin and bowel disease in a Lebanese family[239]. Of the three children who were born to consanguineous unaffected parents, one child was unaffected, whilst two suffered from the syndrome. The syndrome presented with neonatal onset chronic diarrhoea and lesions of the skin. The skin lesions were perioral and perianal erythema (redness of the skin due to inflammation) with fissures (breaks and tears of the skins), a generalised pustular (pus filled, blister like lesions) rash which developed into psoriaform erythroderma and recurrent infections with *Staphylococcal aureus (S. aureus).* In addition, the children also presented with short or broken hair, wiry and disorganised eyebrows and eyelashes, and thickened nails with had repeated pseudomonas and candida infections. The cutaneous phenotype of the affected boy is illustrated in figure 1.2.3

Figure 1.2.3: Cutaneous phenotype of boy with ADAM17 LOF mutation. Facial erythema (reddening), short hair and wiry disorganised eyebrows (**A**), widespread pustular rash (**B**) and thickened nails (**C**)

(Images taken from[239])

Homozygosity mapping using single nucleotide polymorphism (SNP) arrays, which enable detection of single nucleotide variations within the DNA sequence, was performed on the parents and siblings of the family[239]. Analysis of the SNP data detected segregation to long stretches of SNP homozygosity on chromosomes 2, 5 and 21. Sequencing of exons within this region subsequently revealed a 4 base pair deletion in exon 5 of ADAM17 (c.603-606delCAGA) on chromosome 2. The mutation introduces a premature stop codon truncating the ADAM17 protein. The resulting protein contains only the signal sequence and prodomain, and lacks the metalloprotease, disintegrin, transmembrane and cytoplasmic domains. When peripheral blood mononuclear cells (PBMCs) were stimulated with the bacterial cell wall component lipopolysaccharide (LPS), with PMA, or by T cell activation using an anti-cluster-of-differentiation (CD) 3 or 28 antibody, TNFα secretion was not detected. This was consistent with a loss of functional ADAM17 expression by the patient. *ADAM17*$^{-/-}$ mice die perinatally. Although the affected girl died at 12 years of age from Parvovirus-B19-associated myocarditis, despite repeated skin infections, the affected boy has survived until adulthood and now lives a normal life. This highlights the potential differences in function and requirements of ADAM proteins between humans and mice.

1.2.8 Tylosis with oesophageal cancer

Tylosis with oesophageal cancer (TOC) is a rare condition which is inherited in an autosomal dominant manner. To date five pedigrees have been reported from the UK[244], USA[245], Germany[246], Spain[247] and Finland[248]. TOC is characterised by non-epidermolytic palmoplantar keratoderma (thickening of the skin on the palms and soles), oral leukoplakia (white keratotic patches on the mucous membranes of the oral cavity, e.g. the tongue) and follicular hyperkeratosis. The clinical presentation of TOC is illustrated in figure 1.2.4. While the risk of developing oesophageal cancer is increased by up to 95% by the age of 65 in TOC patients, the incidence of other malignancies is not affected. Linkage and haplotype analysis has allowed researchers to map the TOC locus to a region on chromosome 17q25c[249-251]. Our group has recently identified mutations in the *RHBDF2* gene as the cause of TOC. *RHBDF2*

encodes the inactive Rhomboid 2 (iRhom2) protein. We identified three missense mutations in exon 6 of iRhom2: c.557T>C (p.Ile186Thr) in the UK and USA pedigrees; and c.566C>T (p.Pro189Leu) in the German pedigree[252]. An additional mutation, c.562 G > A (p.Pro189Leu) was identified in the Finnish pedigree in a separate study[248].

Figure 1.2.4: Clinical presentation of tylosis with oesophageal cancer (TOC). Palmoplantar keratoderma (thickening of skin on palms and soles (**A**) and oral leukoplakia (white patches on mucous membranes of the oral cavity (**B**).

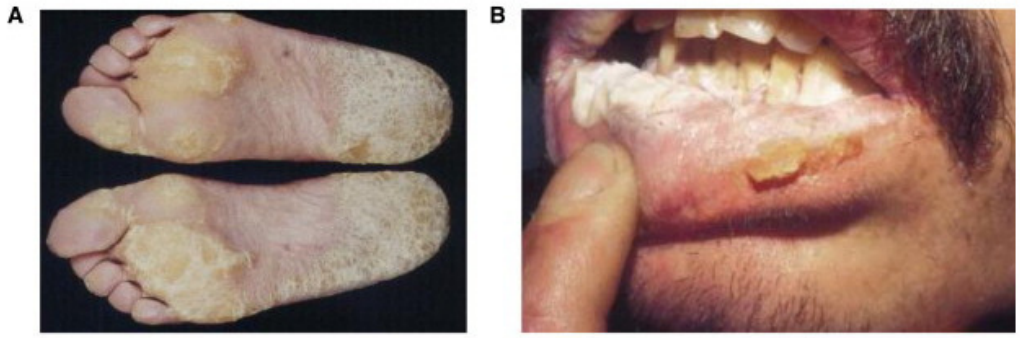

(Images taken from[252])

1.2.9 iRhom2

iRhom2 is a member of the rhomboid family of seven transmembrane spanning intramembrane serine proteases. The active site of rhomboid proteins is contained within the transmembrane domain of rhomboids which cleave substrates within, or immediately adjacent to, their transmembrane domain[253]. The *Rhomboid* gene was first identified in *Drosophila* for its role in development, where it was named after an embryonic mutant phenotype, which resulted in the formation of a rhomboid shaped head[254]. Rhomboids were subsequently discovered to control developmental processes in *Drosophila* through regulation of the EGFR signalling pathway. In *Drosophila*, rhomboids cleave membrane bound members of the EGF ligand family, analogous to their cleavage by specific ADAM proteins in mammals.

A recent study has identified three subgroups of eukaryotic Rhomboid proteins, including the catalytically active proteases, and a group of inactive rhomboid-like proteins (iRhoms)[255]. iRhoms closely resemble rhomboids, but they lack

catalytic residues. Specific members of the iRhom group are missing different catalytic residues. For example, some members lack either the histidine or serine or both residues. iRhom2 misses the catalytic serine721 residue[252]. All iRhom family members have an additional proline residue in the first x position of the rhomboid catalytic GxSx motif, which is absent in active proteases[255]. Although the function of the proline residue is unknown, because of its close proximity to the catalytic serine, it is believed to inhibit the proteolytic activity of the protein[253]. Compared to active rhomboid proteases, iRhoms also have an extended cytoplasmic N-terminal domain, and a conserved 'iRhom homology' loop domain between the first two transmembrane domains (figure 1.2.5). The 'iRhom homology' domain contains 16 cysteine residues which have been proposed to form disulphide bridges; this could be important to maintain the stability of the folded protein[253,255].

Figure 1.2.5: Structure of iRhom proteins. iRhoms lack one or both of the catalytic serine and histidine residues and have an additional proline inserted into the catalytic motif. iRhoms also have an extended cytoplasmic N-terminus and an iRhom homology domain.

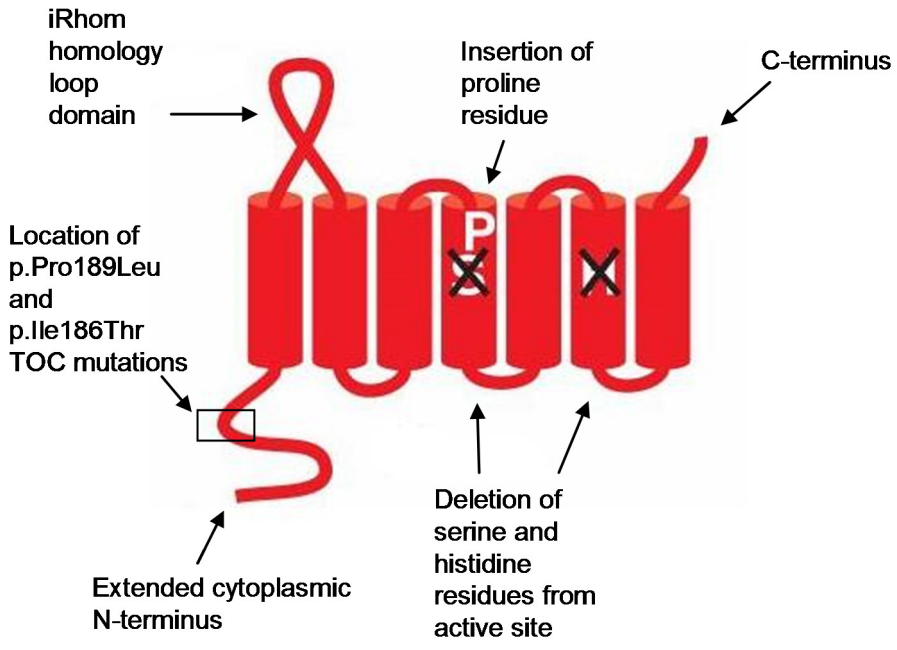

(Image modified from[256])

1.2.9.1 Function of iRhom2

Whereas the EGFR signalling pathway is activated by active rhomboid proteases, *iRhom* has recently been shown to inhibit EGFR signalling in *Drosophila*, a function which is also shared by mammalian iRhom proteins[257]. iRhom localises to the ER where it can bind to EGF ligand family members, promoting their destabilisation and targeting them for endoplasmic reticulum associated degradation (ERAD) (figure 1.2.6). ERAD is a system which targets misfolded proteins of the ER for degradation, and consequently this represents one way in which iRhom2 can regulate the availability of EGF ligand family members which can be shed by ADAM17.

The analysis of *iRhom2*$^{-/-}$ mice in two separate studies has revealed that iRhom2 functions to regulate the localisation and subsequent ability of ADAM17 to interact with its substrates. In the first study, it was observed that iRhom2 is required to function as a cargo receptor, binding to pro-ADAM17 at its site of synthesis in the ER, and mediating its transport to its site of activation within the Golgi apparatus (figure 1.2.6)[256]. TNFα secretion following LPS stimulation was completely reduced in macrophages from *iRhom2*$^{-/-}$ mice compared to macrophages from WT mice, because mature ADAM17 failed to traffic to the cell surface[256]. In the second study, TNFα shedding was also impaired in *iRhom2*$^{-/-}$ mice, and they were more susceptible to infection with *Listeria monocytogenes* than WT mice[258]. WT mice were better able to control the replication of bacteria, such that the bacteria titres recovered from organs of *iRhom2*$^{-/-}$ mice were significantly greater than those recovered from WT mice[258]. These two studies thus highlight that iRhom2 plays a role in the regulation of the ADAM17 dependent immune response. The iRhom2 mediated transport of pro-ADAM17 from the ER represents a crucial step required for the activation and maturation of ADAM17. In the absence of iRhom2, ADAM17 fails to traffic to the cell surface, which has consequences for protection during bacterial infection.

Figure 1.2.6: Functions of iRhom2 in the ER. iRhom2 regulates EGF signalling by binding to ligands of the EGF family and targeting them for ER associated degradation (ERAD). Concurrently, iRhom2 regulates ADAM17 maturation and traffics pro-ADAM17 from its site of synthesis in the ER to the Golgi apparatus ,where it undergoes further processing required for its maturation.

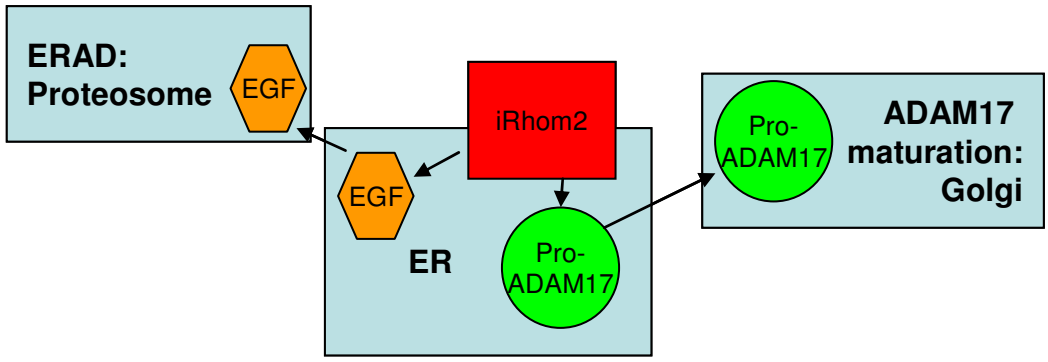

Image modified from[259]

S. aureus is an important pathogen associated with skin disease and as already mentioned in section 1.2.7, the ADAM17 deficient patient suffered from repeated *Staphylococcal* infections. *S. aureus* will therefore be discussed in detail in sections 1.2.10-15.

1.2.10 *S. aureus*

S. aureus causes a wide spectrum of diseases including localised skin disease (e.g. wound infection and impetigo), toxinoses (e.g. toxic shock syndrome and scalded shock syndrome) and systemic diseases (e.g. pneumonia, bacteraemia and endocarditis)[260,261]. It is the most common cause of skin and soft tissue infections[262] and additionally, it exists as a component of the flora in approximately 30% of healthy individuals who are asymptomatically colonised. In such individuals, whilst the bacteria persist without causing infection, they have an increased risk of developing a subsequent infection[261]. Other risk factors for *S. aureus* infections include those whose skin barrier function is compromised, and those who are immunocompromised, for example individuals who suffer from AIDS or an immune deficiency[261]. Strains of *S. aureus* including Methicillin-resistant *S. aureus (*MRSA*)* are associated with both community-acquired and hospital-acquired infections[261]. *S. aureus* is usually transmitted directly by skin-to-skin contact with a colonised or infected individual [261].

1.2.11 *S. aureus* adherence factors and colonisation

S. aureus is primarily an extracellular pathogen. Colonisation with *S. aureus* is initiated when bacteria adhere to plasma or components of the ECM[260]. Adhesion is mediated by surface adhesins of the microbial surface components recognising adhesive matrix molecules (MSCRAMMs) family of proteins[263,264]. MSCRAMMs harbour an amino-terminal signal sequence, targeting them for transport via the Sec dependent secretion system across the inner membrane, periplasm, and outer membrane to the bacterial surface[263]. Ligand binding domains of MSCRAMMs localise to the N-terminus of the protein[263]. The C-terminus of MSCRAMMs contains a conserved LPXTG cell wall sorting signal motif[263,264], which undergoes cleavage between the threonine and glycine residues. The threonine is then anchored to the bacterial cell wall peptidoglycan (PGN) by a sortase[263,264]. Since PGN is directly linked to the ligand binding domains of the MSCRAMMs, bacteria are able to adhere to host cells. MSCRAMMs include fibronectin-binding-proteins (Fnbp) A and B which bind to fibronectin (ECM), clumping factor A and B which bind to fibrinogen (plasma), and collagen binding protein which binds to collagen (ECM)[263].

1.2.12 Cellular invasion by *S. aureus*

Although *S. aureus* is primarily considered an extracellular pathogen, it can invade a variety of cell types. These may be professional phagocytes including neutrophils, monocytes and macrophages, and non-professional phagocytes including endothelial and epithelial cells and fibroblasts[260,265]. Cellular invasion is mediated by some MSCRAMMs including FnbpA and B. FnbpA and B interact with the host cell α5β1 integrin receptor[264]. Following ligand binding, integrin clustering initiates signalling cascades, to activate RhoA, Rac and Cdc42 (Rho GTPases)[266]. This leads to rearrangement of the host cell actin cytoskeleton, triggering bacterial uptake[264]. Cellular invasion enables the bacteria to escape the host cell immune response[264], and consequently, *S. aureus* which has invaded macrophages can persist in the phagocytic vacuole for 3-4 days, before escaping to the cytoplasm and triggering cell lysis[267]. Thus the bacteria can replicate without being eliminated, which contributes to the

establishment of disease. Cellular invasion may also contribute to the development of systemic disease[264].

1.2.13 Cutaneous immune response to *S. aureus*

In addition to forming a protective barrier against invading pathogens, the skin also initiates immune responses against *S. aureus.* Many immune cells reside within the skin including Langerhans cells which persist in the epidermis, and macrophages, dendritic cells, natural killer (NK) cells and T and B cells which persist in the dermis[268]. During *S. aureus* infection, neutrophils are the first cells recruited to the site of infection from the bloodstream[269]. Initially bacterial components including PGN and lipoteichoic acid are recognised by pattern recognition receptors including TLR2 on the cell surface, and NOD2 within the cytoplasm of a variety of cell types including keratinocytes, Langerhans cells, monocytes and dendritic cells[270]. This leads to the production of proinflammatory cytokines, including TNFα, IL-6 and IL-1β[270]. Subsequently, the expression of adhesion molecules required for leukocyte migration is upregulated including L-selectin and lymphocyte function-associated antigen 1 (LFA1) on the surface of neutrophils, and E-selectin and intracellular adhesion molecule 1 (ICAM1) on the endothelium[262,271]. The initial interaction between the neutrophils and the endothelium is weak, meaning that neutrophils roll along the endothelium[262,271]. However, when the endothelium becomes activated, neutrophils adhere firmly[262,271]. Then they migrate across the endothelium by the process of diapedesis and enter the underlying tissue[262,271]. Additionally, neutrophil recruitment requires the expression of chemokines including chemokine (C-X-C motif) ligand (CXCL) 5 and IL-8, which are upregulated in response to bacterial recognition[262,271]. Chemokines activate receptors expressed on the leukocyte surface, which directs leukocyte migration to the infection site[262,271].

At the site of infection, neutrophils use several mechanisms to kill bacteria. Bacteria are internalised into neutrophil phagosomes. They are coated with opsonins including antibodies produced by B cells and components of the complement cascade (e.g. C3b). Opsonised bacteria are recognised by Fc receptors (recognises the constant, Fc portion of the antibody) and complement

receptors expressed on the neutrophil surface[262]. Within the phagosome bacteria may be killed directly, for example by the respiratory burst, which generates reactive oxygen species, including O_2- and H_2O_2[262,269]. Antimicrobial peptides including cathelicidin and defensins may act to inhibit bacterial growth, or may lyse bacterial membranes to directly kill them. Furthermore, proteinases including Cathepsin D and elastase reside in the phagosome and help kill bacteria by degrading bacterial proteins and components[262]. Neutrophils kill bacteria which have not been internalised. They release antimicrobial peptides and proteases from secretory vesicles by degranulation[262,269]. Neutrophils also release neutrophil extracellular traps, which are chromatin fibre projections that are coated with antimicrobial peptides, which trap and kill invading bacteria[272]. The complement cascade also plays an important role in killing bacteria. When host antibody binds to antigen expressed on the surface of bacteria, it can activate the classical pathway of the complement system, which leads to the killing of the bacteria by two methods[265]. As mentioned previously, opsonins including C3b are generated, which enhance subsequent phagocytosis[273]. Alternatively, the components C5b, C6, C7, C8 and C9 interact with each other and form the membrane attack complex, which forms pores in the bacterial membrane resulting in its lysis[273]

With regards to the T cell response, traditionally mouse models have suggested that T helper (Th) 1 cells provide protection during *S. aureus* infection, because they secrete proinflammatory cytokines which recruit neutrophils to the site of infection[262,274,275]. More recently it has emerged that Th17 cells also play a role during *S. aureus* infection[262]. Together with NK cells and γδ T cells, Th17 cells produce IL-17. This causes neutrophil recruitment through the production of chemokines including CXCL1, CXCL2, CXCL5, and IL-8[276]. IL-17 signalling drives ganulopoiesis factor expression, e.g. colony stimulating factors (CSF) 2 and 3, which are required for the production and maintenance of neutrophil populations[276]. Finally, antimicrobial peptides including cathelicidin and human beta defensins (hBD) 2 and 3 are produced in response to IL-17 signalling[262].

Figure 1.2.7: IL-17 signalling pathway. IL-17 produced by cells in the skin including natural killer (NK cells), Th17 cells and γδ T cells leads to the production of antimicrobial, granulopoiesis and chemotactic factors.

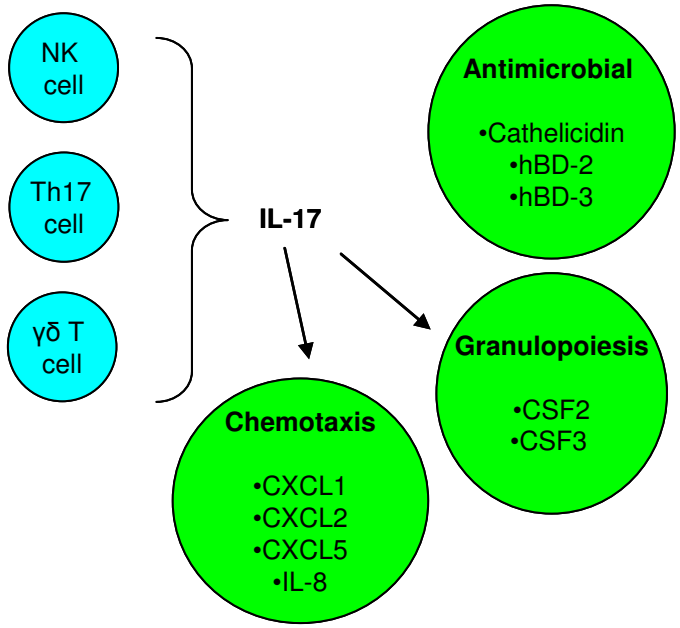

(Adapted from[262])

1.2.14 Immune response evasion by *S. aureus*

Multiple mechanisms exist, which enable *S. aureus* to evade the host immune response. For example, the expression of Staphylococcal Protein A (SpA) on the surface of the bacteria inhibits phagocytosis. SpA is composed of five domains (A-E), each of which can bind to Fcγ on the surface of phagocytes altering its conformation. This prevents the recognition of bacteria opsonised with IgG, thus inhibiting their subsequent uptake[260]. *S. aureus* produces factors which inhibit the complement system. The complement cascade is initiated when the C1q component binds to antibody-antigen complexes. SpA binds to C1q, which in turn inhibits the induction of the cascade[265,277]. The staphylococcal complement inhibitor (SCIN) acts downstream within the complement cascade to inhibit the C3 convertase, thereby preventing the accumulation of the C3b opsonin on the surface of the bacterium[278]. Additionally, components produced by the complement cascade, for example C5a also function as chemoattractants and mediate the recruitment of leukocytes to the site of infection. Their activity can also be inhibited by proteins

expressed by *S. aureus,* for example chemotaxis inhibitory protein of *S. aureus* (CHIPS), which binds to the C5a receptor, and in turn inhibits its activation by C5a [279]. *S. aureus* injects cytolytic toxins including the α- and β-haemolysins and Panton-Valentine leukocidin (PVL) into the host cell plasma membrane to trigger its lysis[260]. Monomer subunits delivered into the cell initially bind to the plasma membrane and oligomerise to form a β barrel pore, which facilitates the influx and efflux of small molecules and ions[260]. This leads to changes in ionic gradients, and an increase in osmotic pressure, which in turn causes water to enter the cell, triggering its subsequent swelling and rupturing[260]. Cytolytic toxins display cytotoxicity towards specific cells types. While α-haemolysin lyses platelets, erythrocytes and monocytes, PVL is particularly cytotoxic towards myeloid cells[265]. Additionally, β-haemolysin has been observed to lyse erythrocytes, monocytes, neutrophils and lymphocytes[265].

The production of the superantigens toxic shock syndrome toxin-1 and the staphylococcal enterotoxins can have detrimental effects on T cell signalling[260,265]. T cell receptors (TCR) expressed on the surface of T cells recognise specific peptides bound to major histocompatibility molecules on the surface of antigen presenting cells[280]. However, TCRs can also be activated non-specifically by bacterial and viral protein superantigens. This leads to a massive inflammatory response, where up to 1 in 5 T cells may be activated, compared to approximately 1 in 10,000 T cells activated during a normal antigen presentation[281]. Superantigen mediated activation of T cells is characterised by non-specific T cell clonal expansion and massive T cell derived pro-inflammatory cytokine release. This is followed by the deletion or anergy of responding T cells, which leads to the substantial loss of the T cell repertoire[280]. Moreover, the uncoordinated release of proinflammatory cytokines can be detrimental to the host and can lead to multi-organ failure and subsequent death[282]. Additionally, SpA has also been shown to act as a superantigen for B cells[260,265,283]. By non-specifically interacting with IgM, Spa induced the polyclonal expansion of non-specific B cells and subsequent depletion of the B cell pool [284].

1.2.15 Regulation of virulence factors

The importance of gene expression regulation has already been discussed for *S. flexneri* and EPEC in section 1.1.20.3. In *S. aureus* gene expression is under the control of several global regulatory systems including the accessory gene regulator (agr) system and the staphylococcal accessory regulator (sarA)[260,265]. Virulence factor expression is controlled in response to stimuli including cell density, nutrient availability, and environmental cues such as temperature, pH and osmolarity[260,265,285]. The production of specific virulence factors is controlled in a temporal manner, which means that specific virulence factors are expressed at the appropriate time point during infection, and in quantities which are sufficient for their survival within the host depending on the conditions of the local environment[260,265,285]. For example, the co-ordinated actions of the regulatory systems ensures that surface proteins including adhesins are expressed during the early stages of infection, whilst secreted proteins are upregulated during the later stages of infection[260]. The control of gene regulation is pivotal for *S. aureus* to establish a successful infection.

1.2.16 Aims and hypotheses (Results chapter 5)

As described in section 1.2.7, loss of functional ADAM17 leads to recurrent *Staphylococcal* infections in a patient suffering from an inflammatory skin and bowel syndrome[239], suggesting that ADAM17 acts to provide protection during bacterial infection. It has recently been shown that iRhom2 is required for ADAM17 maturation and consequently plays a role in the regulation of the ADAM17 dependent immune response[256]; iRhom2$^{-/-}$ mice are more susceptible than WT mice to infection with *L. monocytogenes* (section 1.2.9)[258]. The skin condition TOC is caused by mutations in *RHBDF2* (section 1.2.8), which make iRhom2 overactive and therefore, TOC mutations are predicted to increase ADAM17 activity. The aim of this project was to consider how bacterial infection was affected by ADAM17 activity, using *S. aureus* which is a relevant pathogen to skin disease as an *in vitro* model of infection. Attempts made to immortalise keratinocytes from the ADAM17 deficient patient were unsuccessful, so to mimic loss of functional ADAM17 expression in *vitro*, keratinocyte cell lines

were treated with siRNA against ADAM17. Infection was then compared in untreated keratinocytes and keratinocytes treated with ADAM17 siRNA. Knocking down ADAM17 was predicted to increase *S. aureus* adhesion and invasion. The effect of increased ADAM17 activity on infection was then investigated by comparing infection in control and TOC keratinocytes. It was predicted that ADAM17 would provide protection, with TOC keratinocytes exhibiting reduced infection compared to control keratinocytes. Assuming that the results obtained suggest that functional ADAM17 reduced infection, the way in which ADAM17 acts will subsequently be explored.

~ Chapter 2 ~

Materials and Methods

2.1 Cell Culture

2.1.1. Cell lines

Caco-2 and HT-29 cells are human intestinal epithelial cell lines derived from a colorectal adenocarcinoma. The cell lines are obtained from two different patients. HT-29 cells and Caco-2 cells are derived from well differentiated and moderately differentiated adenocarcinomas respectively. Caco-2 cells spontaneously express differentiation markers and form polarised monolayers with microvilli and tight junctions upon reaching confluence[286]. HT-29 cells however, remain undifferentiated under normal culture conditions unless they are treated with drugs including colchicine, nocodazole and taxol[287]. Both cell lines were obtained from Dr Sahira Khalaf at the Blizard Institute, Whitechapel, London. HeLa cells are derived from a cervical carcinoma and lack endogenous Cx expression. NEB1 and K17 cells are control keratinocyte (skin) cell lines, whilst TYLK1 and TYLK2 cells are TOC keratinocyte (skin) cell lines. TYLK1 and TYLK2 cells are derived from biopsies taken from the skin of a male and female TOC patient respectively, from which primary keratinocytes were isolated and grown in the presence of a γ-irradiated 3T3 mouse fibroblast feeder layer, and were immortalised with HPV16 (E6/E7)[252]. HeLa, NEB1, K17, TYLK1 and TYLK2 cells were obtained from the Kelsell group.

2.1.2 Cell culture conditions

Cells were grown in Dulbecco's Modified Eagle Medium (DMEM) supplemented with 2 mM L-glutamine, 10% foetal bovine serum (FBS) (% v/v), 5,000 U/ml penicillin and 5,000 µg/ml streptomycin (complete media) at 37°C in an incubator supplemented with 5% CO_2. Before passaging cells, the culture media was removed and the cells were washed with phosphate buffered saline (PBS) to remove serum, which inhibits trypsinisation. The cells were detached from the culture flask using 0.05% Trypsin (% w/v) with 0.53 mM ethylenediaminotetraacetic acid (EDTA) (Invitrogen). Trypsin detaches cells by cleaving proteins responsible for the adherence of cells to the culture flask, while EDTA is an ion chelator which enhances the actions of trypsin.

Trypsinising cells were incubated at 37ºC until cells had detached. Subsequently, the activity of trypsin was inhibited by quenching cells in an equal volume of cell culture medium, before centrifugation at 1000 RPM for 5 minutes. The supernatant was then removed, and the pellet was resuspended in the required volume of complete medium.

2.1.3 Cryopreservation of cells: generation of cell line stocks

Cells were trysinised as described in section 2.1.2, centrifuged and the supernatant was removed from the pellet. The pellet was resuspended in the required volume of 10% DMSO (dimethyl sulphoxide) (% v/v) / 90% FBS (% v/v) and aliquoted into cryovials. Cells were frozen slowly at -80ºC for 24 hours before transfer to vapour phase liquid nitrogen for long-term storage. To bring cells up from frozen, cryovials were incubated on dry ice prior to defrosting in a water bath heated to 37ºC. Cells were added to pre-warmed cell culture media and centrifuged at 1000 RPM for 5 minutes to remove the DMSO which is toxic to cells. The supernatant was removed and the pellet was resuspended in complete medium before incubation at 37ºC.

2.1.4 Transfecting HeLa cells with plasmid constructs

The plasmid constructs used to transfect HeLa cells are listed in table 2.1. A vector map of the pmCherry-N1 vector is shown in figure 2.1. HeLa cells were seeded in a 12-well plate at a density of 7.5×10^4 24 hours prior to transfection. 500 ng/well of plasmid construct and 1.5 µl/well of FuGENE 6 (Roche, Basel, Switzerland) transfection reagent were mixed in 50 µl of serum and antibiotic free DMEM, and incubated at room temperature for 20 minutes. The transfection complex was then added drop-wise to cell culture media prior to incubation at 37ºC. Twenty-four hours later, the media was replaced with fresh complete media. A further twenty-four hours later, transfected cells were processed for bacterial infections and immunofluorescence. The transfection efficiency was approximately 50% 48 hours post-transfection.

Table 2.1: Plasmid constructs

Plasmid Construct	Description	Ref/ Source
p-(WT)Cx26-mCherry	WT Cx26 cDNA was cloned and inserted into the EcoRI (GAATTC) and BamHI (CGATCC) restriction sites of the pmCherry-N1 vector (Commercially available Clontech, California, USA)	Dr P. Martin, Glasgow Caledonia University, Glasgow, Scotland
p-(R143W)Cx26-mCherry	The p.R143W mutation was introduced into the (WT)Cx26-mCherry vector construct by site directed mutagenesis	This study
pmCherry	Vector only: the WT Cx26 insert was removed from the (WT)Cx26-mCherry vector construct and the EcoRI and BamHI restriction sites were made blunt ended and then ligated	This study
pGFP	Plasmid pFPV25.1 expressing *gfpmut3a* gene	[288]

Figure 2.1: Vector map and multiple cloning site of pmCherry-N1. Vector backbone **(a)** and multiple cloning site (MCS) sequence (**b)**. In the p-(WT)Cx26-mCherry construct the Cx26 insert is cloned into the EcoRI and BamHI restriction sites. In the pmCherry construct, the Cx26 insert has been removed, and the EcoRI and BamHI restriction sites have been made blunt ended and then ligated. In the p-(WT)Cx26-mCherry and p-(R143W)Cx26-mCherry plasmid constructs, the coding region of Cx26 is upstream of mCherry. The expression of mCherry or the Cx26-mCherry fusion protein is under the control of the cytomegalovirus (CMV) promoter. The translational efficiency of the plasmid construct is enhanced in eukaryotic systems by the Kozak consensus sequence, located immediately upstream of the mCherry gene. The vector contains a *kanamycin* (*kan*) resistant gene, thus meaning that the plasmid can be selected for using LB agar or LB broth containing kanamycin.

a)

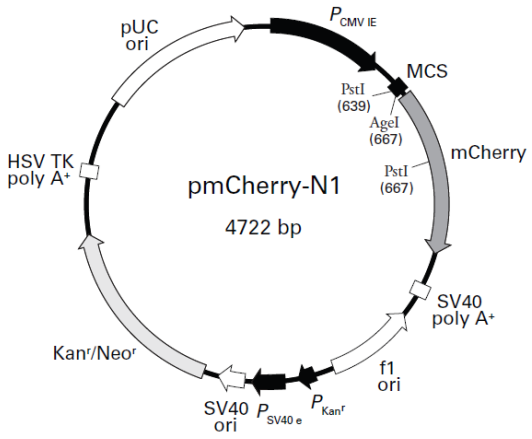

b)

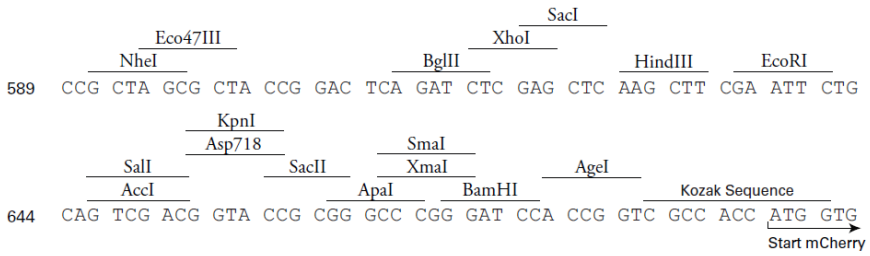

(Taken from pmCherry-N1 vector information at http://www.clontech.com/xxclt_ibcGetAttachment.jsp?cItemId=44287&minisite=10030&secItmId=16172)

2.1.5 siRNA knock down

ON-TARGET plus SMART pool siRNA directed against human *GJB2,* human *ADAM17,* human *ITGB1* and a non-targeting pool (NTP) siRNA (negative control) (all reagents, Thermo Fisher Dharmacon, Colorado, USA) were used for siRNA studies. *GJB2* was knocked down in HT-29 and Caco-2 cells. *ADAM17* was knocked down in HT-29, K17, NEB1, TYLK1 and TYLK2 cells. *ITGB1* was knocked down in K17 and NEB1 cells.

Cells were seeded in a 12-well plate at a density of 1×10^5 per well 24 hours prior to transfection. Serum and antibiotic free DMEM was mixed with siRNA in one tube and DharmaFECT I (Thermo Fisher Dharmacon, Colorado, USA) transfection reagent in another tube. *GJB2* siRNA was used at a final concentration of 25 nM/well and *ADAM17*, *ITGB1* and NTP siRNAs were used at final concentrations of 100 nM/well. The two tubes were incubated for 5 minutes, before mixing the contents of both tubes, and incubating for a further 20 minutes at room temperature. Subsequently, antibiotic free DMEM was added to the transfection complex. The cells were washed with antibiotic free DMEM, and then incubated with the transfection complex at 37ºC. Twenty-four hours later for *GJB2* knockdowns, and forty-eight hours later for *ADAM17* and *ITGB1* knockdowns, cells were processed for bacterial infections, quantitative RT-PCR, immunofluorescence and western blotting.

2.16 Peripheral blood mononuclear cell (PBMC) isolation and culture

PBMC isolations were performed by Matthew Brooke (Centre for Cutaneous Research). PBMCs were isolated from venous blood samples collected from the ADAM17 deficient male patient, his mother, the male and female TOC patients and two age-matched controls. Heparin was added to the blood samples to prevent them from clotting. Equal volumes of blood and PBS were then pipetted into a 50 ml tube, and subsequently underlain with 10 ml of Ficoll. The tube was then spun at 1600 RPM with the brake off for 30 minutes, to ensure that deceleration of the centrifuge did not disrupt the density gradient, meaning that components of the blood were found in different layers. The top plasma layer was then removed and discarded, before drawing off the lymphocyte layer at the density gradient interphase, using a plastic Pasteur pipette. PBMCs were then transferred into a 15 ml tube, which was topped up with PBS, and underwent two subsequent wash steps in PBS by centrifugation at 1000 RPM for 10 minutes. PBMCs ($2x10^5$/well of a 96 well plate (BD Biosciences, Franklin Lakes, New Jersey, USA)) were then cultured in complete media for 24 hours in the presence or absence of 1 ng/ml of lipopolysaccharide (LPS, InvivoGen, San Diego, California, USA), 100 ng/ml of phorbol 12-myrisate 13-acetate (PMA, Sigma-Aldrich, Dorset, UK), or in anti-CD3-coated-96 well plates (BD

Biosciences, Franklin Lakes, New Jersey, USA) with 1 µg/ml of anti-CD28 antibody (eBioscience, San Diego, California, USA). Concentrations of CXCL5, IL-12/23, IL-17-A, IL-17-F, IL-24 and TNFα were measured by ELISA (section 2.8).

2.2 DNA and RNA

2.2.1 DNA quantification

The concentration and purity of DNA samples were measured using a Nanodrop ND-1000 spectrophotometer, which measured the optical density of samples. The concentration of the DNA sample was measured by absorbance at 260 nm. The purity of the DNA sample was measured by absorbance at 260 nm and 280 nm. A ratio of greater than 1.8 for 260/280 and 260/230 was accepted as pure, as 260/280 ratios below 1.8 may indicate protein contamination, while 260/230 ratios below 1.8 many indicate contamination with salts or solvents.

2.2.2 Primer design

Gene sequences were obtained from NCBI Gene (available from http://www.ncbi.nlm.nih.gov/gene). The primer and probe sequences used in this study are listed in table 2.2. Primer and probe sequences for normal and quantitative RT-PCR were designed using Primer-BLAST (available from http://www.ncbi.nlm.nih.gov/tools/primer-blast/). Primers for quantitative RT-PCR were designed so that they spanned an exon-exon junction, to prevent non-coding DNA sequences (introns) within genomic DNA being amplified, thereby ensuring accurate quantification of mRNA. Primer sequences for site directed mutagenesis were designed using PrimerX (available from http://www.bioinformatics.org/primerx/). Primers were obtained from Sigma Aldrich, Dorset, UK.

Table 2.2: Primer and probe sequences

Gene	Primer pair and sequence (5' to 3')	Product size (bp)	AT (℃)	Ref/ Source
ADAM17	ADAM17 Forward 5'-GGTTCCTTTCGTGCTGGCGC-3' ADAM17 Reverse 5' AAGCTTCTCGAGTCTCTGGTGGG-3' Probe 5'-[6FAM]- CGCGACCTCCGGATGACCCGGGCT- [BHQ1]-3'	73	60	Designed by Matthew Brooke
CSF2	CSF2 Forward 5'-AGCCCTGGGAGCATGTGAAT-3' CSF2 Reverse 5'-ACTGTTTCATTCATCTCAGCAGC-3'	88	60	This study
CSF3	CSF3 Forward 5'-AGCTTCCTGCTCAAGTGCTTA-3' CSF3 Reverse 5'-TTGTAGGTGGCACACTCACT-3'	95	60	This study
CXCL5	CXCL5 Forward 5'-ACGCAAGGAGTTCATCCCAA-3' CXCL5 Reverse 5'- GTTCTTCAGGGAGGCTACCAC-3'	96	60	This study
DEFB103A	hBD-3 Forward 5'-TGGTGCCTGTTCCAGGTCA-3' hBD-3 Reverse 5'-TGTTCCTCCTTTGGAAGGCA-3'	109	56	This study
DEFB4A	hBD-2 Forward 5'-AGACTCAGCTCCTGGTGAAGC-3' hBD-2 Reverse 5'-CAAAAACACCTGGAAGAGGCATCAG-3'	103	56	This study
GAPDH	GAPDH Forward 5'- TGGCCCCTCCGGGAAACTGT-3' GAPDH Reverse 5'- CCTTGCCCACAGCCTTGGCA-3' Probe 5'-[HEX]- CGTGATGGCCGCGGGGCTCTCCA-[BHQ1]- 3'	92 -	60	Designed by Matthew Brooke
GJB2	Cx26 BF 5'- CCAGGCTGCAAGAACGTGTG-3' Cx26 BR 5'- GGGCAATGCGTTAAACTGGC -3'	522	60	[289]
	Cx26 RT-QPCR Forward 5'-CCTCCCGACGCAGAGCAAACC-3' Cx26 RT-QPCR Reverse 5'-GCTGGTGGAGTGTTTGTTCACACC-3'	92	60	This study

	Probe 5'-[6FAM]- GGGGCACGCTGCAGACGATCCTGGGG- [BHQ1]-3'			
	CMVF 5'-CGCAAATGGGCGGTAGGCGTG-3' Mcherry Reverse 5'- AAGCTGTCCTTCCCCGAG- 3'	442	60	This study and Clontech
	p.143W Site Directed Mutagenesis Forward 5'- AAGCAGCATCTTCTTCTGGGTCATCTTCG AAGCC-3' p.143W Site Directed Mutagenesis Reverse 5'- GGCTTCGAAGATGACCCAGAAGAAGATGC TGCTTG-3'	-	-	This study
IL-24	IL-24 Forward 5'-TGAATGGTGAAGGTGCCTGT-3' IL-24 Reverse 5'-TCTTGTCCCTCTGGTCCTGT-3'	99	60	This study
MMP9	MMP9 Forward 5'-TTCTGCCCGGACCAAGGATA-3' MMP9 Reverse 5'ACATAGGGTACATGAGCGCC-3'	109	60	This study

2.2.3 Reverse transcriptase polymerase chain reaction (RT-PCR): normal and quantitative

2.2.3.1 Total RNA extraction from cells

Total RNA was extracted from cells using the QIAGEN RNeasy mini RNA extraction kit (QIAGEN, Crawley, UK) according to the manufacturers' protocol. Briefly, cells were lysed in denaturing buffer, which had 1% (v/v) β-mercaptoethanol added to it. They were then mixed with 70% (v/v) ethanol, which facilitated the binding of RNA to the spin column. The column was then incubated with RNAse-free DNAse, which degraded any DNA contamination of the RNA sample. RNA was subsequently eluted in 30 µl of RNAse free H_2O. The concentration and purity of the RNA sample was then quantified using a Nanodrop ND-1000 spectrophotometer.

2.2.3.2 cDNA synthesis

cDNA synthesis was performed using the SuperScript® II Reverse Transciptase kit (Invitrogen, California, USA) according to the manufacturers' protocol. Briefly, reactions contained 200 ng of total RNA, 0.5 µl of 200 µM random hexamers, and 1 µl of 10 mM dNTPs, made up to a 12 µl final volume with dH_2O. The reactions were incubated at 65ºC for 5 minutes, chilled on ice, and 4 µl of 5x first strand buffer, 2 µl of 0.1 M DTT and 1 µl of RNase OUT (all Invitrogen, California, USA) were added to the reaction. RNase OUT is a recombinant ribonuclease inhibitor, which prevents the degradation of RNA. Reactions were incubated at 25ºC for 2 minutes and chilled on ice, before 1 µl (200 U/µl) of superscript II reverse transcriptase (Invitrogen, California, USA) was added. Samples were then incubated at 42ºC for 50 minutes, and then 70ºC for 15 minutes.

2.2.3.3 cDNA amplification by normal RT-PCR

PCR was performed in a 25 µl reaction containing: 200 ng of cDNA, 2.5 µl of NH_4 Reaction Buffer, 0.75 µl of 50 mM $MgCl_2$, 0.5 µl of dNTP mix (200 nM of each dNTP), 0.25 µl of BIOTAQ DNA Polymerase (all BIOLINE, London, UK), 2.5 µl of 50 µM of each primer and dH_20. Reactions were carried out using a DNA engine tetrad PCR system. PCR conditions were: initial denaturation at 95°C for 1 minute, 35 cycles at 95°C for 15 seconds (denaturation), annealing for 15 seconds (temperature dependent on primer pair, see table 2.2) and 72° for 30 seconds (extension), followed by final extension at 72°C for 5 minutes.

2.2.3.4 Agarose gel electrophoresis

PCR products were analysed on agarose gels. Agarose (Sigma-Aldrich, Dorset, UK) was dissolved in 1x TBE (0.89 M tris base, 0.89 M boric acid, 0.2 M EDTA, pH 8.0) in a microwave to give 1-1.3% (w/v) gels. The mixture was cooled, before the addition of ethidium bromide to a final concentration of 20 µg/ml. Gels were poured into a casting gel tray containing combs, allowed to set, and samples were loaded into wells with DNA loading buffer (6x DNA loading buffer:

0.25% (v/v) bromophenol blue, 0.25% (v/v) xylene cyanol FF, 30% (v/v) glycerol) diluted to 1x in TE buffer (10 mM Tris, 1 mM EDTA, pH 8.0) (alongside a 1 kB Plus ladder (Invitrogen, California, USA), which was used to determine product size. Gels were run in 1x TBE at 110 V. Bands were visualised on a UV transilluminator and photographed.

2.2.3.5 cDNA amplification by quantitative RT-PCR (qRT-PCR)

While normal PCR shows the amount of DNA in a sample which has been amplified at the end of the PCR reaction, qPCR makes it possible to quantify the cycle at which DNA amplification begins. The method relies on the use of fluorescent dyes including SYBR Green I, which bind to DNA, or for more accurate quantification, fluorescently labeled probes which bind to specific DNA sequences.

GJB2 and *ADAM17* QPCRs were carried out using the Rotor-Gene Multiplex PCR kit (Qiagen, Crawley, UK). The reaction was carried out in a 25 µl mixture containing: 12.5 µl of 2x Rotor-Gene Multiplex PCR Buffer (Qiagen, Crawley, UK), 1 µl of 10 µM of each primer, 0.5 µl of 10 µM of GAPDH and ADAM17 probes, or 0.5 µl of 10 µM of GAPDH and 0.125 µl of 10 µM of Cx26 probes, 400 ng of cDNA and dH_2O.

CSF2, CSF3, CXCL5, DEFB103A, DEFB4A, IL24 and *MMP9* PCRs were carried out in two separate reactions, one which quantified the expression of *GAPDH*, and the other which quantified the expression of the gene of interest. The *GAPDH* reaction was carried out as described in the previous paragraph using the Rotor-Gene Multiplex PCR kit (Qiagen, Crawley, UK), i.e. in a 25 µl mixture containing: 12.5 µl of 2x Rotor-Gene Multiplex PCR Buffer (Qiagen, Crawley, UK), 1 µl of 10 µM of each primer, 0.5 µl of 10 µM of GAPDH probe, 400 ng of cDNA and dH_2O. The other reaction was carried out using the QuantiTect SYBR Green PCR Kit (Qiagen, Crawley, UK), also in a 25 µl mixture containing: 12.5 µl of 2x QuantiTect SYBR Green PCR Master Mix (Qiagen, Crawley, UK), 1 µl of 10 µM of each primer, 400 ng of cDNA and dH_2O.

For all qRT-PCRs, PCR conditions were: initial denaturation at 95°C for 10 minutes, and 45 cycles at 95°C for 45 seconds and 60°C for 50 seconds.

Thermal cycling and fluorescent monitoring were performed on a Rotor-Gene Q (Qiagen, Crawley, UK). The expression of the gene of interest was calculated relative to the expression of the reference gene *GAPDH*, using the ΔΔCT method. The formula used was: Relative expression (RE) = 2^ (-ΔΔCT) where:

- CT = PCR cycle in which the sample fluorescent intensity exceeds that of the background
- ΔCT of sample (siRNA treated sample) = CT target gene – CT reference gene
- ΔCT of calibrator (NTP siRNA treated sample) = CT target gene – CT reference gene
- ΔΔCT = ΔCT (sample) – ΔCT (calibrator)

2.2.4 *Illumina™* Gene Expression Profiling

Gene expression was analysed in four comparisons:

- Uninfected NTP siRNA treated K17 keratinocytes vs uninfected ADAM17 siRNA treated K17 keratinocytes
- Uninfected NTP siRNA treated TYLK1 keratinocytes vs uninfected ADAM17 siRNA treated TYLK1 keratinocytes
- *S. aureus* infected NTP siRNA treated K17 keratinocytes vs *S. aureus* infected ADAM17 siRNA treated K17 keratinocytes
- *S. aureus* infected NTP siRNA treated TYLK1 keratinocytes vs *S. aureus* infected ADAM17 siRNA treated TYLK1 keratinocytes

Total RNA extracted from cells using the QIAGEN RNeasy mini RNA extraction kit (Qiagen, Crawley, UK) was hybridised to *Illumina*™ Sentrix Human HT12v4 Expression BeadChips in triplicate by Ms Mimoza Hoti at the Genome Centre, Charterhouse Square, London. Each chip contains 47,231 probes and can measure the gene expression for twelve samples in parallel. The probes are sequences of 50 base pairs in length, which target the 3' end of genes. Hybridisation was detected using fluorescently labeled targets which bind to probe sequences, and the strength of the signal generated depended on the

amount of total RNA bound by the probe. Data analysis was subsequently performed using *Illumina*'s BeadStudio™ Data Analysis Software. A list of a minimum of 200 differentially expressed genes for each comparison, with diff scores of ±22 was compiled and analysed using GeneGo pathway analysis software (Thomas Reuters). Information about specific genes of interest was obtained using the online GeneCards encyclopedia (http://www.genecards.org). Additionally, lists of genes with the 30 most upregulated and downregulated genes for each comparison were complied.

2.2.5 Sequencing

The pmCherry construct was sequenced using CMVF and Mcherry reverse primers (table 2.1). The p-(R143W)Cx26-mCherry construct was sequenced using Cx26 BF and Cx26 BR primers. Direct sequencing of plasmid constructs was performed by the cycle sequencing chain termination method. The incorporation of fluorescently-labelled dideoxynucleotides into the extending chain of nucleotides causes chain termination, and the fluorescent signal is detected and converted into a sequence. Constructs were sequenced in forward and reverse directions in independent reactions using the BigDye Terminator version 3.1. Cycle Sequencing kit (Applied Biosystems, Foster City, Canada). The sequencing reaction was carried out in an 11.5 µl mixture containing: 500 ng of plasmid, 1 µl of 10 µM of primer, 1 µl of BigDye Terminator mix (v 3.1) (Applied Biosystems, Foster City, Canada), 3 µl of Better Buffer (Microzone, Ottawa, Canada) and dH_2O. PCR conditions were 25 cycles of 96°C for 1 minute (denaturation), 50°C for 15 seconds (annealing), and 60°C for 1 minute (extension).

The sequencing reactions were subsequently transferred to plates. The samples were precipitated by the addition of 2 µl of 125 mM EDTA and 30 µl of ice-cold 100% (v/v) ethanol, incubation on ice for 10 minutes, and centrifugation at 4000 RPM for 20 minutes. Plates were inverted and centrifuged at 250 RPM for 30 seconds to remove the supernatant. 130 µl of 70% (v/v) ethanol was subsequently added to the samples, which were incubated at room temperature for 5 minutes. The samples were then centrifuged at 4000 RPM for 5 minutes, and then the supernatant was removed as before. Samples were dried in a

heating block at 95ºC for 10 seconds. The following steps were performed by Dr Claire Scott. Samples were resuspended in 10 µl of HiDi™ formamide, transferred to an ABI plate (both Applied Biosystems, Foster City, Canada,) and denatured by incubation at 95ºC for 3 minutes, before loading onto the sequencer.

2.2.5.1 Sequence analysis

Sequence traces were viewed using Chromas Lite 2.1 software (available from http://technelysium.com.au/). The nomenclature for nucleotide positions is given by the position from the start of the ATG (methionine) start codon where A=+1. The sequence traces were compared to WT sequences obtained from the Ensembl Genome browser (available from http://www.ensembl.org/index.html) using MultAlin (available from http://multalin.toulouse.inra.fr/multalin/).

2.3 Plasmid molecular biology

2.3.1 pmCherry construct generation

A restriction digest was performed to remove the Cx26 insert from the p-(WT)Cx26-mCherry plasmid construct, to generate the pmCherry (vector only) construct. Restriction enzymes recognise, and cleave specific DNA sequences (termed restriction sites) within DNA molecules. The reaction was carried out in a 20 µl volume containing: 1 µg of p-(WT)Cx26-mCherry construct, 2 µl of NEB buffer, 0.2 µg of bovine serum albumin (BSA), 1 µl of EcoRI and BamHI restriction enzymes (all New England Biolabs (NEB), Massachusetts, USA), and dH_2O, incubated at 37°C for 90 minutes. The digested product was run on a 1% (w/v) agarose gel at 100 V, and the vector DNA was excised and purified using a MinElute Gel Extraction kit (Qiagen, Crawley, UK).

In preparation for EcoRI and BamHI restriction site ligation, purified vector DNA was made blunt ended using an End-It™ DNA End-Repair kit (Epicentre Biotechnologies, Madison, Wisconsin, USA). Whereas DNA molecules with sticky ends have a stretch of unpaired nucleotides at the end of one DNA

strand, both DNA strands in a DNA molecule with blunt ends terminate in a base pair. The reaction performed made both portions of the vector DNA compatible for ligation. The reaction was performed according to the manufacturer's protocol. Briefly, a 40 µl reaction volume containing: 0.5 µg of purified DNA, 4 µl of End-Repair Buffer, 4 µl of dNTP mix, 4 µl of ATP (all Epicentre Biotechnologies, Madison, Wisconsin, USA), and dH_2O, was incubated at room temperature for 45 minutes. The reaction was terminated by heating at 70°C for 10 minutes.

The ligation was set up in a 20 µl reaction containing: 12 µl of blunt ended vector DNA, 2 µl of ligation buffer, 1 µl of T4 DNA Ligase (400,000 U/ml) (NEB, Massachusetts, USA) and dH_2O. The reaction was incubated at 16°C overnight and heat inactivated at 65°C for 10 minutes. The plasmid was subsequently transformed in bacteria, selected for by antibiotic resistance and prepared as described in sections 2.3.2 and 2.3.3. Finally, the plasmid was sequenced as described in section 2.2.5.

2.3.2 Transformation of chemically-competent E. coli with plasmid constructs

One vial containing 50 µl of One Shot® TOP10 chemically-competent *E. coli* cells (Invitrogen, Massachusetts, USA) was thawed on ice and then mixed with 5 µl of DNA. The transformation mixtures were incubated on ice for 30 minutes, and then heat shocked at 42°C for 30 seconds to incorporate the DNA into cells. They were subsequently incubated on ice for 2 minutes. 250 µl of SOC medium (Invitrogen, Massachusetts, USA) prewarmed to 37°C was then added to the transformation mixtures, which were then shaken at 225 RPM at 37°C for 1 hour. Subsequently 50 µl of the transformation mixture was spread onto Luria-Bertani (LB) Agar (12-15 g/l agar, 10 g/l tryptone, 5 g/ml yeast extract and 10 g/l NaCl) plates containing 50 µg/ml kanamycin, and incubated at 37°C overnight.

2.3.3 Plasmid constructs DNA extraction from *E. coli*

As the plasmid constructs contain a kanamycin resistance gene, bacteria which have incorporated them grew on the plate. Single colonies were isolated from the plate and grown in LB Broth (10 g/l of tryptone, 5 g/l of yeast extract and 10 g/l of NaCl) containing 50 µg/ml kanamycin overnight at 37℃ in an orbital shaker. DNA was subsequently extracted using a QIAprep® Spin MiniPrep kit according to the manufacturer's protocol.

2.3.4 Site directed mutagenesis: p-(R143W)Cx26-mCherry construct generation

The p.R143W mutation was introduced into the p-(WT)Cx26-mCherry construct by site directed mutagenesis using the QuickChange® Site-Directed Mutagenesis Kit (Stratagene Agilent, Stockport, Cheshire). Primer sequences containing the p.R143W substitution are shown in table 2.1. Primers were purified by polyacrylamide gel electrophoresis. PCR was carried out in a 50 µl volume containing: 20 ng of double stranded plasmid DNA, 125 ng of each primer, 1 µl of dNTPs, 1 µl of *PfuTurbo* DNA polymerase (2.5 units/µl), 5 µl of reaction buffer (all Stratagene Agilent, Stockport, Cheshire) and dH_2O. PCR conditions were: initial denaturation at 95℃ for 30 seconds; and 16 cycles at 95℃ for 30 seconds (denaturation), 55℃ for 1 minute (annealing) and 68℃ for 6 minutes (extension). The samples were cooled by incubation on ice for 2 minutes, before the addition of 1 µl of DpnI restriction enzyme (10 units/µl) (Stratagene Agilent, Stockport, Cheshire. Samples were subsequently incubated at 37℃ for 1 hour to digest parental methylated and hemimethylated DNA. Analogous to the pmCherry construct, the p-(R143W)Cx26-mCherry construct plasmid was transformed in bacteria, selected for by antibiotic resistance and prepared as described in sections 2.3.2 and 2.3.3. Finally the plasmid was sequenced as described in section 2.2.5.

2.4 Bacteria

The bacterial strains used in this study are listed in table 2.3. Bacteria were grown in LB Broth in an orbital shaker at 37℃, or in serum and antibiotic free DMEM statically at 37℃ in a 5% CO_2 atmosphere.

Table 2.3: Bacterial strains

Strain	Description	Ref/ Source
EPEC E69	Wild type EPEC	[290]
EPEC E69 Δ*escN*	EPEC deficient in type III secretion	Dr O Marchès, Queen Mary, University of London
EPEC JPN15	EPEC which is missing the EAF plasmid	[290]
EPEC JPN15 Δ*escN*	EPEC which is missing the EAF plasmid and deficient in type III secretion	Dr O Marchès, Queen Mary, University of London
***S. aureus* Staph. Oxford (NCTC 6571)**	Wild type *S. aureus*	[291]
***S. flexneri* serotype 2a (2457T)**	Wild type *S. flexneri*	ATCC

EPEC E69 Δ*escN* was selected for by kanamycin resistance. In this study, EPEC JPN15 and EPEC JPN15 Δ*escN* were transformed with pGFP expression plasmids. EPEC JPN15 was selected for solely by ampicillin resistance, whilst EPEC JPN15 Δ*escN* was selected for by ampicillin and kanamycin resistance.

2.4.1 Bacterial glycerol stocks

Isolated bacteria colonies were added to beads in 20% (v/v) glycerol in cryovials. The cryovials were inverted, the liquid was removed, and they were stored at -80ºC. Samples were streaked onto LB agar (Sigma Aldrich, Dorset, UK) plates or used to grow overnight cultures in LB Broth (Sigma Aldrich, Dorset, UK) as required.

2.4.2 EPEC adherence assays

Overnight EPEC cultures in LB Broth were diluted 1:50 into serum and antibiotic free DMEM, and pre-activated by incubation for 3 hours at 37℃ in a 5% CO_2 atmosphere before infection. The media on cells was replaced with serum and antibiotic free DMEM, and EPEC was added at a multiplicity of infection (MOI) of 120 bacteria per cell, and incubated at 37℃/10% CO_2 for 2 hours. Cells were then washed three times with PBS. Cells were trypsinised and collected in a tube, before lysis with 0.5% (v/v) Trition-X-100 in PBS. Lysates were serially diluted in PBS and were plated onto LB agar plates. Bacteria were cultivated overnight at 37℃. The number of colonies was counted, and the percentage adhesion efficiency relative to the inoculum was quantified.

For immunofluorescence quantification, cells were fixed in 4% paraformaldehyde (PFA) in PBS for 15 minutes after infection. Cells were mounted using Immuno-Mount (Thermo. Scientific, Pittsburgh, PA, USA) containing 10 µg/ml of 4'6-diamidino-2-phenylindole (DAPI), and viewed under a Leica DM5000 automated epifluorescence microscope (Milton Keynes, UK). Images were processed using MetaMorph (Molecular Devices) and ImageJ software program (version 1.47, downloaded from website http://rsb.info.nih.gov/ij/). In an experiment 50 cells were sampled, where the total percentage of cells positive for adhering EPEC was quantified, along with the number of bacteria which adhered per cell. Additionally, EPEC infection could be quantified by calculating the percentage of cells positive for actin pedestal formation.

For flow cytometry quantification, after infection, cells were trypsinised, collected in polystyrene tubes and kept at 4℃ until FACS analysis. Samples were run on a BD LSRII analyser (Becton Dickinson, New Jersey, USA), where 20,000 cells were counted, and then analysed using FlowJo software program (version 8.77, Treestar, California, USA). EPEC adhesion was quantified by calculating the percentage of cells which were GFP positive within the total population of cells.

2.4.3 *S. flexneri* invasion assay

The media on cells was replaced with serum and antibiotic free DMEM. *S. flexneri* was added at an MOI of 100 bacteria per cell. The plate was centrifuged at 1000 RPM for ten minutes to bring the cells and bacteria into contact, thereby initiating infection. The plate was incubated at 37°C/10% CO_2 for 4 hours. Cells were washed three times with PBS, and DMEM containing 75 µg/ml of gentamycin was added, before incubation at 37°C for 1 hour. Gentamicin treatment killed extracellular bacteria, but preserved those which had been internalised. Following three washes in PBS, cells were trypsinised and collected in a tube before lysis with 0.5% (v/v) Triton X-100 in PBS. Lysates were serially diluted in PBS and were plated onto LB agar. Bacteria were grown overnight at 37°C. The number of colonies was counted, and the percentage invasion efficiency relative to the inoculum was quantified.

2.4.4 *S. aureus* infection assay

Two wells of a 12 well plate were used in each infection assay. The media on cells was replaced with serum and antibiotic free DMEM. *S. aureus* was added at an MOI of 200 bacteria per cell. The plate was centrifuged at 1000 RPM for ten minutes and incubated at 37°C/10% CO_2 for 3 hours. The supernatants were removed and the concentrations of CXCL5, IL-6, IL-8, IL-17-A, IL-24 and MMP9 were analysed by ELISA (section 2.8). Cells were then washed three times with PBS. One well used to determine the cell associated bacteria was lysed immediately post infection. Media containing 75 µg/ml of gentamicin was added to the other well, which was used to determine the internalised bacteria. The plate was incubated at 37°C for 1 hour and washed three times with PBS. Cells were trypsinised, collected in a tube and lysed with 0.5 % (v/v) Triton X-100 in PBS. Lysates were serially diluted in PBS and were plated onto LB agar. Bacteria were grown overnight at 37°C and the number of colonies was counted. The number of adhering bacteria was calculated by subtracting the internalised bacteria from the cell associated bacteria. The percentage adhesion and invasion efficiencies were calculated relative to the inoculum.

2.5 Western blotting

Cells were scraped into 100 µl of PBS, collected in sample buffer (200 mM Tris (pH 7.4), 8% (w/v) sodium-dodecyl-sulphate (SDS), 40% (v/v) glycerol, 0.01% (w/v) bromophenol blue) and sonicated for 15 seconds. The proteins in a volume of lysate were separated by electrophoresis on a 12% (w/v) SDS-polyacrylamide gel at 12 mA per gel in 1x running buffer (25 mM Tris, 192 mM glycine, 0.1% (w/v) SDS). Each gel cast consisted of a 12% resolving gel (in 5 ml total volume: 1.6 ml of dH_2O, 2.0 ml of 30% acrylamide mix (0.8% (w/v) Bisacrylamide, 30% (w/v) Acrylamide) (National Diagnostics, Hull, UK)), 1.3 ml of 1.5 M Tris (pH 8.8), 50 µl of 10% (w/v) SDS, 50 µl of 10% (w/v) ammonium persulphate, 2 µl of TEMED) and a 5% stacking gel (in 5 ml total volume: 3.4 ml of dH_2O, 830 µl of 30% acrylamide mix, 630 µl of 1.0 M Tris (pH 6.8), 50 µl of 10% (w/v) SDS, 50 µl of 10% (w/v) ammonium persulphate, 5 µl of TEMED). Lysates were run alongside a rainbow marker (GE Healthcare UK Ltd, Buckinghamshire, UK) which was used to determine protein band size.

Electrophoretic transfer transferred the proteins onto a Hybond C nitrocellulose membrane (GE Healthcare UK Ltd, Buckinghamshire, UK). The membrane, filter paper and foam pads were pre-soaked in 1x transfer buffer (48 mM Tris, 30 mM glycine, 0.037% (w/v) SDS, 20% (v/v) methanol). A sandwich was made which consisted of two pieces of filter paper with the gel placed on top, the membrane on top of the gel, and another two pieces of filter paper on top of the membrane. This was placed between foam pads in a transfer cassette in a transfer tank. The tank was filled with 1x transfer buffer and the proteins were transferred at 300 mA for 2 hours, or at 100 mA overnight.

The membrane was blocked in 10% (w/v) non-fat milk/1x Tris buffered saline (TBS)-Tween 20 (50 mM Tris, pH 7.5, 0.15 M NaCl, 1% (v/v) of Tween-20) for 1 hour at room temperature, before incubation with primary antibody diluted in blocking buffer at 4ºC overnight on a shaker. GAPDH was used as a loading control. The membrane was washed three times for 5 minutes in TBS-Tween 20, and incubated with horseradish peroxidase (HRP) conjugated secondary antibody, diluted in TBS-Tween 20, for 1 hour at room temperature on a shaker. The membrane was then washed five times for 5 minutes in TBS-Tween 20.

20x LumiGlO® Reagent and 20x Peroxide (Cell Signaling Technology®, Massachusetts, USA) was used to detect the signal. The membrane was exposed to Hyperfilm (GE Healthcare UK Ltd, Buckinghamshire, UK) and developed with an automated developer.

Table 2.4: Antibodies used in immunofluorescence and western blotting

Antibody	Dilution	Product code
ADAM17, rabbit polyclonal	1/500 WB	Abcam (Cambridge, UK) ab2051
Cx26, rabbit polyclonal	1/100 IF (PFA fixation)	Invitrogen (Massachusetts, USA) 71-0500
GAPDH, rabbit polyclonal	1/1000 WB	Abcam (Cambridge, UK) ab9485
hBD-2, rabbit polyclonal	1/500 WB 1/50 IF (acetone fixation)	Abcam (Cambridge, UK) ab63982
hBD-3, rabbit polyclonal	1/500 WB	Abcam (Cambridge, UK) ab19270
Integrin β1, mouse monoclonal	1/50 IF (acetone fixation) 1/500 WB	Abcam (Cambridge, UK) ab30388
MMP9, mouse monoclonal	1/50 IF (PFA fixation)	Thermo Scientific Pittsburgh, PA, USA) MAI-12894
Alexa-Fluor 488, Goat anti-rabbit	1/200 IF	Invitrogen (Massachusetts, USA) A11008
Alexa-Fluor 488, Rabbit anti-mouse		Invitrogen (Massachusetts, USA) A11059
Alexa-Fluor 546, Goat anti-rabbit		Invitrogen (Massachusetts, USA) A11010
Immunoglobulin conjugated to HRP, Rabbit anti-mouse	1/1000 WB	
Immunoglobulin conjugated to HRP, Swine anti-rabbit		

2.6. Immunofluorescence

Cells were either fixed in 4% (w/v) PFA in PBS for 30 minutes, or 100% (v/v) acetone for 10 minutes at -20°C. PFA fixation results in the formation of disulphide intermolecular bridges between free amino groups on the proteins expressed within the cell, thus creating a network of cross-linked proteins. On the other hand, acetone is an organic solvent which functions to dehydrate the cells and remove lipids from them, whilst precipitating proteins on the surface of the cells. Although PFA fixation preserves the structure of the cells better than methanol or acetone fixation, it requires an additional permeabilisation step to

ensure that antibodies can enter the cells and bind to their appropriate antigen. Permeabilisation steps were not required if cells were fixed with acetone.

Cells which had been fixed with PFA were permeabilised in 0.5% (v/v) Triton-X-100 in PBS for 15 minutes at room temperature. Subsequently all cells were blocked with 10% (v/v) goat serum in PBS for 1 hour at room temperature, to prevent antibody from binding non-specifically to proteins within the cell. Cells were incubated with primary antibodies diluted in 10% (v/v) goat serum, by inverting the coverslip onto parafilm with 40 µl of antibody on its surface, for 1 hour at room temperature, or at 4℃ overnight, before washing three times for 5 minutes with PBS. Cells were incubated for a subsequent hour with secondary antibodies diluted in 10% (v/v) goat serum at room temperature, before washing five times for 5 minutes with PBS. Cells that were just incubated with secondary antibody without the primary antibody were used as a negative control. For phalloidin staining, following permeabilisation, cells were incubated with AlexaFluor 555 phalloidin (Invitrogen, Massachusetts, USA), diluted 1/100 in PBS for 30 minutes at room temperature. Cells were mounted using Immuno-Mount (Thermo. Scientific, Pittsburgh, PA, USA) containing 10 µg/ml of 4'6-diamidino-2-phenylindole (DAPI) and viewed under a Leica DM5000 automated epifluorescence microscope (Milton Keynes, UK).

2.7 Immunohistochemistry

Skin biopsies were obtained from the ADAM17 deficient male patient, the male and female TOC patients and healthy age-matched controls. Skin samples were cryoembedded and sectioned by a technician in the Pathology core facility, Blizard Institute, Whitechapel. Prior to staining, sections were defrosted and left to air dry for 30 minutes. The samples were subsequently fixed and stained following a protocol analogous to the one described for immunofluorescence in section 2.6.

2.8 ELISAs

The concentrations of CXCL5, IL-6, IL-8, IL-17-A, IL-24 and MMP9 in the supernatants from uninfected and *S. aureus infected* keratinocytes were measured using a sandwich ELISA technique with specific ELISA kits (R&D Systems, Abingdon, UK). CXCL5, IL-17A, IL-24 and MMP9 were also measured in the supernatants from K17 and TYLK1 keratinocytes, and in control and TOC PBMCs, which had undergone 24 hour stimulations with 100 ng/ml of PMA/ 500 ng/ml of ionomycin and 1 ng/ml of LPS. Finally, IL-17-A, IL-17-F, IL-12/IL-23 and IL-22 were measured in PBMCs from the ADAM17 deficient patient and control subjects following stimulation with 100 ng/ml of PMA/500 ng/ml of ionomycin, or CD3/CD28 activation for 24 hours. This final experiment was also carried out in the presence of three inhibitors: two small molecule inhibitors, GI254023X which blocks ADAM10 activity, and GW280264X which targets both ADAM17 and ADAM10[292], and an ADAM17 neutralising antibody[293].

ELISAs were carried out according to manufacturer's protocols. Briefly, the wells of a microtitre plate were coated with capture antibody diluted 1/180 in standard reagent diluent (1% (w/v) BSA in PBS), or specific IL-8 reagent diluent (0.1% (w/v) BSA, 0.05% (v/v) Tween 20 in TBS), and incubated at 4℃ overnight. The plate was washed three times by filling the wells with wash buffer (0.05% (v/v) Tween 20 in PBS). Remaining protein binding sites within the wells which had not been coated with capture antibody were blocked with standard reagent diluent or IL-8 blocking solution (1% (w/v) BSA, 0.05% (w/v) NaN_3 in PBS) for 1 hour at room temperature. The plate was then washed three times with wash buffer, and 100 µl of supernatants were added to each well. Serial dilutions of standard antibody were also included. The plate was incubated for 2 hours at room temperature, and then washed three times with wash buffer. 100 µl of detection antibody, which had been diluted 1/180 in reagent diluent, was added to each well, and the plate was incubated for a further 2 hours at room temperature. The plate was washed three times with wash buffer, and then incubated with 100 µl of HRP-conjugated streptavidin, diluted 1/200 in reagent diluent, which binds to the detection antibody, for 20 minutes at room temperature in the dark. The plate was then washed a further three times, and 100 µl of substrate was added to each well, and the plate was incubated for 20

minutes at room temperature in the dark. Cleavage of the substrate by the enzyme produces a colour change. The reaction was stopped by the addition of 50 µl of 1 M H_2SO_4, and the absorbance of each well was measured at 450 nm using a BioTek ELX800 plate reader.

The standard antibodies were serially diluted so that a standard curve could be produced. As the concentration of antibody which produces a particular absorbance is known, it is possible to measure the concentration of antibody present in the well, thus enabling the concentration of cytokines present in the supernatants to be quantified.

2.9 Statistical analysis

All statistical analysis was carried out as unpaired two-tailed t tests, and p-values equal to or less than $5x10^{-2}$ were considered as statistically significant. Statistically significant results presented as *, **, *** or **** represent $p<5x10^{-2}$, $p<5x10^{-3}$ $p<5x10^{-4}$ and $p<5x10^{-5}$ respectively.

2.10 Patient material

The use of patient material was approved by the National Health Services research ethics committees, and all participants gave their informed consent.

~ Chapter 3 ~

EPEC Infection Quantification Assay Development

3.1 Introduction

S. flexneri invasion was quantified by cellular invasion as has been published previously[45,141,200] and therefore no method optimisation was needed. For this study, an initial challenge was being able to accurately quantify EPEC infection. Manually counting infected cells as a means to quantify infection is less reliable than using an automated counting system. Humans may make mistakes over the number of cells which have been counted. They may also be biased with regards to which cells to include in the analysis. Additionally, manually counting cells is a time consuming process so far fewer cells can be counted. In order to quantify EPEC infection accurately without any bias, one of the aims was to develop an automated counting system. Although some error is associated with every system, this should be counteracted by sampling a large enough population of cells, hence generating more accurate quantification of infection than could be achieved manually. The feasibility of using image analysis software and flow cytometry to quantify EPEC infection is considered and described in section 3.2.

3.1.1 Aims

- Consider the reliability of quantifying EPEC infection by bacterial adherence using image analysis software and flow cytometry (method 2.4.2)
- Consider the feasibility of quantifying EPEC infection by actin pedestal formation using image analysis software

3.2 Results

3.2.1 EPEC infection detection by immunofluorescence

Infection can be detected by bacterial adherence to cells, either by infecting cells with EPEC which has been transformed with a green fluorescent protein

expression plasmid (pGFP), or by visualising DAPI stained bacterial DNA that is associated with cells (figure 3.1 a-c). Infection can also be detected by phalloidin staining of actin pedestals formed by the bacteria (figure 3.1 d-f).

Figure 3.1: EPEC infection in HeLa cells. **(a, c)** Nuclei of cells and bacterial DNA (*DAPI* staining in *blue)*. **(b)** EPEC (*green*). **(d).** Actin (*Phalloidin* staining in *red*). **(c, f)** Merged images. Infection can be detected by bacterial adherence to cells **(a-c)**, either by infecting cells with EPEC which has been transformed with a pGFP expression plasmid, or by visualising DAPI stained bacterial DNA that is associated with cells. Infection can also be detected by actin pedestal formation **(d-f)**. Image magnification 40x. *Bars* 20µm.

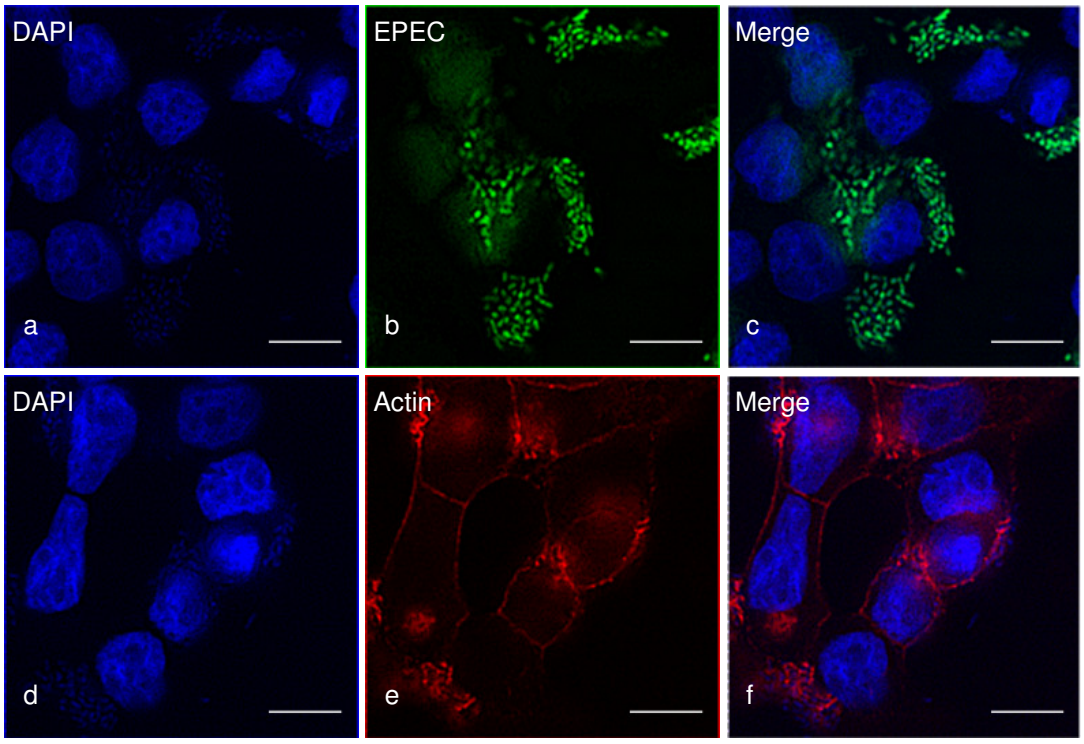

3.2.2 EPEC infection quantification by immunofluorescence and image processing software

As discussed in section 3.1.1, one of the aims of this study was to quantify EPEC infection using an automated counting system, to enable more accurate quantification of infection than would be achieved by manual counting. First, the feasibility of quantifying infection by immunofluorescence using image analysis software (MetaMorph) was investigated. Prior to performing quantification analysis, the clarity of all images was improved by application of convolution filters. Background noise was removed from images by application of a median filter, whilst detail within images was increased by sharpening using a high pass

filter. This processing was necessary to increase the likelihood that the edges of objects of interest would be well defined and included in subsequent analysis; artefacts in the image would be less well defined and therefore less likely to be included in subsequent analysis.

To understand how application of convolution filters to an image improves its subsequent clarity, it is necessary to know the definition of an RGB image, a pixel and an 8 bit image, and these definitions are given in section 3.2.2.1. DAPI stained nuclei and GFP labelled EPEC were sharpened by application of a high pass filter. The way a high pass filter works is depicted in figure 3.2. Subsequently the sharpening of nuclei and bacteria is shown in figure 3.3. Finally the processing of phalloidin staining is illustrated in figure 3.4.

3.2.2.1 RGB image, pixel and 8 bit image definitions

A merged image consists of three channels corresponding to the three primary colours of light – red, blue and green. The smallest unit of an image is a picture element (pixel), with the whole image being composed of thousands or millions of individual pixels arranged in rows and columns.

A bit, which is a binary digit, is the smallest unit of information on a computer. A binary digit is represented by the numbers one or zero, and the number of bits used to represent a pixel in a channel (bits per pixel) determines the number of possible brightness levels of the channel. More bits result in more possible combinations and therefore more levels. Each bit has two possible values, so every bit added doubles the number of combinations. For example, 4 bits give 16 (2^4) combinations, 5 bits give 32 (2^5) combinations, and 8 bits give 256 (2^8) combinations. Humans usually represent these combinations of ones and zeroes as numbers starting from zero, therefore an 8 bit value would be represented by the numbers 0-255 (2^8-1), giving 256 unique values.

For image processing, each channel of the merged image was converted to a separate greyscale 8 bit image. This meant that the image was composed of pixels ranging in value from 0-255, representing the colours black and white respectively, with the values in between representing different shades of grey.

3.2.2.2 Image sharpening by application of a high pass filter

A high pass filter was applied to 8 bit images of DAPI stained nuclei and GFP labelled EPEC to increase their detail (figure 3.3). The filter involves centring a matrix of values termed a kernel on every pixel of the original image. The value for the corresponding pixel in the new image was calculated from the pixels within the kernel. The filter defines the mathematical function used on these pixels. To illustrate how the process of image sharpening using a high pass filter works, DAPI staining has been used as an example (figure 3.2). A section of the original image, highlighted in red (figure 3.2 b) was enlarged (figure 3.2 c). Zooming in further (figure 3.2 d), shows the kernel overlaying the values of the individual pixels in the original image. The 3x3 kernel (figure 3.2 a) was centred on one pixel of the original image (red square, figure 3.2 d). The corresponding pixel in the convoluted image (red pixel, figure 3.2 e) was then calculated. The pixel values covered by the kernel were multiplied by their corresponding kernel values, and then divided by the total of the kernel values to give the sharpened pixel values (figure 3.2 e). Figure 3.2 f shows the same area as figure 3.9 c after sharpening has occurred, while figure 3.2 g shows the final output. Figure 3.3 shows examples of images of cells and bacteria which have been sharpened.

Figure 3.2: Example of using a high pass filter to sharpen DAPI staining. **(a)** 3x3 kernel used in filter. **(b)** Original image used to demonstrate DAPI sharpening using the 3x3 kernel **(a)**. The red square **(b)** is enlarged to show the pixels **(c)**. **(d)** Pixel values of the original image. The pixel values in the convoluted image **(e)** highlighted in red and green are calculated as described. **(e)** Recalculated pixel values in convoluted image. **(f)** Corresponding pixels to **(c)** post processing**. (g)** Final output image processed by the high pass filter.

a

-1	-1	-1
-1	9	-1
-1	-1	-1

b c

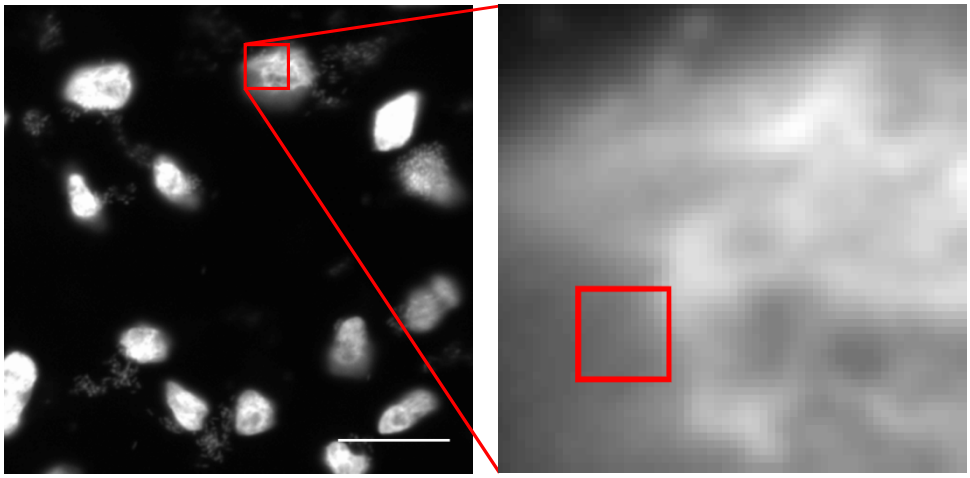

Figure 3.2: Example of using a high pass filter to sharpen DAPI staining - continued

d

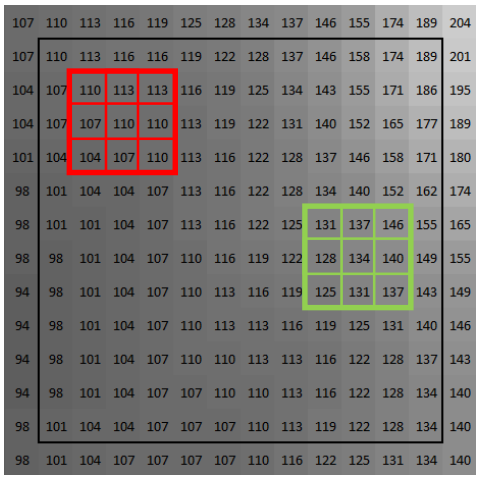

To calculate the red pixel in the processed image, the 3x3 kernel **(a)** is figuratively overlaid on the image. The pixel values are then multiplied by the corresponding kernel values, summed and divided by the total of the kernel values i.e.:

((110 * -1) + (113 * -1) + (113 * -1) + (107 * -1) + (110 * 9) + (110 * -1) + (104 * -1) + (107 * -1) + (110 * -1)) / 1 = 116

e

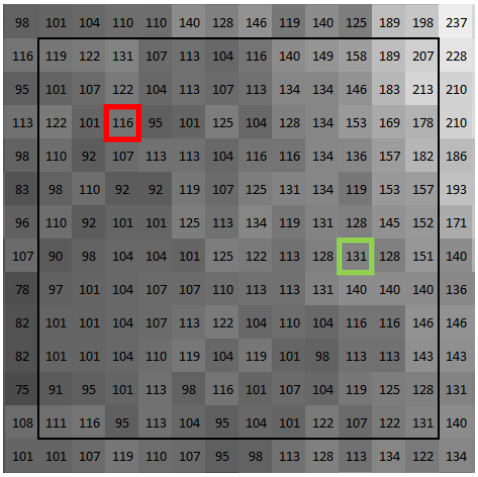

Similarly for the green pixel:

((131 * -1) + (137 * -1) + (146 * -1) + (128 * -1) + (134 * 9) + (140 * -1) + (125 * -1) + (131 * -1) + (137 * -1)) / 1 = 131

f

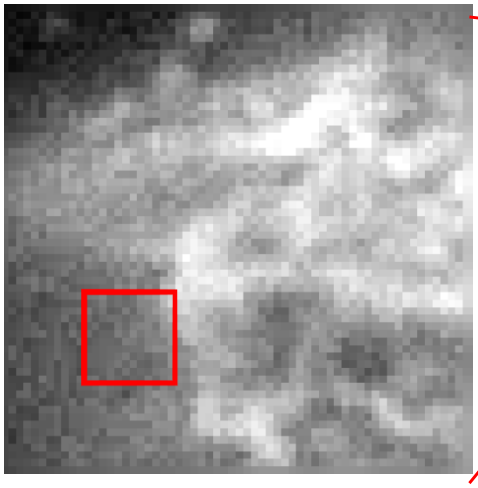

g

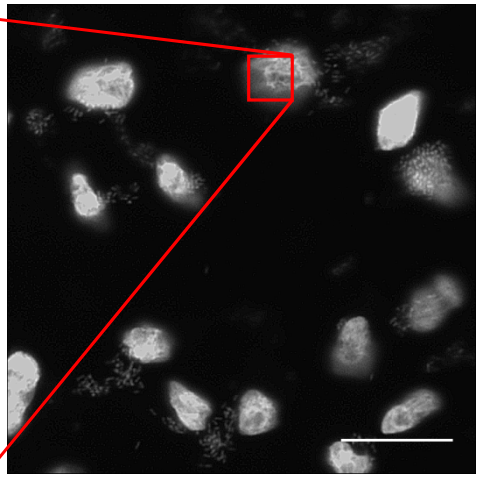

Figure 3.3: Image processing prior to EPEC (E69) adherence quantification. Raw data **(a-c)**. **(a)** Nuclei of cells (*DAPI* staining in *blue*). **(b)** EPEC (*green*). **(c)** Merged images. The blue and green channels were converted to 8 bit greyscale images **(d, e)**. The 3x3 pixel kernel (**figure 3.2 a**) was applied to images **(d)** and **(e)** to produce sharpened images **(f)** and **(g)**. The greyscale images were converted back to RGB images **(h, i)**, and the processed images were merged **(j)**. Image magnification 40x. *Bars* 20µm.

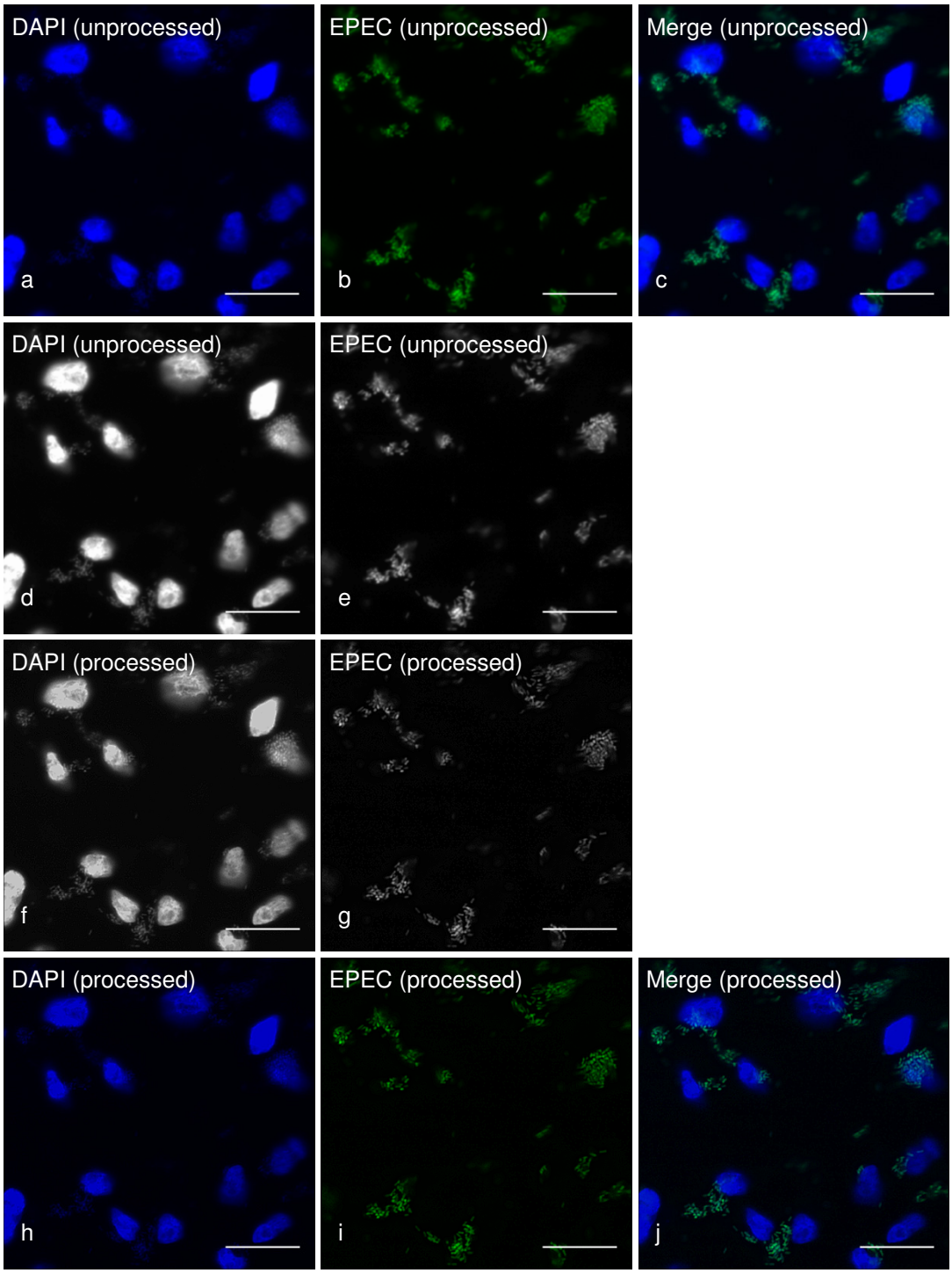

3.2.2.3 Phalloidin staining image processing

A median filter using a 50x50 kernel was first applied to the original image to smooth it (figure 3.4 e). Each individual pixel value in the image was replaced by the median of the pixels within the kernel. Background noise was then removed from the original phalloidin image, by subtracting the pixel values of the median filtered image from the pixel values of the original image (figure 3.4 f). Finally, the detailed actin staining was sharpened and enhanced in the resulting subtracted image, by application of a high pass filter using the 3x3 kernel in figure 3.2 a (figure 3. g).

Figure 3.4: Image processing prior to actin pedestal formation quantification. Raw data **(a-c)**. **(a)** Nuclei of cells (*DAPI* staining in *blue*). **(b)** Actin pedestals (*phalloidin* staining in *red*). **(c)** Merged images. Actin staining image processing **(d-g)**. Image **(b)** was converted to an 8 bit greyscale image **(d)**. A median filter of 50x50 pixels was applied to image **(d)** to produce the smoothed image **(e)**. Image **(e)** was subsequently subtracted from image **(d)** to produce image **(f)**. The 3x3 kernel **(figure 3.2 a)** was then applied to image **(f)** to produce the sharpened image **(g)**. The greyscale image was converted back to an RGB image **(i)**. DAPI stained nuclei were processed analogous to **figure 3.3**. Processed DAPI **(h)** and phalloidin **(i)** images were merged **(j)**. Image magnification 40x. *Bars* 20µm.

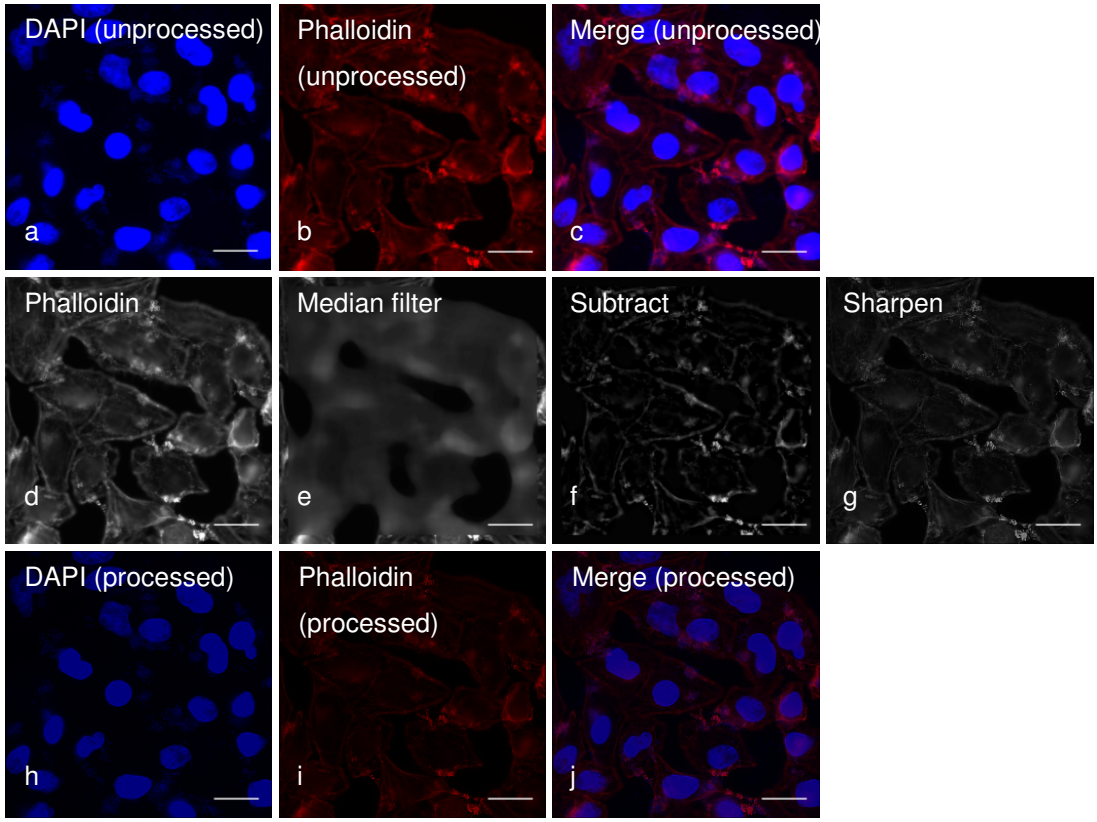

3.2.2.4 Quantifying EPEC E69 adherence

Once images had been processed by application of convolution filters to sharpen their detail and remove background noise, the feasibility of using the image processing software (MetaMorph) to quantify infection was investigated. In order to quantify bacterial adherence to cells, the aim was to use the software to count the number of infected cells within a population of 50 cells. This was initially investigated in a population of cells which had been infected with the prototype WT EPEC strain, E69. Infected cells were defined as those which were positive for adhering bacteria, and uninfected cells as those that were negative for adhering bacteria. Cells and bacteria included in the analysis were identified by DAPI and GFP staining respectively. Those included in the analysis were selected according to their size. The minimum and maximum length of cells and bacteria was measured and set as the limit for what was to be included in the subsequent analysis. This was necessary as it increased the likelihood that the software would accurately identify staining corresponding to cells and bacteria, and omit any staining that was an artefact in the image. A threshold was also applied to the images so that only pixels with a value greater than the background were included in the analysis, which again helped ensure that cells and bacteria were accurately selected, and any non-specific background staining was not.

The 'Cell Scoring' tool was used to count the number of infected cells in the population of cells (figure 3.5). The first requirement was to ensure that the cells and bacteria had been accurately selected for inclusion in the analysis. Cells and bacteria which have been selected for inclusion are displayed by MetaMorph as red and green respectively (figure 3.5 d, e). MetaMorph displays the 'Cell Scoring' analysis results as green cells which are positive for adhering bacteria and red cells which are negative for adhering bacteria (figure 3.5 f).

A requirement for using MetaMorph as an automated counter was that it produces a maximum error of 10%. To validate the results generated by MetaMorph to quantify EPEC adherence to cells, the percentage error between the results from MetaMorph and results obtained by manual counting was calculated. A population of 50 cells was analysed across 3 independent experiments. A population size of 50 was selected as this provided a large

enough number of cells for comparison between the two methods, whilst not sampling too many cells, and thus avoiding the introduction of human error.

Bacterial adherence to cells was compared in a population of cells infected with WT EPEC and an EPEC mutant, *ΔescN*. EPEC *ΔescN* is deficient in type III secretion and unable to deliver effectors into the host cell. Manual counting identified 60% of cells infected with WT EPEC and 25% of cells infected with EPEC *ΔescN* as positive for adhering bacteria (figure 3.5 g). On the other hand, MetaMorph identified 55% of cells infected with WT EPEC and 22% of cells infected with EPEC *ΔescN* as positive for adhering bacteria (figure 3.5 g). The increased adherence to cells exhibited by WT EPEC was significant, and arose because EPEC *ΔescN* was unable to inject effectors into the cells, and consequently could not adhere intimately to them. Percentage errors of 9% for WT EPEC and 10% for EPEC *ΔescN* were calculated between the results obtained by the two methods. This meant that there was a concordance of approximately 90%, and no statistically significant differences between the two methods were calculated (figure 3.5 g), demonstrating that MetaMorph could be used as an automated counter to quantify adherence to cells.

Figure 3.5: Quantifying EPEC (E69) adherence by immunofluorescence in HeLa cells. **(a)** Nuclei of cells (*DAPI* staining in blue). **(b)** EPEC (*green*). **(c)**. Merged images. Cells and bacteria are selected for analysis based on length and pixel intensity, and those included in the analysis are shown in *red* **(d)** and *green* **(e)** respectively. **(f)** Selection results where cells positive and negative for bacteria are shown in *green* and *red* respectively. Magnification 40x. *Bars* 20µm. **(g)** Results obtained by manual counting and MetaMorph for the percentage of cells positive for adhering bacteria (numbers on plot). Data represent mean ± the SEM; *n*=3 Comparison was carried out by using a two-tailed unpaired t test where a significantly greater percentage of cells positive for WT EPEC compared to EPEC *ΔescN* was observed (* represents $p<5x10^{-2}$). No significant difference was observed between the results generated by the two methods.

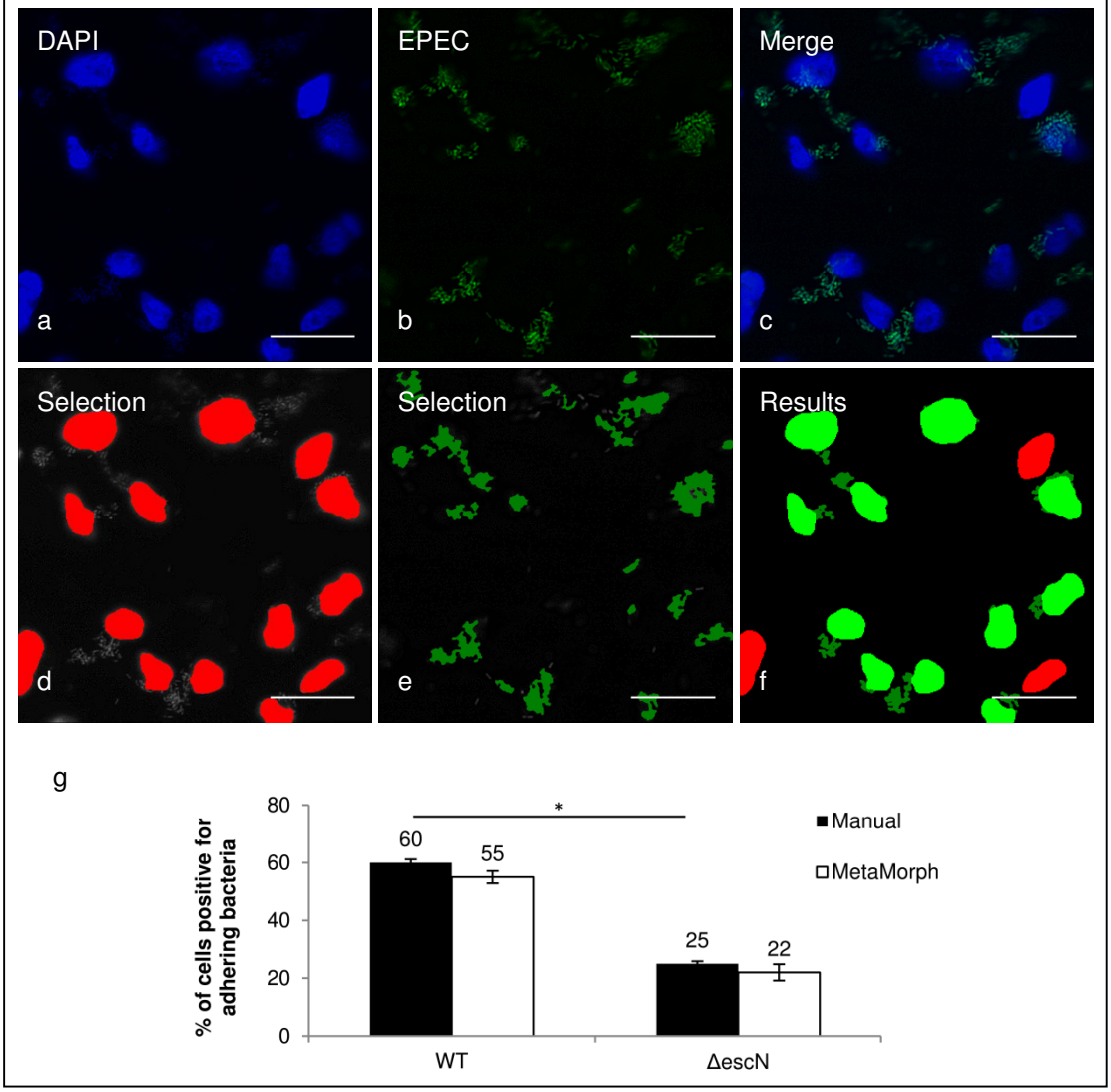

3.2.2.5 Quantifying EPEC JPN15 adherence

One of the limitations of simply quantifying the percentage of cells which are positive or negative for adhering bacteria is that it may not give an accurate indication of the level of infection. EPEC E69 harbours the EPEC adherence factor (EAF) plasmid, which encodes bundle forming pili (BFP), and the bacteria undergo localised adherence to cells. BFP are proteinaceous fibrillar organelles which extend out of the surface of the bacterium, facilitating the adhesion of the bacterium to the host cell, and the recruitment of additional bacteria into micro-colonies on the cell[143,178]. Multiple bacteria adhere making it difficult to determine the actual number of adhering bacteria per cell. This was dealt with by infecting cells with EPEC JPN15. EPEC JPN15 is missing the EAF plasmid and does not undergo localised adherence to cells, meaning that individual bacteria can be seen adhering per cell. The aim, therefore, was to use MetaMorph not only to quantify the percentage of cells positive for adhering bacteria, but also to count the number of individual bacteria adhering per cell. For this the 'Granularity' tool of MetaMorph was used. Similarly to quantifying EPEC E69 adherence, cells and bacteria were identified by DAPI and GFP respectively, and were selected based on their size and pixel intensity. MetaMorph displays cells and bacteria which are included in the analysis as green nuclei and white granules respectively (figure 3.6 d). In a population of 50 cells, manual counting and MetaMorph identified 47% and 50% of cells as positive for adhering WT EPEC JPN15, while manual counting and MetaMorph identified 26% and 24% of cells as positive for adhering EPEC *ΔescN* JPN15 (figure 3.6 e). The difference in adherence between WT EPEC and EPEC *ΔescN* was statistically significant and arose because EPEC *ΔescN* was unable to adhere intimately to cells. When the results obtained by MetaMorph were validated, concordances of 94% for WT EPEC JPN15 and 92% for EPEC *ΔescN* JPN15, and no statistically significant differences between the two methods were calculated. This confirmed that MetaMorph could also be used to reliably quantify EPEC JPN15 adherence.

Figure 3.6: Quantifying EPEC JPN15 adherence by immunofluorescence in HeLa cells. **(a)** Nuclei of cells (*DAPI* staining in *blue)*. **(b)** EPEC *(green)*. **(c)** Merged images. Cells and bacteria are selected for analysis based on length and pixel intensity. Nuclei included in the analysis are shown in *green*, whilst bacteria are shown in *white* **(d)**. Magnification 40x. *Bars* 20µm. **(e)** Results obtained by manual counting and MetaMorph for the percentage of cells positive for adhering bacteria (numbers on plot). Data represent mean ± the SEM; *n*=3. Comparison was carried out by using a two-tailed unpaired t test where a significantly greater percentage of cells positive for adhering bacteria was observed for WT EPEC compared to EPEC *ΔescN* infection (***represents $p<5x10^{-4}$). No significant difference was observed between the results generated by the two methods.

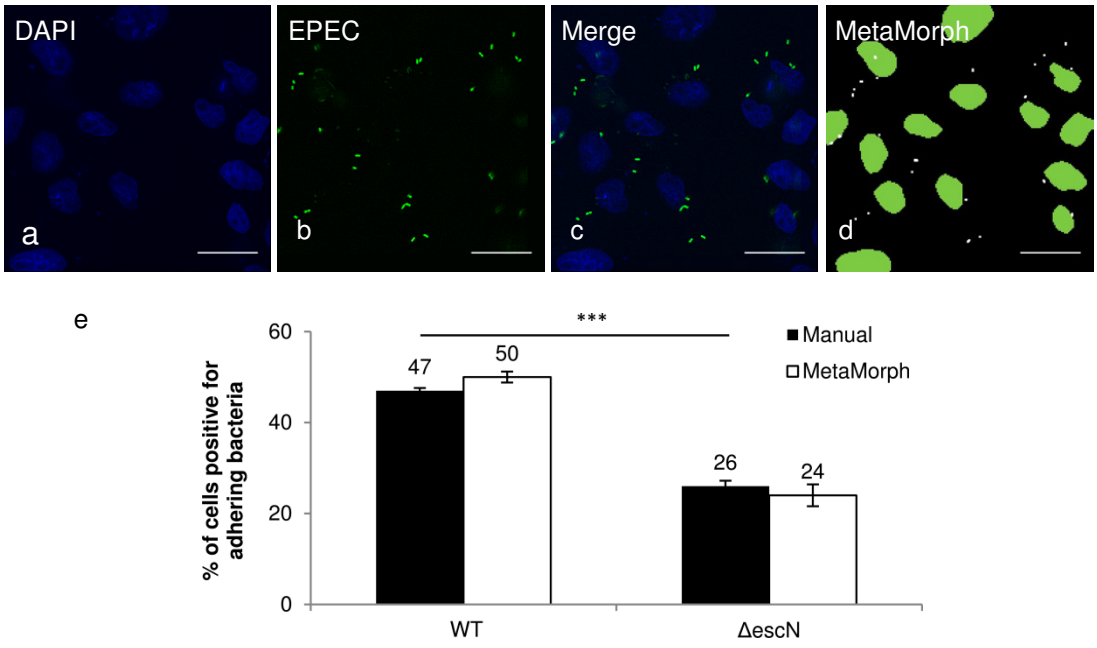

3.2.2.6 Quantifying EPEC E69 actin pedestal formation by immunofluorescence

The 'Granularity' tool was used to quantify the percentage of cells positive for actin pedestal formation (figure 3.7). Cells and actin to be included in the analysis were identified by DAPI and phalloidin staining respectively, and were also selected based on their size and pixel intensity. As EPEC *ΔescN* is deficient in type III secretion, it is unable to induce actin pedestal formation. One of the challenges of using MetaMorph to quantify pedestal formation was to ensure that MetaMorph could discriminate between staining of actin pedestals and background cellular actin staining. This was tested by using MetaMorph to analyse cells that had been infected with both WT EPEC E69 and EPEC *ΔescN* E69 (figure 3.7).

Of a population of 50 cells that had been infected with WT EPEC, manual counting and MetaMorph identified 29% and 32% respectively of cells that were positive for actin pedestal formation (figure 3.7 i). MetaMorph quantified approximately 4% of cells infected with EPEC *ΔescN* as positive for actin pedestals (figure 3.7 i). These were false positive results and were counted because MetaMorph misidentified some background actin staining as actin pedestals. Using MetaMorph to quantify the percentage of cells positive for actin staining during WT EPEC and EPEC *ΔescN* infection, revealed a significantly greater percentage of cells positive for actin staining during WT EPEC infection (figure 3.7 i). When the results obtained by MetaMorph were validated, concordances of 94% and 98% for cells infected with WT EPEC and EPEC *ΔescN* respectively, and no statistically significant differences between the two methods were calculated. This confirmed that MetaMorph could also quantify EPEC infection by actin pedestal formation.

Figure 3.7: Quantifying actin pedestal formation during WT EPEC and EPEC *ΔescN* E69 infection by immunofluorescence in HeLa cells. **(a, e)** Nuclei of cells (*DAPI* staining in *blue)*. **(b, f)** Actin (*phalloidin* staining in *red*) **(c, g)** Merged images. Cells and actin are selected for analysis based on length and pixel intensity. Nuclei included in the analysis are shown in *green,* whilst actin is shown in *white* **(d, h)**. Magnification 40x. *Bars* 20μm. **(i)** Results obtained by manual counting and MetaMorph for the percentage of cells positive for actin staining (numbers on plot). Data represent mean ± the SEM; *n*=3. Comparison was carried out by using a two-tailed unpaired t test where a significantly greater percentage of cells positive for actin staining was observed for WT EPEC compared to EPEC *ΔescN* infection (*** represents $p<5x10^{-4}$). No significant difference was observed between the results generated by the two methods.

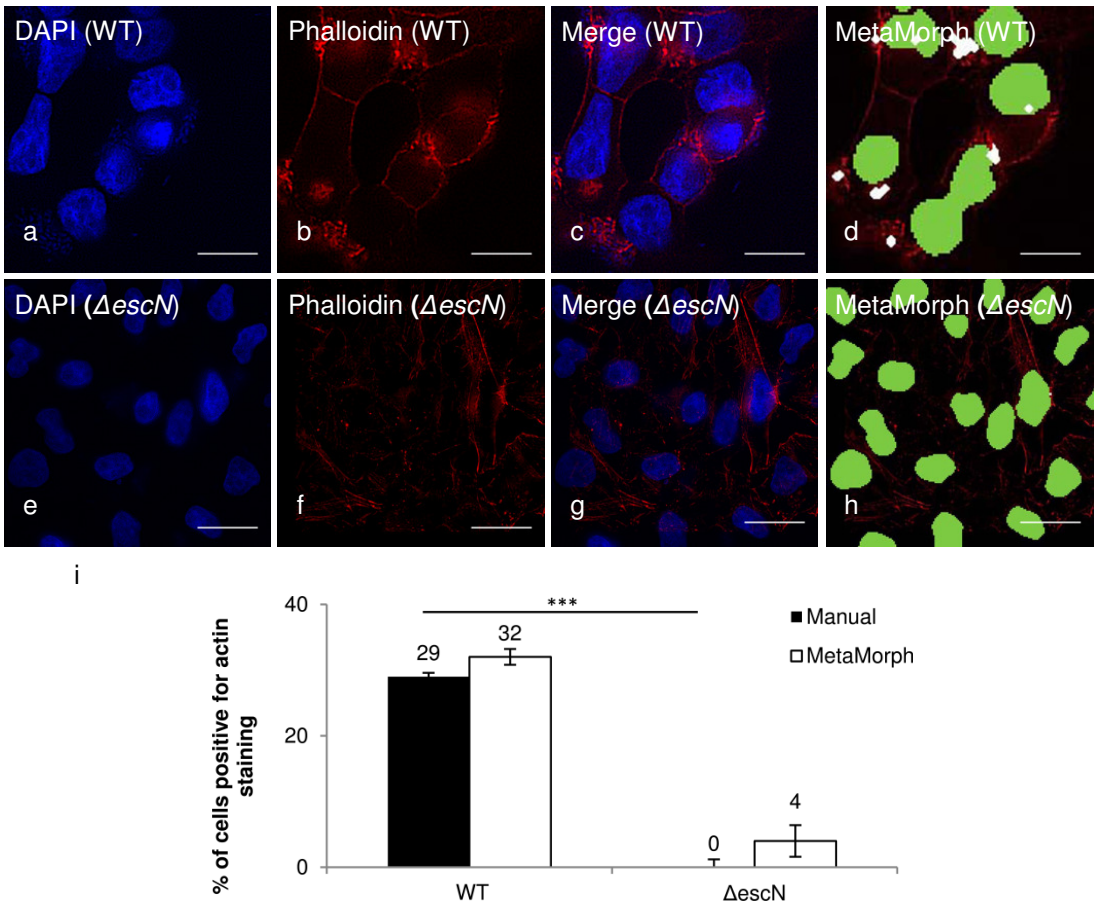

3.2.3 Quantifying EPEC E69 adherence by flow cytometry

Quantifying bacterial adherence by flow cytometry (figure 3.8) was investigated as an additional method by which EPEC E69 infection could be quantified in HeLa cells infected with WT EPEC E69 and EPEC *ΔescN* E69 which had been transformed with pGFP expression plasmids. An example of the gating used to select cells included in the analysis is shown in figure 3.8 a. Cells included in the analysis were selected by forward versus side scatter, which selects cells based on their size and granularity respectively. Cells were further gated for GFP expression into GFP negative and positive populations. An uninfected

population of cells provided a negative control to establish where to set the gate to discriminate between GFP negative and positive populations for infected cells.

The percentages of GFP negative and positive cells were determined for cells infected with WT EPEC and EPEC *ΔescN* (figure 3.8 b). Within the population of cells, 84.5% and 18.6% were GFP positive for WT EPEC and EPEC *ΔescN* infection. This difference was statistically significant. The mean fluorescent intensities (MFI) of the GFP negative and GFP positive populations were also analysed (figure 3.8 c). The MFIs of GFP negative cells were 445 and 361 for WT EPEC and EPEC *ΔescN* infections, while the MFIs of GFP positive cells were 25731 and 2998 for WT EPEC and EPEC *ΔescN* infections. This confirmed that there was increased fluorescence in the GFP positive population. To compare the MFI shift for cells infected with WT EPEC and EPEC *ΔescN*, the MFI of the GFP negative population was subtracted from the MFI of the GFP positive population (figure 3.8 d). The MFI shifts calculated were 26685 and 2637.5 for WT EPEC and EPEC *ΔescN*. This difference was also statistically significant. A greater MFI shift suggests increased GFP expression by a cell population. Taken together, the flow cytometry results demonstrate increased GFP expression by cells infected with WT EPEC compared to EPEC *ΔescN,* suggesting that adherence to cells by WT EPEC was greater than EPEC *ΔescN*.

Figure 3.8: Quantifying EPEC E69 adherence by flow cytometry in HeLa cells. **(a)** Example of the gating used to select cells included in the analysis. Cells were selected by forward (FSC-A) versus side scatter (SSC-A), and then further gated into GFP (FITC-A) negative and positive populations. The percentage of cells within the GFP negative and positive populations **(b)**, the mean fluorescent intensities (MFIs) of the GFP negative and positive populations **(c)**, and the MFI shift between the GFP negative and positive populations **(d)** were quantified, and are represented by the numbers on the plot. Data represent mean ± the SEM; *n*=2. Unpaired two-tailed t tests revealed a significantly greater percentage of GFP positive cells for cells infected with WT EPEC compared to EPEC *ΔescN* **(b)**, and a significantly increased MFI shift in GFP expression for cells infected with WT EPEC compared to EPEC *ΔescN* **(d)** (* and ** represents $p<5x10^{-2}$ and $p<5x10^{-3}$ respectively).

a

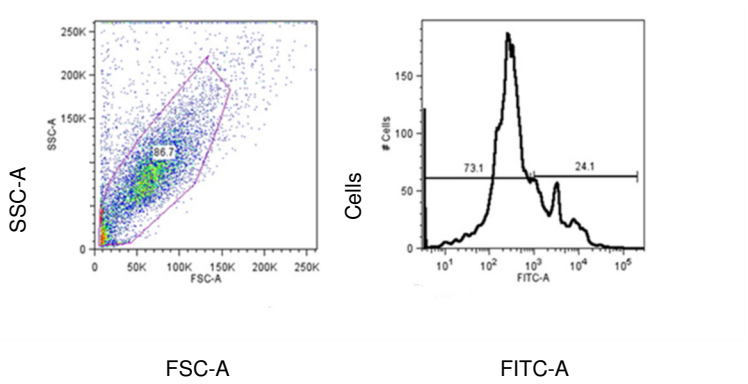

b

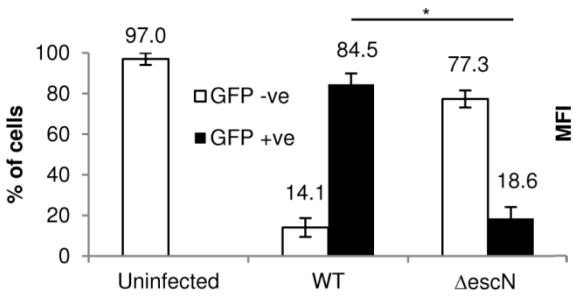

c

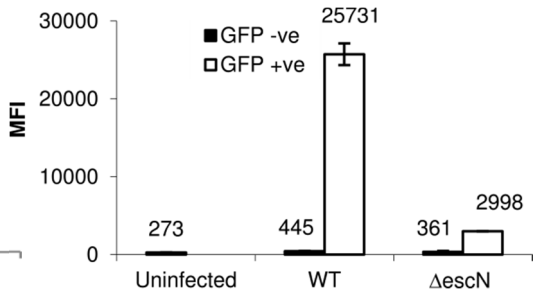

d

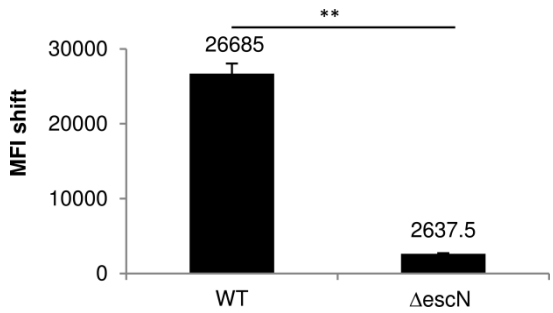

3.3 Discussion

The results described in this chapter have demonstrated that it is possible to use an automated counter to quantify EPEC infection. For immunofluorescence quantification, there was a minimum concordance of approximately 90%, and no statistically significant difference between the results obtained by manual counting and those obtained by image processing software, for both bacterial adherence to cells and actin pedestal formation. MetaMorph could discriminate, to a statistically significant degree, between actin pedestals and background actin staining. It is therefore possible to use MetaMorph to batch process large numbers of images and accurately quantify infection, without the introduction of human error or bias. A much larger sample of cells can be analysed by MetaMorph than by manual counting, which will improve the reliability of the results generated. By immunofluorescence it was possible to quantify both the percentage of cells which were positive for adhering bacteria, and the number of bacteria that adhered per cell, meaning that the infection level of individual cells could be established.

In published studies, actin pedestal formation has traditionally been the more widely used method to quantify EPEC infection. Intimate adherence to intestinal epithelial cells has been thought to be mediated by actin pedestals resulting from bacterial induced actin polymerisation. More recently, however, *in vitro* observations have demonstrated that some strains have failed to induce actin polymerisation, yet were still able to form attaching and effacing lesions on cells[294]. In light of this, in this study EPEC infection will be quantified by bacterial adherence to cells. This will aim to ensure that all infected cells are identified; quantifying actin pedestals alone could possibly miss some infected cells, if any such cells had adhering bacteria and no visible pedestals.

Flow cytometry was explored as a second method by which EPEC adherence could be quantified. The flow cytometry results depicted in figure 3.8 support the immunofluorescence results in figure 3.5, where adherence to cells was significantly greater by WT EPEC than EPEC *ΔescN.* One of the limitations of using flow cytometry, however, is that infection can only be quantified as the percentage of cells within a population that are positive for adhering bacteria. It

is not possible to count the number of bacteria which adhere per cell, and so provides no information on the infection level of individual cells.

In this study EPEC infection has therefore been quantified by immunofluorescence rather than flow cytometry. The methods described in section 3.2 have been used to quantify how EPEC infection is affected by changes in Cx26 and ADAM17 expression. These results are presented in chapters 4 and 5.

~ Chapter 4 ~

Effect of Cx26 Expression on Gastrointestinal Bacterial Infection

4.1 Introduction

Recessive mutations in Cx26 cause non syndromic hearing loss (NSHL). As described in section 1.1.16, there are specific mutations which cause the majority of Cx26 NSHL in certain geographic locations and ethnic groups. Such mutations include c.35delG in European populations[114,115], c.235delG in Japanese populations[116] and p.143W in African[95] populations. It has been hypothesised that these mutations may confer a heterozygote advantage to carriers[45,118-120]. For example, heterozygote carriers of the p.R143W[120] and c.35delG[118] mutations have a significantly thicker epidermis than WT Cx26 homozygotes, which could provide improved protection against bacterial infection. Furthermore, HeLa cells expressing p.R143W are significantly less susceptible to cellular invasion by *S. flexneri* than HeLa cells expressing WT Cx26[45], suggesting that being a carrier of p.R143W may result in decreased susceptibility to gastrointestinal bacterial infection.

4.1.1 Aims

- Consider whether a loss of functional Cx26 expression improves resistance to infection with gastrointestinal bacteria
- Investigate the effect of expressing Cx26 NSHL mutations in transfected HeLa cells on bacterial infection
- Compare EPEC adherence (method 2.4.2) and *S. flexneri* invasion (method 2.4.3), as a positive control, in HeLa cells expressing WT-Cx26 and p.R143W-Cx26
- Confirm the sequences of plasmid constructs (method: 2.2.5) and their localisation in transfected HeLa cells (methods 2.1.4 and 2.6) prior to performing infection studies
- Investigate how EPEC adherence and *S. flexneri* invasion were affected by Cx26 siRNA treatment (method 2.1.5) in intestinal epithelial Caco-2 and HT-29 cells
- Confirm Cx26 expression by qRT-PCR (method 2.2.3.5) and immunofluorescence (method 2.6) in intestinal cells prior to performing infection studies

4.2 Results

4.2.1 Cx26 expression in intestinal HT-29 and Caco-2 cells

To validate models of the intestinal environment which could be used to study how enteric bacterial infection was affected by Cx26 expression, Cx26 mRNA and protein expression were analysed in intestinal HT-29 and Caco-2 cells by qRT-PCR and immunofluorescence. The cell lines are obtained from two different patients; HT-29 cells and Caco-2 cells are derived from well differentiated and moderately differentiated adenocarcinomas respectively. They provide two independent intestinal models, and therefore differences exist between the two cell lines. For example, Caco-2 cells spontaneously express differentiation markers and form polarised monolayers with microvilli and tight junctions upon reaching confluence[286]. HT-29 cells however, remain undifferentiated under normal culture conditions unless they are treated with drugs including colchicine, nocodazole and taxol[287]. In this study, any differences in results obtained in HT-29 and Caco-2 cells could result from different characteristics, for example in terms of cell structure and gene expression between the two cell lines. Both cell lines expressed Cx26 mRNA, but expression was greater in HT-29 cells (figure 4.1). QRT-PCR revealed that Cx26 mRNA was detected at a lower cycle threshold number in HT-29 cells (green population) compared to Caco-2 cells (blue population, figure 4.1 b). When Cx26 mRNA expression was normalised to GAPDH, an expression ratio of 1:0.24 for HT-29 cells: Caco-2 cells was calculated (figure 4.1 c).

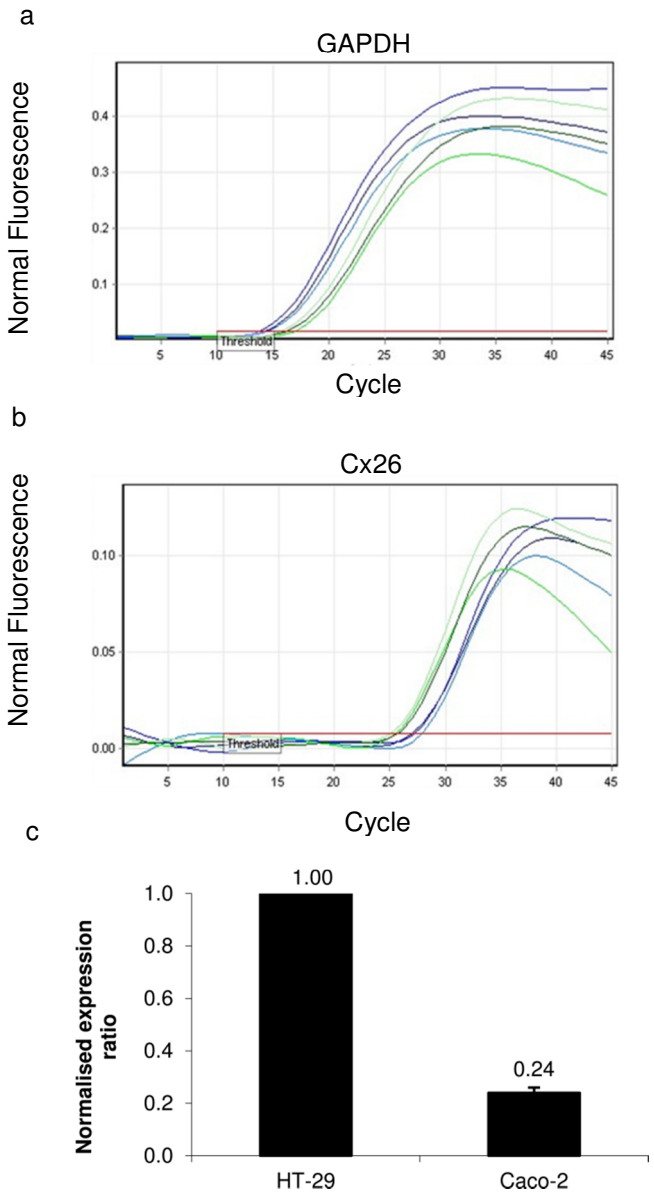

Figure 4.1: Cx26 mRNA expression in intestinal cells by qRT-PCR. (a) GAPDH and **(b)** Cx26 mRNA levels in HT-29 (blue) and Caco-2 (green) cells. Note that Cx26 mRNA expression is greater in HT-29 cells as the green population of cells crosses the cycle threshold (CT) at an earlier cycle number **(b)**. **(c)** Cx26 mRNA expression was quantified relative to GAPDH in HT-29 and Caco-2 cells (numbers on plot). Data represent mean ΔΔCT value ± the SEM; *n*=3.

Cx26 protein expression was analysed by immunofluorescence in Caco-2 and HT-29 cells. To confirm the specificity of any staining detected in intestinal cells, the antibody specificity was first investigated in HeLa cells (figure 4.2). HeLa cells do not express endogenous Cx proteins, making them ideal for use in transfection studies. HeLa cells transfected with p-(WT)Cx26-EGFP and p-(WT)Cx31-EGFP were stained with Cx26 antibody. Colocalisation could be detected between transfected GFP-tagged Cx26 protein and Cx26 antibody staining in p-(WT)Cx26-EGFP transfected HeLa cells (figure 4.2 a-h), confirming that the antibody specifically detected Cx26 protein. The antibody recognised GJ plaques composed of Cx26 between HeLa cells transfected with p-(WT)Cx26-EGFP (figure 3.2 e-h). Additionally, as staining HeLa cells

transfected with p-(WT)Cx31-EGFP did not result in colocalisation between transfected GFP-tagged Cx31 protein and the Cx26 antibody, this showed that the antibody did not cross react with Cx31. Cx26 protein expression was detected in HT-29 (figure 4.3 a-c) and Caco-2 cells (figure 4.3 g-i), and the antibody could specifically detect GJ plaques composed of Cx26. Furthermore, as published previously[67], Cx26 protein could be detected at low levels in the basal layer of the epidermis of normal skin (figure 4.3 m-o). Taken together, these results have shown that both HT-29 and Caco-2 cells express Cx26 and form Cx26 GJ dependent plaques. These two lines can thus be used as models of the intestinal environment to study how gastrointestinal infection is affected by Cx26 expression.

Figure 4.2: Specificity of Cx26 antibody in transfected HeLa cells. **(a-h)** HeLa cells transfected with (WT)Cx26-EGFP. **(i-l)** HeLa cells transfected with (WT)Cx31-EGFP). (**a, e, i)** Nuclei of cells (*DAPI* staining in *blu*e). **(b, f, j)** Transfected protein (*green*). **(c, g, k)** Cx26 antibody staining (*red*). **(d, h, l)** Merged images. Note the colocalisation of Cx26 antibody staining with Cx26 transfeced protein **(d, h)** compared to the absence of any colocalisation of Cx26 antibody with Cx31 transfection protein **(l,)** confirming that the Cx26 antibody recognised Cx26 protein, but did not cross react with Cx31 protein. Note the staining of Cx26 aggregates characteristic of GJ plaques in the extracellular space between (WT)Cx26-EGFP transfected HeLa cells (*white* arrows in **g**, **h**). Image magnification 40x. *Bars* 20µm.

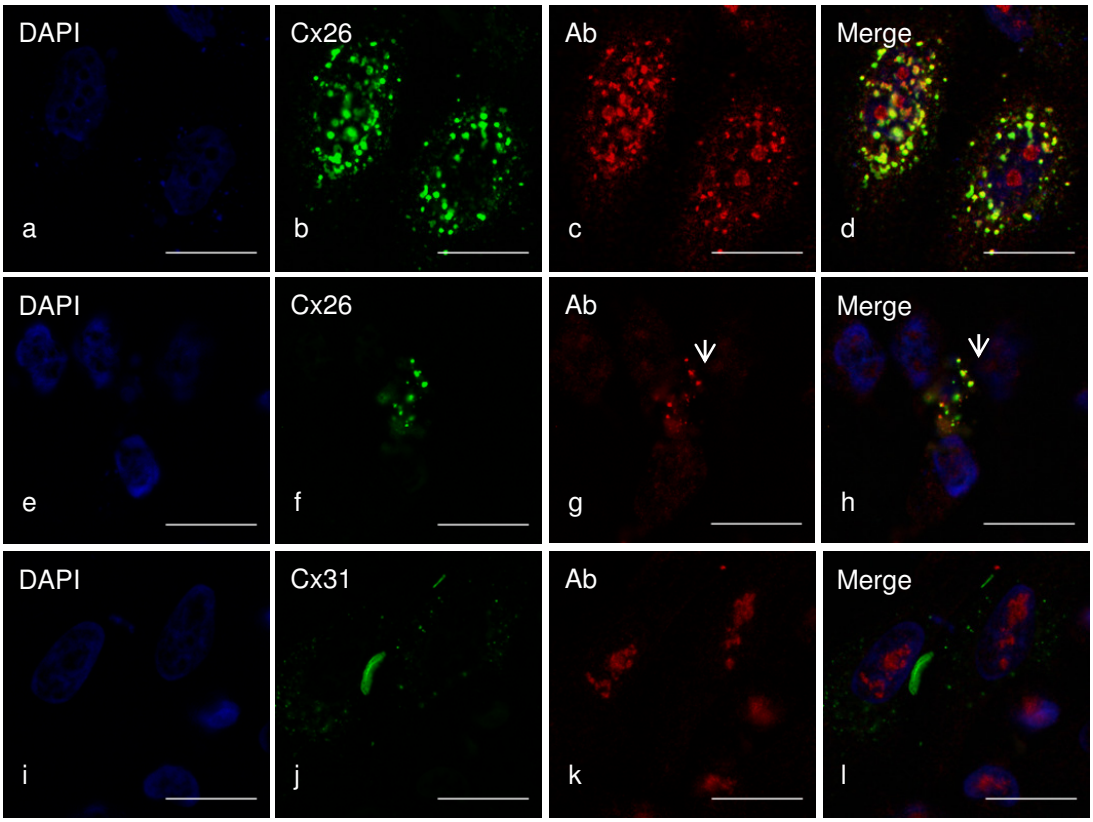

Figure 4.3: Cx26 protein expression in intestinal cells and the epidermis. **(a-c)** HT-29 cells. **(g-i)** Caco-2 cells. **(m-o)** Frozen skin sections**. (a, d, g, j, m, p)** Nuclei of cells (*DAPI* staining in *blue*). **(b, h, n),** Cx26 (*red*). **(d, k, o)** Negative control: unstained cells and tissue section. **(c, f, i, l, o, r)** Merged images. Note the localisation of Cx26 aggregates characteristic of GJ plaques in the extracellular space between cells (*white* arrows in **b, c, h, i**), and Cx26 expression restriction to the basal epidermal layer of frozen skin sections **(n, o)**. Image magnification 40x. *Bars* 20µm.

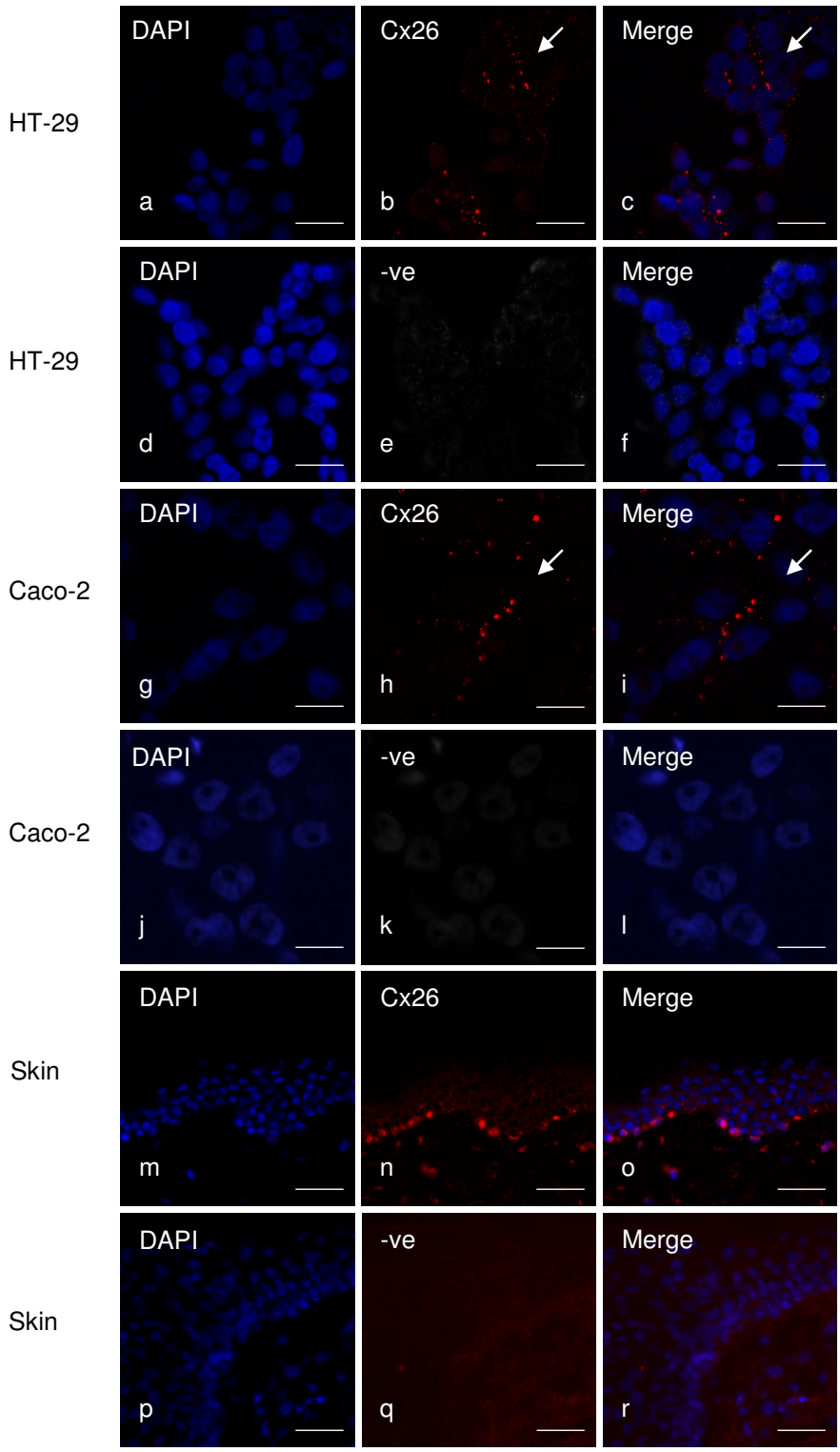

4.2.2 p-(WT)Cx26-mCherry, p-(R143W)Cx26-mCherry and pmCherry constructs

Infection studies were performed using EPEC which had been transformed with a pGFP expression plasmid. To quantify infection in transfected HeLa cells, Cx26 expressing constructs had to be labelled with a different colour reporter tag. Therefore, the constructs used in these studies were tagged with mCherry protein. A p-(WT)Cx26-mCherry construct was obtained from Dr P. Martin. As an empty vector plasmid construct was not available, a restriction digest was performed in this study to remove the Cx26 insert from the p-(WT)Cx26-mCherry construct. This created a negative control pmCherry construct, which was used for mock transfecting cells. To investigate the effect of Cx26 NSHL mutations on bacterial infections, site directed mutagenesis was performed to introduce the p.143W mutation into the p-(WT)Cx26-mCherry construct. Prior to performing infection studies, the sequences of pmCherry and p-(R143W)Cx26-mCherry, and the localisation of p-(WT)Cx26-mCherry, p-(R143W)Cx26-mCherry and pmCherry were verified in transfected in HeLa cells.

4.2.2.1 Sequencing of pmCherry and p-(R143W)Cx26-mCherry constructs

Analysis of the pmCherry construct sequence confirmed removal of the Cx26 insert and ligation of the EcoRI and BamHI restriction sites (black rectangle, figure 4.4 a). This was also shown by alignment with the known pmCherry-N1 vector sequence (pink rectangle, figure 4.4 b). The sequences (black arrows, figure 4.4 c, d) and the alignment between the p-(WT)Cx26-mCherry and p-(R143W)Cx26-mCherry constructs sequences (black arrow, figure 4.4 e), revealed a thymine for cytosine substitution in the (R143W)Cx26-mCherry construct, confirming introduction of the p.R143W mutation.

Figure 4.4: Sequencing of pmCherry and p-(R143W)Cx26-mCherry constructs. (a) pmCherry sequence confirming removal of Cx26 insert and ligation of EcoRI and BamHI restriction sites (black rectangle). **(b)** Sequence alignment between the known pmCherry-N1 vector sequence (top line) and the pmCherry construct (bottom line). EcoRI (pink rectangle) and BamHI (green rectangle) restriction sites. **(c)** p-(WT)Cx26-mCherry, **(d)** p-(R143W)Cx26-mCherry sequences. **(e)** Sequence alignment between p-(WT)Cx26-mCherry (top line) and p-(R143W)Cx26-mCherry (bottom line). Note the thymine for cytosine substitution (black arrows), confirming introduction of the p.R143W mutation by site directed mutagenesis.

a

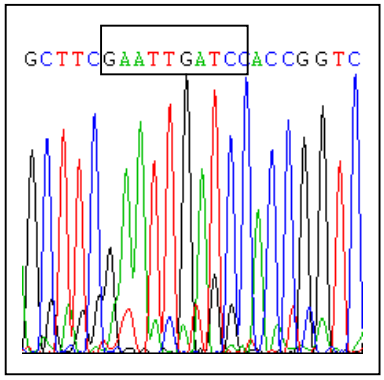

b

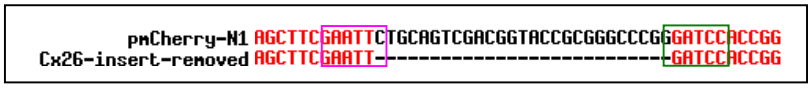

c

p-(WT)Cx26-mCherry

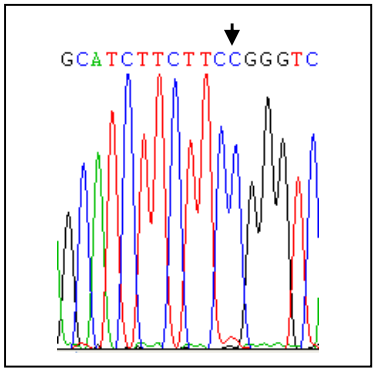

d

p-(R143W)Cx26-mCherry

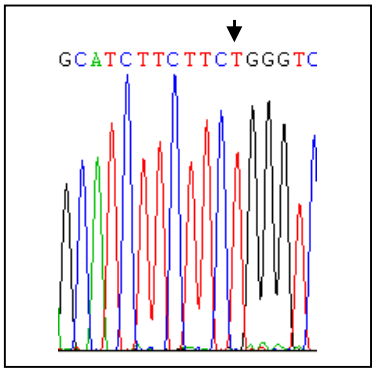

e

4.2.2.2 Localisation of constructs in transfected HeLa cells

The localisation of the three constructs in transfected HeLa cells was visualised by epifluorescence microscopy (figure 4.5). Protein aggregates were observed in the extracellular space between cells transfected with (WT)Cx26-mCherry (white arrows, figure 4.5 b, c), which are indicative of GJ plaques. Such protein aggregates were absent in cells transfected with (R143W)Cx26-mCherry, and in contrast a perinuclear localisation of Cx26 protein was visualised (figure 4.5 d-f). Vector only transfected cells exhibited diffuse cytoplasmic staining of mCherry protein (figure 4.5 g-i).

Figure 4.5: Localisation of plasmid constructs in transfected HeLa cells. **(a-c)** (WT)Cx26-mCherry. **(d-f)** (R143W)Cx26-mCherry. **(g-i)** mCherry (vector only). **(a, d, g)** Nuclei of cells (*DAPI* staining in *blue*). **(b, e, h)** Transfected protein (*red).* **(c, f, l)** Merged images. Note the localisation of (WT)Cx26 aggregates characteristic of gap junction plaques in the extracellular space between cells (*white arrows*, in **b, c)**, compared with perinuclear staining observed with (R143W)Cx26 **(e, f)**, and the cytoplasmic staining observed in vector only transfected cells **(h, i).** Image magnification 40x. *Bars* 40µm.

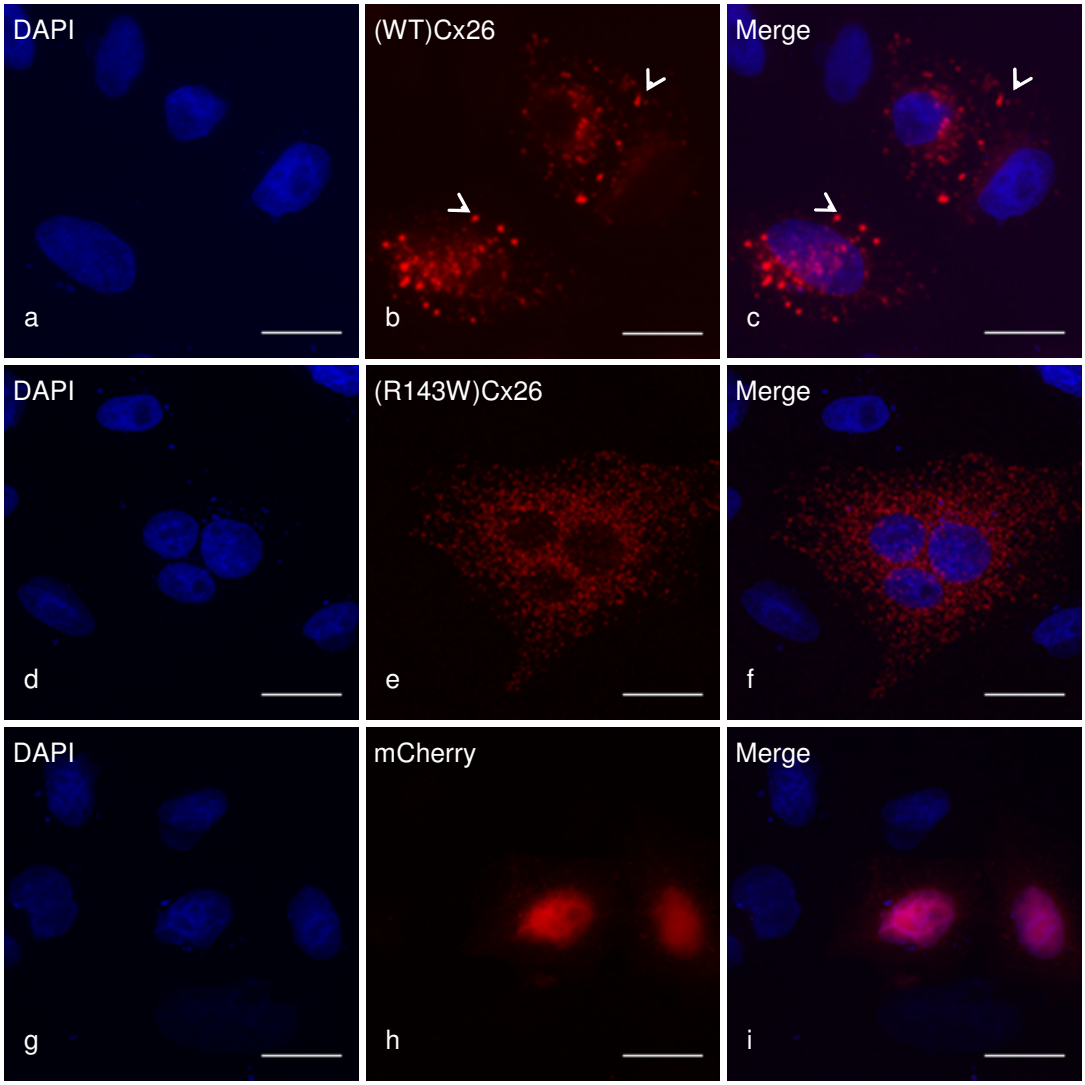

4.2.3 Effect of Cx26 expression on gastrointestinal bacterial infection

4.2.3.1 S. flexneri invasion and EPEC adherence in p-(R143W)Cx26-mCherry expressing HeLa cells

To determine how Cx26 expression affected gastrointestinal bacterial infection, *S. flexneri* and EPEC infection were first analysed in HeLa cells transfected with

p-(WT)Cx26-mCherry and p-(R143W)Cx26-mCherry, and in HeLa cells mock transfected with pmCherry. *S. flexneri* invasion efficiencies were 5.74%, 4.07% and 3.69% in HeLa cells transfected with p-(WT)Cx26-mCherry, p-(R143W)Cx26-mCherry and pmCherry respectively (figure 4.6). This work initially confirmed previous findings[45,141,200]; *S. flexneri* invasion was significantly increased in HeLa cells transfected with p-(WT)Cx26-mCherry compared to mock transfected (mCherry) HeLa cells, and HeLa cells transfected with p-(R143W)Cx26-mCherry (figure 4.6). Although the difference between 5.74% and 4.07% is small, it is possible that this has significant implications for infection level, since very small numbers of bacteria are sufficient to establish disease[127].

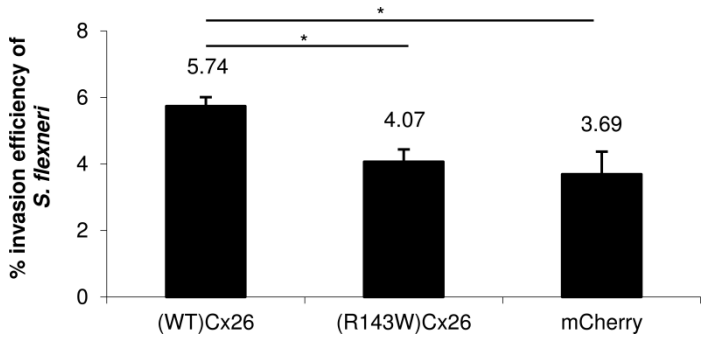

Figure 4.6: *S. flexneri* invasion efficiency in transfected HeLa cells. Data represent mean percentage invasion efficiency (numbers on plot) ± the SEM; *n*=3. Comparison was carried out by using unpaired, two-tailed t-tests, where significant differences were observed between (WT)Cx26 and (R143W)Cx26, and (WT)Cx26 and mCherry (* represents $p<5x10^{-2}$).

To investigate how Cx26 expression affects WT EPEC (E69) infection, the total percentage of transfected cells positive for adhering bacteria was quantified using DAPI stained bacterial DNA (figure 4.7). 83% and 58% of HeLa cells expressing p-(WT)Cx26-mCherry and pmCherry respectively were positive for adhering EPEC (figure 4.7 g). Although bacterial adherence was increased by the expression of p-(WT)Cx26-mCherry, the difference was not significant.

It was hypothesised that any effect which WT Cx26 had on EPEC infection level may be more subtle, for example by altering the number of bacteria which adhered per transfected cell. This may not have been observed by quantifying the total percentage of transfected cells positive for adhering bacteria. This experiment was therefore repeated using EPEC JPN15, which had been transformed with a pGFP expression plasmid. Unlike EPEC E69, EPEC JPN15 does not form microcolonies on cells, so fewer EPEC JPN15 (figure 4.8)

adhered per cell compared to EPEC E69 (figure 4.7). Subsequently the number of adhering EPEC JPN15 per cell was also determined (figure 4.8). HeLa cells transfected with p-(R143W)Cx26-mCherry were included to consider how EPEC adherence was affected by a non-functional deafness associated Cx26 mutation. 80.00%, 34.00% and 42.67% of HeLa cells expressing p-(WT)Cx26-mCherry, p-(R143W)Cx26-mCherry and pmCherry respectively were positive for adhering EPEC JPN15. EPEC JPN15 adherence was significantly increased by the expression of p-(WT)Cx26-mCherry compared to pmCherry or p-(R143W)Cx26-mCherry (figure 4.8 m). There was no significant difference in EPEC adherence to cells expressing p-(R143W)Cx26-mCherry compared to pmCherry (figure 4.8 m). Furthermore, the number of bacteria which adhered per transfected cell was greatest when p-(WT)Cx26-mCherry was expressed (figure 4.8 n). This suggested that Cx26 expression could affect the susceptibility of individual cells to EPEC infection.

Figure 4.7: Wild type EPEC (E69) adherence to transfected HeLa cells. Adherence was quantified by DAPI stained bacterial DNA by manual couting. **(a, d)** Nuclei of cells and bacterial DNA (*white* arrows) are stained with DAPI (*blue*). **(b, e)** Transfected protein (*red*). **(c, f)**, Merged images. Image magnification 40x. *Bars* 40µm. **(g)** Total percentage of transfected cells positive for adhering EPEC (numbers on plot). Data represent mean ± the SEM; *n*=3. Comparison was carried out by using an unpaired, two-tailed t-test where no significant difference was observed between (WT)Cx26 and mCherry.

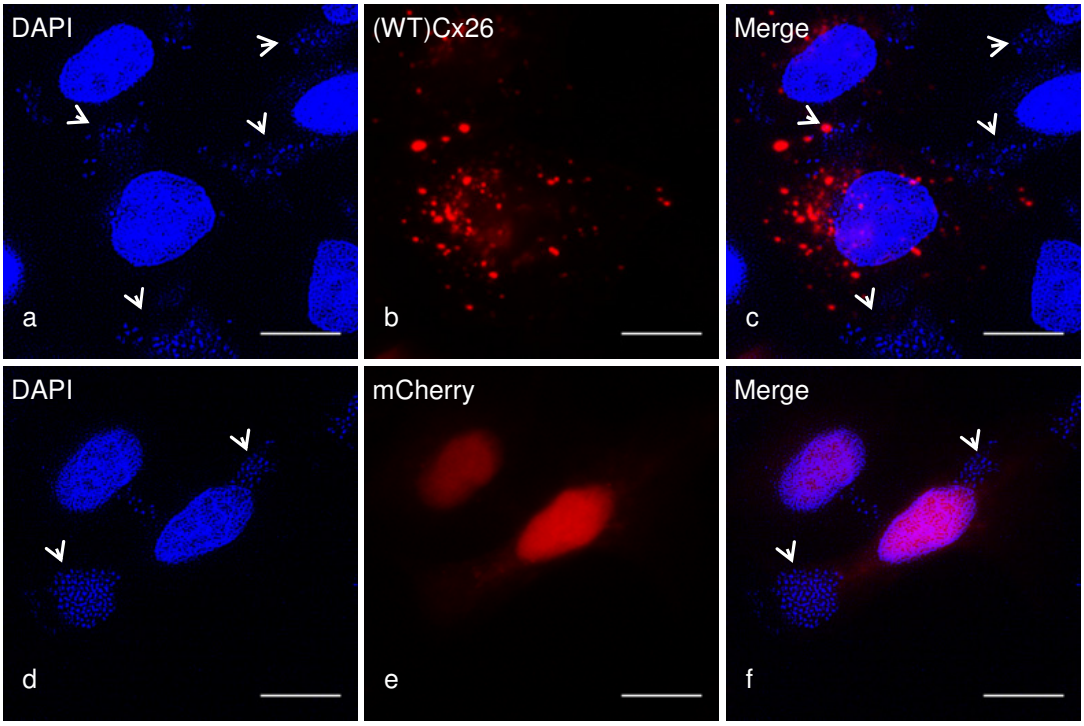

g

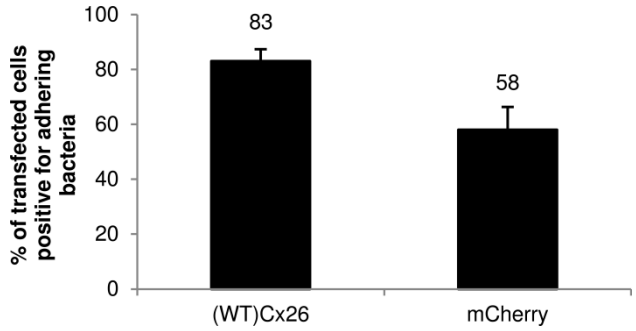

Figure 4.8: Wild type EPEC (JPN15) adherence to transfected HeLa cells. Adherence was quantified by pGFP expression by manual counting. **(a, e, i)** Nuclei of cells are stained with DAPI (*blue*). **(b, f, j)** Transfected protein (*red*). **(c, g, k)** EPEC (*green*). (**d, h, l)** Merged images. Image magnification 40x. *Bars* 40µm. **(m)** Total percentage of transfected cells positive for adhering EPEC (numbers on plot). Data represent mean ± the SEM; *n*=3. Comparison was carried out by using unpaired, two-tailed t-tests; significant differences were observed between (WT)Cx26 and mCherry, and (WT)Cx26 and (R143W)Cx26 (** and *** represents $p<5x10^{-3}$ and $p<5x10^{-4}$ respectively). No significant difference was observed between (R143W)Cx26 and mCherry. **(n)** Number of bacteria that adhered per transfected cell.

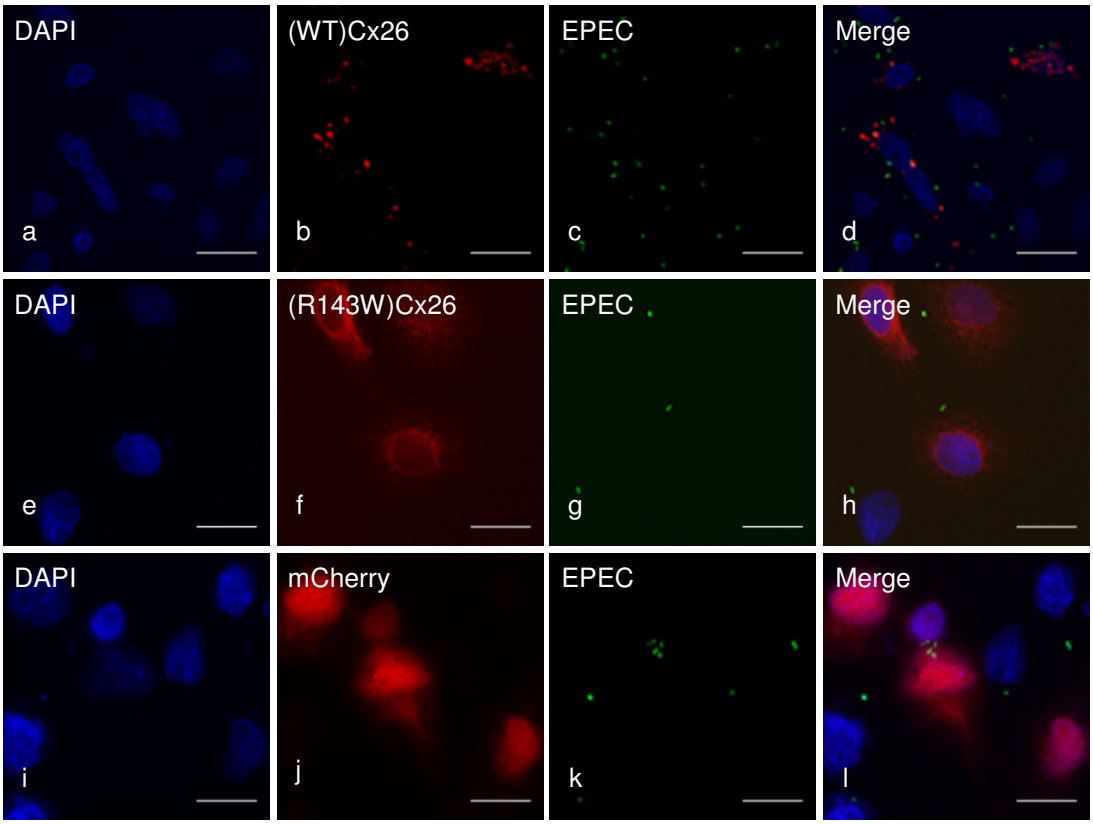

m

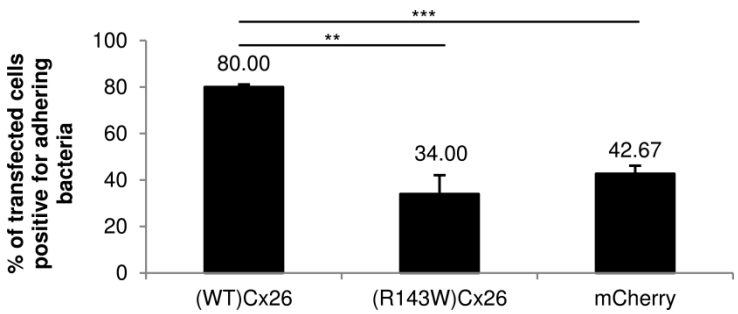

n

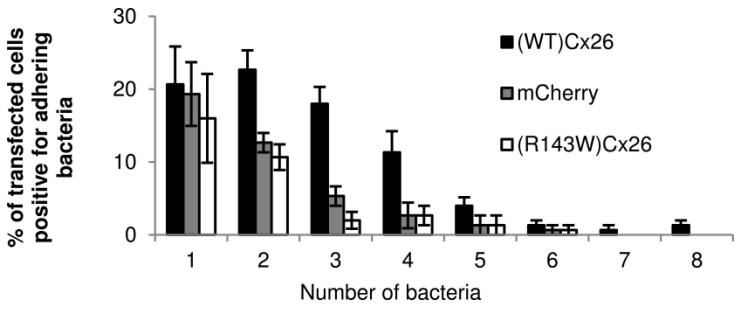

4.2.3.2 EPEC adherence and S. flexneri invasion in intestinal HT-29 and Caco-2 cell lines treated with Cx26 siRNA

Given that EPEC adherence and *S. flexneri* invasion were enhanced by a gain of functional Cx26 expression in transfected HeLa cells, the effect of Cx26 expression on enteric bacterial infection level was next considered in intestinal HT-29 and Caco-2 cells. Unlike HeLa cells, both of these intestinal cell lines express endogenous Cx26, and thus Cx26 expression was manipulated using Cx26 specific siRNA. The use of Cx26 siRNA prevents the production of Cx26 protein, making it possible to replicate *in vitro* many of the autosomal recessive Cx26 NSHL mutations which are termed 'loss of function', as they produce severely truncated non-functional proteins[51].

Following Cx26 siRNA treatment, Cx26 mRNA expression was quantified relative to GAPDH by qRT-PCR. Cx26 mRNA levels were 46.26% and 32.23% in HT-29 and Caco-2 cells respectively (figure 4.9 a). Heterozygous carriers of Cx26 NSHL mutations have one normal copy and one mutated copy of Cx26, so only approximately 50% of the Cx26 protein which they produce is functional. In this study therefore, although there was not a total inhibition in production of Cx26 mRNA following knock down, the levels observed were more representative of carriers of Cx26 NSHL mutations.

The percentage EPEC adhesion efficiencies were significantly reduced from 21.46% to 15.68% and from 14.22% to 7.26% in Caco-2 and HT-29 cells respectively following Cx26 siRNA treatment (figure 4.9 b). The invasion efficiencies of *S. flexneri* were not significantly different in HT-29 cells treated with non-targeting pool (NTP) siRNA (2.64%) and Cx26 siRNA (2.23%) (figure 4.9 c). Finally, treating cells with Cx26 siRNA significantly reduced *S. flexneri* invasion from 3.08% to 2.01% in Caco-2 cells (figure 4.9 c).

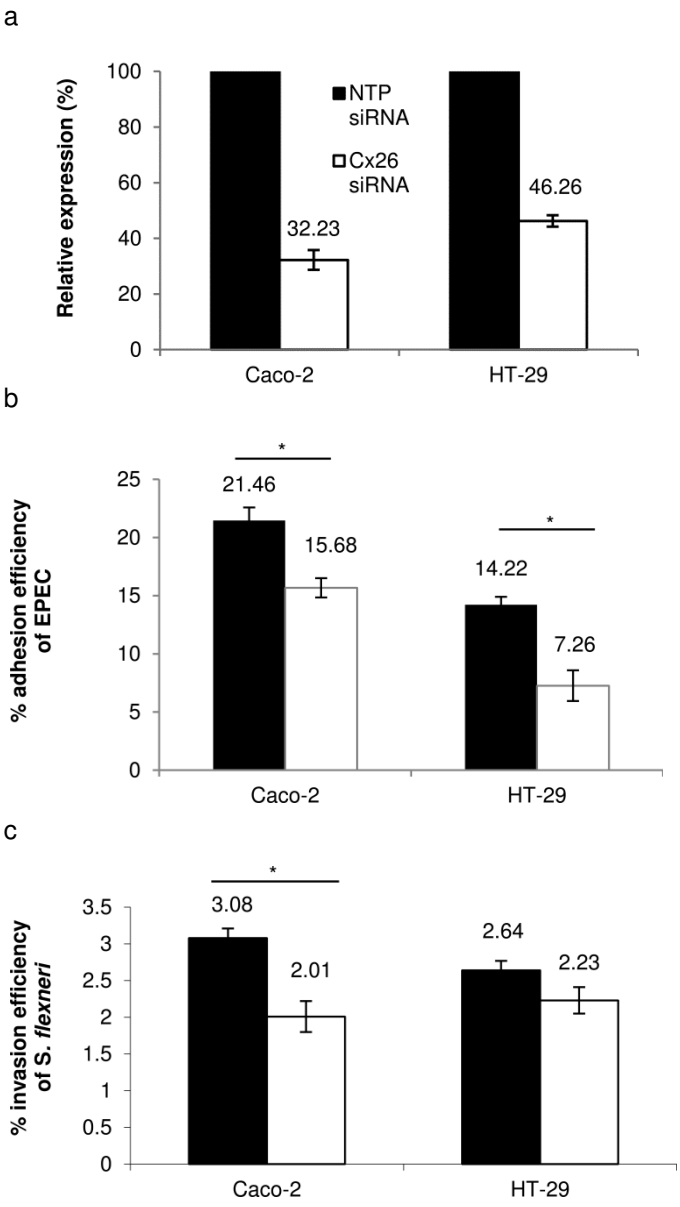

Figure 4.9 *S. flexneri* invasion and EPEC adherence in intestinal cells. (a) Cx26 mRNA expression was quantified relative to GAPDH by qRT-PCR in Caco-2 and HT-29 cells treated with non-targeting pool (NTP) siRNA and Cx26 siRNA (numbers on plot). Data represent mean ΔΔCT value ± the SEM; *n*=4. **(b)** EPEC adhesion efficiencies and **(c)** *S. flexneri* invasion efficiencies were quantified in Caco-2 cells and HT-29 cells which had been treated with NTP siRNA and Cx26 siRNA (numbers on plots). Data represent mean ± SEM; *n*=3. Comparisons were carried out by using unpaired, two-tailed t-tests. A significant reduction in EPEC adhesion efficiency was observed in both Caco-2 and HT-29 cells. Although a significant reduction in *S. flexneri* invasion efficiency was observed in Caco-2 cells, no significant difference was observed in HT-29 cells (* represents $p<5x10^{-2}$).

4.3 Discussion

The results in this study provide evidence to support the hypothesis that Cx26 NSHL mutations, for example p.R143W, may be selected for because they confer a protective advantage to the carrier. While *S. flexneri* invasion is enhanced in HeLa cells transfected with WT Cx26, invasion is significantly reduced in mock transfected HeLa cells, and HeLa cells expressing the p.R143W mutation, as has been previously reported[45,141,200]. EPEC adherence is also significantly increased in HeLa cells expressing WT Cx26 compared to mock transfected cells. A loss of functional Cx26 expression associated with the p.R143W mutation significantly reduced EPEC adherence to a level which was not significantly different to that exhibited by mock transfected cells. Furthermore, reducing endogenous Cx26 expression in intestinal cells by Cx26 specific siRNA, replicated the effects of many Cx26 NSHL mutations, which truncate the Cx26 protein and compromise its function *in vitro*[51]. This led to a significant reduction in the adhesion and invasion efficiencies of EPEC and *S. flexneri*. One explanation to account for the selection of Cx26 NSHL mutations could therefore be that they provide carriers with improved protection against gastrointestinal pathogens including EPEC and *S. flexneri*. This may be most beneficial to carriers of Cx26 NSHL mutations in developing countries, where exposure to such pathogens is greater than in developed countries.

This work could be extended *in vitro* to consider EPEC and *S. flexneri* infection levels in HeLa cells expressing other Cx26 NSHL mutations including c.35delG, c235delC and p.167delT, which are found at high carrier frequencies in European, Japanese and Ashkenazi Jewish populations respectively[114,116,117]. Results obtained from experiments performed in cell monolayers, may not accurately represent what happens in tissues *in vivo*, where multiple cell types are present. Organotypic cultures grown with Caco-2 or HT-29 cells provide a three-dimensional model in which the intestine can be studied *in vitro*, which may mimic what happens in *vivo* more accurately than cell monolayers. It would therefore be interesting to repeat the infection experiments in organotypic cultures, and determine whether the results obtained for cultures treated with NTP siRNA and Cx26 siRNA replicated the results obtained from cell monolayers.

A loss of functional Cx26 expression may result in the host being less susceptible to infection with gastrointestinal bacteria. Heterozygous carriers of the c.35delG[118] and p.R143W[120] alleles have a significantly thicker epithelium than WT Cx26 homozygotes. Furthermore, keratinocytes expressing the p.R143W mutation form a significantly thicker epidermis than keratinocytes expressing WT Cx26 in an *in vitro* organotypic co-culture skin model[45]. A thicker epidermal epithelium may act as a more robust barrier, and in turn, provide improved protection against infection. As similar protective properties of the skin also exist in the gut epithelium, it is plausible that heterozygous carriers of Cx26 NSHL mutations have a thicker gut epithelium, and therefore may be better protected against infection with gastrointestinal pathogens. The effect of Cx26 expression on the thickness of the gut epithelium should be investigated in future experiments. Any difference in epidermal thickness in organotypic cultures grown with Caco-2 or HT-29 cells treated with NTP siRNA and Cx26 siRNA should be measured. Additionally, the epidermal thickness could be measured from gut biopsies taken from homozygotes and heterozygous carriers of a range of Cx26 NSHL mutations including p.R143W, c35delG, c235delC and p.167delT.

Cx26 is expressed in the crypts of human colon enterocytes[199]. After wounding rat epidermis *in vivo*, Cx26 expression is upregulated at the wound site[67]. Cx26 upregulation has been linked to keratinocyte differentiation, proliferation and migration into the wound site[2,68]. Although organotypic cultures with keratinocytes expressing WT Cx26 and the p.R143W mutation do not display differences in cell proliferation, those expressing p.R143W undergo an extended terminal differentiation programme[45]. Performing scratch migration assays also revealed that keratinocytes expressing the p.R143W mutation migrate and close the scratch significantly quicker than keratinocytes expressing WT Cx26[45]. As similar protective properties exist between the gut and skin epithelium, potentially enterocyte proliferation, differentiation or migration could be affected by differential expression of Cx26. This could contribute to a thicker gut epithelium, and could also have implications for gastrointestinal infections which damage the intestinal epithelium, for example *S. flexneri*. *S. flexneri* infection is associated with a massive inflammatory

response, which in combination with ulceration and bleeding, leads to the destruction of the colonic epithelium.

S. flexneri opens Cx26 hemichannels in transfected HeLa cells releasing ATP into the extracellular medium[141,200]. Prior to invasion, the bacteria are captured by filopodial extensions which retract in response to ATP, bringing the bacteria into contact with the cell body where invasion takes place[141]. *S. flexneri* invasion is reduced in HeLa cells expressing the p.143W mutation, and in intestinal cells by siRNA against Cx26. Approximately only 50% of the Cx26 protein produced by heterozygous carriers of Cx26 NSHL mutations, who have one WT and one mutated copy of Cx26, is functional. It is likely that some Cx26 expressed within their intestines is non-functional. Therefore, the number of Cx26 hemichannels which can be utilised by *S. flexneri* for invasion might potentially be reduced in heterozygous carriers compared to WT Cx26 homozygotes. This could possibly explain why they are less susceptible to infection with S. *flexneri.* Functional assays could be performed in future experiments to determine the degree to which intestinal hemichannel activity is affected by differential expression of Cx26. This could include measuring the level of release of molecules such as ATP into the extracellular medium from intestinal HT-29 and Caco-2 cells.

The effect of Cx26 expression on gastrointestinal bacterial infection remains to be investigated *in vivo*. *C. rodentium* is used as an *in vivo* model of human EPEC infection[201]. Unpaired Cx43 hemichannels localise to the apical plasma membrane of mouse colonocytes where they facilitate water secretion into the intestinal lumen, which contributes to diarrhoea development during *C. rodentium* infection[201]. $Cx43^{+/-}$ mice that produce less functional Cx43 than WT mice, also produce less diarrhoea[201], which supports the hypothesis that a loss of functional Cx protein reduces infection by enteric bacteria. An aim of future work therefore, could be to consider how diarrhoea production during *C. rodentium* infection is affected by changes in Cx26 expression. Although $Cx26^{-/-}$ mice are embryonically lethal[50], diarrhoea production could be measured in $Cx26^{+/-}$ mice, or in mice expressing Cx26 NSHL mutations. Additionally, using Cre-lox technology to generate mice where Cx26 is conditionally knocked out in the colon could be utilised to investigate whether diarrhoea production is further reduced by a complete absence of Cx26. Cre lox technology involves tamoxifem inducible Cre recombinase being under the control of an intestinal

specific promoter, and the *GJB2* gene being flanked by loxP sites. Tamoxifem administration activates Cre, leading to the excision of the loxP sites, which in turn results in a loss of Cx26 expression from the tissue.

Cx43 expression has also been linked to *Y. enterocolitica* infection[202]. The bacteria induced tyrosine phosphorylation of Cx43 in transfected HeLa cells, which was thought to trigger hemichannel opening, in turn leading to their internalisation[202]. A reduction in *Y. enterocolitica* invasion was observed following treatment with a hemichannel blocker[202], which further supports the hypothesis that loss of functional Cx expression reduces infection with gastrointestinal bacteria. Additionally, Cx43 has also been linked to *Salmonella*. Tumour cells display reduced levels of GJIC and interestingly, treating them with *Salmonella* stimulated dye transfer between cells[295]. This indicated the presence of functional GJs, which occurred concomitantly with increased Cx43 expression[295]. Combined administration of *Salmonella* and the chemotherapy agent cisplatin reduced tumour growth by 73%, whereas cisplatin alone did not significantly affect tumour growth[295]. While this discovery is promising for cancer therapy, it also provides another example of gastrointestinal bacteria modifying GJIC, and therefore could potentially have implications for the treatment of enteric bacterial infections. In future experiments this work could also be extended to consider how Cx26 expression affects infection with other enteric bacteria including *Shigella, Yersinia*, *Salmonella, Listeria* and *Campylobacter in vivo*. The production of diarrhoea could be measured in living mice. In addition, the disease burden could be measured by sacrificing the mouse and determining the number of bacteria that are recovered from the colon. It would be interesting to confirm whether reductions in diarrhoea production and disease burden correlate with a loss of functional Cx26 expression. Cx26 may represent a potential, new therapeutic target for gastrointestinal bacterial infection. Loss of functional expression of both Cx26 and Cx43 has been associated with reduced enteric bacterial infection. However, since Cx43 is the most widely expressed Cx protein[17], targeting Cx43 may result in more adverse effects systemically than Cx26, and therefore of the two, Cx26 may represent the more attractive target.

During EPEC infection, the structure and function of tight junctions (TJ) and adherens junctions (AJ) is manipulated, which contributes to the production of

diarrhoea. Although a loss of functional Cx26 expression has been shown to reduce bacterial infection and result in a thicker epidermal barrier, other studies have also suggested that functional Cx26 has a role in maintaining the integrity of the epithelial barrier. Cx26 has been shown to colocalise with the TJ proteins occludin and ZO-1 in T84 colonic epithelial cells[296], and the AJ proteins α-catenin and E-cadherin in hepatocytes[297]. These interactions have been postulated to facilitate GJ, TJ and AJ formation. In a more recent study, chemically disrupting Caco-2 cell monolayers stably expressing Cx26 resulted in significantly decreased paracellular permeability and increased transepithelial resistance compared to mock transfected cells[298]. Expression of the TJ protein claudin 4 was also significantly increased in Caco-2 cells stably expressing Cx26[298]. The authors suggested that Cx26 mediated GJIC may therefore improve barrier maintenance in Caco-2 cells[298]. In future experiments it would be interesting to investigate whether differential expression of Cx26 affected the structure and function of the intestinal barrier during EPEC infection. Experiments could be carried out in intestinal HT-29 and Caco-2 cells in the presence and absence of Cx26 specific siRNA, and in HeLa cells transfected with various Cx26 NSHL mutants. Parameters measured could include the localisation of various TJ and AJ proteins, the transepithelial resistance and the paracellular permeability across the intestinal barrier. If these parameters were not significantly different in either uninfected or infected cells with differential expression of Cx26, the reduced infection associated with a loss of functional Cx26 would probably be unrelated to the maintenance of the intestinal barrier. If these parameters were significantly altered, any effect would probably be Cx26 rather than EPEC dependent, since infection is reduced by a loss of functional Cx26 expression. The localisation of TJ and AJ proteins could also be visualised by two photon microscopy in mice with differential expression of Cx26 during *C. rodentium* infection.

Although these results support others studies, which suggest that a loss of functional Cx expression could improve resistance to gastrointestinal infection, Cx expression has also been linked to the induction of immune responses. Infecting A431 cells (derived from a vulva epidermal carcinoma) with *S. flexneri,* leads to the activation of NF-κB and the MAP kinases JNK, p38 and ERK, and the production of IL-8 in both infected, and non-infected bystander cells[157]. IL-8

production by bystander cells is significantly reduced by siRNA against Cx43, or by treatment with the GJ blocker 18β-glycyrrhetinic acid[157]. This suggests that activation of proinflammatory signalling cascades is transferred from infected cells to uninfected neighbouring cells via GJs, in turn amplifying the host immune response during bacterial infection[157]. *Shigella* injects effectors including OspF and OspG, which dampen the host immune response[129,160], during the later stages of infection. During the earlier stages of infection, however, *Shigella* induces a massive inflammatory response, of which IL-8 in particular plays an important role, because it stimulates neutrophil recruitment into the intestine. This damages the epithelial surface allowing more bacteria to cross the intestinal barrier, and gain access to the basolateral pole of epithelial cells where invasion takes place. Thus, propagation of the immune response via GJs could potentially be less beneficial to the host initially, when a strong inflammatory response helps the bacteria establish an infection. During the later stages of infection, when the bacteria try to suppress inflammation, a strong inflammatory response may be more beneficial to the host, and may contribute to the elimination of infection.

Although Cx43 was linked to the induction of immune responses during *S. flexneri* infection *in vitro*, it would be interesting to determine if the immune response was affected by differential expression of either Cx26 or Cx43 during *S. flexneri* infection of mice *in vivo.* If mice were infected with bacteria labelled with a fluorescent reporter tag, two photon microscopy could be employed to determine whether activation of immune cascades was solely in infected cells, or whether it also propagated to uninfected cells. Immune signalling cascade activation could be determined by nuclear localisation of NF-κB and phosphorylation of the MAP kinases JNK, p38 and ERK. The transcription of inflammatory molecules could also be followed if their promoters controlled the expression of the fluorescent luciferase reporter gene[299]. Any effect of differential expression of Cx26 or Cx43 on immune cell recruitment into the intestine could also be followed. If propagation of the immune response via GJs occurred, the potential implications for the host in terms of infection level could be determined by sacrificing mice at different infection time points and quantifying the number of bacteria recovered from the intestine.

Peptidoglycan derived from gram positive bacteria has also been shown to activate the innate immune response, in a process dependent on Cx expression. Stimulating endothelial cells with *S. epidermidis* has been shown to induce Cx43 hemichannel opening, which in turn stimulates TLR2 and IL-6 gene transcription; IL-6 and TLR2 expression is abolished by treatment with hemichannel blockers[300,301]. In a subsequent study, IL-6 mRNA production was also observed 6 hours post stimulation with *S. aureus* in HaCaT keratinocytes which had been transfected with WT Cx26[301]. Interestingly, in this study, expression of IL-6 mRNA was significantly greater in HaCaT cells which had been transfected with keratosis-ichthyosis-deafness (KID) syndrome mutations, but was significantly reduced by blocking hemichannel activity[301]. Many KID patients are prone to infection with gram positive bacteria[301]. Although KID mutations and Cx26 NSHL mutations both prevent the formation of functional GJs, KID mutations may be associated with increased *S. aureus* infection, whereas Cx26 NSHL mutations have been linked to reduced infection by gastrointestinal bacteria. A simple explanation for this could be that different types of bacteria use different methods to set up an infection in the host. However, Cx26 NSHL mutations and KID mutations also behave differently. *S. flexneri* triggers Cx26 hemichannel opening to facilitate invasion and dissemination[141,200]. Therefore, rather than trafficking to the cell surface, if a NSHL mutation such as p.R143W accumulates in the cytoplasm, it follows that infection would be reduced. KID mutants, however, traffic to the cell surface where they induce aberrant hemichannel activity[51],[19]. The hemichannels may be open for longer durations than WT Cx26 hemichannels, as evidenced by their significantly increased release of ATP into the extracellular medium[301]. *Y. enterocolitica* also induces Cx hemichannel opening favouring bacterial uptake[202]. It is potentially possible that *S. aureus* internalisation could be enhanced by open hemichannels, and if Cx26 hemichannels formed from KID mutants were open for longer durations, could suggest why KID patients are prone to infection.

4.4. Conclusion

This chapter has demonstrated that a loss of functional Cx26 expression significantly reduces the adherence and invasion of EPEC and *S. flexneri in vitro*. The results provide support for the hypothesis that Cx26 NSHL mutations may be selected for because they confer a protective advantage to the carrier. Cx26 may represent an alternative therapeutic target for the treatment of gastrointestinal infection. The discovery that cystic fibrosis transmembrane conductance regulator (CFTR) genetic mutations, responsible for cystic fibrosis, confer an advantage to carriers exposed to secretory diarrhoea agents such as *cholera*, has already led to the development of several CFTR inhibitors for antidiarrheal therapy. The development of Cx26 inhibitors in the future would therefore also hopefully improve treatment for enteric bacteria, which are becoming increasingly resistant to multiple antibiotics.

~ Chapter 5 ~

Effect of ADAM17 Expression on Cutaneous Bacterial Infection

5.1 Introduction

ADAM17 acts as a sheddase enzyme cleaving various membrane-bound precursor proteins from the surfaces of cells[203]. This releases the soluble, extracellular portions of the proteins into the bloodstream which subsequently participate in a wide range of biological processes. ADAM17 was the first ADAM protein to be implicated in ectodomain shedding, following its identification as the TNFα converting enzyme (TACE), which sheds a biologically active form of TNFα[203,205,206]. ADAM17 also facilitates proinflammatory cytokine signalling by shedding receptors including the IL-6R[209,224,226,227], and is thus an important stimulator of the immune response. ADAM17 sheds ligands of the epidermal growth factor (EGF) receptor including amphiregulin[230], making it an important upstream regulator of the EGFR signalling pathway. This is important for maintenance of the epidermal[238] and intestinal[243] barriers in mice. These combined activities of ADAM17 suggest that it may play an important role in providing protection during bacterial infection. Loss of function mutations in ADAM17 have been linked to a recessively inherited neonatal onset inflammatory skin and bowel disease in two siblings[239]. The syndrome was associated with recurrent skin infections with *S. aureus*, and chronic diarrhoea which was worsened by gastrointestinal infection[239]. This is consistent with a role for ADAM17 providing protection during infection.

ADAM17 has recently been linked to a major regulator of its activity, inactive rhomboid protein iRhom2. iRhom2 transports pro-ADAM17 from its site of synthesis in the ER, to the Golgi apparatus where it matures[256,258,259]. Gain of function mutations in *RHBDF2*, make iRhom2 overactive, and have recently been identified as the cause of the skin condition tylosis with oesophageal cancer (TOC)[248,252]. Two studies provide evidence suggesting that iRhom2 plays a role in the regulation of the ADAM17 dependent immune response[256,258]. In the first study, TNFα secretion was significantly reduced in macrophages from *iRhom2*$^{-/-}$ mice compared to WT mice[256], whilst in the second study, *iRhom2*$^{-/-}$ mice were more susceptible to infection with *L. monocytogenes* than WT mice[258]. These results are consistent with impaired trafficking of ADAM17 to the cell surface, which in turn compromises the induction of immune responses required to clear bacterial infection.

In a paper being prepared for publication, experiments performed by Matthew Brooke (Centre for Cutaneous Research) using two immortalised keratinocyte cell lines deriving from biopsies taken from TOC patients, have shown that TOC keratinocytes have increased ADAM17 activity compared to control keratinocytes. Immunofluorescence demonstrated increased ADAM17 expression at the plasma membrane, whilst western blotting revealed increased mature ADAM17 protein expression and cleaved pro-domain in TOC keratinocytes. Secretion of cytokines including TNFα, IL-6 and IL-8, and growth factors including amphiregulin and HB-EGF was also increased in TOC keratinocytes. These observations provide support for the hypothesis that overactive iRhom2 in TOC keratinocytes leads to increased trafficking of ADAM17 to the cell surface. Since these results strongly suggest that ADAM17 activity is increased in TOC keratinocytes, and other studies have demonstrated a protective effect for ADAM17 during bacterial infection, it follows that infection levels may be reduced in TOC keratinocytes.

5.1.1 Aims

- Investigative how infection with the gastrointestinal pathogens EPEC (method 2.42) and *S. flexneri* (method 2.43) was affected by loss of functional ADAM17 expression
- Consider how a loss of functional ADAM17 expression affected *S. aureus* adhesion and invasion (method 2.44) in keratinocyte skin cell lines. Since attempts made to immortalise keratinocytes from the ADAM17 deficient patient were unsuccessful, this was replicated by studying how infection was affected by treating keratinocytes with siRNA against ADAM17 (method 2.15)
- Confirm ADAM17 knock down at the mRNA and protein level by qRT-PCR (method 2.2.3) and western blotting (method 2.5)
- Consider how *S. aureus* infection is affected by increased ADAM17 activity; infection will be compared in control and TOC keratinocytes
- Assuming that ADAM17 is shown to protect against bacterial infection, its method of action will be explored in subsequent experiments:
    - Investigate whether the secretion of proinflammatory cytokines is affected by changes in ADAM17 expression in *S. aureus* infected keratinocytes by ELISA (method 2.8)

- Investigate whether ADAM17 affects α5β1 integrin mediated *S. aureus* invasion
- Investigate whether the secretion of the antimicrobial peptides, human beta defensins 2 and 3, is affected by changes in ADAM17 activity
- Carry out gene expression profiling to identify other downstream targets of ADAM17 in control and TOC keratinocytes, in the prescence and absence of ADAM17 siRNA (method 2.24). Following their identification, additional experiments including qRT-PCRs, western blotting, immunohistochemistry and ELISAs (methods 2.23, 2.5, 2.7 and 2.8) will be performed to further investigate whether they are affected by changes in ADAM17 expression

5.2 Results

5.2.1 ADAM17 knock down evaluation

To study how bacterial infection was affected by a loss of ADAM17 expression, cells were treated with siRNA against ADAM17. To confirm that any difference in infection was due to differential expression of ADAM17, the knock down efficiency was first evaluated at the mRNA level by qRT-PCR (figure 5.1 a). This was carried out in HT-29 intestinal epithelial cells, in NEB1 and K17 control keratinocyte skin cells, and in TYLK1 and TYLK2 TOC keratinocyte skin cells. Quantifying ADAM17 mRNA relative to GAPDH 48 hours post knock down, revealed that ADAM17 levels were reduced by approximately 70% in HT-29 cells, 75% in NEB1 cells, 80% in K17 cells, 13% in TYLK1 cells and 10% in TYLK2 cells (figure 5.1 a).

ADAM17 protein expression was analysed by western blotting in HT-29 cells (figure 5.1 b) and keratinocytes (figure 5.1 c) which had been treated with a non-targeting pool (NTP) siRNA and ADAM17 siRNA. Two bands at approximately 100 kDa and 125 kDa corresponding to ADAM17 expression could be detected in cells which had been treated with NTP siRNA (HT-29 cells, figure 5.1 b, TOC and control keratinocytes, figure 5.1 c). ADAM17 is synthesised as a pro-protein, and cleavage of its pro-domain generates mature

ADAM17. Therefore, the band at 125 kDa represents pro-ADAM17, whilst the band at 100 kDa represents mature ADAM17 which has undergone pro-domain removal. Analysis of cells treated with ADAM17 siRNA revealed an absence of the two bands (HT-29 cells, figure 5.1 b, and TOC and control keratinocytes, figure 5.1 c). Together with the qRT-PCR data, these results demonstrate that the knock down of ADAM17 was efficient at the mRNA and protein level in all five cell types.

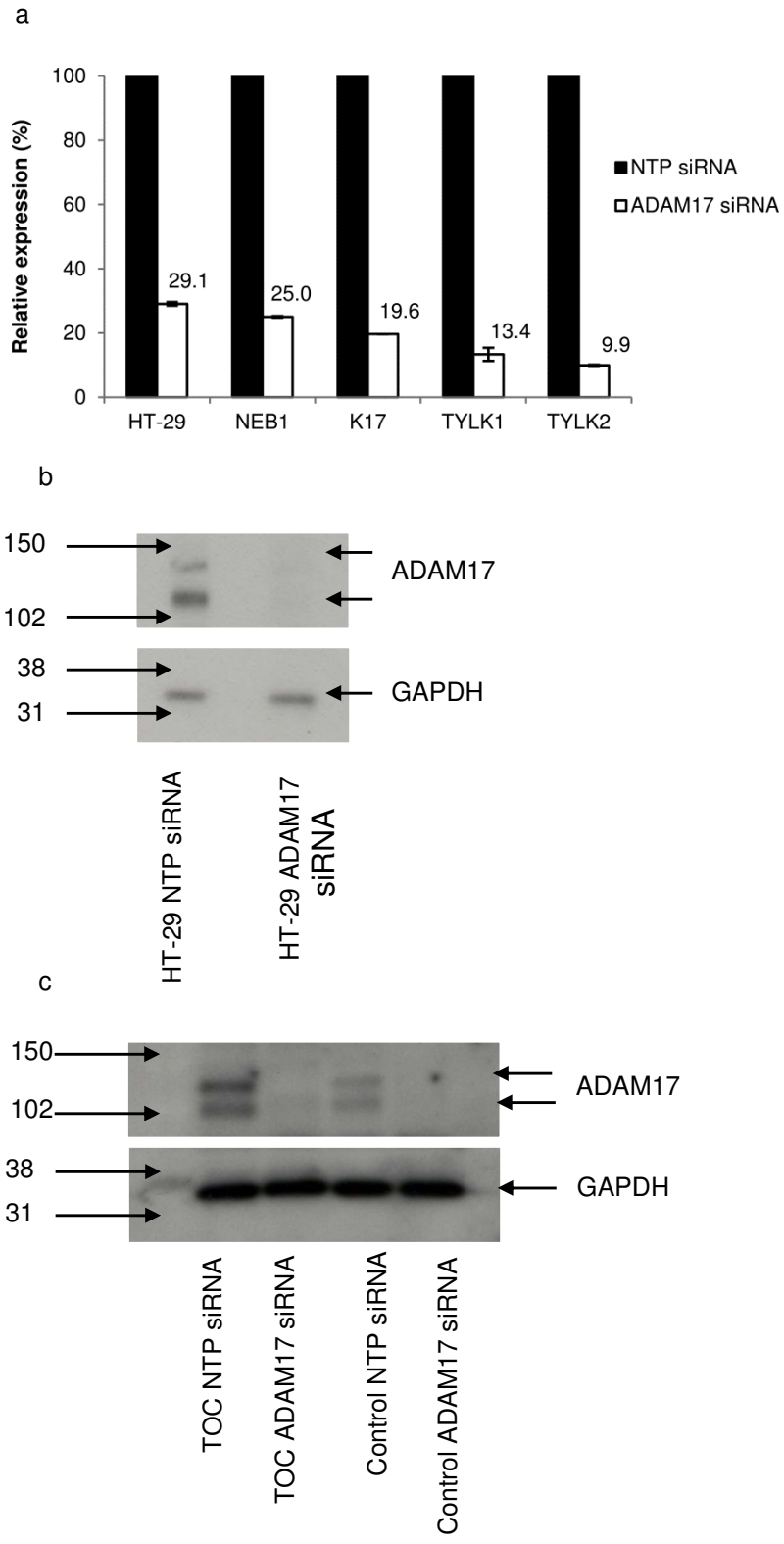

Figure 5.1: ADAM17 knock down evaluation. ADAM17 expression in HT-29 cells, control (NEB1 and K17) and TOC (TYLK1 and TYLK2) keratinocytes treated with NTP siRNA and ADAM17 siRNA. **(a)** Relative expression of ADAM17 mRNA normalised to GAPDH (numbers on plot) quantified by qRT-PCR. Data represent mean ΔΔCT value ± *SEM;* n=3. **(b)** ADAM17 protein expression in HT-29 cells. **(c)** ADAM17 protein expression in TOC (TYLK1 and TYLK2) and control (NEB1 and K17) keratinocytes. Bands at approximately 125 kDa and 100 kDa represent full length and mature ADAM17 expression in cells treated with NTP siRNA, which are absent in cells treated with siRNA to ADAM17, confirming knock down at protein level **(b, c)**. GAPDH is used as a loading control **(b, c)**.

5.2.2 *S. flexneri* invasion and EPEC adherence in intestinal HT-29 cells and control NEB1 keratinocytes treated with ADAM17 siRNA

To consider how bacterial infection was affected by ADAM17 expression, the effect of knocking down ADAM17 on bacterial infection was first investigated. EPEC and *S. flexneri* were initially used as models of infection, as they were the two pathogens which had been worked with previously. Treating HT-29 cells with ADAM17 siRNA resulted in increased bacterial infection. Treating cells with ADAM17 siRNA led to a significant increase in the invasion efficiency of *S. flexneri* from 2.40% to 4.13% (figure 5.2). In a population of HT-29 cells infected with EPEC, 45.56% and 65.74% of cells treated with NTP siRNA and ADAM17 siRNA respectively, were positive for adhering bacteria and this difference was statistically significant (figure 5.3). The number of bacteria that adhered per cell was also greater following treatment with ADAM17 siRNA, suggesting that the infection level of individual cells was higher following knock down (figure 5.3 h). This suggests that ADAM17 provides protection against gastrointestinal pathogens in HT-29 cells.

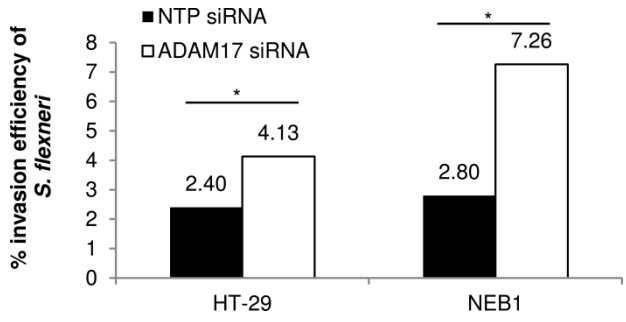

Figure 5.2: *S. flexneri* invasion efficiency in HT-29 cells and NEB1 cells treated with NTP siRNA and ADAM17 siRNA. Data represent mean percentage invasion efficiency (numbers on plot) ± the SEM; *n*=3. Comparisons were carried out by using unpaired, two-tailed t-tests, where significant differences were observed between NTP siRNA and ADAM17 siRNA treated HT-29 and NEB1 cells (* represents $p<5x10^{-2}$).

Figure 5.3: Wild type EPEC (JPN15) adherence to HT-29 cells treated with NTP siRNA and ADAM17 siRNA. Adherence was quantified by pGFP expression by manual counting. NTP siRNA (**a-c)** and ADAM17 siRNA **(d-f). (a, d)** Nuclei of cells and bacterial DNA (*DAPI* staining in *blue)*. (**b**, **e**) EPEC (*green*). **(c, f)** Merged images. Image magnification 40x. *Bars* 20µm. **(g)** Total percentage of cells positive for adhering EPEC (numbers on plot). Data represent mean ± the SEM; *n*=3. Comparison was carried out by using an unpaired, two-tailed t-test, where a significant difference was observed between HT-29 cells treated with NTP siRNA and ADAM17 siRNA (**** represents $p<5x10^{-5}$). **(h)** Number of bacteria that adhered per cell.

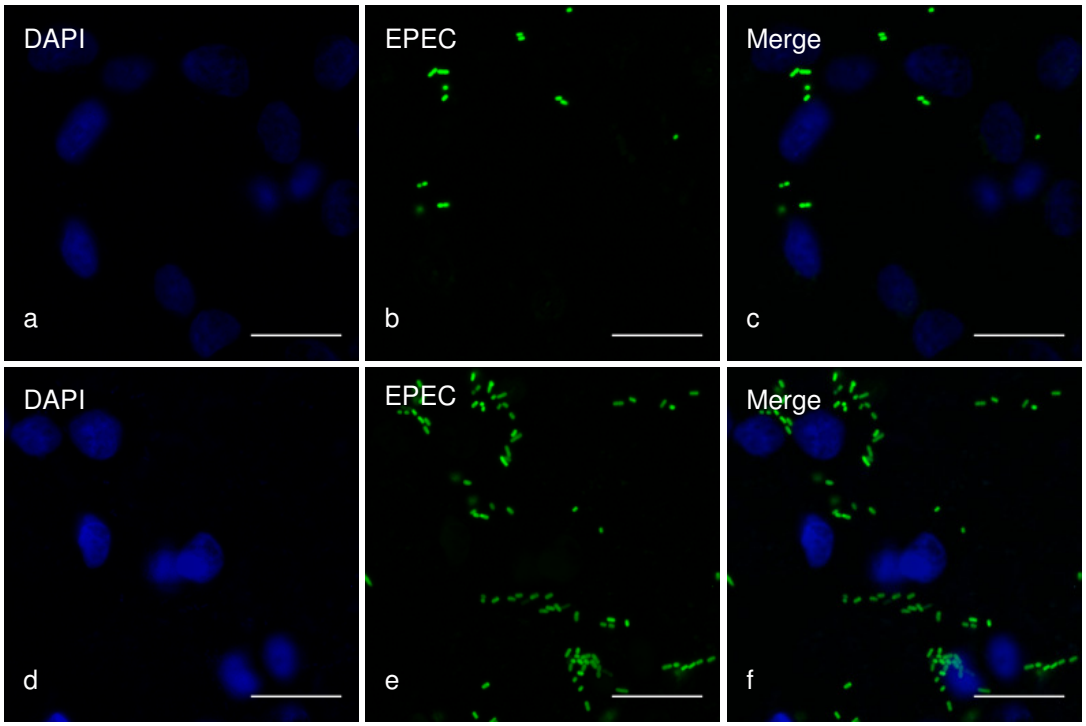

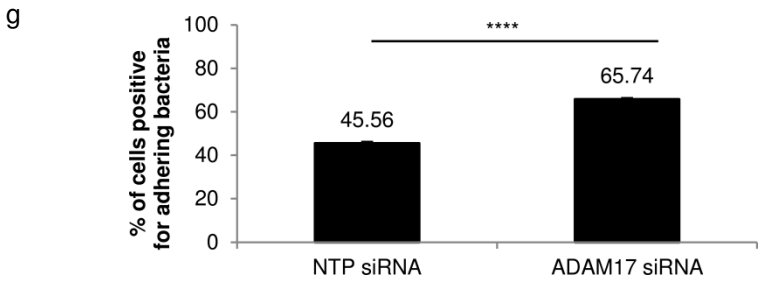

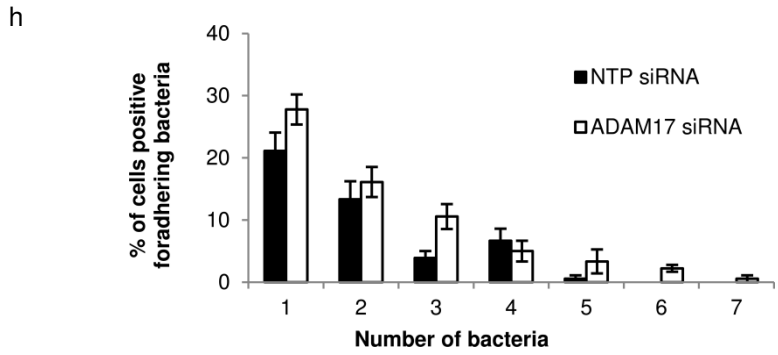

Next, in order to be relevant to the study of skin disease, EPEC and *S. flexneri* infection assays were repeated in NEB1 keratinocytes treated with NTP siRNA and ADAM17 siRNA. In further support of the HT-29 cell infection results, treating NEB1 cells with ADAM17 siRNA resulted in a significant increase in the invasion efficiency of *S. flexneri* from 2.80% to 7.26% (figure 5.2), a significant increase in the total percentage of cells positive for adhering EPEC from 50.00% to 76.67% (figure 5.4 g), and an increase in the number of EPEC which adhered per cell (figure 5.4 h). The consistency of the infection assay results in the two different cell lines strongly suggests that ADAM17 expression reduces infection by gastrointestinal pathogens.

Figure 5.4: Wild type EPEC (JPN15) adherence to NEB1 cells treated with NTP siRNA and ADAM17 siRNA. Adherence was quantified by pGFP expression by manual counting. **(a-c)** NTP siRNA. **(d-f)** ADAM17 siRNA. **(a, d)** Nuclei of cells and bacterial DNA (*DAPI* staining in *blue)*. **(b, e)** EPEC (*green*). **(c, f)** Merged images. Image magnification 40x. *Bars* 20µm. **(g)** Total percentage of cells positive for adhering EPEC (numbers on plot). Data represent mean ± the SEM; *n*=3. Comparison was carried out by using an unpaired, two-tailed t-test, where a significant difference was observed between NEB1 cells treated with NTP siRNA and ADAM17 siRNA (** represents $p<5x10^{-3}$). **(h)** Number of bacteria that adhered per cell.

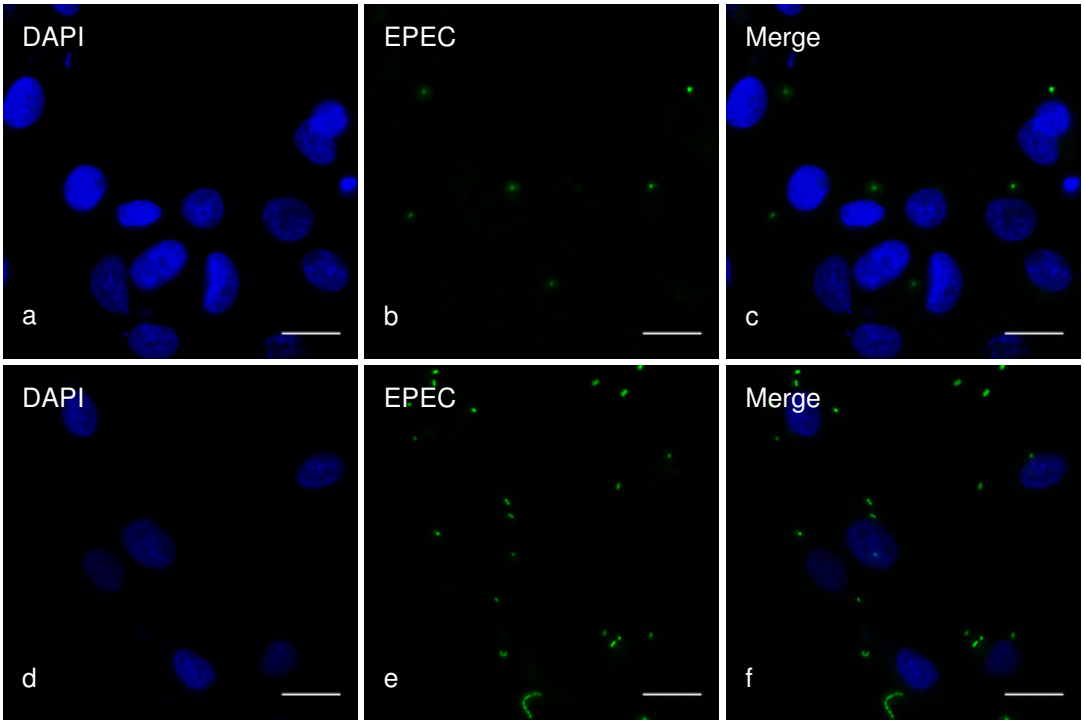

g

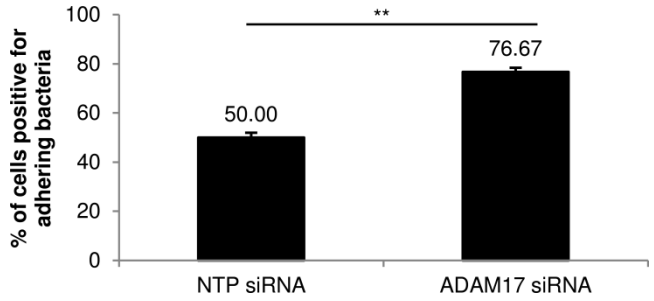

h

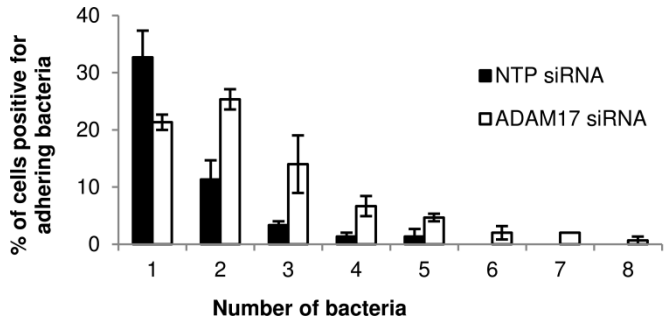

5.2.3 Effect of ADAM17 expression on *S. aureus* infection in control and TOC keratinocytes

S. aureus was considered a more relevant model of infection for studying how ADAM17 expression affects bacterial infection in the skin. *S. aureus* can persist as an extracellular pathogen adhering to components of the plasma membrane and extracellular matrix (ECM), or as an intracellular pathogen following invasion into specific cell types. Therefore, both the adhesion and invasion efficiencies were quantified to measure *S. aureus* infection. Bacterial adherence was measured by subtracting the internalised bacteria from the cell-associated bacteria. For more accurate quantification of infection, two control and two TOC keratinocyte cell lines were analysed. NEB1 and K17 control keratinocytes, and TYLK1 and TYLK2 TOC keratinocytes were pooled for subsequent statistical analysis.

As expected, knocking down ADAM17 in control keratinocytes resulted in significantly increased *S. aureus* adhesion and invasion efficiencies from 21.2% to 70.0% (figure 5.5 a, b) and from 2.6% to 5.5% (figure 5.5 c, d) respectively. This suggested a requirement for ADAM17 in providing protection against *S. aureus* infection. It therefore follows that increased ADAM17 activity may be associated with reduced *S. aureus* infection. To investigate how infection was affected by increased ADAM17 activity, infection levels were compared in control keratinocytes and TOC keratinocytes. The adhesion efficiencies of control and TOC keratinocytes were 21.2% and 13.2% (figure 5.5 b), while the invasion efficiencies were 2.6% and 1.3% (figure 5.5 d). As these results demonstrate that increased ADAM17 activity associated with TOC keratinocytes significantly reduces *S. aureus* infection, this provides additional support for the hypothesis that ADAM17 is required for protection during *S. aureus* infection. This was further demonstrated by knocking down ADAM17 in TOC keratinocytes. As expected, treatment with ADAM17 siRNA led to significant increases in bacterial adhesion and invasion efficiencies to 44.8% and 3.8% respectively (figure 5.5 c, d).

Figure 5.5: Effect of ADAM17 expression on *S. aureus* infection in keratinocytes. *S. aureus* adhesion **(a, b)** and invasion **(c, d)** efficiencies (numbers on plots) in control (NEB1 and K17) and TOC (TYLK1 and TYLK2 keratinocytes treated with NTP siRNA and ADAM17 siRNA. **(a, c)** Results from individual cell lines. **(b, d)** Control and TOC keratinocyte results are pooled for statistical analysis. Data represent mean ± the SEM; **a**, **c** *n*=3; **b**, **d** *n*=6. Comparisons were carried out by using unpaired, two-tailed t tests; where significant differences were observed between control NTP siRNA and control ADAM17 siRNA, control NTP siRNA and TOC NTP siRNA, and TOC NTP siRNA and ADAM17 siRNA for adhesion **(b)** and invasion **(d)** efficiencies (**, *** and **** represents $p<5x10^{-3}$, $p<5x10^{-4}$ and $p<5x10^{-5}$ respectively).

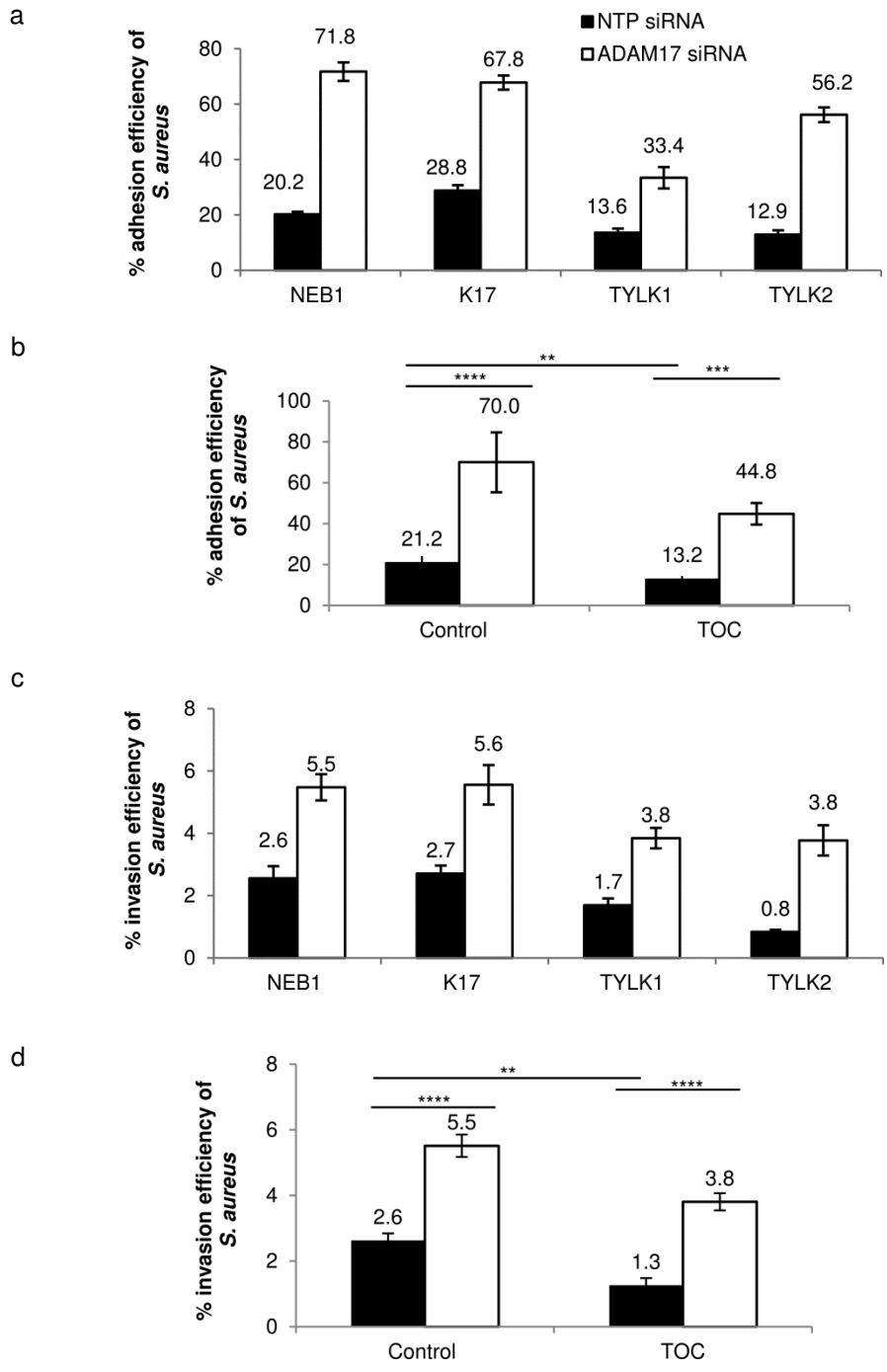

In summary, this set of experiments strongly suggests that ADAM17 is required to reduce *S. aureus* skin infection. Loss of functional ADAM17 in control keratinocytes leads to increased infection, whilst increased ADAM17 activity in TOC cells decreases infection. Furthermore, the protective effect conferred by increased ADAM17 in TOC cells is lost following ADAM17 knock down, when a significant increase in infection is observed. The next set of experiments carried out therefore investigated the mechanisms of ADAM17 mediated protection during bacterial infection.

5.2.4 Effect of ADAM17 expression on the secretion of proinflammatory cytokines IL-6 and IL-8

ADAM17 drives inflammatory responses, first and foremost by cleaving TNFα. TNFα expression coordinates early immune responses, by stimulating the expression of other proinflammatory cytokines including IL-1β and IL-6, and by the induction of adhesion molecules and chemokines which recruit leukocytes to the site of infection[302]. IL-8 is a potent neutrophil recruiter. As discussed in section 1.2.13, neutrophils are the first innate immune cells recruited to the site of infection, and once recruited, they use multiple mechanisms to kill invading pathogens[269].

Although IL-6 and IL-8 are not shed by ADAM17, they are produced in response to TNFα signalling, so their production is affected by changes in ADAM17 expression. As mentioned in section 5.1, experiments performed by Matthew Brooke (Centre for Cutaneous Research) confirmed that IL-6 and IL-8 secretion was increased in TOC keratinocytes compared to control keratinocytes following stimulation with LPS and PMA/ionomycin, but significantly reduced in both cell types following treatment with ADAM17 siRNA. The increased secretion of proinflammatory cytokines by TOC keratinocytes could therefore represent one way by which ADAM17 acts to reduce infection. The next set of experiments carried out considers IL-6 and IL-8 production during *S. aureus* infection in control and TOC keratinocytes, in the presence and absence of ADAM17 siRNA. It was hypothesised that their production would be linked to changes in ADAM17 expression.

In uninfected cells, IL-6 and IL-8 secretion was dependent on ADAM17 expression. Knocking down ADAM17 in control keratinocytes significantly reduced IL-6 production from 106.85 pg/ml to 46.03 pg/ml (figure 5.6 a, b), and IL-8 secretion from 326.98 pg/ml to 220.69 pg/ml (figure 5.6 c, d). Secretion was significantly greater in TOC keratinocytes, which produced 211.03 pg/ml of IL-6 (figure 5.6 a, b) and 611.44 pg/ml of IL-8 (figure 5.6 c, d). In addition, siRNA against ADAM17 in uninfected TOC keratinocytes significantly reduced IL-6 production to 41.22 pg/ml (figure 5.6 a, b), and IL-8 production to 209.78 pg/ml (figure 5.6 c, d).

S. aureus infection increased IL-6 and IL-8 secretion above the basal level produced in uninfected cells. Control keratinocytes displayed significantly reduced IL-6 production from 172.33 pg/ml to 91.92 pg/ml (figure 5.6 a, b), and IL-8 secretion from 473.89 pg/ml to 310.69 pg/ml (figure 5.6 c, d) after treatment with siRNA against ADAM17. Increased ADAM17 activity in TOC keratinocytes correlated with significantly increased cytokine production; they produced 211.03 pg/ml of IL-6 (figure 5.6 a, b) and 834.35 pg/ml of IL-8 (figure 5.6 c, d) respectively. Finally, knocking down ADAM17 in infected TOC keratinocytes significantly decreased IL-6 secretion to 116.75 pg/ml (figure 5.6 a, b), and IL-8 production to 352.70 pg/ml (figure 5.6 c, d).

In summary, this set of experiments has demonstrated that the production of IL-6 and IL-8 in uninfected keratinocytes and during *S. aureus* infection is dependent on ADAM17 expression. On the one hand, a loss of functional ADAM17 expression in both control and TOC keratinocytes is accompanied by a decreased secretion of IL-6 and IL-8. On the other hand, TOC keratinocytes with increased ADAM17 activity, display reduced infection, occurring concomitantly with increased IL-6 and IL-8 secretion. These results may therefore indicate one way that ADAM17 acts to provide protection during skin infection with *S. aureus.*

Figure 5.6: Secretion of IL-6 and IL-8 in keratinocytes. IL-6 **(a, b)** and IL-8 **(c, d)** secretion in control (NEB1 and K17) and TOC (TYLK1 and TYLK2 keratinocytes treated with NTP siRNA and ADAM17 siRNA. **(a, c)** Results from individual cell lines. **(b, d)** Control and TOC keratinocyte results are pooled for statistical analysis. Data represent mean ± the *SEM*; **a**, **c** *n*=3; **b**, **d** *n*=6. Comparisons were carried out by using unpaired, two-tailed t tests. For IL-6 **(b)** and IL-8 **(d)**, significant differences were observed between uninfected and infected, control NTP siRNA and control ADAM17 siRNA, control NTP siRNA and TOC NTP siRNA, and TOC NTP siRNA and ADAM17 siRNA (**** represents $p<5x10^{-5}$).

a

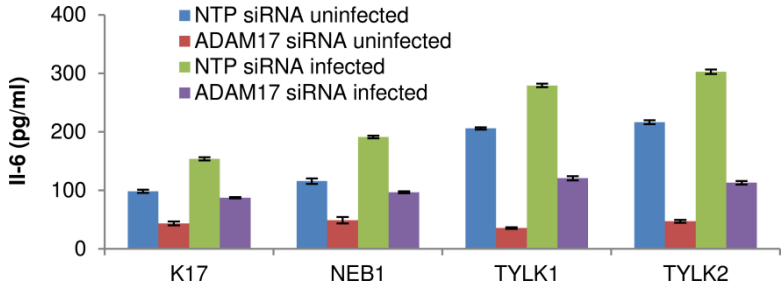

b

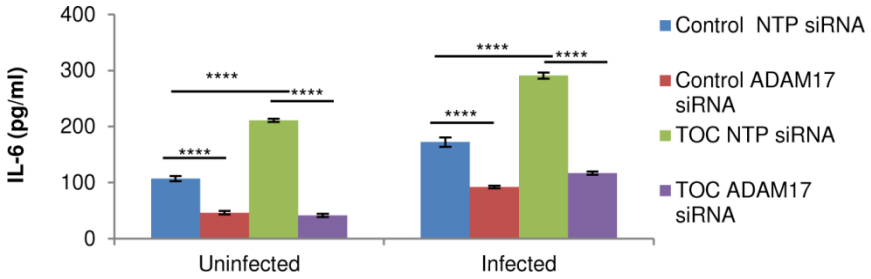

c

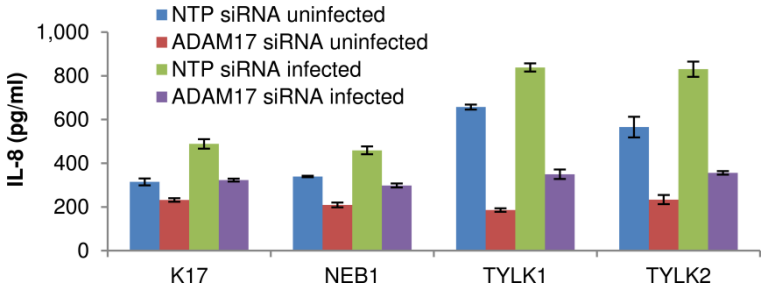

d

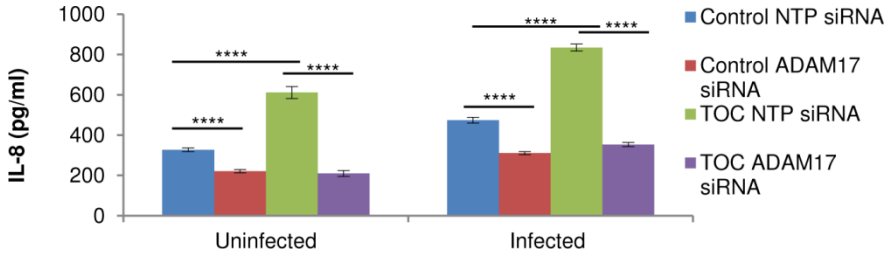

5.2.5 Effect of ADAM17 expression on α5β1 integrin mediated *S. aureus* invasion

Cellular invasion by *S. aureus* can be mediated by the interaction of fibronectin-binding proteins (e.g. FnBPA and FnBPB) expressed on the surface of the bacterium with the host cell α5β1 integrin ECM component[264]. In addition, ADAM17 has been shown to bind to α5β1 integrin through its disintegrin or cysteine-rich domains[218]. As α5β1 integrin has been implicated in *S. aureus* infection and shown to interact with ADAM17, this set of experiments investigated whether changes in ADAM17 expression influenced α5β1 integrin mediated *S. aureus* invasion. One hypothesis considered was that ADAM17 may influence the localisation and availability of α5β1 integrin.

To initially demonstrate a requirement for α5β1 integrin expression during *S. aureus* infection, β1 integrin was knocked down in control NEB1 and K17 keratinocytes. As knocking down β1 integrin significantly reduces the expression of the α5 subunit[303], any differences in infection were assumed to result from an impaired interaction with both the α5 and β1 subunits. Knock down of β1 integrin was confirmed by western blotting and immunofluorescence. The antibody against β1 integrin produced heavy background staining, which made it difficult to detect expression by western blotting (figure 5.7). However, a faint band could be detected at 130 kDa in NEB1 (figure 5.7 a) and K17 cells (figure 5.7 b) which had been treated with NTP siRNA. The same band was absent in cells which had been treated with siRNA against β1 integrin. The expression of β1 integrin was detected by immunofluorescence at the plasma membrane in K17 (figure 5.8 a-c) and NEB1 (figure 5.8 g-i) cell monolayers treated with NTP siRNA. This staining was absent in K17 (figure 5.8 d-f) and NEB1 (figure 5.8 j-l) cell monolayers treated with β1 integrin siRNA. Together, the western blotting and immunofluorescence results demonstrate that the knock down of β1 integrin protein was successful.

Figure 5.7: Western blotting for β1 integrin protein in keratinocytes treated with NTP siRNA and β1 integrin siRNA. **(a)** NEB1 cells. **(b)** K17 cells. The band at 130 kDa corresponds to β1 integrin expression in cells treated with NTP siRNA. It is absent in cells treated with siRNA against β1 integrin, confirming a reduction in β1 integrin protein following knock down. GAPDH is used as a loading control.

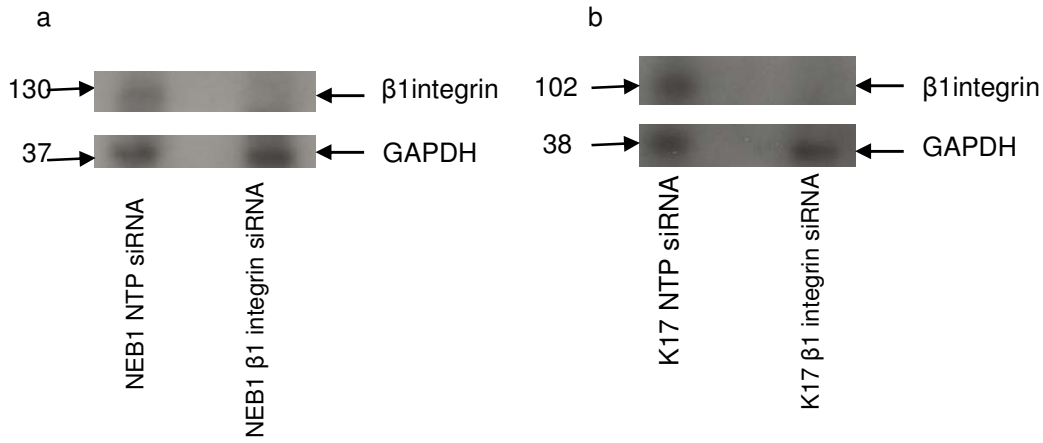

Figure 5.8: Immunofluorescence for β1 integrin expression in keratinocytes treated with NTP siRNA and β1 integrin siRNA. K17 **(a-c)** and NEB1 **(g-i)** cells treated with NTP siRNA and K17 **(d-f)** and NEB1 cells **(j-l)** treated with β1 integrin siRNA. Negative control: cells which have not been stained with β1 integrin antibody. **(a, d, g, j, m)** Nuclei of cells (*DAPI* staining in *blue)*. **(b, e, h, k)** β1 integrin (*green*). **(n)** Unstained cells (negative control). **(c, f, i, l, o)** Merged images. Note the plasma membrane expression of β1 integrin in cells treated with NTP siRNA **(b, c, h, i)**, which is absent in cells treated with β1 integrin siRNA **(e, f, k, l)**. Image magnification 40x. *Bars* 20μm.

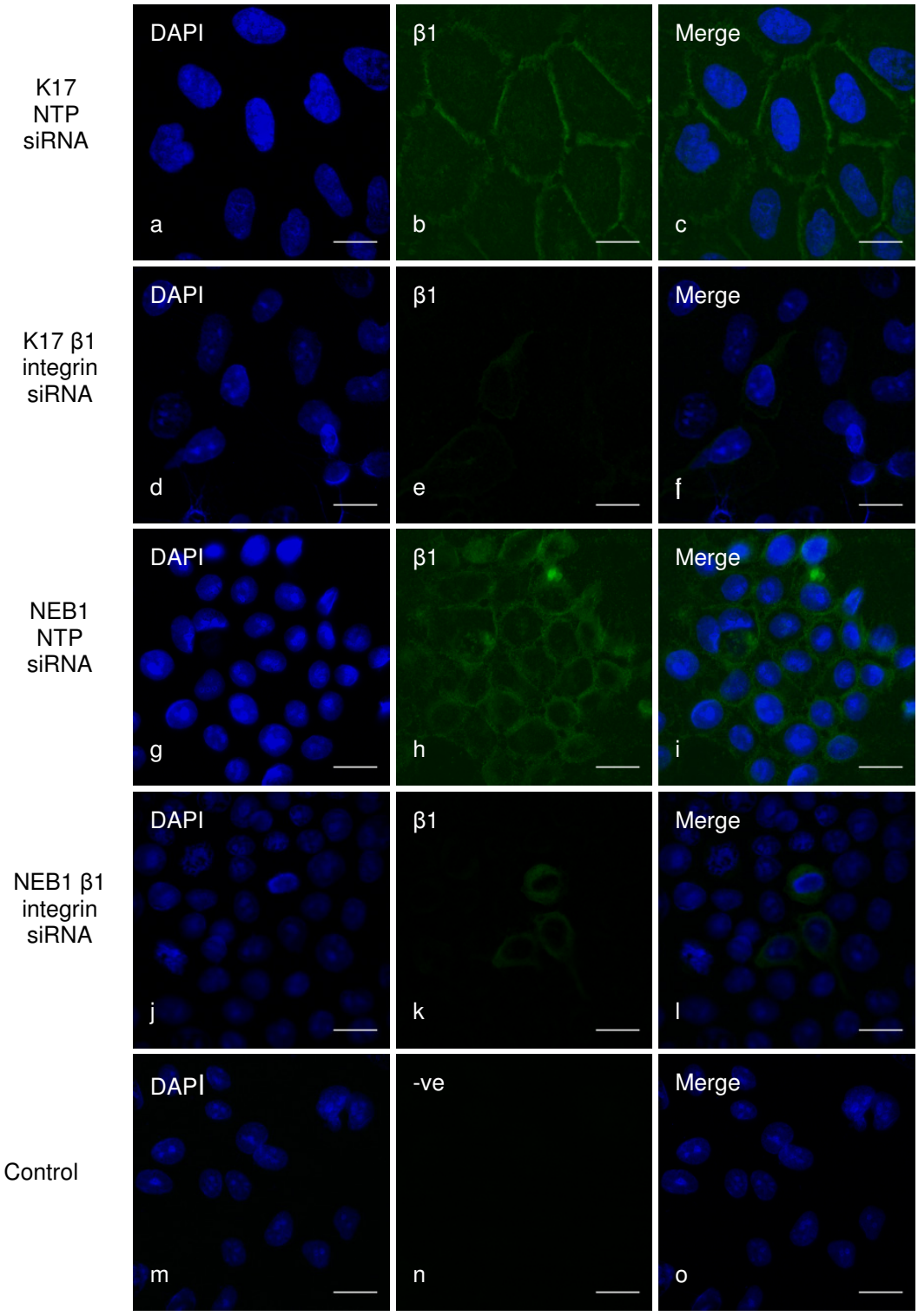

Treating control keratinocytes with β1 integrin siRNA significantly reduced *S. aureus* infection (figure 5.9). The adhesion efficiencies of *S. aureus* decreased from 38.8% to 20.3% in NEB1 keratinocytes, and from 69.2% to 22.5% in K17 keratinocytes following knock down (figure 5.9 a). Treatment with β1 integrin siRNA also reduced the bacterial invasion efficiencies from 4.0% to 2.2% in NEB keratinocytes, and from 4.7% to 2.0% in K17 keratinocytes (figure 5.9 b). Together, these results confirmed a requirement for α5β1 integrin during *S. aureus* infection in control keratinocytes.

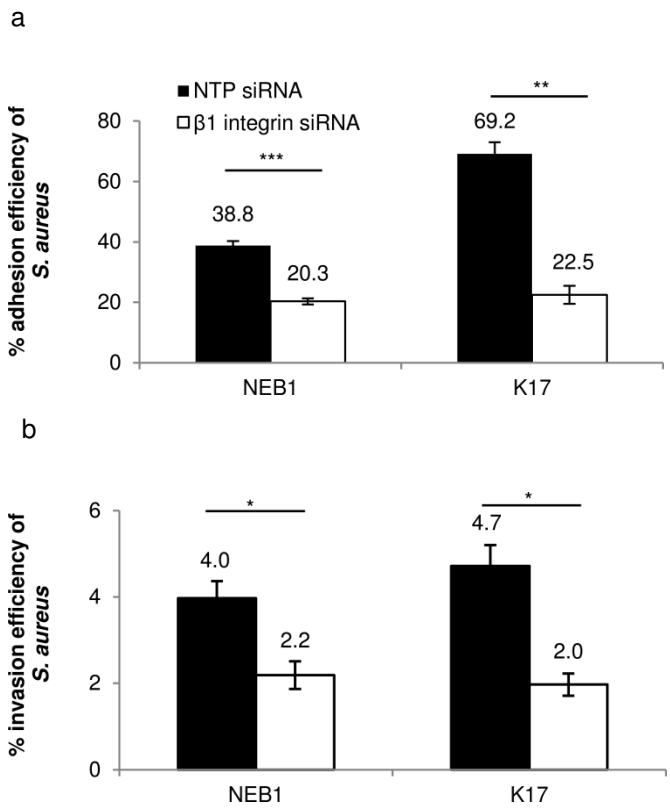

Figure 5.9: Effect of β1 integrin expression on *S. aureus* infection in keratinocytes. *S. aureus* adhesion **(a)** and invasion **(b)** efficiencies (numbers on plot) in NEB1 and K17 keratinocytes treated with NTP siRNA and β1 integrin siRNA. Data represent mean ± the SEM); *n*=3. Comparisons were carried out by using unpaired, two-tailed t tests, where significant differences were observed between NEB1 NTP siRNA and NEB1 β1 integrin siRNA, and K17 NTP siRNA and K17 β1 integrin siRNA for adhesion and invasion efficiencies (*, ** and *** represents $p<5x10^{-2}$, $p<5x10^{-3}$ and $p<5x10^{-4}$ respectively).

In preliminary experiments, the effect of ADAM17 expression on β1 integrin localisation was also investigated by staining frozen normal, TOC and ADAM17 deficient human skin sections (figure 5.10). An identical expression pattern of β1 integrin restricted to the basal epidermal layers was detected in all three specimens (figure 5.10). As changes in ADAM17 expression did not affect the localisation of β1 integrin protein, it suggests that the protective effect of ADAM17 during *S. aureus* infection was not mediated through α5β1 integrin.

Figure 5.10: Effect of ADAM17 expression on β1 integrin expression in skin. β1 integrin expression in frozen normal **(a-c)**, ADAM17 LOF **(d-f)** and TOC **(g-i)** skin sections. Negative control: normal skin section which has not been stained with β1 integrin antibody **(j-l)**. **(a, d, e, i)** Nuclei of cells (*DAPI* staining in *blue)*. **(b, e, g)** β1 integrin (*green*). **(k)** Unstained cells. **(c, f, i, l)** Merged images. Note that the expression of β1 integrin is identical in normal **(a-c)**, ADAM17 LOF **(d-f)** and TOC **(g-i)** skin, and is restricted to the epidermal basal layer. Image magnification 20x. *Bars* 20µm.

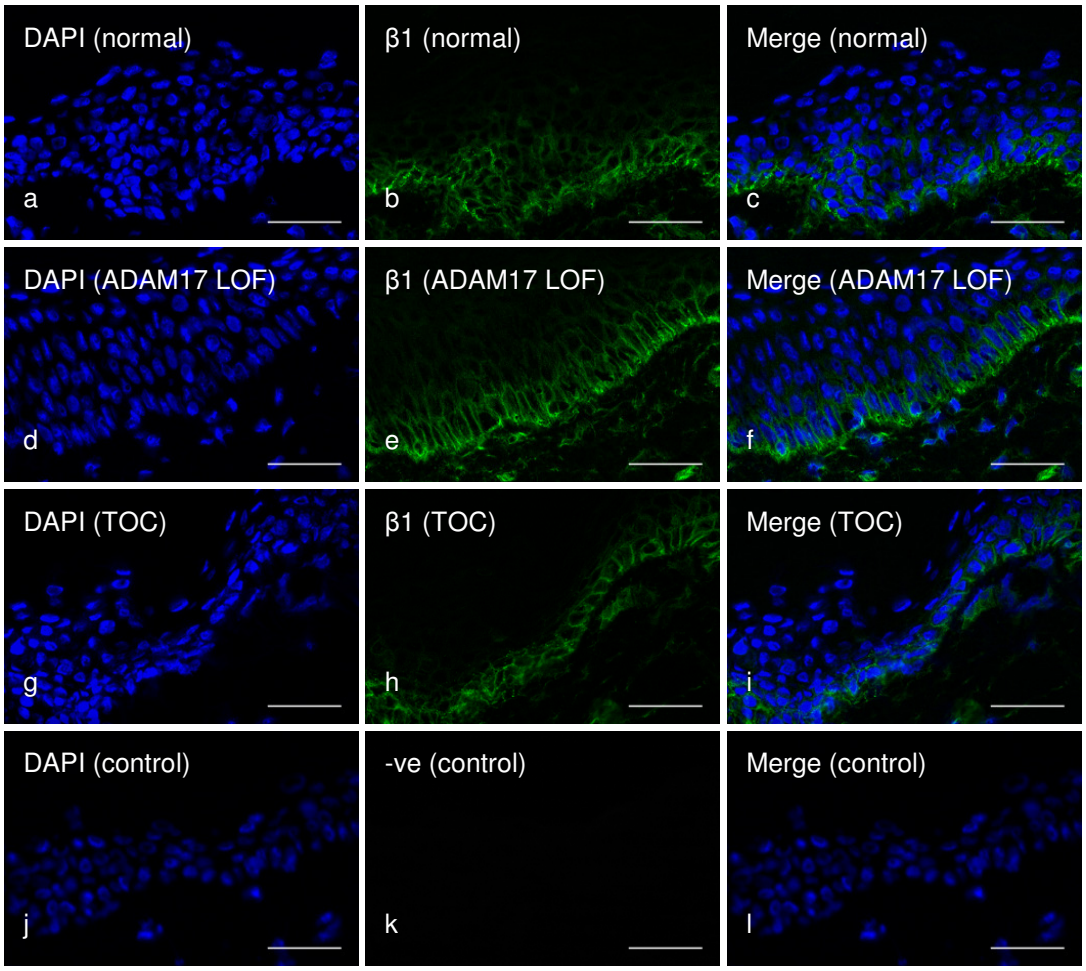

5.2.6 Effect of ADAM17 expression on hBD-2 and hBD-3 expression

In humans, the defensin family of peptides, which consists of α- and β-defensins, plays an important role in innate immunity. Defensins are expressed within neutrophil granules and many different tissue types including the skin[304]. Defensins exhibit antimicrobial activity towards bacteria. They may act to inhibit bacterial growth, or lyse bacterial membranes to directly kill them. Defensins are also chemotactic and recruit immune cells to the site of infection[304].

Candida albicans is a polymorphic yeast which colonises epithelial surfaces within the body as a commensal organism[305]. However, *C. albicans* also causes

invasive disease including candida oesophagitis, which is associated with upregulation of human β-defensins (hBDs) 2 and 3[305]. Recently, *C. albicans* has been shown to induce hBD-2 expression through IL-1β signalling, whilst hBD-3 was induced in response to signalling through the EGFR[305]. ADAM17 is an upstream regulator of EGFR signalling, and as expected, treatment with ADAM17 specific siRNA significantly reduced hBD-3 expression[305]. Although treatment with siRNA against ADAM17 did not affect hBD-2 expression in this study[305], hBD-2 expression is induced by proinflammatory cytokines, including IL-1β, whose expression can be driven by TNFα. It therefore follows that hBD-2 expression could be affected by changes in ADAM17 expression. This set of experiments investigated the effects of ADAM17 activity on hBD-2 and hBD-3 expression. Expression was analysed in the presence and absence of ADAM17 siRNA to consider how it was affected by a loss of functional ADAM17 activity. To investigate whether their expression was affected by increased ADAM17 activity, expression levels were compared in control (K17) and TOC (TYLK1) keratinocytes.

5.2.6.1 Semi quantitative RT-PCR for hBD-2 and hBD-3 mRNA expression

Initially, semi quantitative RT-PCRs for hBD-2 and hBD-3 were performed in uninfected and *S. aureus* infected control (K17) and TOC (TYLK1) keratinocytes. As a positive control, RT-PCRs for GAPDH were also performed. If the mRNA expression of hBD-2 and hBD-3 was affected by changes in ADAM17 expression, it would follow that hBD-2 and hBD-3 cDNA amplification would occur at a lower cycle in TOC keratinocytes than control keratinocytes. At cycle 27, GAPDH was expressed in all of the samples, but neither hBD-2, nor hBD-3 were expressed (figure 5.11 a). At cycle 28, hBD-3 was detected in all samples (figure 5.11 b). As the bands were of similar intensities, it suggested that changes in ADAM17 expression did not affect hBD-3 expression in control and TOC keratinocytes (figure 5.11 b). However, at cycle 28 for hBD-2 expression, two brighter bands of greater intensity could be detected in both uninfected and *S. aureus* infected TOC keratinocytes (figure 5.11 b). As a preliminary result, this suggested that increased ADAM17 expression in TOC keratinocytes was associated with upregulation of hBD-2 mRNA expression.

Figure 5.11: Semi-quantitative RT-PCR for the effect of ADAM17 on hBD-2 and hBD-3 mRNA expression. GAPDH, hBD-2 and hBD-3 expression in uninfected and *S. aureus* infected control (K17) and TOC (TYLK1) keratinocytes at cycles 27 **(a)** and 28 **(b).** Although GAPDH expression is detected, neither hBD-2 nor hBD-3 is expressed at cycle 27 **(a)**. At cycle 28 **(b)**, no difference in hBD-3 expression was observed. Note the bands of brighter intensity (3 and 4) for hBD-2 expression, suggesting increased hBD-2 expression in TOC keratinocytes at cycle 28.

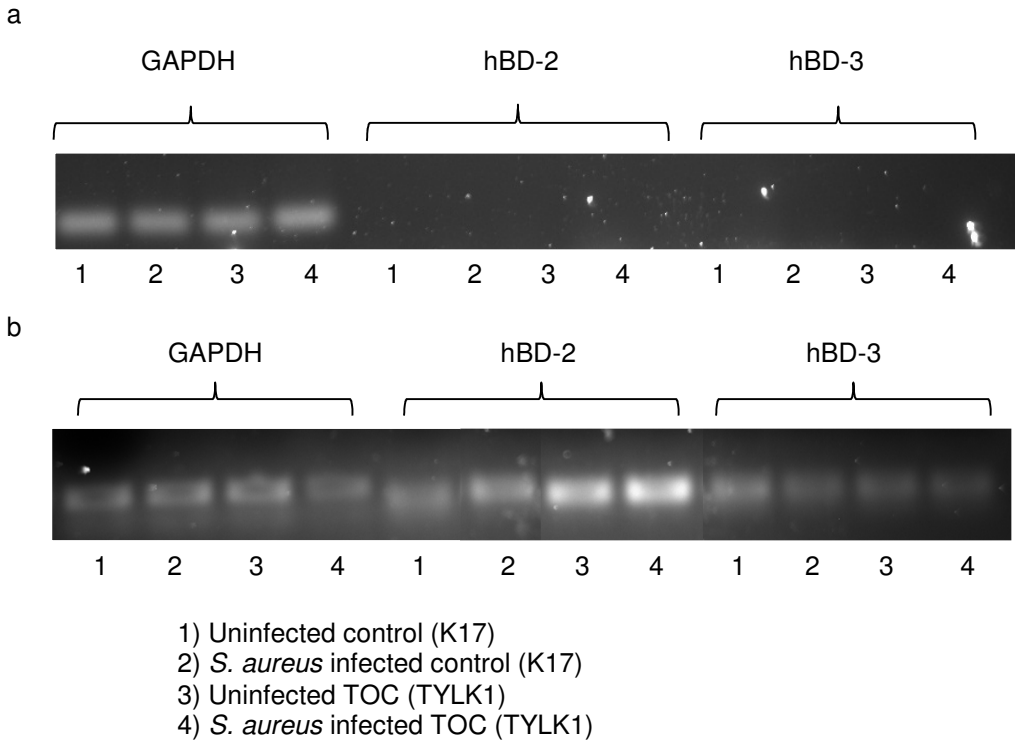

5.2.6.2 qRT-PCR and western blotting for hBD-2 and hBD-3 expression

QRT-PCRs were performed to quantify any ADAM17-dependent effect on hBD-2 (figure 5.12 a, b) and hBD-3 (figure 5.12 c, d) mRNA expression. The expression of mRNA was compared in control keratinocytes treated with NTP siRNA and ADAM17 siRNA (red bars), in control keratinocytes and TOC keratinocytes treated with NTP siRNA (green bars), and in TOC keratinocytes treated with NTP siRNA and ADAM17 siRNA (blue bars). These comparisons were carried out in uninfected (hBD-2 figure 5.12 a, hBD-3, figure 5.12 c) and *S. aureus* infected (hBD-2 figure 5.12 b, hBD-3 figure 5.12 d) keratinocytes. As each comparison performed revealed that there were no significant differences in hBD-2 or hBD-3 mRNA expression, this suggested that neither hBD-2, nor hBD-3 mRNA expression were affected by changes in ADAM17 expression. This finding was later supported by gene expression array data carried out in

section 5.2.7, which confirmed that hBD-2 and hBD-3 were not differentially expressed, in either uninfected or infected control, or TOC keratinocytes, treated with ADAM17 siRNA compared to NTP siRNA.

Figure 5.12: qRT-PCR for the effect of ADAM17 on hBD-2 and hBD-3 mRNA expression. Relative expression of hBD-2 **(a, b)** and hBD-3 **(c, d)** mRNA normalised to GAPDH (numbers on plot) in control (K17) and TOC (TYLK1) keratinocytes treated with NTP siRNA and ADAM17 siRNA. **(a, c)** Uninfected cells. **(b, d)** Infected cells. Data represent mean ΔΔCT value ± *SEM*; *n*=3. Comparisons were carried out by using unpaired, two-tailed t tests where no significant differences were observed between control NTP siRNA and control ADAM17 siRNA (*red* bars), control NTP siRNA and TOC NTP siRNA (*blue* bars), and TOC NTP siRNA and TOC ADAM17 siRNA (*green* bars), for hBD-2 or hBD-3 expression, in uninfected or infected cells.

a

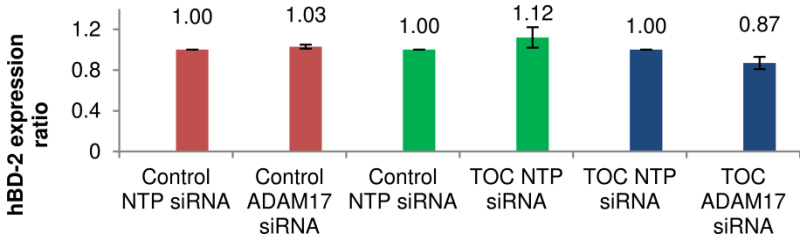

b

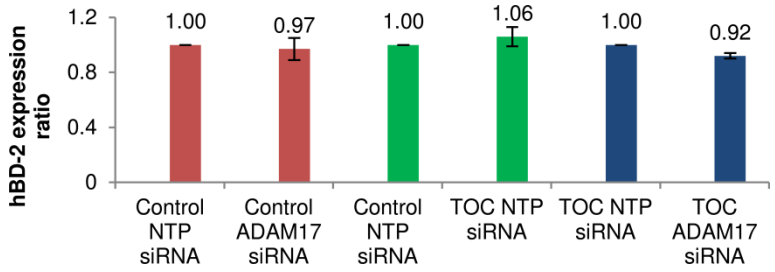

c

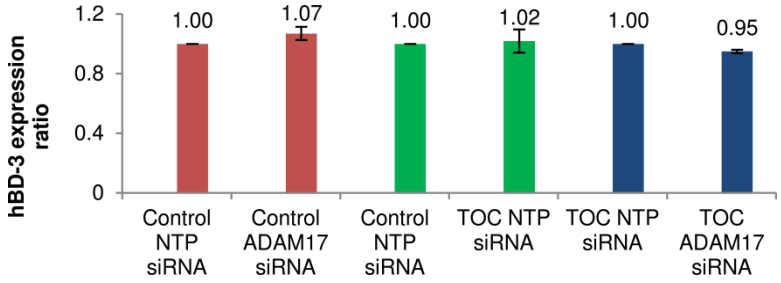

d

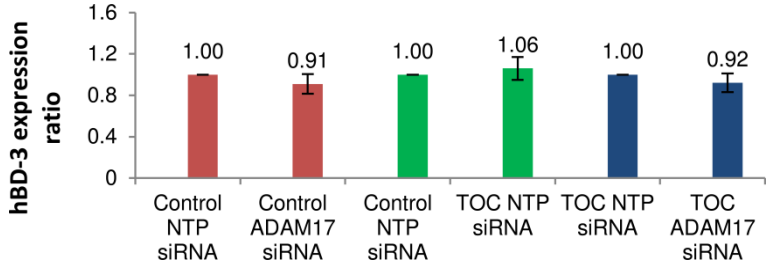

Western blotting also provided further evidence that changes in ADAM17 expression do not affect hBD-2 or hBD-3 protein expression (figure 5.13). Bands of identical intensities of 7 kDa corresponding to hBD-2, and 5 kDa corresponding to hBD-3, were detected in uninfected, and *S. aureus* infected control, and TOC keratinocytes, treated with NTP siRNA, and siRNA against ADAM17. The bands corresponding to hBD-3 are of weaker intensity than the bands corresponding to hBD-2, which could suggest that control and TOC keratinocytes express more hBD-2 than hBD-3 protein (figure 5.13). Taken together, the results depicted in figures 5.12 and 5.13 strongly suggest that the expression of hBD-2 and hBD-3 is not affected at the mRNA or protein level by changes in ADAM17 expression.

It is important to remember, however, that the results in figures 5.12 and 5.13 show mRNA and protein results from cell lines which grow in monolayers. In the skin, along with keratinocytes, neutrophils, macrophages, monocytes, mast cells and sebocytes also produce hBD-2 and hBD-3[306,307]. Consequently, analysis of monolayers which contain one cell type may not give an accurate representation of hBD-2 and hBD-3 expression in tissue. Therefore, their expression was also analysed by immunofluorescence in control, ADAM17 deficient and TOC frozen skin sections. Although the antibody against hBD-3 did not detect any staining in the skin sections, identical expression of hBD-2 restricted to the epidermal layer was detected in all three specimens (figure 5.14). In summary, the expression of hBD-2 and hBD-3 does not appear to be affected by ADAM17 expression. Therefore, it probably does not represent a mechanism by which ADAM17 provides protection during *S. aureus* infection.

Figure 5.13: Western blotting for the effect of ADAM17 on hBD-2 and hBD-3 expression. hBD-2 and hBD-3 protein expression in uninfected, and *S. aureus* infected control (K17), and TOC (TYLK1) keratinocytes, treated with NTP siRNA, and ADAM17 siRNA. Bands of identical intensity at 7 kDa corresponding to hBD-2, and at 5 kDa corresponding to hBD-3, are expressed by all of the samples, suggesting that ADAM17 expression does not affect hBD-2 or hBD-3 protein expression. GAPDH is used as a loading control.

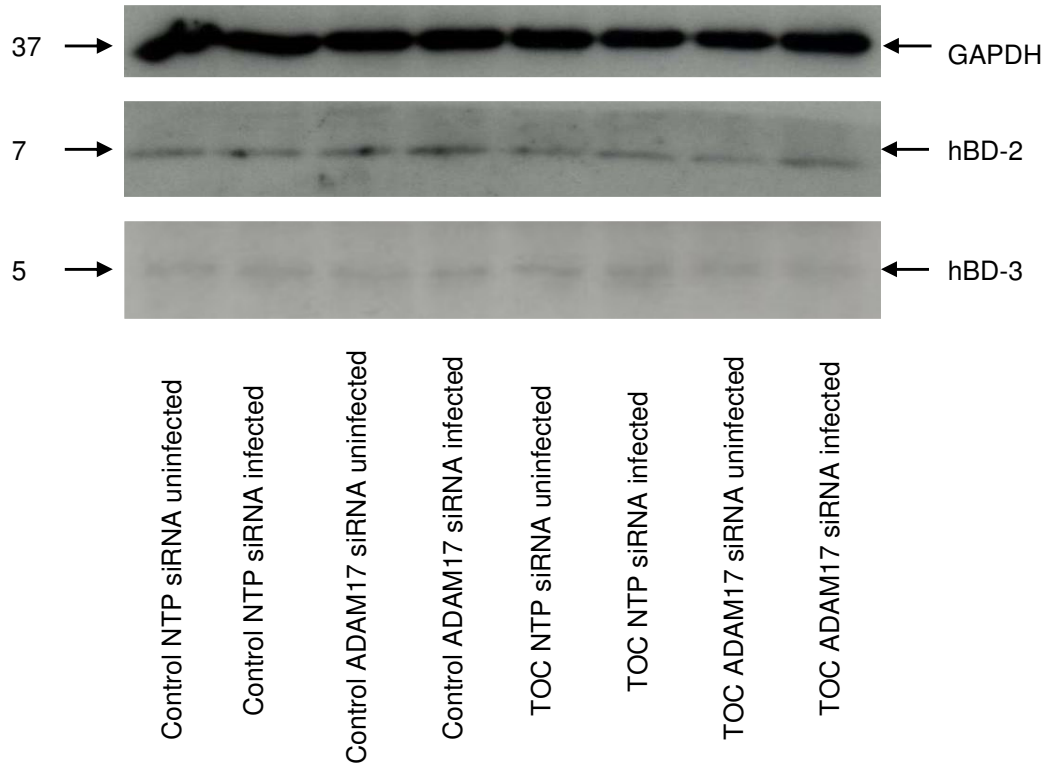

Figure 5.14: Effect of ADAM17 expression on hBD-2 expression in skin. hBD-2 expression in frozen normal **(a-c),** ADAM17 LOF **(d-f)** and TOC **(g-i)** skin sections. Negative control: normal skin section which has not been stained with hBD-2 antibody (**j-l**). **(a, d, e, i)** Nuclei of cells (*DAPI* staining in *blue)*. **(b, e, g)** hBD-2 (*green*). **(k)** Unstained cells. **(c, f, i, l)** Merged images. Note that the expression of hBD-2 is identical in normal **(a-c),** ADAM17 LOF **(d-f)** and TOC **(g-i)** skin, and is restricted to the epidermal basal layer. Image magnification 20x. *Bars* 20µm.

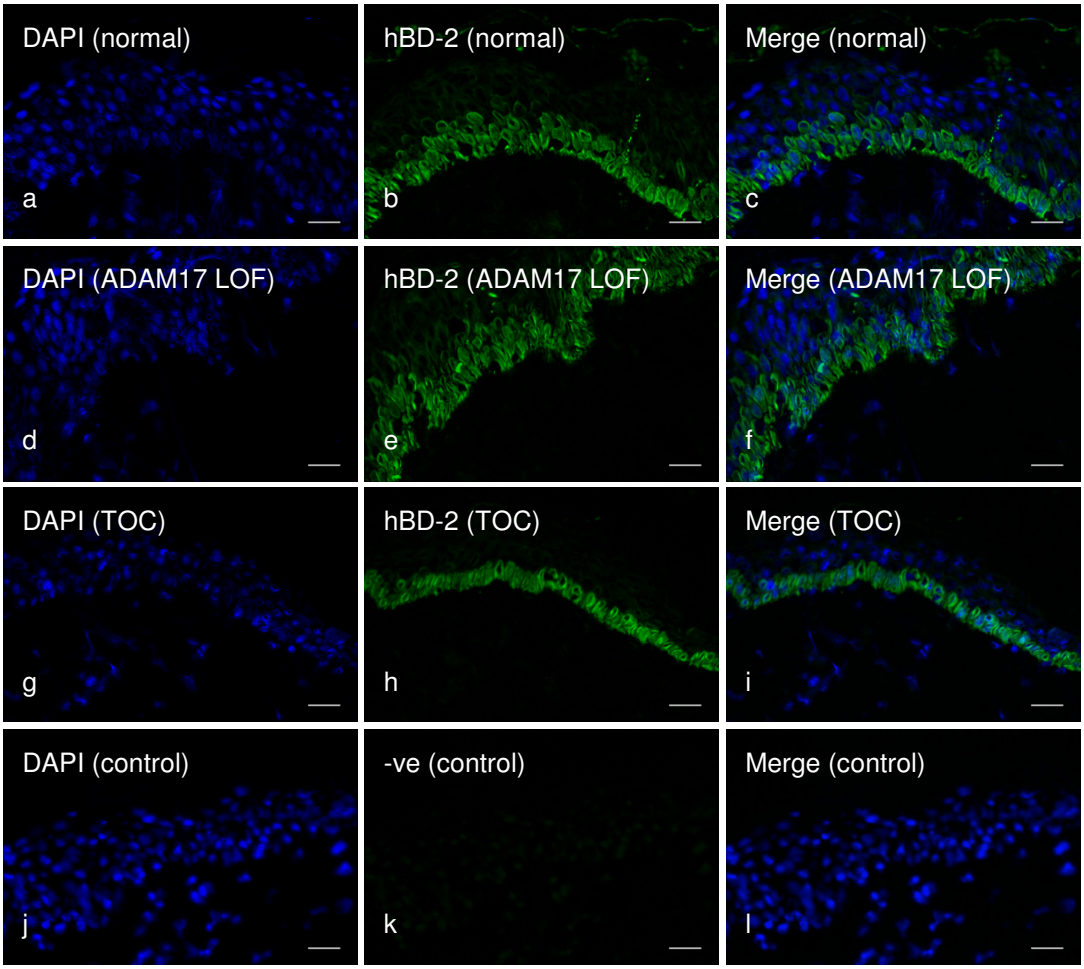

5.2.7 *Illumina™* gene expression profiling analysis

The results in this chapter have suggested that one mechanism used by ADAM17 to provide protection during infection is the induction of proinflammatory cytokine secretion. A gene expression array was then performed as an attempt to identify other downstream targets of ADAM17. Since microarray experiments can measure the transcriptional activity of thousands of genes in a sample simultaneously, it makes it possible to identifty numerous genes whose expression may be affected by changes in ADAM17 expression in a single experiment. While most molecular biology techniques

only permit the strudy of a small number of genes in the sample, carrying out the microarray should make it possible to identify novel targets of ADAM17.

Gene expression profiling was carried out on RNA extracted from uninfected and *S. aureus* infected control (K17) and TOC (TYLK1) keratinocytes, which had been treated with NTP siRNA and ADAM17 specific siRNA. To ensure that the identification of genes expressed within a sample was accurate, the detection p value was analysed. This value shows whether or not the fluorescent intensity of a given probe was significantly higher than the background, which was defined by negative control probes. The data set was filtered to include only genes which had a detection p value of less than $1x10^{-2}$. A detection p value equal to $1x10^{-2}$ means that there is a 1% false positive detection rate. The fold changes and diff scores of gene expression between the control and comparison groups were analysed to identify differentially expressed genes for four comparisons:

1. Uninfected K17 NTP siRNA vs K17 ADAM17 siRNA
2. Uninfected TYLK1 NTP siRNA vs TYLK1 ADAM17 siRNA
3. *S. aureus* infected K17 NTP siRNA vs K17 ADAM17 siRNA
4. *S. aureus* infected TYLK1 NTP siRNA vs TYLK1 ADAM17 siRNA

5.2.7.1 Fold change analysis and IL-24 expression

Lists detailing the 30 most up and downregulated genes for each comparison were compiled, which can be viewed in the appendix. Genes that were differentially expressed in at least two comparisons were of particular interest, since the differential expression was more likely to result from changes in ADAM17 expression than by chance. Most results of genes that were differentially expressed in two comparisons were obtained from comparisons performed on the same cell type. As gene expression may be affected by knocking down ADAM17 in one cell type but not the other, this suggests that differences in gene expression exist between the two cell lines. ADAM17 was downregulated in the four comparisons, which provided a positive control confirming that the microarray had worked. A significant find from this analysis was that IL-24 was the most consistently downregulated gene across all of the

four comparisons. This strongly suggested that IL-24 gene expression was affected by changes in ADAM17 expression in both cell lines. IL-24 has recently been shown to be protective during bacterial infection in mice. For example, in mouse models of *Mycobacterium* tuberculosis (TB)[308] and *Salmonella*[309], IL-24 stimulates IL-12 and interferon (IFN) γ production by neutrophils, which activates cytotoxic CD8+ T cells and leads to the killing of infected cells. In summary, gene expression profiling has identified IL-24 as a potential downstream target of ADAM17. Since IL-24 has been shown to be protective during bacterial infection, it follows that production of IL-24 may represent a protective mechanism of ADAM17.

5.2.7.2 Diff score selection and Genego pathway analysis

RNA hybridised to *Illumina*™ Sentrix Human HT12v4 Expression BeadChips is fluorescently labelled. The fluorescent intensity of each probe corresponds to the level of gene expression within the RNA sample. The diff score is a measurement based on the fluorescent intensity difference between the control group and the comparison group. It is a transformation of the detection p value, and positive and negative diff scores represent genes which are up and downregulated in the comparison group compared to the control group. According to the manufacturers', a p value of $1x10^{-4}$ transforms into a diff score of ±65, and represents the most up and downregulated genes in the comparison group compared to the control group. Detection p values of $1x10^{-3}$ and $1x10^{-2}$ transform into diff scores of ±33 and ±22, and represent less differentially expressed genes between the control and comparison groups.

Lists of differentially expressed genes generated for each of the four comparisons were imported into the pathway analysis MetaCore program from Genego. The program contains information drawn from the literature on signalling pathways, biological processes and diseases that specific proteins are involved in. Diagrams of signalling pathways illustrate interactions of specific proteins within the pathway. Based on the gene lists imported into the program, signalling pathways containing the greatest number of differentially expressed genes for each comparison were identified.

The pathway analysis software required lists of a minimum of 200 differentially expressed genes in the comparisons. This helped identify all of the signalling pathways that may have been affected by changes in ADAM17 expression. Initially genes with diff scores ±65 were considered to generate lists of differentially expressed genes. If this filtering process did not select enough genes, the filtering conditions were broadened to include genes with diff scores of ±33 or ±22. Table 5.1 details the selection criteria used for each comparison, the number of genes that were selected for further analysis, and the number of genes that were up and downregulated for each comparison.

Table 5.1 Selection criteria used to identify differentially expressed genes

Comparison	**Selection criteria**	**Number of genes selected**	**Number of genes upregulated and downregulated**
Uninfected K17 NTP siRNA vs uninfected K17 ADAM17 siRNA	Diff score ±22	322	Upregulated: 181 Downregulated: 141
Uninfected TYLK1 NTP siRNA vs uninfected TYLK1 ADAM17 siRNA	Diff score ± 33	241	Upregulated: 85 Downregulated: 156
***S. aureus* infected K17 NTP siRNA vs *S. aureus* infected K17 ADAM17 siRNA**	Diff score ±22	437	Upregulated: 265 Downregulated:172
***S. aureus* infected TYLK1 NTP siRNA vs *S. aureus* infected TYLK1 ADAM17 siRNA**	Diff score ±22	318	Upregulated:131 Downregulated:187

No comparisons have been carried out between K17 and TYLK1 cells. Selecting genes with diff scores ±65 would have included approximately 3,000 genes in the comparison. Even when this list was further processed to only include those genes which also had detection p values of less than $1x10^{-5}$, more than 1,200 genes were still selected. The massive difference in gene expression probably occurs by chance since K17 and TYLK1 keratinocytes are two different cell lines. Thus, any pathways containing differentially expressed genes identified by the software, would probably result from chance, rather than from differences in ADAM17 expression.

5.2.7.3 IL-17 signalling pathway

Colony stimulating factors (CSF) 2 and 3, chemokine (C-X-C motif) ligand (CXCL) 5, and matrix metalloprotease (MMP) 9 are components of the IL-17 signalling pathway that were differentially expressed between control and comparison groups (figure 5.15). Recently this pathway has been implicated during defence against *S. aureus* infection[262]. The IL-17 family is composed of six members (IL-17 A-F)[310]. IL-17-A and F are produced by several cell types within the skin including natural killer (NK) cells, T helper (Th) 17 cells and γδ T cells. Th17 cells also produce IL-22, and are induced by cytokines including IL-6 and IL-23 produced by dendritic cells, IL-1β produced by macrophages, and IL-21 produced by activated T cells. Consequently, these cytokines are also important components in the IL-17 signalling pathway. IL-17 and IL-22 signalling leads to the production of antimicrobial factors including hBD-2 and hBD-3, chemotactic factors including IL-8, CXCL1, CXCL2 and CXCL5, and the granulopoiesis factors CSF2 and CSF3. CXCL5 (ENA-78) (GeneCard database: GC04M074851) is produced concomitantly with IL-8, and is responsible for neutrophil recruitment to the site of infection. The gene expression array showed that CXCL5 was downregulated in uninfected and *S. aureus* infected K17 cells, treated with ADAM17 siRNA compared to NTP siRNA (figure 5.15). Additionally, fold change analysis revealed that CXCL5 was within the 30 most downregulated genes in both comparisons (appendix). CSF2 (GM-CSF) (GeneCard database: GC05P131409) and CSF3 (G-CSF) (GeneCard database: GC17P038171) control the production, differentiation and function of macrophages and granulocytes. CSF2 and CSF3 downregulation was also observed in uninfected K17 cells treated with ADAM17 siRNA compared to NTP siRNA.

MMP9 exhibited reduced expression in uninfected K17 cells treated with ADAM17 siRNA compared to NTP siRNA. MMP9 expression was also reduced in both uninfected, and *S. aureus* infected, TYLK1 cells treated with ADAM17 siRNA compared to NTP siRNA. MMP9 is induced by stimuli including EGF and TNFα[311], and therefore could be a downstream target of ADAM17. Consistently, ADAM17 has been shown to induce MMP9 expression in lung epithelial cells[312]. According to GeneGo, MMP9 is a downstream target of the EGFR signalling

pathway, suggesting that it may be involved in maintenance of the epidermal barrier. MMP9 also cleaves IL-8 to a more potent form[313], illustrating a role for MMP9 in the immune response. Finally, MMP9 induction by proinflammatory cytokines during *Mycobacterium tuberculosis* infection in mice, suggests that it may play a protective role during bacterial infection[314].

With the exception of a downregulation of IL-1β following siRNA against ADAM17 in uninfected K17 and TYLK1 cells, the expression of cytokine mRNA involved in Th17 cell induction, namely IL-6 and IL-23, was not affected by changes in ADAM17 expression. Additionally, IL-17-A, IL-17-F and IL-22 mRNA was not affected by knocking down ADAM17. This could suggest that ADAM17 expression may affect existing IL-17 signalling cascades, rather than affecting new Th17 cell generation.

Figure 5.15: IL-17 signalling pathway. Th17 cells are important producers of members of the IL-17 family of cytokines including IL-17-A and IL-17-F, and additionally produce IL-22. The yellow rectangle highlights the induction of Th17 cells by cytokines including IL-6 and IL-23 produced by dendritic cells, IL-1β produced by macrophages, and IL-21 produced by activated T cells. The black rectangles highlight particular components of interest of the IL-17 pathway that may be linked to changes in ADAM17 expression. IL-17 signalling increases the mRNA levels of MMP9, granulopoiesis factors G-CSF (CSF3) and GM-CSF (CSF2), and chemotactic factors ENA-78 (CXCL5), IL-8 and GCP2 (CXCL6). Four comparisons were carried out: 1) uninfected K17 NTP siRNA vs ADAM17 siRNA; 2) uninfected TYLK1 NTP siRNA vs ADAM17 siRNA; 3) infected K17 NTP siRNA vs ADAM17 siRNA; 4) infected TYLK1 NTP siRNA vs ADAM17 siRNA. Within the black rectangles, blue bars dictate which comparison(s) the differentially expressed gene(s) was/were downregulated in.

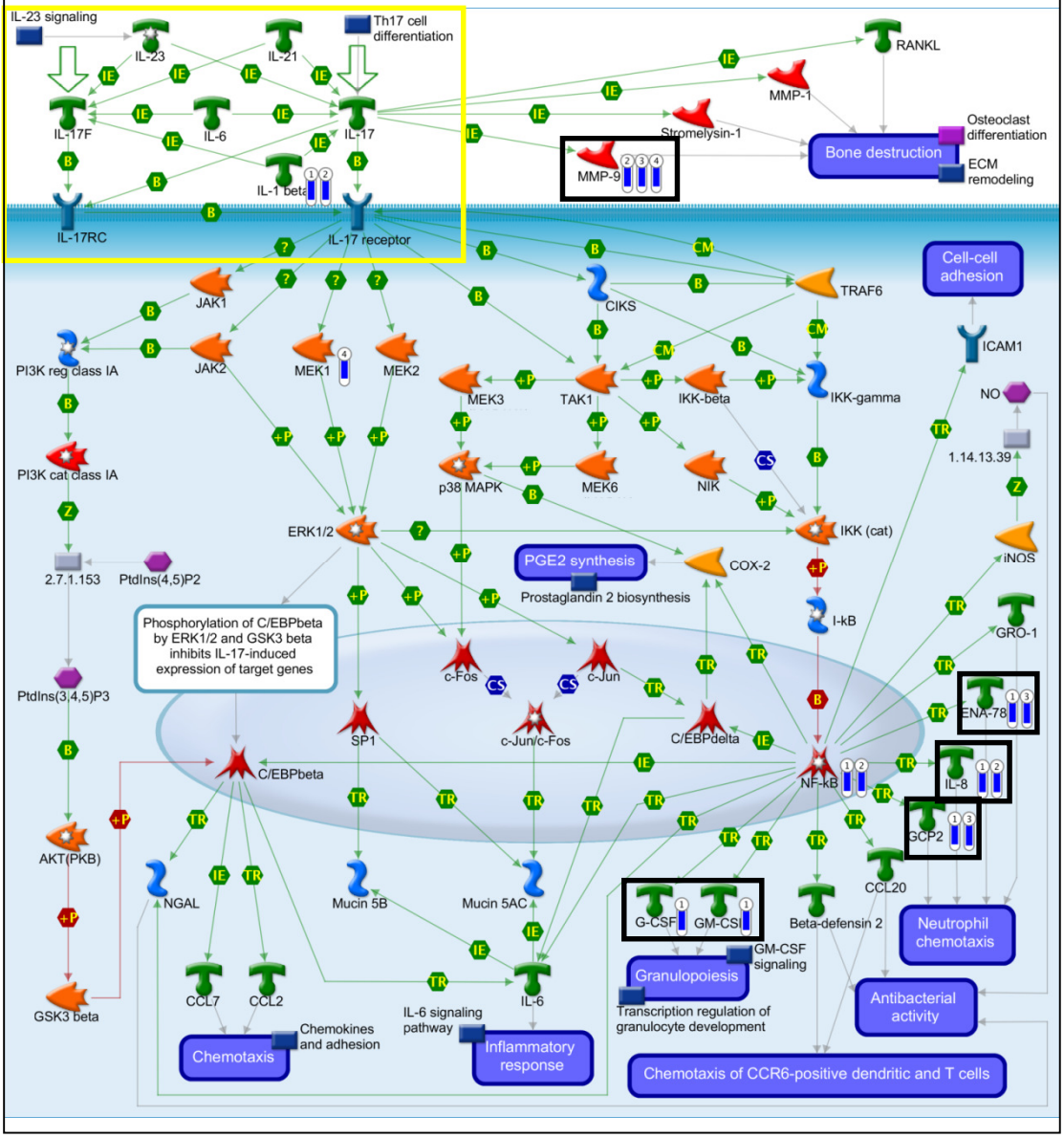

5.2.7.4 Differentially expressed genes summary

Based on the results from the fold change, and diff score selection and pathway analysis, five genes were selected for follow up work. These were CSF2, CSF3, CXCL5, IL-24 and MMP9. Based on their diff score, table 5.2 summarises which of the comparisons the genes were differentially expressed in. The fold changes of these genes along with ADAM17 are shown in figure 5.16.

Table 5.2: Differential expression of genes based on diff score

	Uninfected K17 NTP siRNA vs ADAM17 siRNA	**Uninfected TYLK1 NTP siRNA vs ADAM17 siRNA**	**Infected K17 NTP siRNA vs ADAM17 siRNA**	**Infected TYLk1 NTP siRNA vs ADAM17 siRNA**
CSF2	Yes	No	No	No
CSF3	Yes	No	No	No
CXCL5	Yes	No	Yes	No
IL-24	Yes	Yes	Yes	Yes
MMP9	No	Yes	Yes	Yes

Figure 5.16: Fold change of gene expression array hits. Fold change of ADAM17, CSF2, CSF3, CXCL5, IL-24 and MMP9 in K17 and TYLK1 keratinocytes treated with ADAM17 siRNA. Fold change expressed as the ratio of the log e of the mean signal strength (*n*=3) for cells treated with NTP siRNA and ADAM17 siRNA.

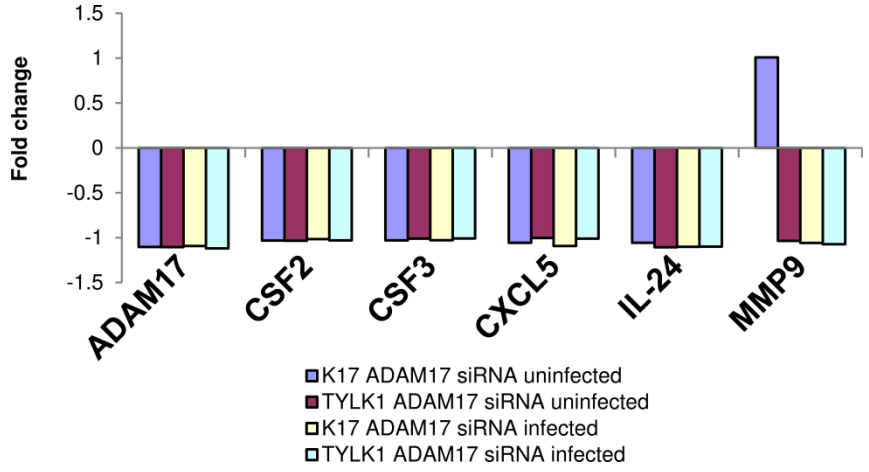

5.2.8 Validation of gene expression array hits by qRT-PCR

The expression of CSF2, CSF3, CXCL5, IL-24 and MMP9 was validated at the mRNA level by qRT-PCR in uninfected, and *S. aureus* infected, K17 and TYLK1 cells for each of the four comparisons (figure 5.17). Both uninfected and *S.*

aureus infected K17 and TYLK1 keratinocytes treated with siRNA against ADAM17, displayed reductions in the mRNA level of each of the five genes. The level of reduction ranged from approximately 30-80% depending on the gene and the comparison (figure 5.17). By qRT-PCR, IL-24 and MMP9 were the two most consistently downregulated genes across the four comparisons (figure 5.17). These results provide support for the gene expression array data, and suggest that ADAM17 may induce the transcription of IL-24 and certain components of the IL-17 signalling pathway, thus making them potential downstream targets of ADAM17.

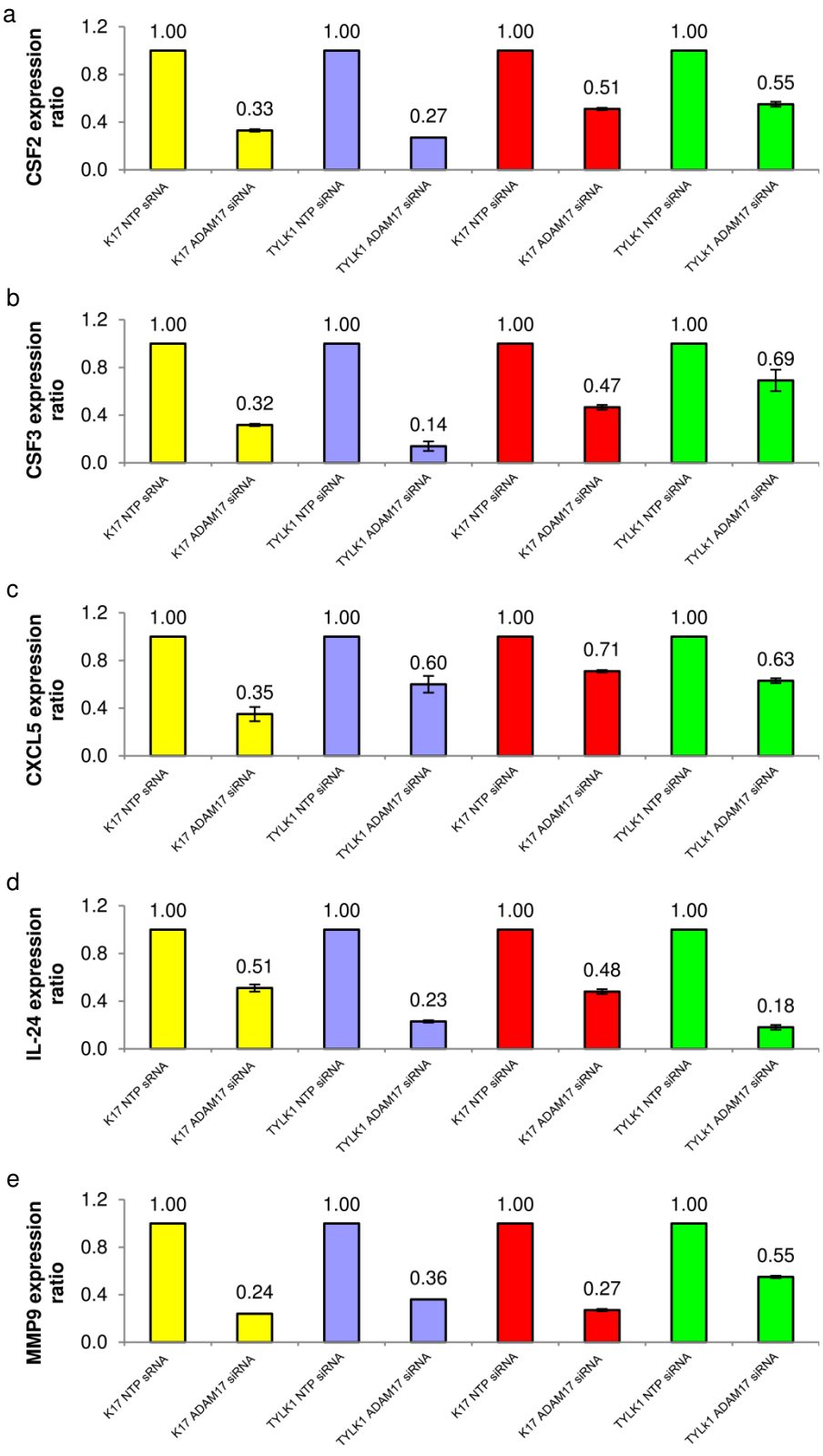

Figure 5.17: Gene expression array hits validation by qRT-PCR. Relative expression of CSF2 **(a),** CSF3 **(b)**, CXCL5 **(c)**, IL-24 **(d)** and MMP9 **(e)** mRNA normalised to GAPDH (numbers on plot) in uninfected, and infected, control (K17), and TOC (TYLK1) keratinocytes, treated with NTP siRNA, and ADAM17 siRNA. Data represent mean ΔΔCT value ± *SEM*; *n*=3. Uninfected K17 NTP siRNA vs ADAM17 siRNA (*yellow* bars), uninfected TYLK1 NTP siRNA vs ADAM17 siRNA (*blue* bars), infected K17 NTP siRNA vs ADAM17 siRNA (*red* bars), infected TYLK1 NTP siRNA vs ADAM17 siRNA (*green* bars).

5.2.9 MMP9 protein expression by immunofluorescence

MMP9 degrades the ECM components collagen IV and V (GeneCard database: GC20P044637) and is involved in ECM remodelling. ECM remodelling occurs during physiological processes including cell proliferation, cell adhesion, cell migration and wound healing, and during some disease processes including metastasis (GeneGo). It is known that MMP9 is induced by EGFR signalling, and in mice, ADAM17 mediated regulation of EGFR signallling is required for epidermal barrier maintenance[238]. One hypothesis considered for the protective role of ADAM17 was that ADAM17 induces MMP9 expression. This in turn could participate in ECM remodelling, and contribute to cell proliferation and migration, which may be important for the structure and function of the epidermal barrier.

MMP9 is secreted as an inactive proprotein of 92 kDa. Following cleavage by the extracellular proteinase plasmin[311], an active protein of 84 kDa is generated. MMP9 expression was analysed in normal, ADAM17 deficient and TOC frozen skin sections by immunofluorescence (figure 5.18). Although results from the expression array and qRT-PCR suggested that MMP9 mRNA expression was affected by changes in ADAM17 expression, immunofluorescence revealed identical MMP9 expression in the three specimens. MMP9 was expressed throughout the epidermis, and particularly by epidermal appendages including sweat glands and hair follicles (figure 5.18). The antibody used for immunofluorescence recognised full length MMP9, and could explain why no differences in MMP9 were detected between the three samples. If ADAM17 expression does not lead to existing MMP9 protein degradation, and if MMP9 transcription occurs more quickly than translation, then the total amount of MMP9 protein expression could potentially be the same between all samples.

.

Figure 5.18: Effect of ADAM17 expression on MMP9 expression in skin. MMP9 expression in frozen normal **(a-c),** ADAM17 LOF **(d-f)** and TOC **(g-i)** skin sections. Negative control: normal skin section which has not been stained with the MMP9 antibody **(j-l). (a, d, e, i)** Nuclei of cells (*DAPI* staining in *blue)*. **(b, e, g)** MMP9 (*green*). **(k)** Unstained cells. **(c, f, i, l)** Merged images. Note that the expression of MMP9 is identical in normal **(a-c)**, ADAM17 LOF **(d-f)** and TOC **(g-i)** skin, and is expressed throughout the epidermis, and in particular by epidermal appendages including sweat glands and hair follicles. Image magnification 20x. *Bars* 20µm.

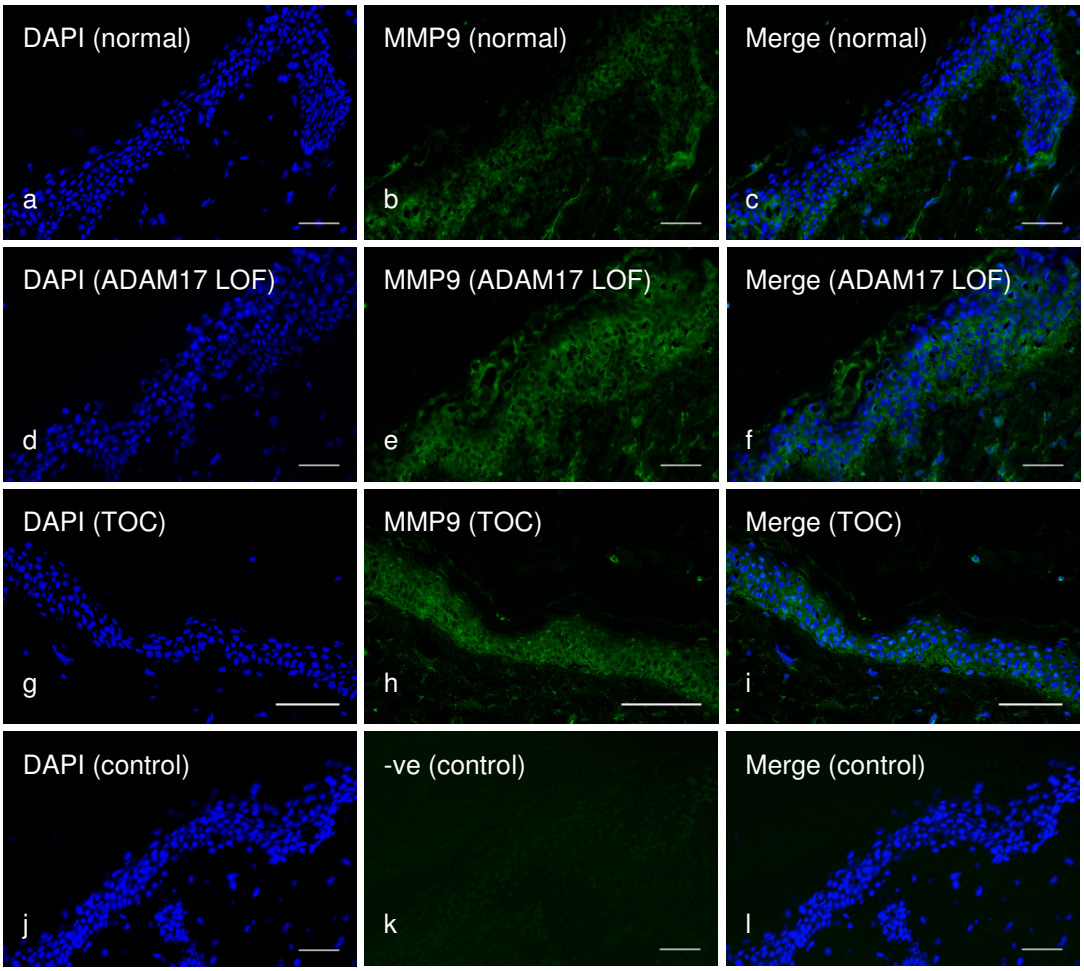

5.2.10 MMP9, CXCL5, IL-24 and IL-17-A secretion by ELISA

Since MMP9 is activated extracellularly, secretion was investigated in both *S. aureus* infected, and PMA/ ionomycin stimulated, control and TOC keratinocytes, in the presence and absence of ADAM17 siRNA. Ionomycin is an ionophore, which increases the intracellular concentration of Ca^{2+}, whilst PMA is a direct activator of Protein kinase C (PKC). When used together to stimulate cells, PKC activation is synergistically enhanced[315], which in turn increases cytokine secretion. MMP9 secretion was significantly reduced in unstimulated control (K17) keratinocytes from 89.75 pg/ml to 29.70 pg/ml, and in *S. aureus* infected K17 keratinocytes from 151.07 pg/ml to 65.85 pg/ml (figure 5.19 a)

following treatment with ADAM17 siRNA. Increased ADAM17 activity correlated with significantly increased MMP9 secretion. MMP9 production was 346.15 pg/ml by uninfected TOC (TYLK1) keratinocytes, and 526.19 pg/ml by *S. aureus* infected TYLK1 cells (figure 5.19 a). Finally, MMP9 secretion was significantly reduced to 235.75 pg/ml and 271.54 pg/ml in unstimulated, and *S. aureus* infected TYLK1 cells when ADAM17 was knocked down (figure 5.19 a), reinforcing that MMP9 secretion is affected by changes in ADAM17 expression. Interestingly, K17 and TYLK1 keratinocytes appeared to be unresponsive to stimulation with PMA/ionomycin since they did not produce any MMP9 following stimulation (figure 5.19 a).

Although the gene expression array did not identify IL-17-A mRNA as being affected by changes in ADAM17 expression, it is an important component of the IL-17 signaling pathway, so when ELISAs were performed on array follow up hits CXCL5 and IL-24, IL-17-A was also included for analysis. A maximum production of 26 pg/ml of CXCL5 (figure 5.19 b) and 9 pg/ml of IL-17A (figure 5.20 a) by keratinocytes was detected following infection with *S. aureus*, or stimulation with PMA/ionomycin. As these values were very low, it suggested that under normal circumstances, keratinocytes do not secrete IL-17A (figure 5.20 a) or CXCL5 (figure 5.19 b).

Figure 5.19: MMP9 and CXCL5 secretion in keratinocytes and PBMCs. MMP9 **(a)** and CXCL5 **(b)** secretion in keratinocytes treated with NTP siRNA and ADAM17 siRNA, and CXCL5 secretion in PBMCs **(c)**. Results from unstimulated, *S. aureus* infected/LPS (1 ng/ml) stimulated, and PMA (100 ng/ml)/ ionomycin (I) (500 ng/ml) stimulated cells. Data represent mean ± the SEM; **a**, **b** *n*=3; **c** *n*=2. Comparisons were carried out by using unpaired, two-tailed t tests. For MMP9, **(a)** significant differences were observed between unstimulated and infected K17 NTP siRNA and ADAM17 siRNA, K17 NTP siRNA and TYLK1 NTP siRNA, and TYLK1 NTP siRNA and ADAM17 siRNA. For CXCL5 **(c)** significant differences were observed between LPS and PMA/I stimulated control and TOC PBMCs (**, *** and **** represents $p<5x10^{-3}$, $p<5x10^{-4}$ and $p<5x10^{-5}$).

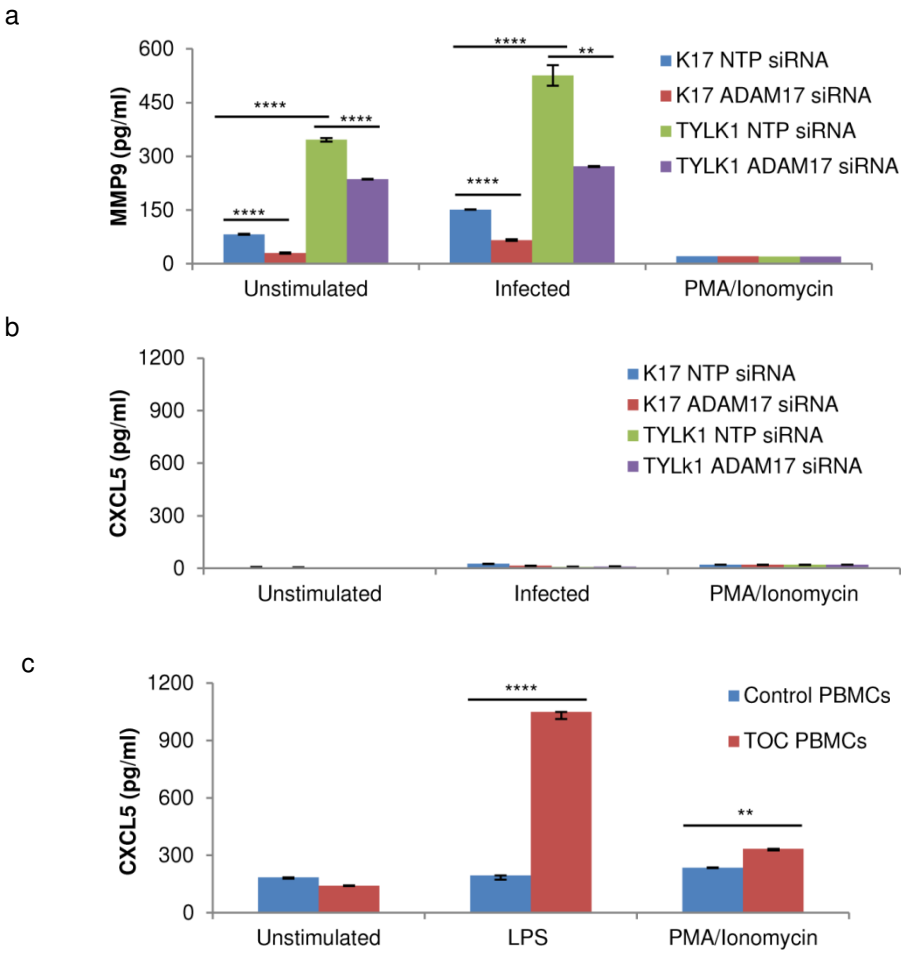

Measurements ranging from approximately 20-110 pg/ml of IL-24 were observed in *S. aureus* infected and PMA/ionomycin stimulated keratinocytes (figure 5.20 c). *S. aureus* infected K17 and TYLK1 keratinocytes, treated with either NTP siRNA or ADAM17 siRNA, produced nearly identical amounts of IL-24 (figure 5.20 c). Following stimulation with PMA/ionmycin, TYLK1 keratinocytes produced more IL-24 than K17 keratinocytes. However, no significant differences were observed in IL-24 production in K17 cells treated with NTP siRNA and ADAM17 siRNA, or between TYLK1 keratinocytes treated with NTP siRNA and ADAM17 siRNA (figure 5.20). Thus, the method of

stimulation used may influence the amount of IL-24 produced by K17 and TYLK1 keratinocytes, but any effect is likely to occur independently of ADAM17.

Western blotting was also performed to determine whether there was any difference in CXCL5, IL-24 and MMP9 protein expression in K17 and TYLK1 cells treated, with NTP siRNA and ADAM17 siRNA. However, all available antibodies produced heavy background staining, which made it impossible to detect bands of 12 kDa, 24 kDa, or 92 kDa corresponding to CXCL5, IL-24, or immature MMP9 respectively. Thus, in this study it was not possible to conclude whether CXCL5, IL-24 or MMP9 protein levels were affected by differential expression of ADAM17.

Next, the production of CXCL5, IL-17-A and IL-24 was measured in PBMCs isolated from control and TOC subjects (figures 5.19 c, 5.20 b and 5.20 d). PBMCs comprise immune cells including T and B lymphocytes, NK cells, monocytes and dendritic cells. PBMCs are likely to produce greater amounts of CXCL5 and IL-17-A than keratinocytes, which secrete little or none. IL-24 secetion is probably also greater in PBMCs than keratinocytes. Therefore, as it should be possible to measure increased volumes of cytokines in PBMCs, this should enable the role of ADAM17 in their production to be further investigated. Due to limited volumes of the control and TOC patients' PBMCs, MMP9 secretion was not investigated. While the results for keratinocyte secretion of MMP9 strongly suggest that MMP9 secretion is affected by changes in ADAM17 expression (figure 5.19 a), the results obtained for keratinocyte secretion of CXCL5, IL-17-A, and IL-24 (figures 5.19 b, 5.20 a and 5.20 c) do not give any real indication as to whether they are affected by ADAM17 activity. Therefore, because of limited sample availability, this was the rationale behind measuring PBMC secretion of CXCL5, IL-17-A and IL-24, and not MMP9. LPS stimulation of PBMCs caused a greater increase in CXCL5 (figure 5.19 c) and IL-24 (figure 5.20 d) than PMA/ionomycin stimulation. No significant difference in IL-24 secretion by control or TOC PBMCs was observed (figure 5.20 d). This suggests that although a loss of functional ADAM17 expression reduces IL-24 mRNA levels in keratinocytes, increased ADAM17 expression in PBMCs does not affect IL-24 secretion. It is possible that PBMCs may have a maximum volume of IL-24 that they secrete. If this level had been reached in control PBMCs, then increased ADAM17 activity might not allow for greater IL-24

production by TOC PBMCs. This could potentially explain why production of IL-24 was not significantly different in control and TOC PBMCs. CXCL5 secretion however, was significantly increased in TOC PBMCs compared to control PBMCs following stimulation with LPS and PMA/ionomycin. In response to LPS and PMA/ionomycin stimulation, TOC PBMCs secreted 1049 pg/ml and 333 pg/ml respectively of CXCL5 (figure 5.19 c). However, control PBMCs only produced 194 pg/ml and 235 pg/ml of CXCL5 following stimulation with LPS and PMA/ionomycin respectively (figure 5.19 c). Although IL-17-A production was not observed in PBMCs following stimulation with LPS, stimulation with PMA/ionomycin led to control PBMCs producing 149 pg/ml of IL-17-A, while TOC PBMCs released a significantly greater volume of 450 pg/ml of IL-17-A (figure 5.20 b). Taken together, these results provide support for changes in ADAM17 expression affecting secreted components of the IL-17 signaling pathway.

Figure 5.20: IL-17-A and IL-24 secretion in keratinocytes and PBMCs. IL-17-A **(a, b)** and IL-24 **(c, d)** secretion in keratinocytes treated with NTP siRNA and ADAM17 siRNA **(a, c)**, and control and TOC PBMCs **(b, d)**. Results from unstimulated, *S. aureus* infected/LPS (1 ng/ml) stimulated, and PMA (100 ng/ml)/ ionomycin (I) (500 ng/ml) stimulated cells. Data represent mean ± the SEM; **a**, **c** *n*=3; **b**, **d** *n*=2. Comparisons were carried out using by unpaired, two-tailed t tests. For IL-17-A **(b)**, no significant differences were observed between PMA/I stimulated control and TOC PBMCs (*** represents $p<5x10^{-4}$). For IL-24, no significant differences were observed in keratinocytes **(c)** or PBMCs **(d)**.

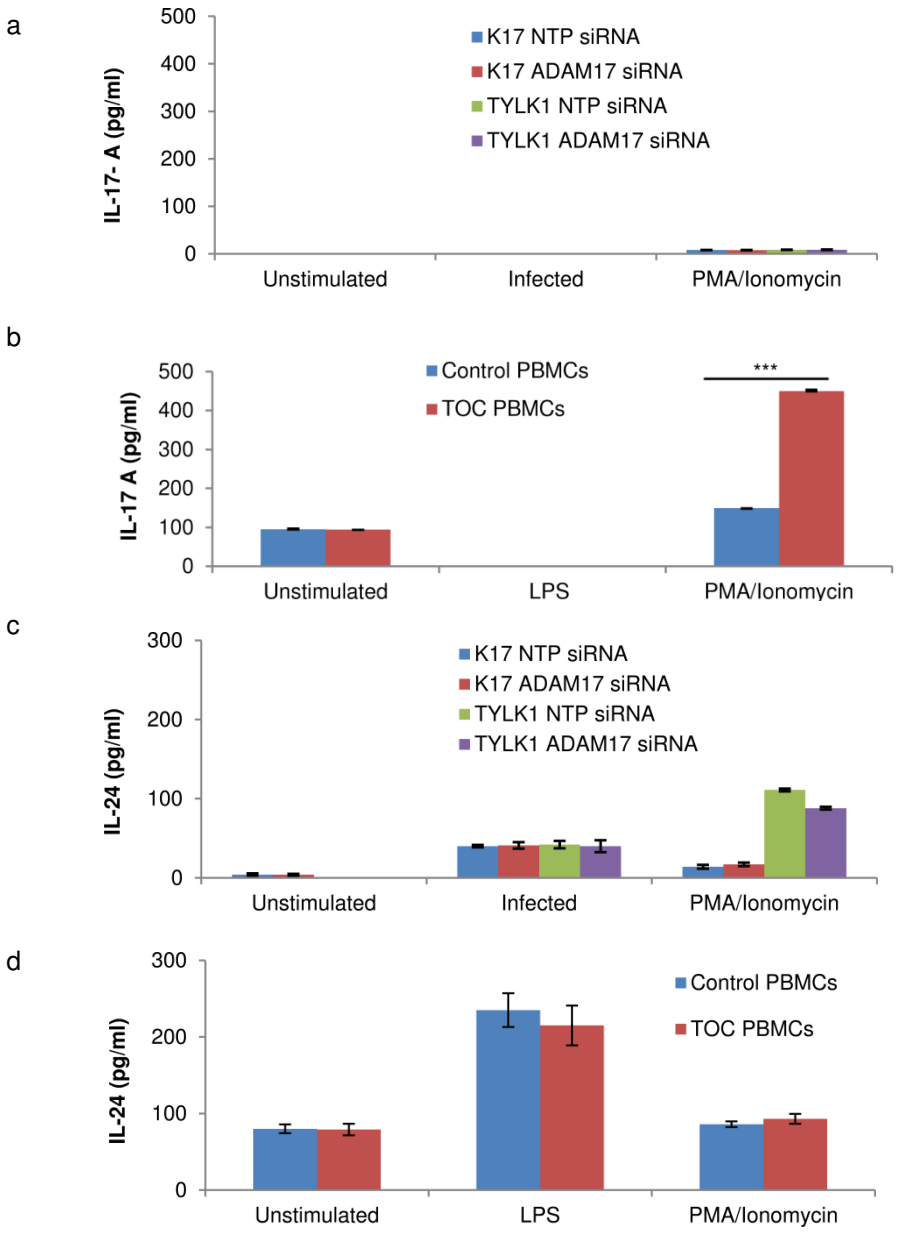

5.2.11 Secretion of IL-17 related cytokines in control and ADAM17 deficient PBMCs

The experiments described in sections 5.2.7-10 suggest that the IL-17 signalling pathway may be a downstream target of ADAM17. To investigate this further,

the secretion of the Th17 inducing cytokine IL-23, and the Th17 cytokines IL-17-A, IL-17-F and IL-22 were measured in PBMCs from the ADAM17 deficient patient, his mother and control subjects. As the mutation which truncates the ADAM17 protein is recessive[239], cytokine production by the mother should be similar to control subjects. IL-23 is a member of the IL-12 family of cytokines. IL-23 is composed of two subunits, p19 and p40. The p19 subunit is only expressed by IL-23, but the p40 subunit is also expressed by IL-12[316]. IL-23 was detected using an ELISA kit which recognised the common IL-12/IL-23 p40 subunit. Cytokine production was investigated in PBMCs stimulated with PMA/ionomycin, and CD3/CD28, which activates T cells. In T cells, CD3 is required for signal transduction following ligand binding to the αβ or γδ receptor, whilst CD28 provides co-stimulatory signals required for T cell activation[317]. In these experiments TNFα secretion was measured as a positive control.

To further investigate how IL-17 cytokine secretion was affected by changes in ADAM17 expression, these experiments were also carried out in the presence of three inhibitors: two small molecule inhibitors; GI254023X which blocks ADAM10 activity, GW280264X which targets both ADAM17 and ADAM10[292], and an ADAM17 neutralising antibody[293]. ADAM10 and ADAM17 are both implicated in the shedding of the IL-6R, CX3CL1 and CXCL16[292]. Constitutive and inducible shedding of these molecules is thought to be mediated by ADAM10 and ADAM17 respectively[292]. Whilst GI254023X potently blocked the constitutive release of the IL-6R, CX3CL1 and CXCL16, it had no effect on the PMA-induced shedding, which was only blocked by GW280264X[292]. This was in line with GI254023X solely blocking ADAM10 activity, and GW280264X targeting both ADAM17 and ADAM10[292]. The ADAM17 neutralising antibody[293], which was the third inhibitor used in this study, has been shown to bind to both the TACE ectodomain and the isolated catalytic domain[293]. This led to an inhibition of the ADAM17 dependent shedding of TNF-α, HB-EGF, TGF-α and amphiregulin[293]. In this study, the ability of the neutralising antibody to block ADAM17 activity was first tested in K17 and TYLK1 keratinocytes by measuring amphiregulin secretion (figure 5.21). Treating K17 cells with 100 nM of neutralising antibody for 4 hours only reduced amphiregulin secretion by 8%. However, ADAM17 activity was significantly reduced in K17 cells treated with 200 nM of neutralising antibody for 4 hours, and in TYLK1 cells treated with

either 100 nM or 200 nM of neutralising antibody, for either 4 or 24 hours. This was shown by decreases in amphiregulin secretion which ranged from approximately 30%-60 (figure 5.21).

Figure 5.21: Effect of ADAM17 neutralising antibody on amphiregulin secretion in keratinocytes. Amphiregulin secretion in K17 **(a)** and TYLK1 keratinocytes **(b)**, treated with 100 nM or 200 nM of ADAM17 neutralising antibody for 4 or 24 hours. Data represent mean ± the SEM; *n*=2. Comparisons were carried out by using unpaired, two-tailed t tests. For K17 keratinocytes **(a),** significant differences were observed between 0 nM and 200 nM for 4 hours; 0 nM and 100 nM for 24 hours; and 0 nM and 200 nM for 24 hours. For TYLK1 keratinocytes **(b),** significant differences were observed between 0 nM and 100 nM for 4 hours; 0 nM and 200 nM for 4 hours; 0 nM and 100 nM for 24 hours; and 0 nM and 200 nM for 24 hours (*, **,*** and **** represents $p<5x10^{-2}$, $p<5x10^{-3}$, $p<5x10^{-4}$ and $p<5x10^{-5}$ respectively).

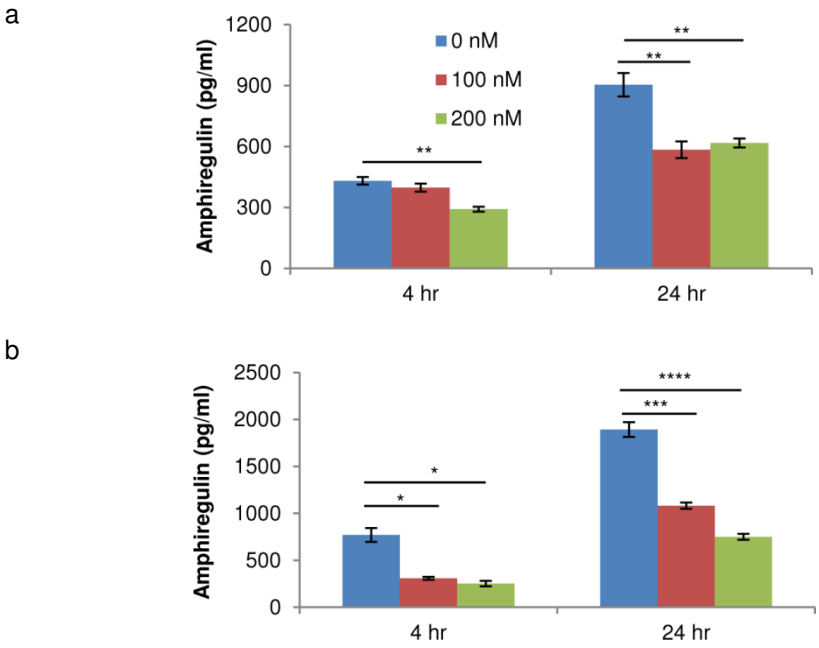

5.2.11.1 TNFα secretion

Although there was variability in TNFα secretion between the mother and two control samples following stimulation with PMA/ionomycin or CD3/CD28, all produced more TNFα than the ADAM17 deficient patient, as expected (figure 5.22 a). The efficacy of the three inhibitors was varied. As the two small molecule inhibitors GI254023X and GW280264X were dissolved in DMSO, measuring TNFα secretion by stimulated keratinocytes in the presence of DMSO alone was used as a positive control. However, rather than producing similar results to PMA/ionomycin or CD3/CD28 stimulated cells in the absence of any inhibitors, TNFα secretion was reduced in the presence of DMSO alone,

suggesting that DMSO interfered with pathways affecting TNFα production. Consistently, DMSO has been shown to reduce TNFα production following stimulation in rat Kuppfer cells[318], and in mouse macrophages[319,320], and has also reduced TNFα induced MMP9 production by human keratinocytes[321]. GW280264X blocks ADAM10 and ADAM17 activity[292], and consequently abolished TNFα secretion following stimulation with either PMA/ionomycin or CD3/CD28. While TNFα secretion was reduced in cells treated with GI254023X compared to untreated PMA/ionomycin or CD3/CD28 stimulated cells, it was not significantly different to TNFα production in PMA/ionomycin or CD3/CD28 stimulated cells treated with DMSO. This suggests that the GI254023X inhibitor had little effect on TNFα secretion, which is consistent with it blocking ADAM10 rather than ADAM17[292]. The ADAM17 neutralising antibody activity is best displayed in CD3/CD28 stimulated PBMCs. The IgG1 antibody is used as an isotype control, meaning that it is the same immunoglobulin class, and raised in the same species as the ADAM17 neutralising antibody. It therefore confirms that results obtained by the neutralising antibody are specific, and result from an inhibition of ADAM17. TNFα production by CD3/CD28 stimulated PBMCs treated with the neutralising antibody is reduced compared to untreated CD3/CD28 stimulated PBMCs. Out of all of the three inhibitors, the neutralising antibody has least effect on TNFα secretion. While treating PMA/ionomycin stimulated PBMCs with the neutralising antibody leads to a small decrease in TNFα secretion, little difference is observed in TNFα production between PMA/ionomycin stimulated PBMCs treated with the neutralising antibody and the isotype control antibody. This experiment has therefore not worked well enough to draw any conclusions from and should be repeated in the future.

5.2.11.2 IL-17 related cytokine production

IL-17 related cytokine production by PBMCs was not affected by changes in ADAM17 expression. Although IL-17-F and IL-22 production were not detected in PBMCs, no differences in IL-17-A or IL-12/IL-23 production in control and ADAM17 deficient PBMCs were observed (figure 5.22 b, c). Likewise, their secretion was not affected by any of the three inhibitors. The data from ELISAs performed on control and ADAM17 deficient PBMCs (figure 5.22 b, c) contrast

the results from ELISAs performed on control and TOC PMBCs (figures 5.19 c, 5.20 b). Rather than suggesting that IL-17 related cytokine production is affected by changes in ADAM17 expression, these results suggest that their secretion may occur independently of ADAM17 activity. This will be discussed in detail in section 5.3.

Figure 5.22: TNFα, IL-17-A and IL-12/IL-23 secretion in PBMCs. TNFα **(a),** IL-17-A **(b)** and IL-12/IL-23 **(c)** secretion in PBMCs from the ADAM17 LOF patient, mother and two controls, following stimulation with PMA/Ionomycin and activation of CD3/CD28. Experiments were carried out in the presence of three inhibitors: two small molecule inhibitors, GW280264X (GW) which blocks ADAM10 and ADAM17, and GI254023X (GI) which blocks ADAM10, and a neutralising antibody against ADAM17 (αA17). DMSO and IgG1 provided controls for the small molecule inhibitors and αADAM17 respectively. Data represent mean ± the SEM; *n*=2.

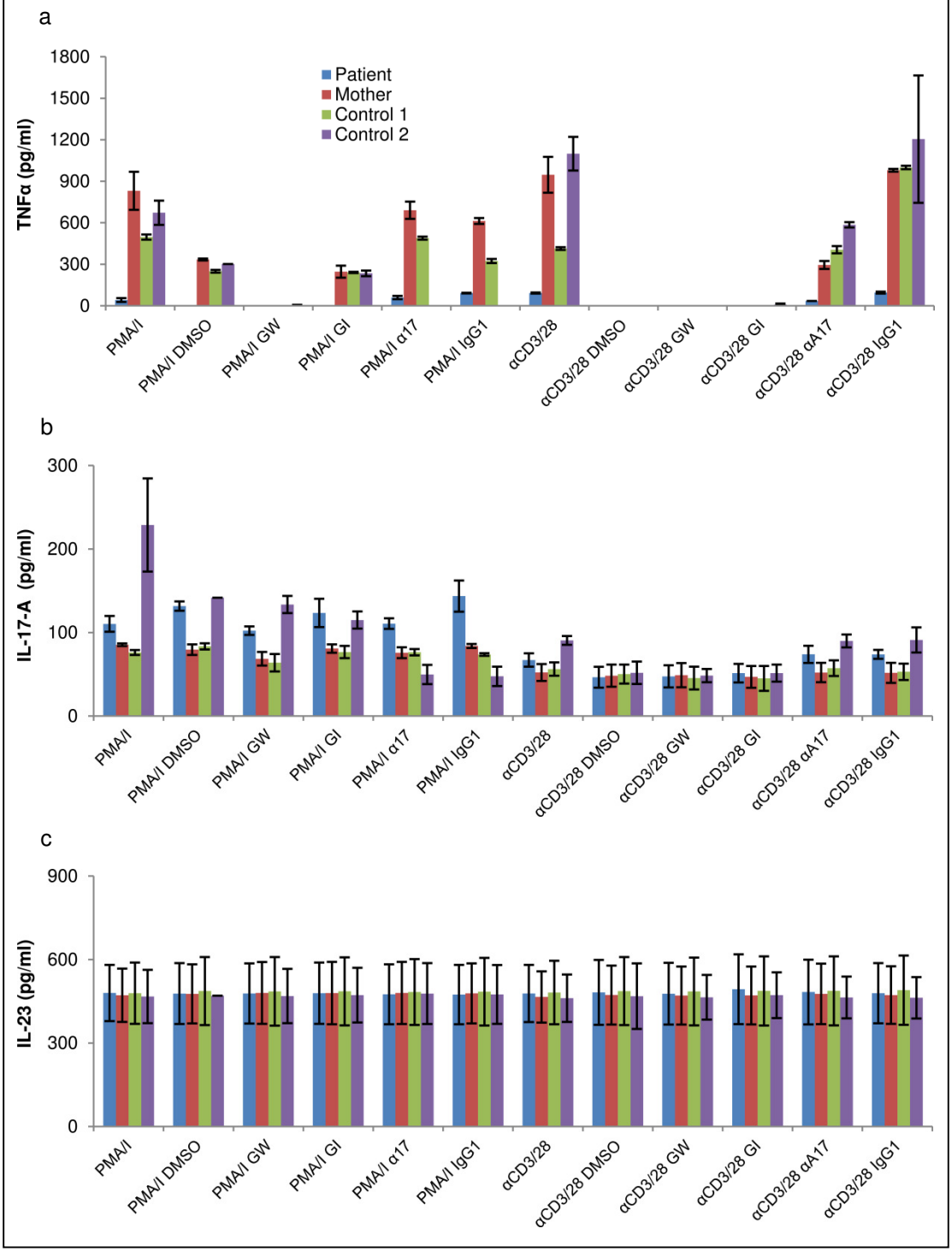

5.3 Discussion

The results in this chapter strongly suggest that ADAM17 acts to provide protection during cutaneous *S. aureus* skin infection. ADAM17 deficiency is associated with recurrent *Staphylococcal* skin infections in a patient suffering from an inflammatory skin and bowel syndrome[239]. While attempts made to immortalise keratinocytes from this patient were unsuccessful, using siRNA against ADAM17 provided a way to study the loss of functional ADAM17 expression in *vitro*. Knocking down ADAM17 in control keratinocytes resulted in significantly increased *S. aureus* adhesion and invasion. Furthermore, ADAM17 is probably also important during gastrointestinal bacterial infection, as treating intestinal cells with siRNA against ADAM17 increased EPEC adhesion and *S. flexneri* invasion.

Immortalised keratinocytes from TOC patients carrying the gain of function mutation p.ILe136Thr in iRhom2[252], were utilised to study the effects of increased ADAM17 activity. iRhom2 has recently been shown to transport pro-ADAM17 from the ER to its site of maturation in the Golgi apparatus, and is thus a key regulator of ADAM17 activity. Macrophages from *iRhom2*$^{-/-}$ mice exhibit abrogated secretion of TNFα secretion compared to WT mice[256,258]. Experiments performed by Matthew Brooke (Centre for Cutaneous Research) demonstrate increased ADAM17 activity in TOC keratinocytes compared to control keratinocytes, with elevated expression of mature ADAM17 at the plasma membrane, together with enhanced release of ADAM17 dependent cytokines and growth factors. Increased ADAM17 activity in TOC keratinocytes correlates with reductions in *S. aureus* infection, which is consistent with a hypothesis that ADAM17 is required for protection during bacterial infection. Furthermore, treating TOC keratinocytes with siRNA against ADAM17 abolishes this protective effect, leading to increases in infection.

One limitation of these experiments is they were only performed in one cell type grown in a monolayer. In addition to epithelial cells, *S. aureus* invades other non-professional phagocytes including endothelial cells and fibroblasts, as well as professional phagocytes including neutrophils, monocytes and macrophages[260,265] . For future experiments it would be interesting to consider

how infection is affected by changes in ADAM17 expression in other cell types. It remains to be investigated how *S. aureus* is affected by changes in ADAM17 expression in *vivo.* Although *ADAM17*$^{-/-}$ mice exhibit perinatal lethality[203], mice in which ADAM17 is conditionally knocked out in keratinocytes (*ADAM17*$^{-/-}$) have been descibed[238]. If a transgenic mouse model of TOC, carrying either the p.Ile186Thr or p.Pro189Leu mutations were available, it would be interesting to investigate if there were differences in *S. aureus* infection in such mice compared to WT mice and *ADAM17*$^{-/-}$ mice.

Perhaps the most obvious way ADAM17 acts to provide protection during bacterial infection is by stimulating an immune response. ADAM17 drives inflammatory responses, first and foremost by its cleavage of TNFα. TNFα expression coordinates early immune responses, by stimulating expression of other proinflammatory cytokines including IL-1β and IL-6, and by induction of chemokines and adhesion molecules, which recruit leukocytes to the site of infection[302]. Proinflammatory cytokine expression also enhances bacterial killing by upregulating phagocytosis, antimicrobial peptide and proteinase production, lysosomal production of reactive oxygen species, degranulation, and by production of neutrophil extracellular traps[322]. In this study, the production of IL-6 and IL-8 in *S. aureus* infected keratinocytes was shown to be ADAM17 dependent, with production being significantly greater in TOC keratinocytes compared to control keratinocytes, and being significantly reduced following treatment with ADAM17 siRNA. This supports observations made by Matthew Brooke (Centre for Cutaenous Research), where proinflammatory cytokine secretion was linked to changes in ADAM17 expression. Furthermore, as the elevated secretion of IL-6 and IL-8 is indicative of an enhanced inflammatory response in TOC keratinocytes, and correlates with a reduction in *S. aureus* infection, this could represent one way ADAM17 acts to provide protection during bacterial infection. It would be interesting to investigate whether other components of the immune response are affected by changes in ADAM17 expression. The effect of manipulating ADAM17 expression in a neutrophil or macrophage cell line on bacterial killing could be investigated by a number of different methods. The level of phagocytosis could be measured by quantifying the number of internalised bacteria. Production of proteinases including cathepsin D and elastase, which degrade bacterial proteins and components[262],

could be measured by immunofluorescence and western blotting. Immunofluorescence could also be used to investigate lysosomal production of reactive oxygen species (ROS). Dyes including aminophenylfluorescein (AFP) become fluorescent in the presence of ROS. Neutrophil degranulation could also be measured *in vitro* by quantifying the release of components including myeloperoxidase[323]. For example, 3,3',5,5'-tetramethylbenzidine is a substrate of myeloperoxidase, and an interaction between the two molecules produces a quantifiable colour change[323]. Finally, recruitment of immune cells to the site of infection could be measured *in vivo* by two photon microscopy. Immune cells could be labelled according to cell surface marker expression, for example neutrophils by L-selectin, or macrophages or dendritic cells with CD11 (http://www.biolegend.com/cell_markers).

Upstream regulation of EGFR signalling by ADAM17, which sheds EGFR ligands including amphiregulin, TGF-α and HB-EGF[230], may represent a second way in which ADAM17 acts to provide protection during bacterial infection. In mice EGFR signalling maintains the epidermal barrier[238]. It drives the terminal differentiation of keratinocytes as they migrate through the suprabasal layers to the epidermal surface. It also activates transglutaminases (TGM) 1 and 3, which initiate cornified envelope formation, by cross linking structural components of keratinocytes. Mice with a conditional knock out of ADAM17 in keratinocytes (*ADAM17*$^{-/-}$) have a defective epidermal barrier resulting from defects in keratinocyte terminal differentiation, and reduced TGM activity, preventing cornified envelope formation[238]. Blaydon *et al*[252] suggested that EGFR signalling is increased in TOC keratinocytes compared to control keratinocytes. In the absence of EGF within the culture media, control keratinocytes exhibited very low levels of proliferation and migration, whilst TOC keratinocytes displayed increased proliferative and migratory potentials. Consistent with increased EGFR signalling, experiments performed by Matthew Brooke (centre for Cutaenous Research) demonstrated that the shedding of ADAM17 dependent growth factors is increased in TOC keratinocytes. As keratinocyte wound healing relies on cell proliferation and migration, increased EGFR signalling in TOC keratinocytes could lead to keratinocyte hyperproliferation[324]. Additionally, a recent study in rats has shown that ADAM17 mRNA is upregulated in the epidermis and dermis following wound healing[325], providing

further evidence that ADAM17 is likely to be important for epidermal barrier maintenance. MMP9 is a downstream target of the EGFR pathway, whose expression was shown to be affected at the mRNA and secretion level by changes in ADAM17 expression in this study. As already mentioned, MMP9 plays a role in ECM remodelling which occurs during processes including cell growth, cell migration and wound healing. Matthew Brooke (Centre for Cutaenous Research) has also shown by immunofluorescence that frozen TOC keratinocytes have increased TGM1 activity, which is likely to enhance the cornification process. In combination with keratinocyte hyperproliferation and MMP9 induced ECM remodelling, increased TGM1 activity could potentially contribute to a thicker epidermal barrier and provide improved protection against invading pathogens in TOC cells.

In the *ADAM17*$^{-/-}$ mice, the defective epidermal barrier was shown by increased transepithelial water loss (TWL)[252]. If a mouse model of TOC was available, it would be interesting to measure how TWL compared to WT mice, to determine whether there is any effect of increased ADAM17 activity on epidermal barrier function *in vivo*. It would also be interesting to visualise how TGM1 and terminal differentiation marker expression is affected by increased ADAM17 activity i*n vivo*. Finally, measuring the epidermal thickness of organotypic cultures grown with control and TOC keratinocytes, in the presence and absence of ADAM17 siRNA, could provide an insight into whether epidermal thickness is affected by changes in ADAM17 expression.

The gene expression array and qRT-PCR data first suggested that the IL-17 signalling pathway may be affected by ADAM17 expression, with siRNA against ADAM17 leading to decreases in CSF2, CSF3, CXCL5 and MMP9 mRNA levels. Keratinocyte secretion of MMP9 appeared to correlate with ADAM17 expression, but other ELISA data suggested that IL-17-A secretion might occur independently of ADAM17 activity. Keratinocytes do not produce IL-17-A, but there was no significant difference in secretion between PBMCs from control subjects and PBMCs from the ADAM17 deficient patient. Furthermore, reducing ADAM17 activity with various inhibitors had no effect on the secretion of IL-17-A or the Th17 inducing cytokines IL-12/IL-23, providing further evidence that it may be ADAM17 independent. TOC PBMCs produced significantly more IL-17-A and CXCL5 than control PBMCs. This could potentially result from increased

endogenous expression of IL-17-A and CXCL5, in turn leading to increases in their secretion following stimulation with PMA/ionomycin.

Two different skin conditions with a similar clinical presentation have been shown to have different levels of ADAM17 expression and IL-17 signalling compared to healthy controls. At one end of the spectrum, ADAM17 expression is increased in psoriasis, with psoriatic lesions displaying elevated levels of ADAM17 mRNA compared to control skin[225]. Psoriasis is a chronic skin disease which presents with inflamed lesions covered by scaly patches of dead skin. It is associated with dysregulated inflammation, keratinocyte hyperproliferation and abnormal keratinocyte terminal differentiation[225]. The IL-17 signalling pathway is also overactive in psoriatic patients, and increased levels of IL-17-A, IL-17-C and IL-17-F have been observed in psoriatic lesions[326]. Interestingly, at the other end of the spectrum, the impaired function of ADAM17 causes an inflammatory skin disease which has a similar clinical presentation to psoriasis[239]. A recent study in mice has shown that conditionally knocking out ADAM17 in the epidermis of mice leads to atopic dermatitis[1]. Interestingly, these mice also have increased IL-17 signalling[1]. They display chronic inflammation with Th17 and IL-17-A producing γδ T cell infiltration, along with increased production of IL-17-A, IL-22, and two Th17 cell inducing cytokines, IL-1β and IL-23[1]. So these are two different skin conditions with a similar phenotype, with very different levels of ADAM17 expression, yet they share the common feature of elevated IL-17 signalling. This could suggest that rather than being directly regulated by ADAM17, the IL-17 signalling pathway may be activated by an unknown upstream factor. If IL-17 pathway activation is the common factor responsible for the chronic inflammation in both diseases, they may share a common event which induces IL-17 signalling cascades. ADAM17 may therefore not have a role in the IL-17 signalling pathway, and could explain why PBMCs from the ADAM17 deficient patient produce similar levels of IL-17-A to PBMCs from control subjects. An aim of future work, therefore should be to identify any common upstream factor that may lead to IL-17 signalling in both diseases.

When ADAM17 was knocked out in the epidermis of mice, the mRNA expression of IL-17 related cytokines increased[1], yet in this study, keratinocytes 48 hours post knock down displayed no differences in the mRNA

expression of Th17 inducing cytokines, IL-17-A/F or IL-22, but reduced expression of the downstream components CXCL5, MMP9, CSF2 and CSF3 . These differences in results could arise for a variety of reasons. Firstly, differential gene expression may exist between humans and mice. Secondly, mRNA expression is measured in cell monolayers in human keratinocytes, whilst its expression is measured within the epidermis in mice. Other cell types exist within the epidermis, and therefore the mRNA level measured includes cells other than just keratinocytes. Thirdly, gene expression may vary depending on the time point it is measured at. In human keratinocytes, IL-17 related cytokine mRNA could potentially have been degraded independently of ADAM17, and new mRNA synthesis may not have occurred at the time point when expression is measured. The study in mice does not indicate the time point at which gene expression is measured. If mRNA expression were measured at a later time point, this could potentially give more time for an increase in its synthesis.

While these results may suggest that the IL-17 signalling pathway is not a direct downstream target of ADAM17, and therefore may not be a way ADAM17 acts to provide protection during infection, more work is needed to determine this. Firstly, as different cell types including NK, Th17 and γδT cells producing IL-17 reside in the epidermis, it would be interesting to measure mRNA expression of different cytokines in the IL-17 pathway in different epidermal cell types. Carrying out mRNA expression analysis at different time points post knock down, for example, 24, 48, 72 and 96 hours should provide an insight into the time point, if any, at which they are affected by ADAM17 activity. Any effect could be transient, or occur over a long time period, and could be affected directly by ADAM17 activity, or indirectly in response to other signalling pathways or cellular processes. The cytokines analysed could include Th17 inducing cytokines (IL-1β, IL-6, IL-21 and IL-23), IL-17-A, IL-17-F, IL-22 and more downstream components (MMP9, CSF2, CSF3 and CXCL5). Frozen skin sections are available from biopsies taken from the ADAM17 deficient patient, control and TOC subjects. If RNA were extracted from these samples, qRT-PCRs could be performed to determine if there is any difference in the total RNA level of IL-17 related cytokines in the epidermis of the three specimens.

Total RNA could also be measured in PBMCs from control, ADAM17 deficient and TOC PBMCs.

It would also be interesting to measure whether ADAM17 affects IL-17 related cytokine protein expression. This could be determined by extracting protein from the frozen samples, making lysates and analysing by western blotting. Protein expression level and localisation could also be determined by immunofluorescence if suitable antibodies were available. Most of the components of the IL-17 signalling pathway described in the previous paragraphs are secreted, so their expression should also be measured by ELISA. PBMCs are significantly greater producers of IL-17 related cytokines than keratinocytes. Measuring IL-17-A and IL-12/23 should therefore be repeated and include the ADAM17 deficient patient, control and TOC PBMCs in the same experiment. The experiment should be extended to include the other IL-17 related cytokines described in the previous paragraphs. This should be carried out in unstimulated, *S. aureus* infected and LPS and PMA/ionomycin stimulated PBMCs at different time points. Using ADAM17 inhibitors would further clarify whether secretion is affected by ADAM17 activity. Additionally, whether increased production of IL-17-A and CXCL5 by TOC PBMCs compared to control PBMCs is due to differences in ADAM17 activity should be clarified by treating TOC PBMCs with ADAM17 inhibitors. If there were no differences in their secretion in TOC PBMCs following inhibitor treatment, this would support the idea that TOC PBMCs express a higher endogenous level of IL-17A and CXCL5 than control PBMCs.

Finally, flow cytometry and immunofluorescence could be used to investigate whether differences exist between the numbers of IL-17 producing cells, namely Th17, γδ T cells and NK cells in ADAM17 deficient, control and TOC subjects. The number of cells within a population of PBMCs could be analysed by flow cytometry by quantifying $CD4^{+}$/IL-17A^{+} (Th17), γδ-TCR^{+}[327] (γδ) and $CD3^{-}$/$CD56^{+}$[328] (NK) cells. Similarly, performing single staining for γδ T cells, and double staining for Th17 and NK cells on frozen control, ADAM17 LOF and TOC skin specimens, should provide insights as to whether the numbers of IL-17-A producing cells in the epidermis are affected by different levels of ADAM17 expression.

5.4 Conclusion

The results in this chapter strongly suggest that ADAM17 provides protection during cutaneous bacterial skin infection *in vitro*. ADAM17 mediated protection probably results in part from its roles in the induction of immune responses and in the maintenance of the epidermal barrier. This study suggests that ADAM17 probably does not influence α5β1 integrin mediated *S. aureus* invasion, or affect the expression of the antimicrobial peptides hBD-2 or hBD-3. Finally, research over recent years has demonstrated the importance of the IL-17 signalling pathway during *S. aureus* infection. However, whether ADAM17 targets the IL-17 signalling pathway as a way to provide protection during bacterial infection remains to be investigated.

~ Chapter 6 ~

Final Discussion

This study began with investigating how gastrointestinal bacterial infection was affected by a loss of functional Cx26 expression. Within certain geographic locations and ethnic groups, high carrier frequencies of specific recessive mutations account for the majority of Cx26 related non-syndromic hearing loss (NSHL), for example c.35delG and p.R143W in Europe[114,115] and Ghana respectively[95]. The common occurrence of specific mutations in different populations is possibly due to geographic isolation. Given that mutations have remained in populations for thousands of years, however, suggests that they may provide a heterozygous advantage to carriers. Heterozygote carriers of the NSHL mutations c.35delG and p.R143W alleles were previously shown to have a thicker epidermis than wild type (WT) Cx26 homozygotes[118,120], and cells expressing the p.143W mutant were also significantly less susceptible to invasion by *S. flexneri* than cells expressing WT Cx26[45]. This study investigated how infection by the attaching and effacing pathogen EPEC was affected by expression of the p.143W mutation. Subsequently, EPEC and *S. flexneri* infection were measured in intestinal cells treated with Cx26 siRNA.

S. flexneri infection was quantified using cellular invasion as has been published previously[45,141,200], so no method optimisation was needed. In this study however, an automated system was developed to quantify EPEC infection by bacterial adherence and actin pedestal formation. This made it possible to quantify infection within a large population of cells, and without the introduction of human error or bias. In addition to solely quantifying the total percentage of infected cells within a given population, it was also possible to measure the infection level of individual cells. By measuring the adhesion of individual bacteria to cells, more subtle effects of differential expression of Cx26 on infection could be determined. The methods described in chapter 3 could also be applied to quantify infection of different types of bacteria that are fluorescently labelled by immunofluorescence.

The *in vitro* results presented in chapter 4 demonstrate that a loss of functional Cx26 expression provides improved protection against gastrointestinal bacterial pathogens. EPEC adherence was significantly reduced by expression of a Cx26 NSHL mutation. Additionally, when endogenous Cx26 expression was reduced by siRNA in intestinal cells, *S. flexneri* invasion and EPEC adherence were

significantly decreased. Therefore, although inheriting two Cx26 recessive mutations causes deafness in homozygous individuals, such mutations may remain in the population if they are beneficial to heterozygous carriers. If heterozygotes were less susceptible to gastrointestinal bacterial infection, this could potentially explain the high carrier frequencies of specific Cx26 NSHL mutations.

Bacterial infection was also hypothesised to be affected by differential expression of a second host protein, ADAM17. Since ADAM17 sheds the proinflammatory cytokine TNFα[203,205,206] and ligands of the EGFR[230], it plays important roles in the stimulation of immune responses and in the maintenance of the epidermal barrier. These combined activities suggest that ADAM17 may provide protection during bacterial infection. Consistently, a loss of functional ADAM17 expression led to recurrent *Staphyloccocal* skin infections in a patient with an inflammatory skin and bowel syndrome[239]. The results described in chapter 5 show that a loss of functional ADAM17 expression was associated with significantly increased *S. aureus* infection *in vitro*. Furthermore, iRhom2 is required for ADAM17 maturation[256,258,259], and TOC keratinocytes which have increased iRhom2 and ADAM17 activity, also have significantly reduced *S. aureus* infection. These findings strongly suggest that ADAM17 is required for protection during skin infection. Experiments performed in this study and by Matthew Brooke (Centre for Cutaneous Research), have shown that shedding of proinflammatory cytokines and growth factors positively correlates with ADAM17 activity. Increased ADAM17 in TOC keratinocytes may contribute to reduced infection by production of an enhanced inflammatory response and stronger epidermal barrier. In this chapter, gene expression profiling was also carried out. This identified the IL-17 signalling pathway, which is important during *S. aureus* infection, as a potential downstream target of ADAM17. However, whether or not ADAM17 activates the IL-17 signalling pathway during bacterial infection remains to be investigated.

Cx26 and ADAM17 may represent two potential alternative therapeutic targets for treatment of bacterial infections. Some patients with bacterial infections may benefit from a reduction in functional Cx26 expression, whilst others may benefit from a stimulation of ADAM17 activity. This may be beneficial for bacterial

infections which may be difficult to treat with current therapies, in part because of the development of resistance to multiple antibiotics. The next major step for considering the role of either protein during bacterial infection probably involves investigating the infection of a broader range of bacterial pathogens in an *in vivo* setting.

~ Bibliography ~

1 Abstracts of the 2013 International Investigative Dermatology Meeting. May 8-11, 2013. Edinburgh, Scotland, United Kingdom. *J Invest Dermatol* **133 Suppl 1**, S1-311 (2013).
2 Scott, C. A. & Kelsell, D. P. Key functions for gap junctions in skin and hearing. *Biochem J* **438**, 245-254 (2011).
3 Caspar, D. L., Goodenough, D. A., Makowski, L. & Phillips, W. C. Gap junction structures. I. Correlated electron microscopy and x-ray diffraction. *J Cell Biol* **74**, 605-628 (1977).
4 Makowski, L., Caspar, D. L., Phillips, W. C. & Goodenough, D. A. Gap junction structures. II. Analysis of the x-ray diffraction data. *J Cell Biol* **74**, 629-645 (1977).
5 Vinken, M. *et al.* Connexins and their channels in cell growth and cell death. *Cell Signal* **18**, 592-600 (2006).
6 Kumar, N. M. & Gilula, N. B. The gap junction communication channel. *Cell* **84**, 381-388 (1996).
7 Rackauskas, M., Neverauskas, V. & Skeberdis, V. A. Diversity and properties of connexin gap junction channels. *Medicina (Kaunas)* **46**, 1-12 (2010).
8 White, T. W. & Paul, D. L. Genetic diseases and gene knockouts reveal diverse connexin functions. *Annu Rev Physiol* **61**, 283-310 (1999).
9 Maeda, S. & Tsukihara, T. Structure of the gap junction channel and its implications for its biological functions. *Cell Mol Life Sci* **68**, 1115-1129 (2011).
10 Paul, D. L. Molecular cloning of cDNA for rat liver gap junction protein. *J Cell Biol* **103**, 123-134 (1986).
11 Sohl, G. & Willecke, K. An update on connexin genes and their nomenclature in mouse and man. *Cell Commun Adhes* **10**, 173-180 (2003).
12 Wright, C. S., Becker, D. L., Lin, J. S., Warner, A. E. & Hardy, K. Stage-specific and differential expression of gap junctions in the mouse ovary: connexin-specific roles in follicular regulation. *Reproduction* **121**, 77-88 (2001).
13 Rabionet, R., Lopez-Bigas, N., Arbones, M. L. & Estivill, X. Connexin mutations in hearing loss, dermatological and neurological disorders. *Trends Mol Med* **8**, 205-212 (2002).
14 Panchin, Y. V. Evolution of gap junction proteins--the pannexin alternative. *J Exp Biol* **208**, 1415-1419 (2005).
15 Orellana, J. A. *et al.* Modulation of brain hemichannels and gap junction channels by pro-inflammatory agents and their possible role in neurodegeneration. *Antioxid Redox Signal* **11**, 369-399 (2009).
16 Phelan, P. *et al.* Innexins: a family of invertebrate gap-junction proteins. *Trends Genet* **14**, 348-349 (1998).
17 Laird, D. W. Life cycle of connexins in health and disease. *Biochem J* **394**, 527-543 (2006).
18 Wagner, C. Function of connexins in the renal circulation. *Kidney Int* **73**, 547-555 (2008).

19 Mese, G., Richard, G. & White, T. W. Gap junctions: basic structure and function. *J Invest Dermatol* **127**, 2516-2524 (2007).

20 Stergiopoulos, K. *et al.* Hetero-domain interactions as a mechanism for the regulation of connexin channels. *Circ Res* **84**, 1144-1155 (1999).

21 Zhang, J. T., Chen, M., Foote, C. I. & Nicholson, B. J. Membrane integration of in vitro-translated gap junctional proteins: co- and post-translational mechanisms. *Mol Biol Cell* **7**, 471-482 (1996).

22 Musil, L. S. & Goodenough, D. A. Multisubunit assembly of an integral plasma membrane channel protein, gap junction connexin43, occurs after exit from the ER. *Cell* **74**, 1065-1077 (1993).

23 Koval, M., Harley, J. E., Hick, E. & Steinberg, T. H. Connexin46 is retained as monomers in a trans-Golgi compartment of osteoblastic cells. *J Cell Biol* **137**, 847-857 (1997).

24 Martin, P. E., Errington, R. J. & Evans, W. H. Gap junction assembly: multiple connexin fluorophores identify complex trafficking pathways. *Cell Commun Adhes* **8**, 243-248 (2001).

25 Lauf, U. *et al.* Dynamic trafficking and delivery of connexons to the plasma membrane and accretion to gap junctions in living cells. *Proc Natl Acad Sci U S A* **99**, 10446-1045 (2002).

26 Johnson, R. G. *et al.* Gap junctions assemble in the presence of cytoskeletal inhibitors, but enhanced assembly requires microtubules. *Exp Cell Res* **275**, 67-80 (2002).

27 Goldberg, G. S., Valiunas, V. & Brink, P. R. Selective permeability of gap junction channels. *Biochim Biophys Acta* **1662**, 96-101 (2004).

28 Gaietta, G. *et al.* Multicolor and electron microscopic imaging of connexin trafficking. *Science* **296**, 503-507 (2002).

29 Traub, O. *et al.* Comparative characterization of the 21-kD and 26-kD gap junction proteins in murine liver and cultured hepatocytes. *J Cell Biol* **108**, 1039-1051 (1989).

30 Lampe, P. D. & Lau, A. F. The effects of connexin phosphorylation on gap junctional communication. *Int J Biochem Cell Biol* **36**, 1171-1186 (2004).

31 TenBroek, E. M., Lampe, P. D., Solan, J. L., Reynhout, J. K. & Johnson, R. G. Ser364 of connexin43 and the upregulation of gap junction assembly by cAMP. *J Cell Biol* **155**, 1307-1318 (2001).

32 Cooper, C. D. & Lampe, P. D. Casein kinase 1 regulates connexin-43 gap junction assembly. *J Biol Chem* **277**, 44962-44968 (2002).

33 Leithe, E. & Rivedal, E. Epidermal growth factor regulates ubiquitination, internalization and proteasome-dependent degradation of connexin43. *J Cell Sci* **117**, 1211-1220 (2004).

34 Ebihara, L. & Steiner, E. Properties of a nonjunctional current expressed from a rat connexin46 cDNA in Xenopus oocytes. *J Gen Physiol* **102**, 59-74 (1993).

35 Li, H. *et al.* Properties and regulation of gap junctional hemichannels in the plasma membranes of cultured cells. *J Cell Biol* **134**, 1019-1030 (1996).
36 Hofer, A. & Dermietzel, R. Visualization and functional blocking of gap junction hemichannels (connexons) with antibodies against external loop domains in astrocytes. *Glia* **24**, 141-154 (1998).
37 Kondo, R. P., Wang, S. Y., John, S. A., Weiss, J. N. & Goldhaber, J. I. Metabolic inhibition activates a non-selective current through connexin hemichannels in isolated ventricular myocytes. *J Mol Cell Cardiol* **32**, 1859-1872 (2000).

38 Valiunas, V. Biophysical properties of connexin-45 gap junction hemichannels studied in vertebrate cells. *J Gen Physiol* **119**, 147-164 (2002).
39 Beahm, D. L. & Hall, J. E. Hemichannel and junctional properties of connexin 50. *Biophys J* **82**, 2016-2031(2002).

40 Goodenough, D. A. & Paul, D. L. Beyond the gap: functions of unpaired connexon channels. *Nat Rev Mol Cell Biol* **4**, 285-294 (2003).

41 Evans, W. H., De Vuyst, E. & Leybaert, L. The gap junction cellular internet: connexin hemichannels enter the signalling limelight. *Biochem J* **397**, 1-14 (2006).

42 Parpura, V., Scemes, E. & Spray, D. C. Mechanisms of glutamate release from astrocytes: gap junction "hemichannels", purinergic receptors and exocytotic release. *Neurochem Int* **45**, 259-264 (2004).

43 Cherian, P. P. *et al.* Mechanical strain opens connexin 43 hemichannels in osteocytes: a novel mechanism for the release of prostaglandin. *Mol Biol Cell* **16**, 3100-3106 (2005).

44 Brini, M., Cali, T., Ottolini, D. & Carafoli, E. Intracellular calcium homeostasis and signaling. *Met Ions Life Sci* **12**, 119-168 (2013).
45 Man, Y. K. *et al.* A deafness-associated mutant human connexin 26 improves the epithelial barrier in vitro. *J Membr Biol* **218**, 29-37 (2007).
46 Ey, B., Eyking, A., Gerken, G., Podolsky, D. K. & Cario, E. TLR2 mediates gap junctional intercellular communication through connexin-43 in intestinal epithelial barrier injury. *J Biol Chem* **284**, 22332-22343, (2009).

47 Wilders, R. & Jongsma, H. J. Limitations of the dual voltage clamp method in assaying conductance and kinetics of gap junction channels. *Biophys J* **63**, 942-953 (1992).

48 Van Rijen, H. V., Wilders, R., Van Ginneken, A. C. & Jongsma, H. J. Quantitative analysis of dual whole-cell voltage-clamp determination of gap junctional conductance. *Pflugers Arch* **436**, 141-151 (1998).
49 Goldberg, G. S. *et al.* Evidence that disruption of connexon particle arrangements in gap junction plaques is associated with inhibition of gap junctional communication by a glycyrrhetinic acid derivative. *Exp Cell Res* **222**, 48-53 (1996).

50 Gabriel, H. D. *et al.* Transplacental uptake of glucose is decreased in embryonic lethal connexin26-deficient mice. *J Cell Biol* **140**, 1453-1461 (1998).
51 Lee, J. R. & White, T. W. Connexin-26 mutations in deafness and skin disease. *Expert Rev Mol Med* **11**, e35 (2009).

52 Alberti, P. *THE ANATOMY AND PHYSIOLOGY OF THE EAR AND HEARING (World Health Organisation Occupational Health Publications)*, <http://www.who.int/occupational_health/publications/noise2.pdf>
53 Martinez, A. D., Acuna, R., Figueroa, V., Maripillan, J. & Nicholson, B. Gap-junction channels dysfunction in deafness and hearing loss. *Antioxid Redox Signal* **11**, 309-322 (2009).
54 Hibino, H. & Kurachi, Y. Molecular and physiological bases of the K+ circulation in the mammalian inner ear. *Physiology (Bethesda)* **21**, 336-345 (2006).

55 Cohen-Salmon, M. *et al.* Targeted ablation of connexin26 in the inner ear epithelial gap junction network causes hearing impairment and cell death. *Curr Biol* **12**, 1106-1111 (2002).
56 Proksch, E., Brandner, J. M. & Jensen, J. M. The skin: an indispensable barrier. *Exp Dermatol* **17**, 1063-1072 (2008).
57 CliffsNotes.com. *The Dermis*, <http://www.cliffsnotes.com/study_guide/topicArticleId-277792,articleId-277540.html>
58 CliffsNotes.com. *The Hypodermis*, <http://www.cliffsnotes.com/study_guide/topicArticleId-277792,articleId-277542.html>
59 University-of-Leeds. *Epithelia: How to classify them*, <http://www.histology.leeds.ac.uk/tissue_types/epithelia/epithelia_classify.php>
60 Candi, E., Schmidt, R. & Melino, G. The cornified envelope: a model of cell death in the skin. *Nat Rev Mol Cell Biol* **6**, 328-340 (2005).

61 Garrod, D. & Chidgey, M. Desmosome structure, composition and function. *Biochim Biophys Acta* **1778**, 572-587 (2008).

62 Garrod, D. R., Merritt, A. J. & Nie, Z. Desmosomal cadherins. *Curr Opin Cell Biol* **14**, 537-545 (2002).
63 Gros, E. & Novak, N. Cutaneous dendritic cells in allergic inflammation. *Clin Exp Allergy* **42**, 1161-1175 (2012).
64 Di, W. L., Rugg, E. L., Leigh, I. M. & Kelsell, D. P. Multiple epidermal connexins are expressed in different keratinocyte subpopulations including connexin 31. *J Invest Dermatol* **117**, 958-964 (2001).

65 Salomon, D. *et al.* Topography of mammalian connexins in human skin. *J Invest Dermatol* **103**, 240-247 (1994).
66 Di, W. L. *et al.* Connexin interaction patterns in keratinocytes revealed morphologically and by FRET analysis. *J Cell Sci* **118**, 1505-1514 (2005).

67 Lucke, T. *et al.* Upregulation of connexin 26 is a feature of keratinocyte differentiation in hyperproliferative epidermis, vaginal epithelium, and buccal epithelium. *J Invest Dermatol* **112**, 354-361 (1999).
68 Scott, C. A., Tattersall, D., O'Toole, E. A. & Kelsell, D. P. Connexins in epidermal homeostasis and skin disease. *Biochim Biophys Acta* **1818**, 1952-1961(2012).

69 Goliger, J. A. & Paul, D. L. Wounding alters epidermal connexin expression and gap junction-mediated intercellular communication. *Mol Biol Cell* **6**, 1491-1501 (1995).
70 Coutinho, P., Qiu, C., Frank, S., Tamber, K. & Becker, D. Dynamic changes in connexin expression correlate with key events in the wound healing process. *Cell Biol Int* **27**, 525-541(2003).
71 Djalilian, A. R. *et al.* Connexin 26 regulates epidermal barrier and wound remodeling and promotes psoriasiform response. *J Clin Invest* **116**, 1243-1253 (2006).
72 Labarthe, M. P., Bosco, D., Saurat, J. H., Meda, P. & Salomon, D. Upregulation of connexin 26 between keratinocytes of psoriatic lesions. *J Invest Dermatol* **111**, 72-76 (1998).
73 White, T. W. Functional analysis of human Cx26 mutations associated with deafness. *Brain Res Brain Res Rev* **32**, 181-183 (2000).
74 Zelante, L. *et al.* Connexin26 mutations associated with the most common form of non-syndromic neurosensory autosomal recessive deafness (DFNB1) in Mediterraneans. *Hum Mol Genet* **6**, 1605-1609 (1997).
75 D'Andrea, P. *et al.* Hearing loss: frequency and functional studies of the most common connexin26 alleles. *Biochem Biophys Res Commun* **296**, 685-691 (2002).
76 Thomas, T., Telford, D. & Laird, D. W. Functional domain mapping and selective trans-dominant effects exhibited by Cx26 disease-causing mutations. *J Biol Chem* **279**, 19157-19168 (2004).

77 Richard, G. *et al.* Functional defects of Cx26 resulting from a heterozygous missense mutation in a family with dominant deaf-mutism and palmoplantar keratoderma. *Hum Genet* **103**, 393-399 (1998).
78 Rouan, F. *et al.* trans-dominant inhibition of connexin-43 by mutant connexin-26: implications for dominant connexin disorders affecting epidermal differentiation. *J Cell Sci* **114**, 2105-2113 (2001).
79 Bakirtzis, G. *et al.* Targeted epidermal expression of mutant Connexin 26(D66H) mimics true Vohwinkel syndrome and provides a model for the pathogenesis of dominant connexin disorders. *Hum Mol Genet* **12**, 1737-1744 (2003).
80 Montgomery, J. R., White, T. W., Martin, B. L., Turner, M. L. & Holland, S. M. A novel connexin 26 gene mutation associated with features of the keratitis-ichthyosis-deafness syndrome and the follicular occlusion triad. *J Am Acad Dermatol* **51**, 377-382 (2004).

81 Petit, C., Levilliers, J. & Hardelin, J. P. Molecular genetics of hearing loss. *Annu Rev Genet* **35**, 589-646 (2001).

82 Ballana E, Estivill X. *Connexins and deafness homepage*, < http://www.crg.es/deafness>

83 Hutchin, T. *et al.* Assessment of the genetic causes of recessive childhood non-syndromic deafness in the UK - implications for genetic testing. *Clin Genet* **68**, 506-512 (2005).

84 Guilford, P. *et al.* A non-syndrome form of neurosensory, recessive deafness maps to the pericentromeric region of chromosome 13q. *Nat Genet* **6**, 24-28 (1994).

85 Chaib, H. *et al.* A gene responsible for a dominant form of neurosensory non-syndromic deafness maps to the NSRD1 recessive deafness gene interval. *Hum Mol Genet* **3**, 2219-2222 (1994).

86 Kelsell, D. P. *et al.* Connexin 26 mutations in hereditary non-syndromic sensorineural deafness. *Nature* **387**, 80-83 (1997).

87 Kelsell, D. P. *et al.* Connexin mutations associated with palmoplantar keratoderma and profound deafness in a single family. *Eur J Hum Genet* **8**, 141-144 (2000).

88 Houseman, M. J. *et al.* Genetic analysis of the connexin-26 M34T variant: identification of genotype M34T/M34T segregating with mild-moderate non-syndromic sensorineural hearing loss. *J Med Genet* **38**, 20-25 (2001).

89 Brobby, G. W., Muller-Myhsok, B. & Horstmann, R. D. Connexin 26 R143W mutation associated with recessive nonsyndromic sensorineural deafness in Africa. *N Engl J Med* **338**, 548-550 (1998).

90 Fuse, Y. *et al.* Three novel connexin26 gene mutations in autosomal recessive non-syndromic deafness. *Neuroreport* **10**, 1853-1857 (1999).

91 Denoyelle, F. *et al.* Connexin 26 gene linked to a dominant deafness. *Nature* **393**, 319-320 (1998).

92 Loffler, J. *et al.* Sensorineural hearing loss and the incidence of Cx26 mutations in Austria. *Eur J Hum Genet* **9**, 226-230 (2001).

93 Matos, T. D. *et al.* A novel M163L mutation in connexin 26 causing cell death and associated with autosomal dominant hearing loss. *Hear Res* **240**, 87-92 (2008).

94 Primignani, P. *et al.* A novel dominant missense mutation--D179N--in the GJB2 gene (Connexin 26) associated with non-syndromic hearing loss. *Clin Genet* **63**, 516-521 (2003).

95 Hamelmann, C. *et al.* Pattern of connexin 26 (GJB2) mutations causing sensorineural hearing impairment in Ghana. *Hum Mutat* **18**, 84-85, (2001).

96 Morle, L. *et al.* A novel C202F mutation in the connexin26 gene (GJB2) associated with autosomal dominant isolated hearing loss. *J Med Genet* **37**, 368-370 (2000).

97 Bondeson, M. L., Nystrom, A. M., Gunnarsson, U. & Vahlquist, A. Connexin 26 (GJB2) mutations in two Swedish patients with atypical Vohwinkel (mutilating keratoderma plus deafness) and KID syndrome both extensively treated with acitretin. *Acta Derm Venereol* **86**, 503-508 (2006).

98 Maestrini, E. *et al.* A missense mutation in connexin26, D66H, causes mutilating keratoderma with sensorineural deafness (Vohwinkel's syndrome) in three unrelated families. *Hum Mol Genet* **8**, 1237-1243 (1999).

99 Snoeckx, R. L. *et al.* GJB2 mutations and degree of hearing loss: a multicenter study. *Am J Hum Genet* **77**, 945-957 (2005).

100 Richard, G., Brown, N., Ishida-Yamamoto, A. & Krol, A. Expanding the phenotypic spectrum of Cx26 disorders: Bart-Pumphrey syndrome is caused by a novel missense mutation in GJB2. *J Invest Dermatol* **123**, 856-863 (2004).

101 Alexandrino, F., Sartorato, E. L., Marques-de-Faria, A. P. & Steiner, C. E. G59S mutation in the GJB2 (connexin 26) gene in a patient with Bart-Pumphrey syndrome. *Am J Med Genet A* **136**, 282-284 (2005).

102 Akiyama, M. *et al.* A novel GJB2 mutation p.Asn54His in a patient with palmoplantar keratoderma, sensorineural hearing loss and knuckle pads. *J Invest Dermatol* **127**, 1540-1543 (2007).

103 Heathcote, K., Syrris, P., Carter, N. D. & Patton, M. A. A connexin 26 mutation causes a syndrome of sensorineural hearing loss and palmoplantar hyperkeratosis (MIM 148350). *J Med Genet* **37**, 50-51 (2000).

104 Leonard, N. J., Krol, A. L., Bleoo, S. & Somerville, M. J. Sensorineural hearing loss, striate palmoplantar hyperkeratosis, and knuckle pads in a patient with a novel connexin 26 (GJB2) mutation. *J Med Genet* **42**, e2 (2005).

105 de Zwart-Storm, E. A. *et al.* A novel missense mutation in GJB2 disturbs gap junction protein transport and causes focal palmoplantar keratoderma with deafness. *J Med Genet* **45**, 161-166 (2008).

106 Uyguner, O. *et al.* The novel R75Q mutation in the GJB2 gene causes autosomal dominant hearing loss and palmoplantar keratoderma in a Turkish family. *Clin Genet* **62**, 306-309 (2002).

107 Iossa, S. *et al.* New evidence for the correlation of the p.G130V mutation in the GJB2 gene and syndromic hearing loss with palmoplantar keratoderma. *Am J Med Genet A* **149A**, 685-688 (2009).

108 de Zwart-Storm, E. A. *et al.* A novel missense mutation in the second extracellular domain of GJB2, p.Ser183Phe, causes a syndrome of focal palmoplantar keratoderma with deafness. *Am J Pathol* **173**, 1113-1119 (2008).

109 Richard, G. *et al.* Missense mutations in GJB2 encoding connexin-26 cause the ectodermal dysplasia keratitis-ichthyosis-deafness syndrome. *Am J Hum Genet* **70**, 1341-1348 (2002).

110 Arita, K. *et al.* A novel N14Y mutation in Connexin26 in keratitis-ichthyosis-deafness syndrome: analyses of altered gap junctional communication and molecular structure of N terminus of mutated Connexin26. *Am J Pathol* **169**, 416-423 (2006).

111 Janecke, A. R. *et al.* GJB2 mutations in keratitis-ichthyosis-deafness syndrome including its fatal form. *Am J Med Genet A* **133A**, 128-131 (2005).

112 Yotsumoto, S. *et al.* Novel mutations in GJB2 encoding connexin-26 in Japanese patients with keratitis-ichthyosis-deafness syndrome. *Br J Dermatol* **148**, 649-653 (2003).

113 van Geel, M. *et al.* HID and KID syndromes are associated with the same connexin 26 mutation. *Br J Dermatol* **146**, 938-942 (2002).

114 Kelley, P. M. *et al.* Novel mutations in the connexin 26 gene (GJB2) that cause autosomal recessive (DFNB1) hearing loss. *Am J Hum Genet* **62**, 792-799 (1998).

115 Gasparini, P. *et al.* High carrier frequency of the 35delG deafness mutation in European populations. Genetic Analysis Consortium of GJB2 35delG. *Eur J Hum Genet* **8**, 19-23 (2000).

116 Abe, S., Usami, S., Shinkawa, H., Kelley, P. M. & Kimberling, W. J. Prevalent connexin 26 gene (GJB2) mutations in Japanese. *J Med Genet* **37**, 41-43 (2000).

117 Morell, R. J. *et al.* Mutations in the connexin 26 gene (GJB2) among Ashkenazi Jews with nonsyndromic recessive deafness. *N Engl J Med* **339**, 1500-1505 (1998).

118 D'Adamo, P. *et al.* Does epidermal thickening explain GJB2 high carrier frequency and heterozygote advantage? *Eur J Hum Genet* **17**, 284-286 (2009).

119 Common, J. E., Di, W. L., Davies, D. & Kelsell, D. P. Further evidence for heterozygote advantage of GJB2 deafness mutations: a link with cell survival. *J Med Genet* **41**, 573-575 (2004).

120 Meyer, C. G. *et al.* Selection for deafness? *Nat Med* **8**, 1332-1333 (2002).

121 Luzzatto, L. Sickle cell anaemia and malaria. *Mediterr J Hematol Infect Dis* **4**, e2012065 (2012).

122 Patanayindee, J., Muanprasat, C., Soodvilai, S. & Chatsudthipong, V. Antidiarrheal efficacy of a quinazolin CFTR inhibitor on human intestinal epithelial cell and in mouse model of cholera. *Indian J Pharmacol* **44**, 619-623 (2012).

123 Pier, G. B. *et al.* Salmonella typhi uses CFTR to enter intestinal epithelial cells. *Nature* **393**, 79-82 (1998).

124 Phalipon, A. & Sansonetti, P. J. Shigella's ways of manipulating the host intestinal innate and adaptive immune system: a tool box for survival? *Immunol Cell Biol* **85**, 119-129 (2007).

125 PubMed-Health. *A.D.A.M. Medical Encylopedia Hypoglycemia*, <http://www.ncbi.nlm.nih.gov/pubmedhealth/help/>

126 PubMed-Health. *A.D.A.M. Medical Encyclopedia Toxic megacolon*, <http://www.ncbi.nlm.nih.gov/pubmedhealth/PMH0001294/>

127 DuPont, H. L., Levine, M. M., Hornick, R. B. & Formal, S. B. Inoculum size in shigellosis and implications for expected mode of transmission. *J Infect Dis* **159**, 1126-1128 (1989).

128 Kotloff, K. L. *et al.* Global burden of Shigella infections: implications for vaccine development and implementation of control strategies. *Bull World Health Organ* **77**, 651-666 (1999).

129 Kaper, J. B., Nataro, J. P. & Mobley, H. L. Pathogenic Escherichia coli. *Nat Rev Microbiol* **2**, 123-140 (2004).

130 Nataro, J. P. & Kaper, J. B. Diarrheagenic Escherichia coli. *Clin Microbiol Rev* **11**, 142-201 (1998).

131 Lapointe, T. K., O'Connor, P. M. & Buret, A. G. The role of epithelial malfunction in the pathogenesis of enteropathogenic E. coli-induced diarrhea. *Lab Invest* **89**, 964-970 (2009).

132 Todar, K. *Online Textbook Of Bacteriology*, <http://www.textbookofbacteriology.net/e.coli_4.html> (2008-2012).

133 Spears, K. J., Roe, A. J. & Gally, D. L. A comparison of enteropathogenic and enterohaemorrhagic Escherichia coli pathogenesis. *FEMS Microbiol Lett* **255**, 187-202 (2006).

134 Trabulsi, L. R., Keller, R. & Tardelli Gomes, T. A. Typical and atypical enteropathogenic Escherichia coli. *Emerg Infect Dis* **8**, 508-513 (2002).

135 Cornelis, G. R. The type III secretion injectisome. *Nat Rev Microbiol* **4**, 811-825 (2006).

136 Buchrieser, C. *et al.* The virulence plasmid pWR100 and the repertoire of proteins secreted by the type III secretion apparatus of Shigella flexneri. *Mol Microbiol* **38**, 760-771(2000).

137 Niebuhr, K. *et al.* IpgD, a protein secreted by the type III secretion machinery of Shigella flexneri, is chaperoned by IpgE and implicated in entry focus formation. *Mol Microbiol* **38**, 8-19 (2000).

138 Garmendia, J., Frankel, G. & Crepin, V. F. Enteropathogenic and enterohemorrhagic Escherichia coli infections: translocation, translocation, translocation. *Infect Immun* **73**, 2573-2585 (2005).

139 Galan, J. E. & Collmer, A. Type III secretion machines: bacterial devices for protein delivery into host cells. *Science* **284**, 1322-1328 (1999).

140 Veenendaal, A. K. *et al.* The type III secretion system needle tip complex mediates host cell sensing and translocon insertion. *Mol Microbiol* **63**, 1719-1730 (2007).

141 Romero, S. *et al.* ATP-mediated Erk1/2 activation stimulates bacterial capture by filopodia, which precedes Shigella invasion of epithelial cells. *Cell Host Microbe* **9**, 508-519 (2011).

142 Schroeder, G. N. & Hilbi, H. Molecular pathogenesis of Shigella spp.: controlling host cell signaling, invasion, and death by type III secretion. *Clin Microbiol Rev* **21**, 134-156 (2008).

143 Donnenberg, M. S. Interactions between enteropathogenic Escherichia coli and epithelial cells. *Clin Infect Dis* **28**, 451-455 (1999).

144 Jarvis, K. G. *et al.* Enteropathogenic Escherichia coli contains a putative type III secretion system necessary for the export of proteins involved in attaching and effacing lesion formation. *Proc Natl Acad Sci U S A* **92**, 7996-8000 (1995).

145 Dean, P. & Kenny, B. The effector repertoire of enteropathogenic E. coli: ganging up on the host cell. *Curr Opin Microbiol* **12**, 101-109 (2009).

146 Elliott, S. J. *et al.* A gene from the locus of enterocyte effacement that is required for enteropathogenic Escherichia coli to increase tight-junction permeability encodes a chaperone for EspF. *Infect Immun* **70**, 2271-2277 (2002).

147 Creasey, E. A. *et al.* CesAB is an enteropathogenic Escherichia coli chaperone for the type-III translocator proteins EspA and EspB. *Microbiology* **149**, 3639-3647 (2003).
148 Le Gall, T. *et al.* Analysis of virulence plasmid gene expression defines three classes of effectors in the type III secretion system of Shigella flexneri. *Microbiology* **151**, 951-962 (2005).

149 Rosenshine, I., Ruschkowski, S. & Finlay, B. B. Expression of attaching/effacing activity by enteropathogenic Escherichia coli depends on growth phase, temperature, and protein synthesis upon contact with epithelial cells. *Infect Immun* **64**, 966-973 (1996).
150 Vanmaele, R. P. & Armstrong, G. D. Effect of carbon source on localized adherence of enteropathogenic Escherichia coli. *Infect Immun* **65**, 1408-1413 (1997).
151 Mellies, J. L., Barron, A. M. & Carmona, A. M. Enteropathogenic and enterohemorrhagic Escherichia coli virulence gene regulation. *Infect Immun* **75**, 4199-4210 (2007).

152 Sperandio, V., Mellies, J. L., Nguyen, W., Shin, S. & Kaper, J. B. Quorum sensing controls expression of the type III secretion gene transcription and protein secretion in enterohemorrhagic and enteropathogenic Escherichia coli. *Proc Natl Acad Sci U S A* **96**, 15196-15201 (1999).
153 N. Aguilera Montilla, M. P. B., M. López Santalla, J.M. Martín Villa. Mucosal immune system: A brief review. *Inmunología* **23**, 207-216 (2004).
154 Ogawa, M., Handa, Y., Ashida, H., Suzuki, M. & Sasakawa, C. The versatility of Shigella effectors. *Nat Rev Microbiol* **6**, 11-16 (2008).

155 Mita, Y., Dobashi, K., Nakazawa, T. & Mori, M. Induction of Toll-like receptor 4 in granulocytic and monocytic cells differentiated from HL-60 cells. *Br J Haematol* **112**, 1041-1047(2001).
156 Girardin, S. E. *et al.* Nod1 detects a unique muropeptide from gram-negative bacterial peptidoglycan. *Science* **300**, 1584-1587 (2003).

157 Kasper, C. A. *et al.* Cell-cell propagation of NF-kappaB transcription factor and MAP kinase activation amplifies innate immunity against bacterial infection. *Immunity* **33**, 804-816 (2010).

158 Disanza, A. *et al.* Actin polymerization machinery: the finish line of signaling networks, the starting point of cellular movement. *Cell Mol Life Sci* **62**, 955-970, doi:10.1007/s00018-004-4472-6 (2005).
159 Diwan, J. J. *Actin cytoskeleton*, <http://www.rpi.edu/dept/bcbp/molbiochem/MBWeb/mb2/part1/actin.htm>
160 Poukkula, M., Kremneva, E., Serlachius, M. & Lappalainen, P. Actin-depolymerizing factor homology domain: a conserved fold performing diverse roles in cytoskeletal dynamics. *Cytoskeleton (Hoboken)* **68**, 471-490 (2011).
161 Elam, W. A., Kang, H. & De la Cruz, E. M. Biophysics of actin filament severing by cofilin. *FEBS Lett* **587**, 1215-1219 (2013).

162 Yamashiro, S., Gokhin, D. S., Kimura, S., Nowak, R. B. & Fowler, V. M. Tropomodulins: pointed-end capping proteins that regulate actin filament

architecture in diverse cell types. *Cytoskeleton (Hoboken)* **69**, 337-370 (2012).
163 Cooper, J. A. & Sept, D. New insights into mechanism and regulation of actin capping protein. *Int Rev Cell Mol Biol* **267**, 183-206 (2008).

164 Campellone, K. G. & Welch, M. D. A nucleator arms race: cellular control of actin assembly. *Nat Rev Mol Cell Biol* **11**, 237-251 (2010).

165 Rotty, J. D., Wu, C. & Bear, J. E. New insights into the regulation and cellular functions of the ARP2/3 complex. *Nat Rev Mol Cell Biol* **14**, 7-12 (2013).

166 Carlsson, A. E., Wear, M. A. & Cooper, J. A. End versus side branching by Arp2/3 complex. *Biophys J* **86**, 1074-1081 (2004).

167 Boureux, A., Vignal, E., Faure, S. & Fort, P. Evolution of the Rho family of ras-like GTPases in eukaryotes. *Mol Biol Evol* **24**, 203-216 (2007).

168 Moon, S. Y. & Zheng, Y. Rho GTPase-activating proteins in cell regulation. *Trends Cell Biol* **13**, 13-22 (2003).
169 Bourdet-Sicard, R., Egile, C., Sansonetti, P. J. & Tran Van Nhieu, G. Diversion of cytoskeletal processes by Shigella during invasion of epithelial cells. *Microbes Infect* **2**, 813-819 (2000).
170 Bulgin, R. *et al.* Bacterial guanine nucleotide exchange factors SopE-like and WxxxE effectors. *Infect Immun* **78**, 1417-1425 (2010).

171 Handa, Y. *et al.* Shigella IpgB1 promotes bacterial entry through the ELMO-Dock180 machinery. *Nat Cell Biol* **9**, 121-128 (2007).

172 Niebuhr, K. *et al.* Conversion of PtdIns(4,5)P(2) into PtdIns(5)P by the S.flexneri effector IpgD reorganizes host cell morphology. *EMBO J* **21**, 5069-5078 (2002).
173 Cossart, P. & Sansonetti, P. J. Bacterial invasion: the paradigms of enteroinvasive pathogens. *Science* **304**, 242-248 (2004).

174 Tran Van Nhieu, G., Bourdet-Sicard, R., Dumenil, G., Blocker, A. & Sansonetti, P. J. Bacterial signals and cell responses during Shigella entry into epithelial cells. *Cell Microbiol* **2**, 187-193 (2000).
175 Carayol, N. & Tran Van Nhieu, G. Tips and tricks about Shigella invasion of epithelial cells. *Curr Opin Microbiol* **16**, 32-37 (2013).

176 Ramarao, N. *et al.* Capping of actin filaments by vinculin activated by the Shigella IpaA carboxyl-terminal domain. *FEBS Lett* **581**, 853-857 (2007).

177 Yoshida, S. *et al.* Microtubule-severing activity of Shigella is pivotal for intercellular spreading. *Science* **314**, 985-989 (2006).

178 Zahavi, E. E. *et al.* Bundle-forming pilus retraction enhances enteropathogenic Escherichia coli infectivity. *Mol Biol Cell* **22**, 2436-2447 (2011).

179 Kenny, B. *et al.* Enteropathogenic E. coli (EPEC) transfers its receptor for intimate adherence into mammalian cells. *Cell* **91**, 511-520 (1997).

180 Goosney, D. L., Gruenheid, S. & Finlay, B. B. Gut feelings: enteropathogenic E. coli (EPEC) interactions with the host. *Annu Rev Cell Dev Biol* **16**, 173-189 (2000).

181 Goosney, D. L. *et al.* Enteropathogenic E. coli translocated intimin receptor, Tir, interacts directly with alpha-actinin. *Curr Biol* **10**, 735-738 (2000).

182 Niessen, C. M. Tight junctions/adherens junctions: basic structure and function. *J Invest Dermatol* **127**, 2525-2532 (2007).

183 Hartsock, A. & Nelson, W. J. Adherens and tight junctions: structure, function and connections to the actin cytoskeleton. *Biochim Biophys Acta* **1778**, 660-669 (2008).

184 Hossain, Z. & Hirata, T. Molecular mechanism of intestinal permeability: interaction at tight junctions. *Mol Biosyst* **4**, 1181-1185 (2008).

185 Laukoetter, M. G., Nava, P. & Nusrat, A. Role of the intestinal barrier in inflammatory bowel disease. *World J Gastroenterol* **14**, 401-407 (2008).

186 Manjarrez-Hernandez, H. A. *et al.* Phosphorylation of myosin light chain at distinct sites and its association with the cytoskeleton during enteropathogenic Escherichia coli infection. *Infect Immun* **64**, 2368-2370 (1996).

187 Berkes, J., Viswanathan, V. K., Savkovic, S. D. & Hecht, G. Intestinal epithelial responses to enteric pathogens: effects on the tight junction barrier, ion transport, and inflammation. *Gut* **52**, 439-451 (2003).

188 McNamara, B. P. *et al.* Translocated EspF protein from enteropathogenic Escherichia coli disrupts host intestinal barrier function. *J Clin Invest* **107**, 621-629 (2001).

189 Zhang, Q., Li, Q., Wang, C., Li, N. & Li, J. Redistribution of Tight Junction Proteins During EPEC Infection In Vivo. *Inflammation* **35**, 23-32 (2012).

190 Dean, P. & Kenny, B. Intestinal barrier dysfunction by enteropathogenic Escherichia coli is mediated by two effector molecules and a bacterial surface protein. *Mol Microbiol* **54**, 665-675 (2004).

191 Guttman, J. A. *et al.* Attaching and effacing pathogen-induced tight junction disruption in vivo. *Cell Microbiol* **8**, 634-645 (2006).

192 Hamada, D., Hamaguchi, M., Suzuki, K. N., Sakata, I. & Yanagihara, I. Cytoskeleton-modulating effectors of enteropathogenic and enterohemorrhagic Escherichia coli: a case for EspB as an intrinsically less-ordered effector. *FEBS J* **277**, 2409-2415 (2010).

193 Field, M. Intestinal ion transport and the pathophysiology of diarrhea. *J Clin Invest* **111**, 931-943 (2003).

194 Bowen, R. *Secretion in the Small Intestine*, <http://www.vivo.colostate.edu/hbooks/pathphys/digestion/smallgut/secretion.html>

195 Hodges, K., Alto, N. M., Ramaswamy, K., Dudeja, P. K. & Hecht, G. The enteropathogenic Escherichia coli effector protein EspF decreases sodium hydrogen exchanger 3 activity. *Cell Microbiol* **10**, 1735-1745 (2008).

196 Shaw, R. K. *et al.* Enteropathogenic Escherichia coli type III effectors EspG and EspG2 disrupt the microtubule network of intestinal epithelial cells. *Infect Immun* **73**, 4385-4390 (2005).

197 Dean, P., Maresca, M., Schuller, S., Phillips, A. D. & Kenny, B. Potent diarrheagenic mechanism mediated by the cooperative action of three enteropathogenic Escherichia coli-injected effector proteins. *Proc Natl Acad Sci U S A* **103**, 1876-1881 (2006).

198 Guttman, J. A. *et al.* Aquaporins contribute to diarrhoea caused by attaching and effacing bacterial pathogens. *Cell Microbiol* **9**, 131-141 (2007).

199 Kanczuga-Koda, L., Sulkowski, S., Koda, M., Sobaniec-Lotowska, M. & Sulkowska, M. Expression of connexins 26, 32 and 43 in the human colon--an immunohistochemical study. *Folia Histochem Cytobiol* **42**, 203-207 (2004).

200 Tran Van Nhieu, G. *et al.* Connexin-dependent inter-cellular communication increases invasion and dissemination of Shigella in epithelial cells. *Nat Cell Biol* **5**, 720-726 (2003).

201 Guttman, J. A. *et al.* Gap junction hemichannels contribute to the generation of diarrhoea during infectious enteric disease. *Gut* **59**, 218-226 (2010).

202 Velasquez Almonacid, L. A. *et al.* Role of connexin-43 hemichannels in the pathogenesis of Yersinia enterocolitica. *Vet J* **182**, 452-457 (2009).

203 Blobel, C. P. ADAMs: key components in EGFR signalling and development. *Nat Rev Mol Cell Biol* **6**, 32-43 (2005).

204 Huovila, A. P., Turner, A. J., Pelto-Huikko, M., Karkkainen, I. & Ortiz, R. M. Shedding light on ADAM metalloproteinases. *Trends Biochem Sci* **30**, 413-422 (2005).

205 Moss, M. L. *et al.* Cloning of a disintegrin metalloproteinase that processes precursor tumour-necrosis factor-alpha. *Nature* **385**, 733-736 (1997).

206 Black, R. A. *et al.* A metalloproteinase disintegrin that releases tumour-necrosis factor-alpha from cells. *Nature* **385**, 729-733 (1997).

207 Stocker, W. & Bode, W. Structural features of a superfamily of zinc-endopeptidases: the metzincins. *Curr Opin Struct Biol* **5**, 383-390 (1995).

208 Murphy, G. The ADAMs: signalling scissors in the tumour microenvironment. *Nat Rev Cancer* **8**, 929-941 (2008).

209 Scheller, J., Chalaris, A., Garbers, C. & Rose-John, S. ADAM17: a molecular switch to control inflammation and tissue regeneration. *Trends Immunol* **32**, 380-387 (2011).

210 Seals, D. F. & Courtneidge, S. A. The ADAMs family of metalloproteases: multidomain proteins with multiple functions. *Genes Dev* **17**, 7-30 (2003).

211 Weber, S. & Saftig, P. Ectodomain shedding and ADAMs in development. *Development* **139**, 3693-3709 (2012).

212 Bode, W., Gomis-Ruth, F. X. & Stockler, W. Astacins, serralysins, snake venom and matrix metalloproteinases exhibit identical zinc-binding environments (HEXXHXXGXXH and Met-turn) and topologies and should be grouped into a common family, the 'metzincins'. *FEBS Lett* **331**, 134-140 (1993).
213 Van Wart, H. E. & Birkedal-Hansen, H. The cysteine switch: a principle of regulation of metalloproteinase activity with potential applicability to the entire matrix metalloproteinase gene family. *Proc Natl Acad Sci U S A* **87**, 5578-5582 (1990).
214 Schlondorff, J., Becherer, J. D. & Blobel, C. P. Intracellular maturation and localization of the tumour necrosis factor alpha convertase (TACE). *Biochem J* **347 Pt 1**, 131-138 (2000).
215 Gould, R. J. *et al.* Disintegrins: a family of integrin inhibitory proteins from viper venoms. *Proc Soc Exp Biol Med* **195**, 168-171 (1990).
216 Nath, D. *et al.* Interaction of metargidin (ADAM-15) with alphavbeta3 and alpha5beta1 integrins on different haemopoietic cells. *J Cell Sci* **112 (Pt 4)**, 579-587 (1999).
217 Zhu, X. & Evans, J. P. Analysis of the roles of RGD-binding integrins, alpha(4)/alpha(9) integrins, alpha(6) integrins, and CD9 in the interaction of the fertilin beta (ADAM2) disintegrin domain with the mouse egg membrane. *Biol Reprod* **66**, 1193-1202 (2002).
218 Bax, D. V. *et al.* Integrin alpha5beta1 and ADAM-17 interact in vitro and co-localize in migrating HeLa cells. *J Biol Chem* **279**, 22377-22386 (2004).
219 Soond, S. M., Everson, B., Riches, D. W. & Murphy, G. ERK-mediated phosphorylation of Thr735 in TNFalpha-converting enzyme and its potential role in TACE protein trafficking. *J Cell Sci* **118**, 2371-2380 (2005).
220 Edwards, D. R., Handsley, M. M. & Pennington, C. J. The ADAM metalloproteinases. *Mol Aspects Med* **29**, 258-289 (2008).
221 Primakoff, P. & Myles, D. G. The ADAM gene family: surface proteins with adhesion and protease activity. *Trends Genet* **16**, 83-87 (2000).
222 Nishimura, H., Kim, E., Nakanishi, T. & Baba, T. Possible function of the ADAM1a/ADAM2 Fertilin complex in the appearance of ADAM3 on the sperm surface. *J Biol Chem* **279**, 34957-34962 (2004).
223 Cho, C. *et al.* Fertilization defects in sperm from mice lacking fertilin beta. *Science* **281**, 1857-1859 (1998).
224 Pruessmeyer, J. & Ludwig, A. The good, the bad and the ugly substrates for ADAM10 and ADAM17 in brain pathology, inflammation and cancer. *Semin Cell Dev Biol* **20**, 164-174 (2009).
225 Saftig, P. & Reiss, K. The "A Disintegrin And Metalloproteases" ADAM10 and ADAM17: novel drug targets with therapeutic potential? *Eur J Cell Biol* **90**, 527-535 (2011).
226 Mullberg, J. *et al.* The soluble interleukin-6 receptor is generated by shedding. *Eur J Immunol* **23**, 473-480 (1993).

227 Rose-John, S., Scheller, J., Elson, G. & Jones, S. A. Interleukin-6 biology is coordinated by membrane-bound and soluble receptors: role in inflammation and cancer. *J Leukoc Biol* **80**, 227-236 (2006).

228 McDermott, M. F. *et al.* Germline mutations in the extracellular domains of the 55 kDa TNF receptor, TNFR1, define a family of dominantly inherited autoinflammatory syndromes. *Cell* **97**, 133-144 (1999).

229 Yarden, Y. & Sliwkowski, M. X. Untangling the ErbB signalling network. *Nat Rev Mol Cell Biol* **2**, 127-137 (2001).

230 Sahin, U. *et al.* Distinct roles for ADAM10 and ADAM17 in ectodomain shedding of six EGFR ligands. *J Cell Biol* **164**, 769-779 (2004).

231 Hynes, N. E. & Lane, H. A. ERBB receptors and cancer: the complexity of targeted inhibitors. *Nat Rev Cancer* **5**, 341-354 (2005).

232 Bublil, E. M. & Yarden, Y. The EGF receptor family: spearheading a merger of signaling and therapeutics. *Curr Opin Cell Biol* **19**, 124-134 (2007).

233 Chen, S. *et al.* Neuregulin 1-erbB signaling is necessary for normal myelination and sensory function. *J Neurosci* **26**, 3079-3086 (2006).

234 Normanno, N. *et al.* Epidermal growth factor receptor (EGFR) signaling in cancer. *Gene* **366**, 2-16 (2006).

235 Peschon, J. J. *et al.* An essential role for ectodomain shedding in mammalian development. *Science* **282**, 1281-1284 (1998).

236 Luetteke, N. C. *et al.* Targeted inactivation of the EGF and amphiregulin genes reveals distinct roles for EGF receptor ligands in mouse mammary gland development. *Development* **126**, 2739-2750 (1999).

237 Jackson, L. F. *et al.* Defective valvulogenesis in HB-EGF and TACE-null mice is associated with aberrant BMP signaling. *EMBO J* **22**, 2704-2716 (2003).

238 Franzke, C. W. *et al.* Epidermal ADAM17 maintains the skin barrier by regulating EGFR ligand-dependent terminal keratinocyte differentiation. *J Exp Med* (2012).

239 Blaydon, D. C. *et al.* Inflammatory skin and bowel disease linked to ADAM17 deletion. *N Engl J Med* **365**, 1502-1508 (2011).

240 Moriyama, H. *et al.* Azasugar-based MMP/ADAM inhibitors as antipsoriatic agents. *J Med Chem* **47**, 1930-1938 (2004).

241 Maretzky, T. *et al.* ADAM10 mediates E-cadherin shedding and regulates epithelial cell-cell adhesion, migration, and beta-catenin translocation. *Proc Natl Acad Sci U S A* **102**, 9182-9187 (2005).

242 Maretzky, T. *et al.* ADAM10-mediated E-cadherin release is regulated by proinflammatory cytokines and modulates keratinocyte cohesion in eczematous dermatitis. *J Invest Dermatol* **128**, 1737-1746 (2008).

243 Chalaris, A. *et al.* Critical role of the disintegrin metalloprotease ADAM17 for intestinal inflammation and regeneration in mice. *J Exp Med* **207**, 1617-1624 (2010).

244 Ellis, A. *et al.* Tylosis associated with carcinoma of the oesophagus and oral leukoplakia in a large Liverpool family--a review of six generations. *Eur J Cancer B Oral Oncol* **30B**, 102-112 (1994).
245 Stevens, H. P. *et al.* Linkage of an American pedigree with palmoplantar keratoderma and malignancy (palmoplantar ectodermal dysplasia type III) to 17q24. Literature survey and proposed updated classification of the keratodermas. *Arch Dermatol* **132**, 640-651 (1996).
246 Hennies, H. C., Hagedorn, M. & Reis, A. Palmoplantar keratoderma in association with carcinoma of the esophagus maps to chromosome 17q distal to the keratin gene cluster. *Genomics* **29**, 537-540 (1995).

247 Varela, A. B., Blanco Rodriguez, M. M., Boullosa, P. E. & Silva, J. G. Tylosis A with squamous cell carcinoma of the oesophagus in a Spanish family. *Eur J Gastroenterol Hepatol* **23**, 286-288 (2011).
248 Saarinen, S. *et al.* Analysis of a Finnish family confirms RHBDF2 mutations as the underlying factor in tylosis with esophageal cancer. *Fam Cancer* **11**, 525-528 (2012).
249 Kelsell, D. P. *et al.* Close mapping of the focal non-epidermolytic palmoplantar keratoderma (PPK) locus associated with oesophageal cancer (TOC). *Hum Mol Genet* **5**, 857-860 (1996).
250 Risk, J. M. *et al.* Characterization of a 500 kb region on 17q25 and the exclusion of candidate genes as the familial Tylosis Oesophageal Cancer (TOC) locus. *Oncogene* **21**, 6395-6402 (2002).
251 Langan, J. E. *et al.* Novel microsatellite markers and single nucleotide polymorphisms refine the tylosis with oesophageal cancer (TOC) minimal region on 17q25 to 42.5 kb: sequencing does not identify the causative gene. *Hum Genet* **114**, 534-540 (2004).
252 Blaydon, D. C. *et al.* RHBDF2 mutations are associated with tylosis, a familial esophageal cancer syndrome. *Am J Hum Genet* **90**, 340-346 (2012).

253 Freeman, M. Rhomboid proteases and their biological functions. *Annu Rev Genet* **42**, 191-210 (2008).
254 Mayer, U. & Nusslein-Volhard, C. A group of genes required for pattern formation in the ventral ectoderm of the Drosophila embryo. *Genes Dev* **2**, 1496-1511 (1988).
255 Lemberg, M. K. & Freeman, M. Functional and evolutionary implications of enhanced genomic analysis of rhomboid intramembrane proteases. *Genome Res* **17**, 1634-1646 (2007).

256 Adrain, C., Zettl, M., Christova, Y., Taylor, N. & Freeman, M. Tumor necrosis factor signaling requires iRhom2 to promote trafficking and activation of TACE. *Science* **335**, 225-228 (2012).

257 Zettl, M., Adrain, C., Strisovsky, K., Lastun, V. & Freeman, M. Rhomboid family pseudoproteases use the ER quality control machinery to regulate intercellular signaling. *Cell* **145**, 79-91 (2011).

258 McIlwain, D. R. *et al.* iRhom2 regulation of TACE controls TNF-mediated protection against Listeria and responses to LPS. *Science* **335**, 229-232 (2012).

259 Lichtenthaler, S. F. Cell biology. Sheddase gets guidance. *Science* **335**, 179-180 (2012).

260 Bien, J., Sokolova, O. & Bozko, P. Characterization of Virulence Factors of Staphylococcus aureus: Novel Function of Known Virulence Factors That Are Implicated in Activation of Airway Epithelial Proinflammatory Response. *J Pathog* **2011**, 601905, (2011).

261 Chambers, H. F. & Deleo, F. R. Waves of resistance: Staphylococcus aureus in the antibiotic era. *Nat Rev Microbiol* **7**, 629-641 (2009).

262 Krishna, S. & Miller, L. S. Innate and adaptive immune responses against Staphylococcus aureus skin infections. *Semin Immunopathol* **34**, 261-280 (2012).

263 Foster, T. J. & Hook, M. Surface protein adhesins of Staphylococcus aureus. *Trends Microbiol* **6**, 484-488 (1998).

264 Bartlett, A. H. & Hulten, K. G. Staphylococcus aureus pathogenesis: secretion systems, adhesins, and invasins. *Pediatr Infect Dis J* **29**, 860-861 (2010).

265 Parker, D. & Prince, A. Immunopathogenesis of Staphylococcus aureus pulmonary infection. *Semin Immunopathol* **34**, 281-297 (2012).

266 Brakebusch, C. & Fassler, R. The integrin-actin connection, an eternal love affair. *EMBO J* **22**, 2324-2333 (2003).

267 Kubica, M. *et al.* A potential new pathway for Staphylococcus aureus dissemination: the silent survival of S. aureus phagocytosed by human monocyte-derived macrophages. *PLoS One* **3**, e1409 (2008).

268 Nestle, F. O., Di Meglio, P., Qin, J. Z. & Nickoloff, B. J. Skin immune sentinels in health and disease. *Nat Rev Immunol* **9**, 679-691 (2009).

269 Segal, A. W. How neutrophils kill microbes. *Annu Rev Immunol* **23**, 197-223 (2005).

270 Fournier, B. & Philpott, D. J. Recognition of Staphylococcus aureus by the innate immune system. *Clin Microbiol Rev* **18**, 521-540 (2005).

271 Ley, K., Laudanna, C., Cybulsky, M. I. & Nourshargh, S. Getting to the site of inflammation: the leukocyte adhesion cascade updated. *Nat Rev Immunol* **7**, 678-689 (2007).

272 Kaplan, M. J. & Radic, M. Neutrophil extracellular traps: double-edged swords of innate immunity. *J Immunol* **189**, 2689-2695 (2012).

273 Goldman AS, P. B. *The Complement System. in: Baron's Medical Microbiology*. 4th edn, (University of Texas Medical Branch, 1996).

274 McLoughlin, R. M., Lee, J. C., Kasper, D. L. & Tzianabos, A. O. IFN-gamma regulated chemokine production determines the outcome of Staphylococcus aureus infection. *J Immunol* **181**, 1323-1332 (2008).

275 McLoughlin, R. M. *et al.* CD4+ T cells and CXC chemokines modulate the pathogenesis of Staphylococcus aureus wound infections. *Proc Natl Acad Sci U S A* **103**, 10408-10413 (2006).

276 Korn, T., Bettelli, E., Oukka, M. & Kuchroo, V. K. IL-17 and Th17 Cells. *Annu Rev Immunol* **27**, 485-517 (2009).

277 Nguyen, T., Ghebrehiwet, B. & Peerschke, E. I. Staphylococcus aureus protein A recognizes platelet gC1qR/p33: a novel mechanism for staphylococcal interactions with platelets. *Infect Immun* **68**, 2061-2068 (2000).
278 Rooijakkers, S. H. *et al.* Immune evasion by a staphylococcal complement inhibitor that acts on C3 convertases. *Nat Immunol* **6**, 920-927 (2005).
279 Postma, B. *et al.* Chemotaxis inhibitory protein of Staphylococcus aureus binds specifically to the C5a and formylated peptide receptor. *J Immunol* **172**, 6994-7001 (2004).
280 Li, H., Llera, A., Malchiodi, E. L. & Mariuzza, R. A. The structural basis of T cell activation by superantigens. *Annu Rev Immunol* **17**, 435-466 (1999).
281 Todar, K. *Staphylococcus Todar's Online Textbook Of Bacteriology*, <http://textbookofbacteriology.net/staph_4.html> (2008-2012).
282 Alouf, J. E. & Muller-Alouf, H. Staphylococcal and streptococcal superantigens: molecular, biological and clinical aspects. *Int J Med Microbiol* **292**, 429-440 (2003).
283 Roben, P. W., Salem, A. N. & Silverman, G. J. VH3 family antibodies bind domain D of staphylococcal protein A. *J Immunol* **154**, 6437-6445 (1995).
284 Hakoda, M. *et al.* Molecular basis for the interaction between human IgM and staphylococcal protein A. *Clin Immunol Immunopathol* **72**, 394-401(1994).
285 Novick, R. P. Autoinduction and signal transduction in the regulation of staphylococcal virulence. *Mol Microbiol* **48**, 1429-1449 (2003).
286 Bolte, G. B., K.; Stern, M. The Cell Lines Caco-2, T84, and Ht-29: Models of Enterocytic Differentiation and Function. *Journal of Pediatric Gastroenterology and Nutrition* **24**, 473 (1997).
287 Cohen, E., Ophir, I. & Shaul, Y. B. Induced differentiation in HT29, a human colon adenocarcinoma cell line. *J Cell Sci* **112 (Pt 16)**, 2657-2666 (1999).
288 Valdivia, R. H. & Falkow, S. Bacterial genetics by flow cytometry: rapid isolation of Salmonella typhimurium acid-inducible promoters by differential fluorescence induction. *Mol Microbiol* **22**, 367-378 (1996).
289 Rickard, S. *et al.* Recurrent mutations in the deafness gene GJB2 (connexin 26) in British Asian families. *J Med Genet* **38**, 530-533 (2001).
290 Jerse, A. E., Yu, J., Tall, B. D. & Kaper, J. B. A genetic locus of enteropathogenic Escherichia coli necessary for the production of attaching and effacing lesions on tissue culture cells. *Proc Natl Acad Sci U S A* **87**, 7839-7843 (1990).
291 Mayr-Harting, A. The acquisition of penicillin resistance by Staphylococcus aureus, strain Oxford. *J Gen Microbiol* **13**, 9-21 (1955).
292 Ludwig, A. *et al.* Metalloproteinase inhibitors for the disintegrin-like metalloproteinases ADAM10 and ADAM17 that differentially block constitutive and phorbol ester-inducible shedding of cell surface molecules. *Comb Chem High Throughput Screen* **8**, 161-171 (2005).
293 Tape, C. J. *et al.* Cross-domain inhibition of TACE ectodomain. *Proc Natl Acad Sci U S A* **108**, 5578-5583 (2011).

294 Frankel, G. & Phillips, A. D. Attaching effacing Escherichia coli and paradigms of Tir-triggered actin polymerization: getting off the pedestal. *Cell Microbiol* **10**, 549-556 (2008).

295 Chang, W. W. *et al.* Salmonella enhance chemosensitivity in tumor through connexin 43 upregulation. *Int J Cancer* **133**, 1926-1935 (2013).

296 Nusrat, A. *et al.* The coiled-coil domain of occludin can act to organize structural and functional elements of the epithelial tight junction. *J Biol Chem* **275**, 29816-29822 (2000).

297 Fujimoto, K. *et al.* Dynamics of connexins, E-cadherin and alpha-catenin on cell membranes during gap junction formation. *J Cell Sci* **110 (Pt 3)**, 311-322 (1997).

298 Morita, H. *et al.* Connexin 26-mediated gap junctional intercellular communication suppresses paracellular permeability of human intestinal epithelial cell monolayers. *Exp Cell Res* **298**, 1-8, (2004).

299 Zhang, W. *et al.* A transgenic mouse model with a luciferase reporter for studying in vivo transcriptional regulation of the human CYP3A4 gene. *Drug Metab Dispos* **31**, 1054-1064 (2003).

300 Robertson, J., Lang, S., Lambert, P. A. & Martin, P. E. Peptidoglycan derived from Staphylococcus epidermidis induces Connexin43 hemichannel activity with consequences on the innate immune response in endothelial cells. *Biochem J* **432**, 133-143 (2010).

301 Donnelly, S. *et al.* Differential susceptibility of Cx26 mutations associated with epidermal dysplasias to peptidoglycan derived from Staphylococcus aureus and Staphylococcus epidermidis. *Exp Dermatol* **21**, 592-598 (2012).

302 Harris, J., Hope, J. C. & Keane, J. Tumor necrosis factor blockers influence macrophage responses to Mycobacterium tuberculosis. *J Infect Dis* **198**, 1842-1850 (2008).

303 Brockbank, E. C., Bridges, J., Marshall, C. J. & Sahai, E. Integrin beta1 is required for the invasive behaviour but not proliferation of squamous cell carcinoma cells in vivo. *Br J Cancer* **92**, 102-112 (2005).

304 Bowdish, D. M., Davidson, D. J. & Hancock, R. E. Immunomodulatory properties of defensins and cathelicidins. *Curr Top Microbiol Immunol* **306**, 27-66 (2006).

305 Pahl, R. *et al.* IL-1beta and ADAM17 are central regulators of beta-defensin expression in Candida esophagitis. *Am J Physiol Gastrointest Liver Physiol* **300**, G547-553 (2011).

306 Gallo, R. L. & Nakatsuji, T. Microbial symbiosis with the innate immune defense system of the skin. *J Invest Dermatol* **131**, 1974-1980, (2011).

307 Lai, Y. & Gallo, R. L. AMPed up immunity: how antimicrobial peptides have multiple roles in immune defense. *Trends Immunol* **30**, 131-141 (2009).

308 Ma, Y. *et al.* Interleukin 24 as a novel potential cytokine immunotherapy for the treatment of Mycobacterium tuberculosis infection. *Microbes Infect* **13**, 1099-1110 (2011).

309 Ma, Y. *et al.* IL-24 protects against Salmonella typhimurium infection by stimulating early neutrophil Th1 cytokine production, which in turn activates CD8+ T cells. *Eur J Immunol* **39**, 3357-3368 (2009).
310 Pappu, R., Ramirez-Carrozzi, V. & Sambandam, A. The interleukin-17 cytokine family: critical players in host defence and inflammatory diseases. *Immunology* **134**, 8-16 (2011).
311 Patil DP, K. G. MMP9 (matrix metallopeptidase 9 (gelatinase B, 92kDa gelatinase, 92kDa type IV collagenase)). *Atlas of Genetics and Cytogenetics in Oncology and Haematology* (2006).
312 Li, Y. Q. *et al.* ADAM17 mediates MMP9 expression in lung epithelial cells. *PLoS One* **8**, e51701 (2013).

313 Klein, T. & Bischoff, R. Physiology and pathophysiology of matrix metalloproteases. *Amino Acids* **41**, 271-290 (2011).
314 Quiding-Jarbrink, M., Smith, D. A. & Bancroft, G. J. Production of matrix metalloproteinases in response to mycobacterial infection. *Infect Immun* **69**, 5661-5670 (2001).
315 Chatila, T., Silverman, L., Miller, R. & Geha, R. Mechanisms of T cell activation by the calcium ionophore ionomycin. *J Immunol* **143**, 1283-1289 (1989).
316 Oppmann, B. *et al.* Novel p19 protein engages IL-12p40 to form a cytokine, IL-23, with biological activities similar as well as distinct from IL-12. *Immunity* **13**, 715-725 (2000).
317 Trickett, A. & Kwan, Y. L. T cell stimulation and expansion using anti-CD3/CD28 beads. *J Immunol Methods* **275**, 251-255 (2003).
318 Nakamuta, M. *et al.* Dimethyl sulfoxide inhibits dimethylnitrosamine-induced hepatic fibrosis in rats. *Int J Mol Med* **8**, 553-560 (2001).
319 von Maltzan, K., Tan, W. & Pruett, S. B. Investigation of the role of TNF-alpha converting enzyme (TACE) in the inhibition of cell surface and soluble TNF-alpha production by acute ethanol exposure. *PLoS One* **7**, e29890 (2012).

320 Eberlein, M. *et al.* Anti-oxidant inhibition of hyaluronan fragment-induced inflammatory gene expression. *J Inflamm (Lond)* **5**, 20 (2008).

321 Majtan, J. & Majtan, V. Dimethyl sulfoxide attenuates TNF-alpha-induced production of MMP-9 in human keratinocytes. *J Toxicol Environ Health A* **74**, 1319-1322 (2011).
322 Keshari, R. S. *et al.* Cytokines induced neutrophil extracellular traps formation: implication for the inflammatory disease condition. *PLoS One* **7**, e48111 (2012).

323 Palic, D., Andreasen, C. B., Menzel, B. W. & Roth, J. A. A rapid, direct assay to measure degranulation of primary granules in neutrophils from kidney of fathead minnow (Pimephales promelas Rafinesque, 1820). *Fish Shellfish Immunol* **19**, 217-227 (2005).

324 Etheridge, S. L., Brooke, M. A., Kelsell, D. P. & Blaydon, D. C. Rhomboid proteins: a role in keratinocyte proliferation and cancer. *Cell Tissue Res* **351**, 301-307 (2013).
325 Kawaguchi, M. & Suzuki, T. Gene expression and in situ localization of ADAM17 during skin wound healing. *Int J Dermatol*, doi:10.1111/ijd.12119 (2013).

326 Johansen, C. *et al.* Characterization of the interleukin-17 isoforms and receptors in lesional psoriatic skin. *Br J Dermatol* **160**, 319-324 (2009).

327 Andreu-Ballester, J. C. *et al.* Association of gammadelta T cells with disease severity and mortality in septic patients. *Clin Vaccine Immunol* **20**, 738-746 (2013).

328 Saito, S. *et al.* Ex vivo generation of highly purified and activated NK cells from human peripheral blood. *Hum Gene Ther Methods* (2013).

~ Appendix ~

Gene Expression Array

Figure A1: RNA integrity. **(a)** Control. **(b)** Example of RNA sample (all samples produced identical traces). The total RNA sample was composed of over 80% ribosomal RNA compared to approximately 1-3% mRNA, so ribosomoal RNA was used to check the quality of the RNA. Peaks 1, 2 and 3 correspond to small RNA (non-coding RNA that is not translated into protein), 18S RNA (small eukaryotic cytoplasmic ribosomal unit), and 28S RNA (large eukaryotic nuclear ribosomal unit) respectively. An RNA integrity number (RIN) is assigned to the sample, and level 10 represents RNA which was completely intact.

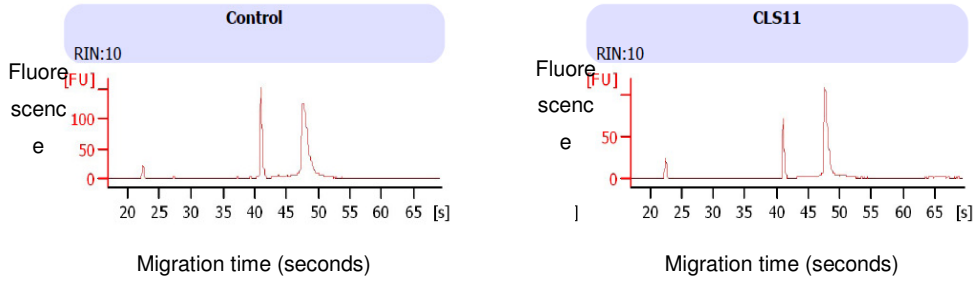

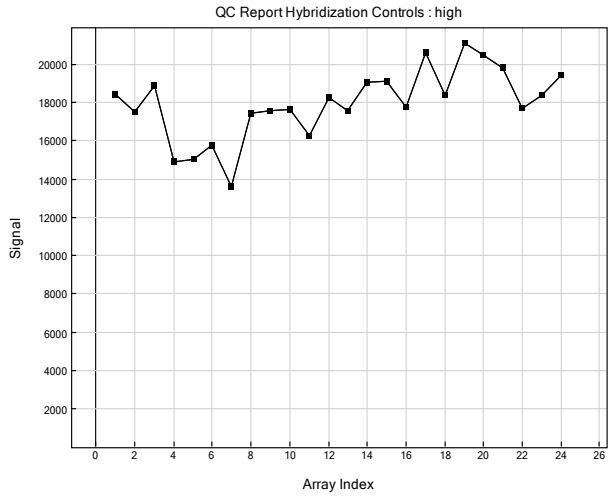

Figure A2: Control probe hybridisation. Hybridisation of control probes to all samples is high, suggesting that there are no problems with the quality of the RNA samples.

Figure A3: Number of genes detected on the gene expression array. The detection p values were set at either 0.01 (blue) or 0.05 (red). Values below the defined p value indicate that gene expression was detected. The detection score represents the confidence that a given gene is expressed above the background defined by negative probes.

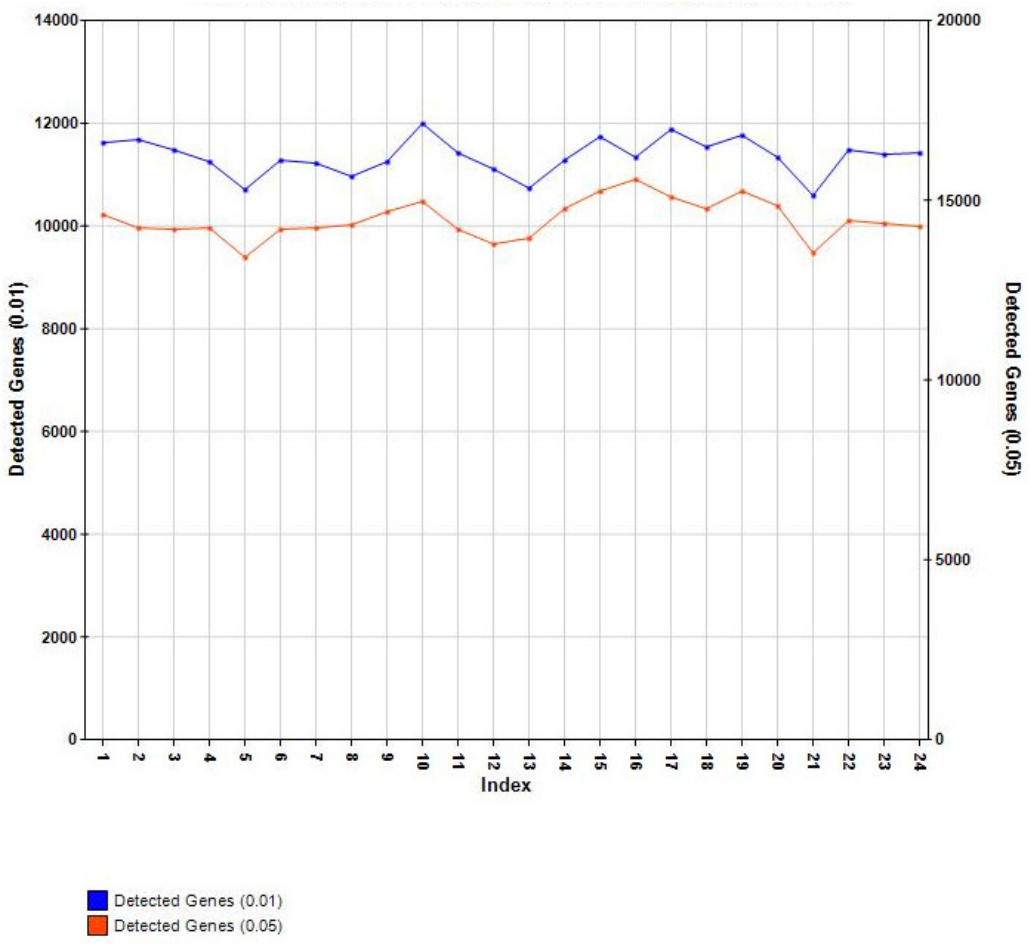

Figure A4: Scatter plot example of gene expression between two comparisons. Black dots represent genes whose expression is similar between samples, whilst blue dots represent genes whose expression is different between samples. Scatter plots provide an overall indication of sample similarity, but do not identify differences in expression of individual genes.

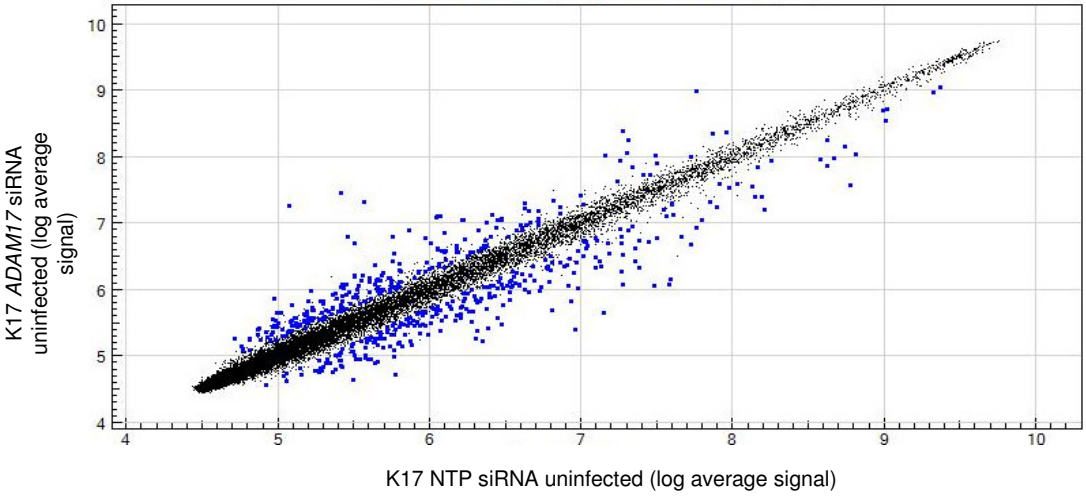

Figure A5: Dendrogram representing differential expression of probes within the eight samples.

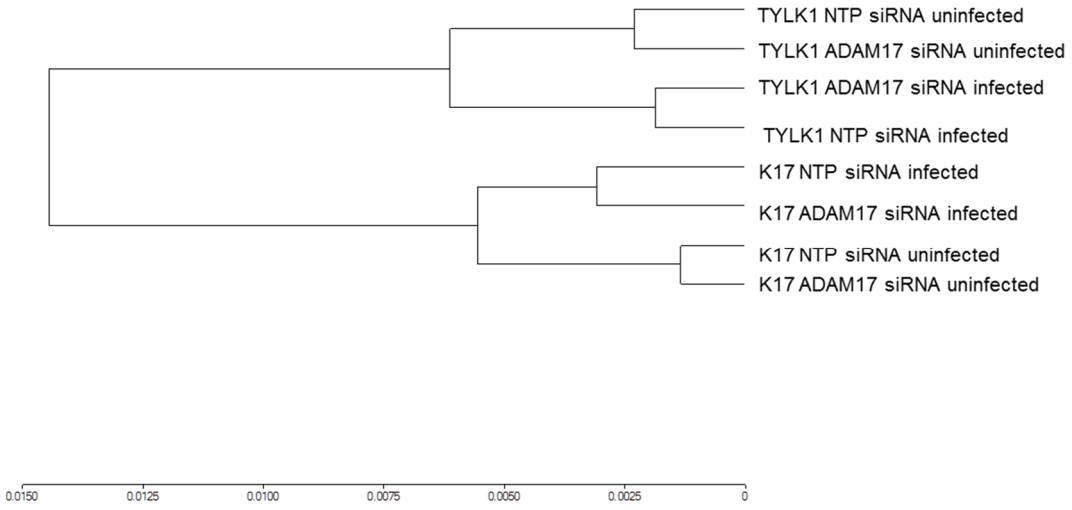

Table A1: 30 most up and downregulated genes: uninfected K17 NTP siRNA vs ADAM17 siRNA

Upregulated genes	Gene	Fold change
1	LOC100129882	1.125804643
2	CD55	1.068279631
3	KPRP	1.060597687
4	DAAM1	1.054105982
5	CYP1B1	1.052573291
6	PATE3	1.048643718
7	CXCL10	1.046565766
8	LCE2D	1.046314122
9	PHACTR3	1.044932632
10	NMI	1.044587262
11	ZC3HAV1	1.043712682
12	LCE2C	1.042311106
13	WEE1	1.041983602
14	LPAR2	1.041348699
15	MAFB	1.041103853
16	CCNE2	1.040913707
17	MX1	1.040365147
18	LCE2B	1.038941527
19	AMMECR1	1.03817924
20	SNORD13	1.037917934
21	CTDSP2	1.036914947
22	NIPAL1	1.036906988
23	ASPRV1	1.03689018
24	AMMECR1	1.036183063
25	KLF4	1.036046925
26	IGFBP3	1.035447888
27	NDNL2	1.034913972
28	OAS1	1.034802892
29	OAS2	1.034385387
30	RRM2	1.034357772
Downregulated genes	**Gene**	**Fold change**
-30	LOC387934	-1.038959385
-29	HOXA10	-1.039004043
-28	LOC441481	-1.039610035
-27	CXCL2	-1.040010231
-26	HSPA1A	-1.040144974
-25	VIM	-1.040150281
-24	RBM47	-1.040438106
-23	LOC653438	-1.041793542

-22	LOC728285	-1.04217377
-21	0	-1.042259216
-20	SH2D5	-1.042278081
-19	NFKB2	-1.042563088
-18	LOC650909	-1.042697801
-17	IL1B	-1.042781987
-16	DKK1	-1.043285303
-15	ANKRD57	-1.044684813
-14	ROD1	-1.047893949
-13	CHMP2B	-1.049134702
-12	SECISBP2	-1.04932171
-11	NFKB2	-1.051486535
-10	CXCL5	-1.052734744
-9	ANKRD46	-1.055014357
-8	CA12	-1.055379347
-7	CXCL5	-1.056899052
-6	IL24	-1.056993167
-5	TAGLN3	-1.058322808
-4	TAGLN3	-1.066804581
-3	OSTM1	-1.075961244
-2	HSPE1	-1.082000813
-1	ADAM17	-1.103718766

Table A2: 30 most up and downregulated genes: uninfected TYLK1 NTP siRNA vs ADAM17 siRNA

Upregulated genes	Gene	Fold change
1	CCNE2	1.077591364
2	LOC650909	1.073346644
3	SCNN1G	1.06892277
4	LOC389286	1.059661307
5	CHRNA5	1.057462568
6	NINJ1	1.054561969
7	ID2	1.054159233
8	ZNF394	1.053429287
9	TRIM31	1.052151671
10	TNNI2	1.051546851
11	KRT15	1.051448176
12	GCNT3	1.051206828
13	OXR1	1.050809401
14	SPRR1A	1.05029158
15	CYP1B1	1.04941924
16	LOC643446	1.049040505
17	LOC148430	1.048528978
18	LEP	1.048022305
19	TRIM22	1.047865441
20	SDCBP2	1.04767403
21	LOC390530	1.047633341
22	ST6GALNAC2	1.047594797
23	RETSAT	1.047239884
24	PSKH1	1.046935223
25	LOC202781	1.046398749
26	KRT4	1.046182595
27	LOC100133551	1.046015469
28	LOC283953	1.04582053
29	ID1	1.045460356
30	MMP7	1.045395169
Downregulated genes	**Gene**	**Fold change**
-30	VIM	-1.047707049
-29	GMCL1	-1.04907743
-28	CA12	-1.049134176
-27	FUT4	-1.049316164
-26	CDS1	-1.049504629
-25	NFKB2	-1.049529157
-24	GMCL1	-1.050117301
-23	GNB4	-1.050800236

-22	DPY19L1	-1.05125417
-21	KIAA1524	-1.051450845
-20	ADAMTS1	-1.052006314
-19	IL1RAP	-1.052058277
-18	TAGLN3	-1.052692632
-17	DCP2	-1.053126961
-16	LBR	-1.053430827
-15	PLAU	-1.053488821
-14	VIM	-1.054097014
-13	SECISBP2	-1.055775184
-12	TSPAN5	-1.056744219
-11	ANTXR2	-1.058643447
-10	AGPAT9	-1.06133046
-9	NLRP3	-1.063569356
-8	CYP27B1	-1.064562815
-7	SH2D5	-1.065061685
-6	CXCL2	-1.066018175
-5	ANKRD57	-1.066805436
-4	OSTM1	-1.07041002
-3	ANKRD46	-1.099538151
-2	ADAM17	-1.10639641
-1	IL24	-1.107274036

Table A3: 30 most up and downregulated genes: *S. aureus* infected K17 NTP siRNA vs ADAM17 siRNA

Upregulated genes	Gene	Fold change
1	LOC100132761	1.137316133
2	LOC441763	1.109812343
3	LOC100134364	1.106725282
4	LOC100008589	1.101679823
5	LOC100008589	1.094560072
6	LOC100132394	1.092860342
7	LOC389286	1.090583125
8	LOC100008588	1.08002524
9	SNORD3D	1.075083213
10	SNORA12	1.073320417
11	LOC100132564	1.07323868
12	SNORD3A	1.073080056
13	LOC100133565	1.071791974
14	CXCL10	1.071398081
15	MYC	1.071055618
16	LOC100130332	1.070549184
17	EPR1	1.067160447
18	IFI6	1.066738708
19	LOC650909	1.06564464
20	GFOD2	1.061610251
21	PRKDC	1.061561892
22	LOC100129882	1.061187435
23	SLC25A22	1.061160977
24	LOC728969	1.059947837
25	SNORD13	1.056897242
26	RN7SK	1.05612386
27	SCAP	1.055206138
28	MRPS25	1.05514912
29	ATF5	1.054887828
30	ARRDC3	1.054184229
Downregulated genes	**Gene**	**Fold change**
-30	FBLIM1	-1.064143508
-29	PPDPF	-1.064901968
-28	LOC645979	-1.066535026
-27	BAT2	-1.066625498
-26	PKMYT1	-1.067139708
-25	RPLP1	-1.067699738
-24	LOC642828	-1.069203204
-23	CRTC2	-1.070430588

-22	CDC42BPB	-1.070830601
-21	JUP	-1.071213109
-20	PKM2	-1.071358059
-19	PABPC1	-1.074119038
-18	NPDC1	-1.074155549
-17	GPR1	-1.075429139
-16	SERPINE1	-1.07718653
-15	UBTD1	-1.077204848
-14	OSTM1	-1.077819078
-13	YWHAE	-1.078345585
-12	LOC100128485	-1.078953869
-11	PKM2	-1.079191943
-10	ANKRD57	-1.079407622
-9	NFKB2	-1.079755528
-8	AGRN	-1.080157261
-7	TMEM132A	-1.080286359
-6	LOC644936	-1.085242869
-5	CXCL5	-1.092714141
-4	ADAM17	-1.093444959
-3	LOC100130009	-1.09421618
-2	SH3BP1	-1.09991806
-1	IL24	-1.102001538

Table A4: 30 most up and downregulated genes: *S. aureus* infected TYLK1 NTP siRNA vs ADAM17 siRNA

Upregulated genes	Gene	Fold change
1	EZH2	1.070358104
2	KRT4	1.060893423
3	CCNE2	1.052223195
4	TSC22D3	1.052029506
5	DEFB1	1.051162118
6	RRM2	1.050387712
7	SAA1	1.047708253
8	NCCRP1	1.047488427
9	CYP1B1	1.047448647
10	SLC1A3	1.047312752
11	LOC441155	1.047127808
12	WEE1	1.047072088
13	TRIM31	1.046495986
14	MPZL2	1.045718104
15	CD83	1.045376564
16	PTPRU	1.044872903
17	MMP7	1.044700475
18	SLC15A3	1.044431818
19	WNT10A	1.043686516
20	ABHD12	1.043142162
21	WHAMM	1.042978657
22	FBXO5	1.042763374
23	BRP44L	1.042660686
24	ARID4B	1.042555833
25	LOC652330	1.042514467
26	CCNE1	1.042379616
27	RHOV	1.042230941
28	CD83	1.0414525
29	FOXA1	1.041343558
30	RPL28	1.04129627
Downregulated genes	**Gene**	**Fold change**
-30	LOC100130154	-1.052644147
-29	EHBP1L1	-1.05341574
-28	0	-1.053983707
-27	CXCL2	-1.054129298
-26	LOC100132425	-1.054236345
-25	CYP27B1	-1.054284996
-24	SH2D5	-1.054670561
-23	C7orf11	-1.054702569

-22	CTSC	-1.05475049
-21	DPY19L1	-1.055107191
-20	FAM73A	-1.055275504
-19	ADAMTS1	-1.055615006
-18	LAMC2	-1.055833544
-17	SYAP1	-1.05587409
-16	IL1RAP	-1.057943808
-15	ANKRD46	-1.058439211
-14	TNFRSF6B	-1.059590787
-13	TXNL1	-1.059860783
-12	TNFRSF6B	-1.060494823
-11	FAM116A	-1.065151392
-10	AGPAT9	-1.066113199
-9	TERC	-1.072617247
-8	VIM	-1.072968177
-7	MMP9	-1.07300177
-6	VIM	-1.076060757
-5	OSTM1	-1.077422531
-4	TFPI2	-1.077909652
-3	IL24	-1.10002384
-2	ANKRD57	-1.109590277
-1	ADAM17	-1.121039695